UNIVERSIDADE DE BRASÍLIA – UnB
INSTITUTO DE GEOCIÊNCIAS – IG
PROGRAMA DE PÓS-GRADUAÇÃO EM GEOLOGIA - PPGGeo
AREA DE CONCENTRAÇÃO EM GEOLOGIA ECONÔMICA
E EXPLORAÇÃO MINERAL

AVALIAÇÃO DO POTENCIAL PARA DEPÓSITOS DE NI-CU-PGE SULFETADO ASSOCIADOS A KOMATIITOS NO BRASIL

Tiago Felipe Arruda Maia

TESE DE DOUTORADO Nº 216

Orientador: Cesar Fonseca Ferreira Filho

Brasília-DF, 27 de março de 2025

Ficha catalográfica elaborada automaticamente,
com os dados fornecidos pelo(a) autor(a)

Ma

Maia, Tiago Felipe Arruda
AVALIAÇÃO DO POTENCIAL PARA DEPÓSITOS DE NI-CU-PGE SULFETADO ASSOCIADOS A KOMATIITOS NO BRASIL / Tiago Felipe Arruda Maia; orientador César Fonseca Ferreira Filho. Brasília, 2025.
211 p.

Tese(Doutorado em Geologia) Universidade de Brasília, 2025.

1. Komatiito. 2. Depósitos magmáticos de Ni-Cu-PGE. 3. Greenstone Belt. 4. Brasil. I. Ferreira Filho, César Fonseca, orient. II. Título.

AGRADECIMENTOS

Não tem como ser diferente eu não iniciar os meus agradecimentos, fazendo isso a minha querida esposa Samia Darcila Barros Maia, que foram meus braços, pernas e muitas vezes coração, durante todo esse período de doutorado. Me deu um suporte e apoio incondicional, me levantando quando eu caia e não deixando eu me desmotivar nunca. Te amo hoje e sempre, você é uma inspiração e um exemplo para mim.

Agradeço em segundo lugar ao meu orientador o Professor Doutor César F. Ferreira Filho, que me ajudou desde o meu primeiro dia em Brasília. Seu apoio e orientação foram cruciais para que essa tese ocorresse bem. Destaco conversas interessantes durante as orientações, conversas sobre a vida, o mundo, família, clima, futebol, tudo como parte de deixar a orientação mais natural possível e repassando o seu conhecimento ímpar sobre depósitos associados ao magmatismo máfico-ultramáfico. Particularmente, para mim, as melhores conversar eram sobre os projetos de exploração em Ni-Cu-PGE sulfetados que estavam surgindo no Brasil.

Agradecer a minha família, minhas irmãs Renata e Paula Maia, Yara e Kyara Teixeira, a meus pais Ricardo Maia e Fernanda Patrícia Arruda, sem o apoio e motivação eles não teriam conseguido.

Aos meus amigos, Paulo Jerry, Kegan Ponce, Wagner, Letícia, Luisa Gomes, Valéria, Ster, Yeimmy, Valentina Bocanegra, Daniela, Sebastin, Yuri Tatiana, Angel, Gabriella, Emiliano, Adriana, Maria Masella, Vivian, André e Lucas, muito obrigado pelas conversar geológicas e não geológicas, muitas vezes nos bares ao redor da UnB em Manaus. Uma especial menção a Marcel, Marcia Caroline, Michele e Mariana pelos momentos durante a pandemia que ficamos enclausurados e por morar muito perto compartilhávamos momentos juntos, obrigado a todos vocês.

Há também aqueles que ajudaram durante a pesquisa, mas que não foi com contado direto. Aqui agradeço aos diversos e-mails trocados com

pesquisadores brasileiros no exterior, o Eduardo Mansur, o Klaus Kuster e a Claudia Augustin.

Por último quero agradecer ao Michael Lesher, por inúmeros e-mails trocados e reuniões on-line feitas, ele acabou sendo um coorientador extraoficial. O meu muito obrigado por tudo.

Deixo também um muito obrigado a aqueles que me ajudaram de alguma forma e que acabei não mencionando aqui.

Por último e não menos importante, agradeço a CAPES, ao CNPq, pelo financiamento ao programa de pós-graduação em geologia da UnB. Agradeço também a própria UnB e a UFAM, pela disponibilidade de uso de suas dependências, laboratórios e equipamentos.

Maia T.F.M. 2014. Avaliação do potencial para depósitos de Ni-Cu-PGE sulfetado associados a komatiitos no Brasil. Tese (Doutorado em Geologia) - Instituto de Geociências, Universidade de Brasília, Brasília.

Depósitos sulfetado de Ni-Cu-PGE associados a komatiitos são raros no Brasil, com somente duas ocorrências Boa Vista e Fortaleza de Minas. Esse fato levou a seguinte pergunta. Existe alguma justificativa geológica/petrológica para a escassez de depósitos sulfetados de Ni-Cu-EGP associados aos komatiitos brasileiros? Motivado em responder este questionamento, a tese teve como objetivos melhorar o entendimento da gênese dos depósitos magmáticos de Ni-Cu-EGP associados a rochas komatiíticas no Brasil, por meio de estudos sistemáticos nos komatiitos brasileiros e os comparando com os encontrados em outras regiões do planeta. Propôs, também, contribuir para um modelo de exploração mineral mais adaptado paras as condições geológicas encontradas no Brasil. Para isso foram realizados estudos geológicos, petrográficos, litogeoquímicos, geoquímicos no minério, geoquímicos isotópicos em enxofre, no minério e na rocha encaixante nos depósitos de Boa Vista no greenstone belt de Crixás e no depósito de Fortaleza de Minas, a fim de entender detalhes dos aspectos metalogenéticos e exploratórios desses depósitos. Por fim, foi feita uma análise integrada comparativa dos komatiitos brasileiros, mineralizados e não mineralizados, para avaliar o seu potencial metalogenéticos para depósitos sulfetados de Ni-Cu-PGE.

Os resultados obtidos mostraram que para o depósito de Boa Vista, mostraram que o depósito é do tipo I (contato basal), formado preferencialmente por pirrotita, pentlandita e calcopirita, com pirita subordinada em zonas de cisalhamento. Novos dados de litogeoquímica, através de modelagem contaminação crustal e cristalização fracionada concomitante junto com os isótopos de enxofre, mostraram que a rocha encaixante, o grafita xisto, é a fonte de enxofre para o depósito de Boa Vista. Modelagens para calcular o R-factor demostraram valores entre 300-400 para depósito de Boa Vista. A associação de altas concentrações de MgO, Zn e Ni, associado ao fácies de

conduto/canalização de lava podem ser usados para critérios exploratórios para essa classe de depósito mineral.

Para os resultados de Fortaleza de minas, novos dados de geoquímica de semimetais combinado com isótopos de enxofre, mostraram que a formação ferrífera bandada é a fonte externa para o enxofre e os semimetais analisados. Modelagens geoquímicas e isotópicas indicaram que o depósito de fortaleza de Minas tem um R fator entre 150-400. Também foi discutido que o ambiente altamente fracionado de lago de lava não é compatível com os valore de R fator obtidos, e principalmente com a presença do minério alojado nesse fácies. Assim possivelmente foi uma combinação de dois ambientes distintos, um para zona inferior e outro para a zona superior.

Para a análise do potencial metalogenético dos komatiitos brasileiros, uma revisão sistemática foi feita e constatou um total de 26 ocorrências de komatiitos diferentes que foram mapeados no território brasileiros, sendo 2 mineralizados. Número muito baixo, para as dimensões continentais do Brasil. Foi constatado que muitas das descrições, são focadas somente no komatiitos, sem fazer uma interpretação de sucessão de facies komatiíticos, nem das rochas sedimentares que possam ser ricas em enxofre associadas ao komatiitos. Outro ponto é pouca quantidade de dados geoquímicos robustos, o que dificulta a avaliação do potencial metalogenético para essas rochas. Foi possível indicar que os komatiitos de Quebra Osso no greenstone belt Rio das Velhas no Quadrilátero Ferrífero - Craton São Francisco, tem bons indicativos de ter formado um líquido sulfetado imiscível que capturou metais e formou sulfetos.

Localizar os principais condutos de magma em terrenos metamórficos, deformados e mal expostos, avaliar fontes adequadas de enxofre, a presença de armadilhas químicas e físicas para a formação do minério, e restringir o efeito da modificação pós-magmática à geoquímica dos komatiitos regionalmente, se torna essencial para a exploração de depósitos de Ni-Cu-PGE associados a komatiitos, principalmente no Brasil. Por último, os komatiitos brasileiros não são diferentes dos daqueles encontrados por exemplo, na Austrália, Canada e África do Sul, e seu potencial metalogenético existe. Eles só precisam serem melhor

mapeados, descritos, interpretados e analisados, com foco em avaliar os pré-requisitos necessários para a formação de depósitos sulfetados de Ni-Cu-PGE.

Palavras-chave: Komatiito, Brasil, sulfetos de Ni-Cu-PGE, geoquímica, isótopos de enxofre

Maia T.F.M. 2014. Avaliação do potencial para depósitos de Ni-Cu-PGE sulfetado associados a komatiitos no Brasil. Tese (Doutorado em Geologia) - Instituto de Geociências, Universidade de Brasília, Brasília.

Ni-Cu-PGE sulfide deposits associated with komatiites are rare in Brazil, with only two occurrences Boa Vista and Fortaleza de Minas. This fact led to the following question. Is there any geological/petrological justification for the scarcity of sulfide deposits of Ni-Cu-EGP associated with Brazilian komatiites? Motivated to answer this question, the thesis aimed to improve the understanding of the genesis of Ni-Cu-EGP magmatic deposits associated with komatiite rocks in Brazil, through systematic studies in Brazilian komatiites and comparing them with those found in other regions of the planet. It also proposed to contribute to a model of mineral exploration more adapted to the geological and climatic conditions found in Brazil. For this, geological, petrographic, lithogeochemical, geochemical studies in ore, isotopic geochemical in sulfur, ore and in the bedrock were carried out in the Boa Vista deposits in the Crixás greenstone belt and in the Fortaleza de Minas deposit, in order to understand details of the metallogenetic and exploratory aspects of these deposits. Finally, an integrated comparative analysis of Brazilian komatiites, mineralized and non-mineralized, was carried out to evaluate their metallogenetic potential for sulfide deposits of Ni-Cu-PGE.

The results obtained showed that for the Boa Vista deposit they are type I (basal contact), formed preferentially by pyrrhotite, pentlandite and chalcopyrite, with subordinate pyrite in shear zones. New lithogeochemical data, through modeling crustal contamination and concomitant fractional crystallization along with sulfur isotopes, showed that the embedding rock, graphite shale, is the source of sulfur for the Boa Vista deposit. Modeling to calculate the R-factor showed values between 300-400 for Boa Vista deposit. The association of high concentrations of MgO, Zn and Ni, associated with the facies of lava conduit/channeling can be used for exploratory criteria for this class of mineral deposit.

For the results from Fortaleza de Mines, new geochemistry data of semimetals combined with sulfur isotopes, showed that the banded iron formation is the external source for the sulfur and semimetals analyzed. Geochemical and isotopic modeling indicated that the Fortaleza de Minas deposit has a R factor between 150-400. It was also discussed that the highly fractionated lava lake environment is not compatible with the R values factor obtained, and especially with the presence of the ore housed in this facies. Thus, it was possibly a combination of two distinct environments, one for the lower zone and the other for the upper zone.

For the analysis of the metallogenetic potential of Brazilian komatiites, a systematic review was carried out and found a total of 26 occurrences of different komatiitos that were mapped in the Brazilian territory, 2 of which were mineralized. A very low number, for the continental dimensions of Brazil. It was found that many of the descriptions are focused only on komatiitos, without making an interpretation of the succession of komatiitic facies, nor of the sedimentary rocks that may be rich in sulfur associated with komatiitos. Another point is the small amount of robust geochemical data, which makes it difficult to evaluate the metallogenetic potential for these rocks. It was possible to indicate that the komatiitos of Quebra Osso in the Rio das Velhas grenstone belt in the Iron Quadrangle - Craton São Francisco, have good indications of having formed an immiscible sulfide liquid that captured metals and formed sulfides.

Locating the main magma conduits in metamorphic, deformed and poorly exposed terrains, evaluating suitable sources of sulfur, the presence of chemical and physical traps for the formation of the ore, and restricting the effect of post-magmatic modification to the geochemistry of komatiites regionally, becomes essential for the exploration of Ni-Cu-PGE deposits associated with komatiites, especially in Brazil. Finally, Brazilian komatiitos are not different from those found, for example, in Australia, Canada and South Africa, and their metallogenetic potential exists. They just need to be better mapped, described, interpreted and analyzed, with a focus on assessing the prerequisites needed for the formation of Ni-Cu-PGE sulfide deposits.

Keywords: komatiite, Brazil, Ni-Cu-PGE sulfides, geochemistry, sulfur isotopes

Lista de Figuras

Lista de tabelas

SUMÁRIO

INTRODUÇÃO

Depósitos magmáticos de Ni-Cu-PGE sulfetado associados a rochas komatiíticas ocorrem em terrenos tipo *greenstone belts* em diversos locais na Terra, incluindo depósitos de grande porte como, por exemplo, no Canadá e na Austrália (Arndt et al. 2008) No Brasil, apesar da presença de komatiitos em diversos *greenstone belts,* existem apenas dois depósitos de Ni-Cu-EGP conhecidos: Boa Vista – GO (Costa JR. et al., 1997; Ferreira Filho e Lesher, 2001) e Fortaleza de Minas – MG (Brenner et al., 1990; Brenner, 2006; Carvalho e Brenner, 2010) (Figura 01). A baixa quantidade de depósitos deste tipo no Brasil levanta questões sobre as condições em que os komatiitos brasileiros se formaram e, desta maneira, se os fatores controladores de mineralizações associadas estavam ausentes nos cratons e terrenos *greenstones belt* brasileiros. Dessa forma, este projeto propôs investigar as condições de formação dos komatiitos brasileiros e comparar com aquelas associadas aos ambientes mais férteis, em especial os canadenses e australianos, bem mais numerosos e melhor estudados.

Os estudos de komatiitos no Brasil são ainda relativamente restritos. Trabalhos com enfoque geológico/estrutural, petrográfico e geoquímicos permitiram a interpretação da origem, o processo mineralizador e potencial prospectivo em komatiitos e rochas associadas (e.g., Costa JR. et al. 1997; Brenner, 2006; Almeida et al., 2007; Siepierski e Ferreira Filho, 2016), enquanto outros apresentam uma abordagem focada na geoquímica (e.g., Arndt et al. 1989; Kuyumjian and Jost 2006; Menezes Leal et al., 2015; Barbosa et al., 2020; Soares et al., 2020; Martins-Ferreira et al., 2020, Borges et al., 2021; Sampaio et al., 2022). Apesar do conhecimento produzido por estes estudos, algumas questões permanecem sem resposta, como por exemplo: Por que são poucos os depósitos sulfetados de Ni-Cu-EGP associados a rochas komatiíticas no Brasil? Existe alguma justificativa (e.g., estrutura magmática, composição) para a ausência de depósitos de Ni-Cu-EGP sulfetado de grande porte nos komatiitos brasileiros? Quais terrenos komatiíticos brasileiros têm maior potencial para hospedar depósitos de Ni-Cu-EGP sulfetado? As estratégias exploratórias, com sucesso em outros terrenos no mundo, precisam ser ajustadas para as

características geológicas brasileiras? (e.g., metamorfismo, deformação, intemperismo, etc.).

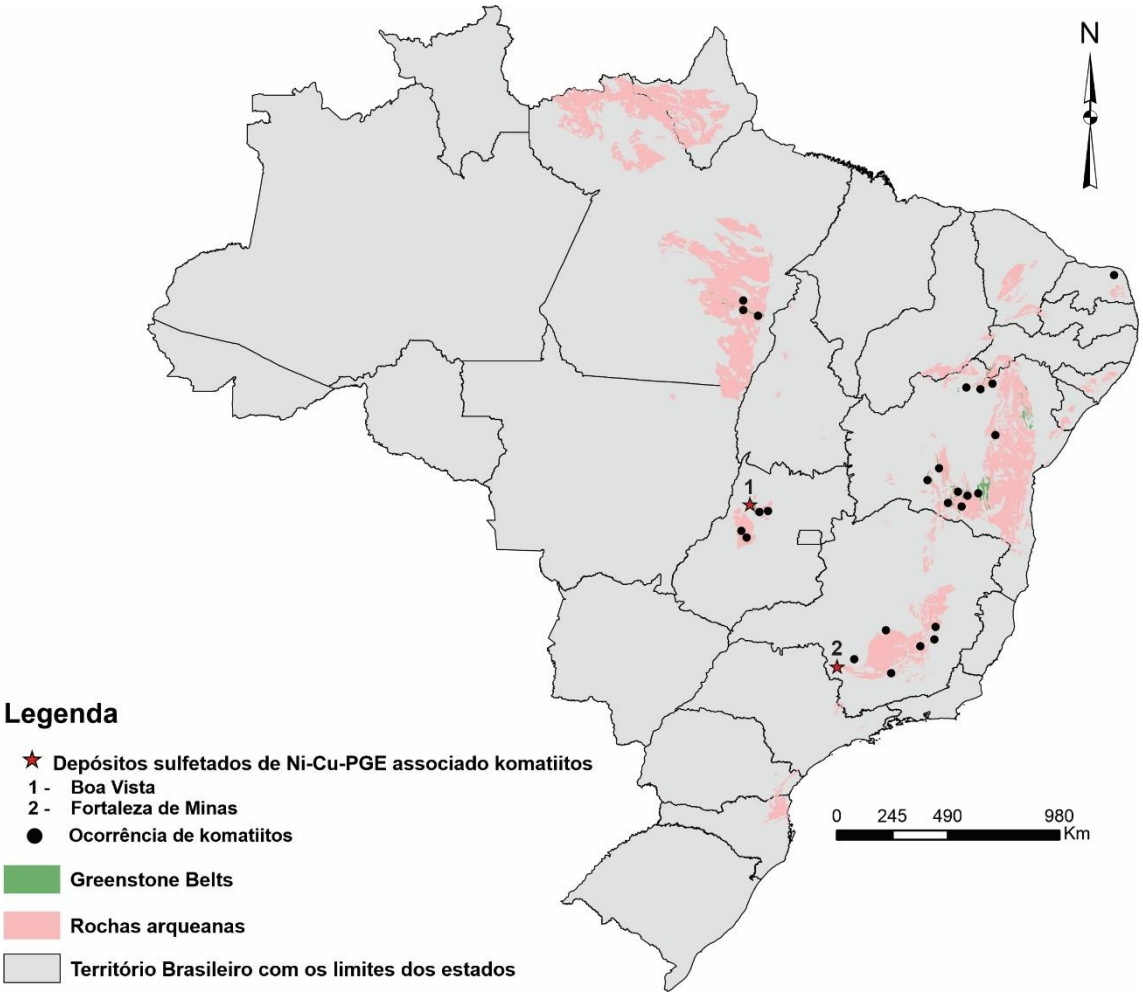

Figura 1 Mapa de localização dos depósitos de Ni-Cu-PGE associado às rochas komatiiticas no Brasil. Fonte: esta tese.

Tendo em vista o contexto geológico e a idade dos *greenstone belts* no Brasil e no mundo, a raridade de komatiitos brasileiros mineralizados é intrigante e merece ser revisitada. Teria o manto subjacente aos crátons brasileiros uma dinâmica de fusão parcial diferente do manto abaixo dos crátons canadense e australiano durante o Arqueano? Quais variáveis foram diferentes durante a formação dos komatiitos brasileiros em relação aos outros? Seria a mineralização diretamente dependente da assimilação de rochas crustais ricas em S, potencialmente ausentes no Brasil e presentes no Canadá e na Austrália?

A perspectiva de aumento de demanda para Ni-Co, com a introdução dos veículos elétricos, motivou a retomada da exploração para depósitos de Ni-Co sulfetado. Comparados aos ambientes mineralizados no Canadá e Austrália, os terrenos komatiitos brasileiros são relativamente pouco conhecidos e

apresentam baixa maturidade exploratória. Assim, komatiitos brasileiros representam alvos potenciais para este novo ciclo exploratório.

A partir de análises químicas, tanto de minerais específicos (exemplo: olivina e piroxênio) quanto de rocha total é possível analisar, quantificar e caracterizar um processo metalogenético específico de um determinado depósito mineral. Uma abordagem múltipla, com a integração e comparação de dados geológicos, geoquímicos, e isotópica pode, portanto, elucidar algumas das questões levantadas acima. O potencial deste tipo de abordagem integrada e comparativa é evidente, dados os inúmeros estudos sobre a metalogenia de depósitos de Ni-Cu-EGP em rochas komatiiticas (Fiorentini *et al*., 2004; Arndt *et al*., 2005; Barnes *et al*., 2007; Barnes & Fiorentini, 2012; Barnes et *al.,* 2016;Le Vaillant et al., 2016; Staude et al., 2017; Staude et al., 2021; Yao and Mungall, 2021; Staude et al., 2022).

Naldrett (2010) mostra que depósitos sulfetados associados a komatiitos contêm aproximadamente 19% dos recursos já descobertos de Ni no mundo, sendo 9% em komatiitos proterozoicos (e.g., Raglan: Lesher, 2007; Thompson: Layton-Matthews *et al.,* 2010) e 10% em komatiitos arqueanos (e.g., Kambalda: Lesher, 1989; Mt Keith: Rosengren *et al.,* 2005; Perseverance: Barnes *et al.,* 1988). Esses depósitos sulfetados produzem ainda quantidades consideráveis de Cu, Co e EGP como subprodutos econômicos. Com base em novos conhecimentos que este projeto pode trazer, o setor mineral brasileiro poderá ter maior entendimento da gênese desse tipo de depósito e aumentar os investimentos na mineração com maior previsibilidade e menor risco, desta forma, gerando mais empregos, aumentando a renda, arrecadando mais impostos e trazendo desenvolvimento socioeconômico.

Do ponto de vista geocientífico, komatiitos são rochas que permitem compreender melhor a dinâmica do manto no período em que elas foram formadas (Arndt et al., 2008; Naldrett, 2010). Este conhecimento é extremamente importante para o entendimento da evolução mantélica desde o arqueano, pois permite compreender a formação de outros tipos de depósitos minerais e rochas geradas na mesma época, como por exemplo aqueles encontrados no Quadrilátero Ferrífero e em Carajás. Além disto, traz um maior entendimento das heterogeneidades do manto no arqueano. Portanto, os dados produzidos neste projeto não só auxiliam no estudo da gênese dos depósitos em

rochas komatiíticas no Brasil, mas também trazem conhecimento para diversas áreas científicas como a geoquímica, geofísica, evolução geológica, petrologia, geologia planetária, entre outras.

Um outro aspecto importante é a preservação dos komatiitos, algo que ele é naturalmente raro, uma vez que essas rochas são preferencialmente arqueanas, compõem geralmente as sequências inferiores dos greenstone belts, tendo sido metamorfisadas, deformadas, soerguidas, intemperizadas e erodidas, por sucessivos eventos orogênicos (Ardnt et al., 2008) que acorreram do território brasileiro ao logo de mais de 2.5 bilhões de anos (ex. eventos Transamazônico, Cariris Velhos, Brasiliano-Panafricano, ruptura do Gondwana etc.) Hasui et al., 2012). Muitos greenstone belts afloram em pequenos sigmoides, domos e quilhas, como faixas alongadas e restritas de alguns quilômetros a centenas de metros de comprimento e largura (ex. Umburanas – Lopes et al., 2002, Mundo Novo – Spreafico et al., 2020; Riacho dos Machados – Leal et al., 2021; etc.).

Dentro desses greenstone belts brasileiros, uma parte, muitas vezes diminuta, aflora os komatiitos, entretanto há exceções com boas exposições, (ex: Crixás - Ardnt et al, 1989; Umburanas – Meneses Leal et al., 2015; Quebra Osso - Verma et al., 2017), mas no geral, há muito poucos afloramentos de komatiitos, com todas as sequências de derrames bem expostos e preservados. Muitos afloramentos são de blocos intemperizados e quando não, são muito pequenos, dificultando o mapeamento geológico dos derrames e a correta interpretação das suas fácies, ou nem exposto estão (ex. Tiquara – Cunha et al., 2012). Vale mencionar o fato de que muitos komatiitos não têm mais a sua mineralogia e estrutura ígnea primárias preservadas, pois foram completamente substituídas por uma paragênese e microestruturas metamórficas (ex. Ibitira-Ubiraçaba – Cunha et al., 2012).

Um último ponto também relevante é a presença de metakomatiitos maciços, combinado com a ausência de textura spinifex, faz com que rochas ultramáficas sejam descritas como peridotitos e não como komatiitos, sendo que apenas 20-40% dos komatiitos tem essa textura (Arndt et al., 2008). Serpentinitos maciços sozinhos não irão indicar qual o tipo exato de protólito ultramáfico, isso dificulta ainda mais o reconhecimento em campo de

metakomatiitos (Ardnt et al., 2008). Todos esses pontos mencionados, tornam a preservação e o posterior reconhecimento dos komatiitos um grande desafio.

OBJETIVOS, PERGUNTAS E HIPÓTESES

O foco desta pesquisa é responder a uma questão principal: ***Existe alguma justificativa geológica/petrológica para a escassez de depósitos sulfetados de Ni-Cu-EGP associados aos komatiitos brasileiros?***

O presente estudo tem por objetivo principal melhorar o entendimento da gênese dos depósitos magmáticos de Ni-Cu-EGP associados a rochas komatiíticas no Brasil por meio de estudos sistemáticos nos komatiitos brasileiros e os comparando com os encontrados em outras regiões do planeta. Propõe, também, contribuir para um modelo de exploração mineral mais adaptado para as condições geológicas e climáticas encontradas no Brasil. Dessa forma são desenvolvidas as seguintes etapas:

(1) Descrever afloramentos de komatiitos mineralizados e não mineralizados, amostras de mão e testemunhos de sondagem em escala macroscópica e microscópica já coletados no Brasil e no Canadá, baseados em rotinas descritas em Houlé & Lesher (2011), como forma de identificar paragêneses minerais, feições, estruturas e texturas típicas desse tipo de rocha e depósito mineral;

(2) Obter e analisar dados geoquímicos provenientes das rochas mineralizadas e não mineralizadas, conforme metodologia elaborada por Lesher *et al*. (2001), Sproule *et al*. (2003); Arndt & Lesher (2004); Arndt *et al*. (2005); e Barnes *et al.* (2007);

(3) Identificar e Integrar os processos mineralizadores que geraram os diferentes depósitos sulfetados de Ni-Cu-EGP associados a komatiitos;

(4) Apresentar a aplicação dos modelos metalogenéticos na exploração e pesquisa mineral;

(5) Comparar os dados e modelos produzidos com os dados geológicos, geoquímicos, metalogenéticos, entre outros que estiverem disponíveis na literatura.

ESTRUTURA DA TESE

Este doutorado está estruturado em três capítulos na forma de artigos (capítulos 1 e 2) e em uma discussão (capítulo 3) em que, um já foi publicado, e o outro está em fase final de submissão para publicação em periódico científico internacional especializado sobre os temas abordados na tese.

Os artigos e discussão contemplam os objetivos e às perguntas estabelecidos no doutorado, que foram submetidos ao decorrer da evolução natural desta pesquisa. Em cada um dos capítulos abaixo, há o detalhamento da metodologia aplicada, da geologia regional, bem como os resultados.

Capítulo 1

Este capítulo apresenta o artigo intitulado “The komatiite-associated Boa Vista Ni-Cu-(PGE) sulfide deposit, Crixás greenstone belt, Central Brazil: insights into komatiite flow facies and exploration”, que foi publicado no periódico Journal of South American Earth Sciences em fevereiro de 2025. O artigo foi reformatado em um capítulo para atender aos padrões de diagramação de Tese do PPGG-UnB.

Este artigo fez uma abordagem integrada de litogeoquímica, litoquímica do minério e de isótopos de enxofre do minério e da rocha encaixante, para definir a rocha fonte externa de enxofre para o minério de Ni-Cu sulfetado de Boa Vista no greenstone belt de Crixás. Além de discutir critérios exploratórios para esse tipo de depósito.

Capítulo 2

Este capítulo apresenta o artigo intitulado “The role of banded iron formations as a source of sulfur and semimetals in komatiite-associated Ni-Cu-PGE deposits: Example from the Fortaleza de Minas deposit, Brazil”, que está em processo de revisão final para ser submetido ao periódico Mineralium Deposita. O artigo foi reformatado em um capítulo para atender aos padrões de diagramação de Tese do PPGG-UnB.

Neste trabalho é apresentado dados geoquímicos de TABS +Se, e dados

isotópicos de enxofre, tanto do minério quanto de BIF, do depósito sulfetado de Ni-Cu-PGE de Fortaleza de Mina. Foi discutido nele a fonte externa do enxofre e dos TABS +Se, e por último a formação do depósito em ambiente de ponded flow.

Capítulo 3

O capítulo é intitulado “Avaliação dos komatiitos brasileiros para mineralização de sulfeto de Ni-Cu-PGE”. Ele não é um artigo e sim uma discussão.

Este último capítulo traz uma discussão dos dados que já existem na literatura dos komatiitos brasileiros, usando uma abordagem integrada que avaliou o potencial dessas rochas para depósitos sulfetados de Ni-Cu-PGE. Além de sugerir critérios exploratórios para o Brasil.

REFERÊNCAS

Almeida C.M. De, Olivo G.R., Carvalho S.G. de 2007. The Ni-Cu-PGE sulfide ores of the komatiite-hosted Fortaleza de Minas deposit, Brazil: Evidence of hydrothermal remobilization. Canadian Mineralogist, **45**:751–773.

Almeida F.F.M. De, Brito Neves B.B. De, Dal Ré Carneiro C. 2000. The origin and evolution of the South American platform. Earth Science Reviews, **50**:77–111.

Anhaeusser C.R. 2014. Archaean greenstone belts and associated granitic rocks - A review. Journal of African Earth Sciences, **100**:684–732.

Arndt N.T., Teixeira N.A., White W.M. 1989. Bizarre geochemistry of komatiites from the Crixás greenstone belt, Brazil. Contributions to Mineralogy and Petrology, **101**:187–197.

Arndt N.T., Lesher C.M., Barnes S.J. 2008. Komatiite (N. T. Arndt, Ed.). Komatiite, 295–327.

Barbosa N., Menezes Leal A.B., Debruyne D., Bastos Leal L.R., Barbosa N.S., Marinho M., Mercês L., Barbosa J.S., Koproski L.M. 2020. Paleoarchean to Paleoproterozoic crustal evolution in the Guanambi-Correntina block (GCB), north São Francisco Craton, Brazil, unraveled by U-Pb Geochronology, Nd-Sr isotopes and geochemical constraints. Precambrian Research, **340**:105614.

Barnes S.-J., Lightfoot P.C. 2005. Formation of Magmatic Nickel Sulfide Deposits and Processes Affecting Their Copper and Platinum Group Element Contents. Society of Economic Geologists, Inc. Economic Geology - One Hundredth Anniversary Volume, 179–213.

Barnes S., Lesher C.M., Keays R.R. 1995. Geochemistry of mineralised and barren komatiites from the Perseverance nickel deposit, Western Australia. Lithos, **34**:209–234.

Barnes S.J. 2006. Komatiite-Hosted Nickel Sulfide Deposits: Geology, Geochemistry, and Genesis. Komatiite-Hosted Nickel Sulfide Deposits:

Geology, Geochemistry, and Genesis, 51–97.

Barnes S.J., Fiorentini M.L. 2012. Komatiite magmas and sulfide nickel deposits: A comparison of variably endowed archean terranes. Economic Geology, **107**:755–780.

Barnes S.J., Godel B., Gürer D., Brenan J.M., Robertson J., Paterson D. 2013. Sulfide-olivine fe-ni exchange and the origin of anomalously ni rich magmatic sulfides. Economic Geology, **108**:1971–1982.

Barnes S.J., Cruden A.R., Arndt N., Saumur B.M. 2016. The mineral system approach applied to magmatic Ni–Cu–PGE sulphide deposits. Ore Geology Reviews, **76**:296–316.

Barnes S.J., Holwell D.A., Le Vaillant M. 2017. Magmatic sulfide ore deposits. Elements, **13**:89–95.

Barnes S.J., Yao Z. Sen, Mao Y.J., Jesus A.P., Yang S., Taranovic V., Maier W.D. 2023. Nickel in olivine as an exploration indicator for magmatic Ni-Cu sulfide deposits: A data review and re-evaluation. American Mineralogist, **108**:1–17.

Bavinton O.A. 1981. The nature of sulfidic metasediments at Kambalda and their broad relationships with associated ultramafic rocks and nickel ores. Economic Geology, **76**:1606–1628.

Begg G.R.C.B., Ronsky J.O.N.A.M.H., Rndt N.I.T.A., Riffin W.I.L.G. 2010. The Craton Margin Model: A Brief History and Description. 1057–1070.

Bleeker W., Macek J. 1996. Evolution of the Thompson nickel belt, Manitoba: Setting of Ni-Cu deposits in the western part of the Circum Superior boundary zone. Joint Annual Meeting, Winnipeg, Manitoba, .

Borges C.C.A., Toledo C.L.B., Silva A.M., Chemale F., Jost H., Lana C. de C. 2017. Geochemistry and isotopic signatures of metavolcanic and metaplutonic rocks of the Faina and Serra de Santa Rita greenstone belts, Central Brazil: Evidences for a Mesoarchean intraoceanic arc. Precambrian Research, **292**:350–377.

Borges C.C.A., Toledo C.L.B., Silva A.M., Kirk J., Ruiz J., Chemale F., Souza

R.G., Santos B.A., Campos M.P., Campos L.M., Santos A.M. 2021a. Archean to Paleoproterozoic evolution of the Crixás greenstone belt, Central Brazil: Insights from two contrasting assemblies of metaigneous rocks. Lithos, **404**–**405**:106493.

Borges C.C.A., Toledo C.L.B., Silva A.M., Chemale F., dos Santos B.A., Figueiredo F.L., Zacchi É.N.P. 2021b. Unraveling a hidden Rhyacian magmatic arc through provenance of metasedimentary rocks of the Crixás greenstone belt, Central Brazil. Precambrian Research, **353**:.

Brenner T.L. 2006.The Fortaleza De Minas Nickel , Copper and Platinoids Deposit : Ore Types , Tectonics and Volcanological Aspects a Jazida De Níquel , Cobre E Platinóides De Fortaleza De Minas : Aspectos Tectônicos , Vulcanológicos E Tipos De Minérios .: A Universidade Estadual Paulista Júlio de Mesquita Filho.

Brenner T.L., Teixeira N.A., Oliveira J.A.L., Franke N.D., Thompson J.F.H. 1990. The O'Toole nickel deposit, Morro do Ferro greenstone belt, Brazil. Economic Geology, **85**:904–920.

Campbell I.H., Naldrett A.J. 1979. The influence of silicate: sulfide ratios on the geochemistry of magmatic sulfides. Economic Geology, **74**:1503–1506.

Carvalho S.G. de, Brenner T.L. 2010. Depósito de Ni-Cu-Co-Au-EGP de Fortaleza de Minas, Minas Gerais. Modelos de depósitos de cobre do Brasil e sua resposta ao Intemperismo, 216.

Chaudhuri T., Satish-Kumar M., Mazumder R., Biswas S. 2017. Geochemistry and Sm-Nd isotopic characteristics of the Paleoarchean Komatiites from Singhbhum Craton, Eastern India and their implications. Precambrian Research, **298**:385–402.

Chavagnac V. 2004. A geochemical and Nd isotopic study of Barberton komatiites (South Africa): Implication for the Archean mantle. Lithos, **75**:253–281.

Choudhuri A., Iyer S.S., Krouse H.R. 1997. Sulfur isotopes in komatiite-hosted ni-cu sulfide deposits from the morro do ferro greenstone belt, southeastern brazil. International Geology Review, **39**:230–238.

Collins J.E., Barnes S.J., Hagemann S.G., McCuaig T.C., Frost K.M. 2012a. Postmagmatic variability in ore composition and mineralogy in the T4 and T5 ore shoots at the high-grade flying fox Ni-Cu-PGE deposit, Yilgarn Craton, western Australia. Economic Geology, **107**:859–879.

Collins J.E., Hagemann S.G., McCuaig T.C., Frost K.M. 2012b. Structural controls on sulfide mobilization at the high-grade flying fox ni-cu-pge sulfide deposit, Forrestania Greenstone Belt, Western Australia. Economic Geology, **107**:1433–1455.

Cordeiro P.F. de O., Oliveira C.G. de 2017. The Goiás Massif: Implications for a pre-Columbia 2.2–2.0 Ga continent-wide amalgamation cycle in central Brazil. Precambrian Research, **298**:403–420.

Corrêa da Costa P.C., Girardi V.A.V., Teixeira W. 2006. 40Ar/39Ar and Rb/Sr geochronology of the Goiás-Crixás dike swarm, central Brazil: Constraints on the neoarchean-paleoproterozoic tectonic boundary in South America, and Nd-Sr signature of the subcontinental mantle. International Geology Review, **48**:547–560.

Costa JR. C.N., Ferreira Filho C.F., Araujo G.A.O.S.M., Lopes R.O. 1997. Geology and Geochemistry of the Boa Vista Nickel Sulfide Deposit, Crixás Greenstone Belt, Central Brazil. Revista Brasileira de Geociências, **27**:365–376.

Cowden A. 1988. EMPLACEMENT OF KOMATIITE LAVA FLOWS AND ASSOCIATED NICKEL SULFIDES AT KAMBALDA, WESTERN AUSTRALIA. Economic Geology, **83**:436–442.

Cowden A., Donaldson M.J., Naldrett A.J., Campbell I.H. 1986. Platinum-group elements and gold in the komatiite-hosted Fe-Ni-Cu sulfide deposits at Kambalda, Western Australia. Economic Geology, **81**:1226–1235.

Cuadros F.A., Botelho N.F., Fuck R.A., Dantas E.L. 2017. The peraluminous Aurumina Granite Suite in central Brazil: An example of mantle-continental crust interaction in a Paleoproterozoic cordilleran hinterland setting? Precambrian Research, **299**:75–100.

Cui X., Jiang X., Wang J., Wang X., Zhuo J., Deng Q., Liao S., Wu H., Jiang Z.,

Wei Y. 2015. Mid-Neoproterozoic diabase dykes from Xide in the western Yangtze Block, South China: New evidence for continental rifting related to the breakup of Rodinia supercontinent. Precambrian Research, **268**:339–356.

Cunha, J.C., Barbosa, J.S.F., Mascarenhas, J.F. 2012. Greenstone Belts e Sequências Similares. In: Barbosa, J. S. F. (Coordenação Geral), Geologia da Bahia: Pesquisa e atualização (v. 1, 101-199). Salvador: CPBM; UFBA.

Ferreira-Filho C.F., Lesher C.M. 2001. The komatiite-associated Ni-sulfide deposit of Boa Vista, Brazil. 4th International Archean Symposium Extended Abstracts, AGSO Record 2001/37, 429–431.

Ferreira B.F., Marques J.C., Frantz J.C., de Souza R.G., Campos M.P., Figueiredo F.L.A. de R., Padilha N.L. 2021. Stratigraphy and U–Pb detrital zircon provenance, Crixás Greenstone Belt, Goiás-Brasil: Gold-bearing vs barren siliciclastic rocks. Journal of South American Earth Sciences, **105**:.

Filgueiras B. de C., Oliveira C.G. de, Sousa I.M.C. de, Cordeiro P. 2020. Further evidence of Rhyacian arc magmatism in the basement of the Brasília Belt, western São Francisco pericraton. Journal of South American Earth Sciences, **103**:102739.

Fiorentini M., Beresford S., Barley M., Duuring P., Bekker A., Rosengren N., Cas R., Hronsky J. 2012. District to camp controls on the genesis of komatiite-hosted nickel sulfide deposits, agnew-wiluna greenstone belt, western australia: Insights from the multiple sulfur isotopes. Economic Geology, **107**:781–796.

Fortes P. de T.F. de O., Martins Pimentel M., Ventura Santos R., Luiz Junges S. 2003. Sm-Nd studies at Mina III gold deposit, Crixás greenstone belt, central Brazil: Implications for the depositional age of the upper metasedimentary rocks and associated Au mineralization. Journal of South American Earth Sciences, **16**:503–512.

Fuck R.A., Dantas E.L., Pimentel M.M., Botelho N.F., Armstrong R., Laux J.H.,

Junges S.L., Soares J.E., Praxedes I.F. 2014. Paleoproterozoic crust-formation and reworking events in the Tocantins Province, central Brazil: A contribution for Atlantica supercontinent reconstruction. Precambrian Research, **244**:53–74.

Gioia S.M.C.L., Pimentel M.M. 2000. The Sm-Nd isotopic method in the Geochronology Laboratory of the University of Brasília. Anais da Academia Brasileira de Ciencias, **72**:218–245.

Giustina M.E.S.D., de Oliveira C.G., Pimentel M.M., de melo L. V., Fuck R.A., Dantas E.L., Buhn B. 2009. U-Pb and Sm-Nd constraints on the nature of the Campinorte sequence and related Palaeoproterozoic juvenile orthogneisses, Tocantins Province, central Brazil. Geological Society Special Publication, **323**:255–269.

Gole M.J., Barnes S.J. 2020. The association between Ni-Cu-PGE sulfide and Ni-Co lateritic ores and volcanic facies within the komatiites of the 2.7 Ga East Yilgarn Craton Large Igneous Province, Western Australia. Ore Geology Reviews, **116**:103231.

Gruau G., Tourpin S., Fourcade S., Blais S. 1992. Loss of isotopic (Nd, O) and chemical (REE) memory during metamorphism of komatiites: new evidence from eastern Finland. Contributions to Mineralogy and Petrology, **112**:66–82.

Hanski E., Huhma H., Rastas P., Kamenetsky V.S. 2001. The palaeoproterozoic komatiite-picrite association of Finnish lapland. Journal of Petrology, **42**:855–876.

Hasui Y., Carneiro C.D.R., de Almeida F.F.M., Bartorelli A. 2012. Geologia do Brasil- São Paulo: Beca,. 900p. ISBN: 978-85-62768-10-1

Heggie G.J., Fiorentini M.L., Barnes S.J., Barley M.E. 2012. Maggie hays Ni deposit: Part 2. Nickel Mineralization and the Spatial Distribution of PGE Ore-Forming Signatures in the Maggie Hays Ni System, Lake Johnston Greenstone Belt, Western Australia. Economic Geology, **107**:797–816.

Hiebert R.S., Bekker A., Houlé M.G., Wing B.A., Rouxel O.J. 2016. Tracing sources of crustal contamination using multiple S and Fe isotopes in the

Hart komatiite-associated Ni–Cu–PGE sulfide deposit, Abitibi greenstone belt, Ontario, Canada. Mineralium Deposita, **51**:919–935.

Hill R.E.T. 2001. Komatiite volcanology, volcanological setting and primary geochemical properties of komatiite-associated nickel deposits. Geochemistry: Exploration, Environment, Analysis, **1**:365–381.

Houlé M.G., Lesher C.M., Davis P.C. 2012. Thermomechanical erosion at the Alexo Mine, Abitibi greenstone belt, Ontario: Implications for the genesis of komatiite-associated Ni-Cu-(PGE) mineralization. Mineralium Deposita, **47**:105–128.

Jahn B. ming, Gruau G., Glikson A.Y. 1982. Komatiites of the Onverwacht Group, S. Africa: REE geochemistry, Sm/Nd age and mantle evolution. Contributions to Mineralogy and Petrology, **80**:25–40.

Jochum K.P., Arndt N.T., Hofmann A.W. 1991. Nb-Th-La in komatiites and basalts: constraints on komatiite petrogenesis and mantle evolution. Earth and Planetary Science Letters, **107**:272–289.

Jost H., De Oliveira A.M. 1991. Stratigraphy of the greenstone belts, Crixás region, Goiás, central Brazil. Journal of South American Earth Sciences, **4**:201–214.

Jost H., Chemale F., Dussin I.A., Tassinari C.C.G., Martins R. 2010. A U-Pb zircon Paleoproterozoic age for the metasedimentary host rocks and gold mineralization of the Crixás greenstone belt, Goiás, Central Brazil. Ore Geology Reviews, **37**:127–139.

Jost H., Junior F.C., Fuck R.A., Dussin I.A.Ô. 2013. Uvá Complex, The Oldest Orthogneisses Of The Archean-Paleoproterozoic Terrane Of Central Brazil. Journal of South American Earth Sciences, **47**:201–212.

Jost H., Hofmann Apollo J.F., Weber W., Salles R. dos R., Marques J.C., Massucatto A.J., Costa D.A., Araújo dos Santos B. 2019. Stratigraphic update, paleotectonic, paleogeographic, and depositional environments of the Crixás Greenstone Belt, Central Brazil. Journal of South American Earth Sciences, **96**:102329.

Keays R.R., Lightfoot P.C. 2010a. Crustal sulfur is required to form magmatic Ni-Cu sulfide deposits: Evidence from chalcophile element signatures of Siberian and Deccan Trap basalts. Mineralium Deposita, **45**:241–257.

Keays R.R., Lightfoot P.C. 2010b. Crustal sulfur is required to form magmatic Ni-Cu sulfide deposits: Evidence from chalcophile element signatures of Siberian and Deccan Trap basalts. Mineralium Deposita, **45**:241–257.

Ketris M.P., Yudovich Y.E. 2009. Estimations of Clarkes for Carbonaceous biolithes: World averages for trace element contents in black shales and coals. International Journal of Coal Geology, **78**:135–148.

Kuyumjian R.M., Jost H. 2006. Low- and high-alumina komatiites of Goiás, Central Brazil. Journal of South American Earth Sciences, **20**:315–326.

Le Vaillant M., Fiorentini M.L., Barnes S.J. 2016. Review of lithogeochemical exploration tools for komatiite-hosted Ni-Cu-(PGE) deposits. Journal of Geochemical Exploration, **168**:1–19.

Leal V.L.S, Kuchenbecker M., Barbuena D., Queiroga G., Pinheiro M.A.P., Freimann M.A. 2021. Geochemistry and U–Pb zircon ages of the metamafic-ultramafic rocks of the Riacho dos Machados metavolcanosedimentary sequence: Evidence of a late Rhyacian back-arc basin during the assembly of São Francisco-Congo paleocontinent, Journal of South American Earth Sciences, Volume 105, 102972, ISSN 0895-9811, doi: https://doi.org/10.1016/j.jsames.2020.102972.

Lesher C.M. 2017a. Roles of xenomelts, xenoliths, xenocrysts, xenovolatiles, residues, and skarns in the genesis, transport, and localization of magmatic Fe-Ni-Cu-PGE sulfides and chromite. Ore Geology Reviews, **90**:465–484.

Lesher C.M. 2017b. Roles of xenomelts, xenoliths, xenocrysts, xenovolatiles, residues, and skarns in the genesis, transport, and localization of magmatic Fe-Ni-Cu-PGE sulfides and chromite. Ore Geology Reviews, **90**:465–484.

Lesher C.M. 2019. Up, down, or sideways: Emplacement of magmatic Fe–Ni–Cu–PGE sulfide melts in large igneous provinces. Canadian Journal of

Earth Sciences, **56**:756–773.

Lesher C.M., Arndt N.T. 1995. REE and Nd isotope geochemistry, petrogenesis and volcanic evolution of contaminated komatiites at Kambalda, Western Australia. Lithos, **34**:127–157.

Lesher C.M., Burnham O.M. 2001a. Multicomponent elemental and isotopic mixing in Ni-Cu-(PGE) ores at Kambalda, Western Australia. Canadian Mineralogist, **39**:421–446.

Lesher C.M., Burnham O.M. 2001b. MULTICOMPONENT ELEMENTAL AND ISOTOPIC MIXING IN Ni – Cu –(PGE) ORES AT KAMBALDA , WESTERN AUSTRALIA. The Canadian Mineralogist, **39**:421–446.

Lesher C.M., Campbell I.H. 1993. Geochemical and fluid dynamic modeling of compositional variations in Archean komatiite-hosted nickel sulfide ores in Western Australia. Economic Geology, **88**:804–816.

Lesher C.M., Keays R.R. 2002. Komatiite-associated Ni-Cu-PGE Deposits: Geology, Mineralogy, Geochemistry, and Genesis. The Geology, Geochemistry, Mineralogy and Mineral Beneficiation of PGE, .

Lesher C.M., Burnham O.M., Keays R.R., Barnes S.J., Hulbert L. 2001. Trace-element geochemistry and petrogenesis of barren and ore-associated komatiites. Canadian Mineralogist, **39**:673–696.

Li C., Ripley E.M. 2005. Empirical equations to predict the sulfur content of mafic magmas at sulfide saturation and applications to magmatic sulfide deposits. Mineralium Deposita, **40**:218–230.

Li C., Ripley E.M. 2009. Sulfur contents at sulfide-liquid or anhydrite saturation in silicate melts:Empirical equations and example applications. Economic Geology, **104**:405–412.

Lightfoot P.C., Keays R.R., Evans-Lamswood D., Wheeler R. 2012. S saturation history of Nain Plutonic Suite mafic intrusions: Origin of the Voisey's Bay Ni-Cu-Co sulfide deposit, Labrador, Canada. Mineralium Deposita, **47**:23–50.

Lima F.G. 2017.Morro do Níquel: Fragmento de manto exumado na faixa Brasília

Meridional: UNIVERSIDADE ESTADUAL PAULISTA - Julio de Mesquita Filho: 127 p.

Lima F.G., Faria Júnior I.R., Zanardo A., Szabó G.A.J., Montibeller C.C. 2021. Caracterização textural e mineralógica das rochas do Morro do Níquel (MG) e correlações com o processo de serpentinização. Geociencias, 567–581.

Lopes, G.A.C.; Garrido, I.A.A.; Oliveira, N.S. 2002 Projeto Guajeru: texto. Salvador: CBPM. 2 v

Luolavirta K. 2018. Magmatic evolution of the Kevitsa igneous complex, northern Finland, and its relation to the associated Ni-Cu-(PGE) mineralization. 68 p.

Lyubetskaya T., Korenaga J. 2007. Chemical composition of Earth's primitive mantle and its variance: 1. Method and results. Journal of Geophysical Research: Solid Earth, **112**:1–21.

Magee C., Muirhead J.D., Karvelas A., Holford S.P., Jackson C.A.L., Bastow I.D., Schofield N., Stevenson C.T.E., McLean C., McCarthy W., Shtukert O. 2016. Lateral magma flow in mafic sill complexes. Geosphere, **12**:809–841.

Martins-Ferreira M.A.C., Dias A.N.C., Chemale F., Campos J.E.G., Seraine M., Novais-Rodrigues E. 2020. Multi-stage crustal accretion by magmatic flare-up and quiescence intervals in the western margin of the São Francisco Craton: U-Pb-Hf and geochemical constraints from the Almas Terrane. Gondwana Research, **85**:32–54.

McDonough W.F., Sun S. s. 1995. The composition of the Earth. Chemical Geology, **120**:223–253.

Menezes Leal A.B.M., Santos A.L.D., Leal L.R.B., Cunha J.C. 2015. Geochemistry of contaminated komatiites from the Umburanas greenstone belt, Bahia State, Brazil, Journal of South American Earth Sciences, Volume 61, Pages 1-13, ISSN 0895-9811, doi: https://doi.org/10.1016/j.jsames.2015.03.006.

Mole D.R., Fiorentini M.L., Thebaud N., Cassidy K.F., Campbell McCuaig T., Kirkland C.L., Romano S.S., Doublier M.P., Belousova E.A., Barnes S.J., Miller J. 2014. Archean komatiite volcanism controlled by the evolution of early continents. Proceedings of the National Academy of Sciences of the United States of America, **111**:10083–10088.

Monster J., Appel P.W.U., Thode H.G., Schidlowski M., Carmichael C.M., Bridgwater D. 1979. Sulfur isotope studies in early Archaean sediments from Isua, West Greenland: Implications for the antiquity of bacterial sulfate reduction. Geochimica et Cosmochimica Acta, **43**:405–413.

Naldrett A.J. 1999. World-class Ni-Cu-PGE deposits: Key factors in their genesis. Mineralium Deposita, **34**:227–240.

Naldrett A.J. 2004a. Komatiite-Related Deposits. Magmatic Sulfide Deposits, 67–136.

Naldrett A.J. 2004b. Magmatic Sulfide Deposits. Geology, geochemistry and exploration. 730 p.

Nesbitt R.W., Sun S.-S., Purvis A.C. 1979. Komatiites: Geochemistry and genesis. Canadian Mineralogist, **17**:165–186.

Oliveira E.P., McNaughton N.J., Zincone S.A., Talavera C. 2020. Birthplace of the São Francisco Craton, Brazil: Evidence from 3.60 to 3.64 Ga Gneisses of the Mairi Gneiss Complex. Terra Nova, **32**:281–289.

Pearce J.A. 2008. Geochemical fingerprinting of oceanic basalts with applications to ophiolite classification and the search for Archean oceanic crust. Lithos, **100**:14–48.

Perring C.S., Barnes S.J., Hill R.E.T. 1995. The physical volcanology of Archaean komatiite sequences from Forrestania, Southern Cross Province, Western Australia. LITHOS, **34**:189–207.

Perring C.S., Barnes S.J., Hill R.E.T. 1996. Geochemistry of komatiites from Forrestania, Southern Cross Province, Western Australia: Evidence for crustal contamination. Lithos, **37**:181–197.

Pimentel M.M. 2016. The tectonic evolution of the Neoproterozoic Brasília Belt,

central Brazil: A geochronological and isotopic approach. Brazilian Journal of Geology, **46**:67–82.

Pimentel M.M., Ferreira Filho C.F. 2002. Idade Sm-Nd de komatiitos do Greestone Belt do Morro do Ferro, Fortaleza de Minas (MG). Revista Brasileira de Geociências, **32**:147–148.

Pinheiro M.A.P., Guice G.L., Reis Magalhães J. 2021. Archean–Ediacaran evolution of the Campos Gerais Domain — a reworked margin of the São Francisco paleocontinent (SE Brazil): Constraints from metamafic–ultramafic rocks. Geoscience Frontiers, 101201.

Queffurus M., Barnes S.J. 2014. Selenium and sulfur concentrations in country rocks from the Duluth complex, Minnesota, USA: Implications for formation of the Cu-Ni-PGE sulfides. Economic Geology, **109**:785–794.

Queffurus M., Barnes S.J. 2015. A review of sulfur to selenium ratios in magmatic nickel-copper and platinum-group element deposits. Ore Geology Reviews, **69**:301–324.

Queiroz C.L., Jost H., da Silva L.C., McNaughton N.J. 2008. U-Pb SHRIMP and Sm-Nd geochronology of granite-gneiss complexes and implications for the evolution of the Central Brazil Archean Terrain. Journal of South American Earth Sciences, **26**:100–124.

Ripley E.M., Li C. 2013. Sulfide saturation in mafic magmas: Is external sulfur required for magmatic Ni-Cu-(PGE) ore genesis? Economic Geology, **108**:45–58.

Robertson J., Ripley E.M., Barnes S.J., Li C. 2015. Sulfur liberation from country rocks and incorporation in mafic magmas. Economic Geology, **110**:1111–1123.

Robin-Popieul C.C.M., Arndt N.T., Chauvel C., Byerly G.R., Sobolev A. V., Wilson A. 2012. A new model for barberton komatiites: Deep critical melting with high melt retention. Journal of Petrology, **53**:2191–2229.

Saboia A.M., de Oliveira C.G., Dantas E.L., Cordeiro P., Scandolara J.E., Rodrigues J.B., de Sousa I.M.C. 2020. The Siderian crust (2.47–2.3 Ga)

of the Goiás Massif and its role as a building block of the São Francisco paleocontinent. Precambrian Research, **350**:105901.

Saboia L.A., Teixeira N.A. 1983. Ultramafic flows of the Crixas greenstone belt, Goias - Brazil. Precambrian Research, **22**:23–40.

Samalens N., Barnes S.-J., Sawyer E.W. 2017. The role of black shales as a source of sulfur and semimetals in magmatic nickel-copper deposits: Example from the Partridge River Intrusion, Duluth Complex, Minnesota, USA. Ore Geology Reviews, **81**:173–187.

Sampaio P.A.B., Corrêa Neto A. V., Brando Soares M., Alves F.E.A., Fabricio-Silva W., Silveira V.D., Gasparotto W. 2022. The record of plume-arc interaction in the Southern São Francisco Craton – Insights from the Pitangui greenstone belt. Journal of South American Earth Sciences, **116**:.

Seat Z., Beresford S.W., Grcuric B.A., Gee M.A.M., Grassineau N. V. 2009. Reevaluation of the role of external sulfur addition in the genesis of Ni-Cu-PGE deposits: Evidence from the nebo-babel Ni-Cu-PGE deposit, west musgrave, Western Australia. Economic Geology, **104**:521–538.

Sharp Z.D. 2017. Principles of Stable Isotope Geochemistry. 385 p.

Siepierski L., Ferreira Filho C.F. 2016. Spinifex-textured komatiites in the south border of the Carajas ridge, Selva Greenstone belt, Carajás Province, Brazil. Journal of South American Earth Sciences, **66**:41–55.

Skrzypek G., Dunn P.J.H. 2020. Absolute isotope ratios defining isotope scales used in isotope ratio mass spectrometers and optical isotope instruments. Rapid Communications in Mass Spectrometry, **34**:1–5.

Smith J.W., Holwell D.A., McDonald I., Boyce A.J. 2016. The application of S isotopes and S/Se ratios in determining ore-forming processes of magmatic Ni-Cu-PGE sulfide deposits: A cautionary case study from the northern Bushveld Complex. Ore Geology Reviews, **73**:148–174.

Soares M., Corrêa Neto A.V., Fabricio-Silva W. 2020. The development of a Meso- to Neoarchean rifting-convergence-collision-collapse cycle over

an ancient thickened protocontinent in the south São Francisco craton, Brazil. Gondwana Research, 77:40–66.

Sossi P.A., Eggins S.M., Nesbitt R.W., Nebel O., Hergt J.M., Campbell I.H., O'Neill H.S.C., Kranendonk M. Van, Rhodri Davies D. 2016. Petrogenesis and geochemistry of Archean Komatiites. Journal of Petrology, **57**:147–184.

Spreafico, R.R., Barbosa J.S.F., Moraes A.M.V., Souza Júnior F.D., 2020. Geology, petrology and U-Pb geochronology of metavolcanic rocks in the Mundo Novo greenstone belt, eastern São Francisco Craton, NE Brazil: considerations about its tectonic setting. Brazilian Jornal Geology, 50 (03).

Sproule R.A., Lesher C.M., Ayer J.A., Thurston P.C., Herzberg C.T. 2002. Spatial and temporal variations in the geochemistry of komatiites and komatiitic basalts in the Abitibi greenstone belt (Precambrian Research (2002) 115 (153-186)). Precambrian Research, **126**:169–172.

Sproule RA, Lesher CM, Ayer JA, Thurston PC 2003. Ontario Geological Survey Open File Report 6073 Geochemistry and Metallogenesis of Komatiitic Rocks in the Abitibi Greenstone Belt, Ontario.

Staude S., Barnes S.J., Le Vaillant M. 2017. Thermomechanical erosion of ore-hosting embayments beneath komatiite lava channels: Textural evidence from Kambalda, Western Australia. Ore Geology Reviews, **90**:446–464.

Staude S., Oelze M., Markl G. 2021. Multi-stage sulfide evolution of the Moran Ni sulfide ore, Kambalda, Western Australia: insights into the dynamics of ore forming processes of komatiite-hosted deposits. Mineralium Deposita, .

Staude, S., Oelze, M. & Markl, G. 2022. Multi-stage sulfide evolution of the Moran Ni sulfide ore, Kambalda, Western Australia: insights into the dynamics of ore forming processes of komatiite-hosted deposits. Miner Deposita 57, 889–909 Doi: https://doi.org/10.1007/s00126-021-01060-5

Staude, S., Martin, L.A., Aleshin, M., et al. (2024).The multiple sulfur isotope

architecture of the Kambalda nickel camp, Western Australia. Miner Deposita 59, 505–518 Doi: https://doi.org/10.1007/s00126-023-01223-6

Stiegler M.T., Cooper M., Byerly G.R., Lowe D.R. 2012. Geochemistry and petrology of komatiites of the Pioneer Ultramafic Complex of the 3.3Ga Weltevreden Formation, Barberton greenstone belt, South Africa. Precambrian Research, **212**–**213**:1–12.

Teixeira N.A., Gaspar J.C., Brenner T.L., Cheney J.T., Marchetto C.M.L. 1987. Geologia e implicações Teotectônicas do Greestone Belt Morro do Ferro (Fortaleza de Minas, MG). Revista Brasileira de Geociências, **17**:209–220.

Törmänen T., Konnunaho J.P., Hanski E., Moilanen M., Heikura P. 2016. The Paleoproterozoic komatiite-hosted PGE mineralization at Lomalampi, Central Lapland Greenstone Belt, northern Finland. Mineralium Deposita, **51**:411–430.

Tourpin S., Gruau G., Blais S., Fourcade S. 1991. Resetting of REE, and Nd and Sr isotopes during carbonitization of a komatiite flow from Finland. Chemical Geology, **90**:15–29.

Turbay C.V.G., Valeriano C. de M., Rossi A., Silva V.G.M. da R. e 2013. Geologia Do Complexo Campos Gerais Ao Sul De Alpinópolis, Sudoeste De Minas Gerais. Geonomos, **16**:79–90.

Verma S.K., Oliveira E.P., Silva P.M., Moreno J.A., Amaral W.S. 2017. Geochemistry of komatiites and basalts from the Rio das Velhas and Pitangui greenstone belts, São Francisco Craton, Brazil: Implications for the origin, evolution, and tectonic setting, Lithos, Volumes 284–285, Pages 560-577, ISSN 0024-4937, doi: https://doi.org/10.1016/j.lithos.2017.04.024.

Vijaya Kumar K., Rathna K., Leelanandam C. 2015. Proterozoic subduction-related and continental rift-zone mafic magmas from the Eastern Ghats Belt, SE India: Geochemical characteristics and mantle sources. Current Science, **108**:184–197.

Waterton P., Arndt N. 2023. Komatiites: their geochemistry and origins. The Archaean Earth: Tempos and Events (2nd Edition of The Precambrian Earth)., .

Waterton P., Mungall J., Pearson D.G. 2021. The komatiite-mantle platinum-group element paradox. Geochimica et Cosmochimica Acta, **313**:214–242.

Wilson A.H. 2003. A new class of silica enriched, highly depleted komatiites in the southern Kaapvaal Craton, South Africa. Precambrian Research, **127**:125–141.

Wilson A.H., Shlrey S.B., Carlson R.W. 2003. Archaean ultra-depleted komatiites formed by hydrous melting of cratonic mantle. Nature, **423**:858–861.

De Wit M.J., Ashwal L.D. 1995. Greenstone belts: what are they? Maarten. South African Journal Geology, **98**:505–250.

Yao Z., Mungall J.E. 2021a. Kinetic controls on the sulfide mineralization of komatiite-associated Ni-Cu-(PGE) deposits. Geochimica et Cosmochimica Acta, **305**:185–211.

Yao Z., Mungall J.E., Qin K. 2020. A Preliminary Model for the Migration of Sulfide Droplets in a Magmatic Conduit and the Significance of Volatiles. Journal of Petrology, 1–35.

Yao Z. sen, Mungall J.E. 2021b. Kinetic controls on the sulfide mineralization of komatiite-associated Ni-Cu-(PGE) deposits. Geochimica et Cosmochimica Acta, **305**:185–211.

Zheng Y.-F., Hermann J. 2014. Geochemistry of continental subduction-zone fluids. Earth, Planets and Space, **66**:93.

Zheng Y.F. 2019. Subduction zone geochemistry. Geoscience Frontiers, **10**:1223–1254.

1. CAPÍTULO 1

The komatiite-associated Boa Vista Ni-Cu-(PGE) sulfide deposit, Crixás greenstone belt, Central Brazil: insights into komatiite flow facies and exploration

The komatiite-associated Boa Vista Ni-Cu-(PGE) sulfide deposit, Crixás greenstone belt, Central Brazil: insights into komatiite flow facies and exploration

Tiago F. A. Maia[1,2], Cesar F. Ferreira Filho[1], Saulo B. de Oliveira[3]

[1]Programa de pós-graduação em geologia do Instituto de Geociências, Universidade de Brasília, Brasília-DF, 70910-900, Brazil

[2]Departamento de Geociências, Universidade Federal do Amazonas, 69080-900, Brazil

[3]Instituto de Energia e Ambiente, Universidade de São Paulo, 05508-900, Brazil

Abstract

The Boa Vista Ni-Cu deposit is an uncommon example of Neoarchean mineralization associated with aluminum-depleted komatiite (ADK). New data for the Boa Vista deposit, including geological and petrographic descriptions, as well as geochemical and isotopic results for komatiites and sulfide ore, are integrated into this study to improve the understanding of the processes associated with its origin. Although the deposit and host rocks were affected by tectonism and greenschist to amphibolite facies metamorphism, primary magmatic textures and compositions are variably preserved throughout the greenstone belt. Our results show that the Boa Vista deposit is hosted by an undifferentiated olivine cumulate channelized/conduit flow facies unit overlying flows of basalts and basaltic komatiites interlayered with sulfide-bearing graphite schist. The Boa Vista deposit is a Type I (basal/contact) of the komatiite-associated Ni-Cu-(PGE) deposit that was variably disrupted along shear zones. The main orebody consists predominantly of matrix ore breccia consisting of pentlandite, pyrrhotite, and minor chalcopyrite and has high Zn contents. Lithogeochemistry, AFC model, ore geochemistry, and sulfur isotopic data support crustal contamination of the komatiitic magma by graphite schist. Strongly positive δ34S isotopic values for the Ni-Cu ore, ranging from +16 to +19, are modeled as resulting from contamination of the komatiitic magma with host graphite schist that contains sulfides with δ34S values ranging from +30 to +34. The relatively low grades of the ores are attributable to relatively low metal tenors, consistent with a magma: sulfide ratio (R factor) calculated between 300-400. High Ni-MgO-Zn content can

be a geochemical exploration criteria guide to finding new targets for komatiite-associated Ni-Cu-(PGE) sulfide deposits in central Brazil.

Keywords: Nickel-cooper sulfide, lithogeochemistry, sulfur isotopes

1.1. INTRODUCTION

With increasing demand for Ni-Cu-Co-PGE (platinum-group elements) over the past decade, mainly due to the use of electric batteries in the automotive industry and clean, green, and renewable energy storage, the search for new Ni-Cu-Co-(PGE) sulfide deposits has also grown. The deposits with the highest Ni grades are hosted by Archean komatiites (e.g., Lesher, 1989; Lesher and Keays, 2002; Barnes, 2006; Arndt et al., 2008; Lesher and Barnes, 2009; Barnes and Fiorentini, 2012; Perring, 2015), and most contain recoverable amounts of Cu, Co, PGE.

Komatiites are volcanic/subvolcanic rocks with >18% MgO, <2% Na2O + K2O, and <1% TiO2 that display spinifex texture or are consanguineous with rocks containing olivine spinifex textures (Arndt et al., 2008). Komatiitic basalts are volcanic rocks containing less than 18% MgO that can be linked to komatiites using petrological, textural, or geochemical arguments (Arndt et al., 2008). Komatiites can be subdivided into several compositional types: Al-depleted komatiites (ADK) and Al-undepleted komatiites (AUK), the latter with Ti-depleted (TDK), Ti-undepleted (TUK), and Ti-enriched (TEK) variants (e.g., Nesbitt et al., 1979; Jahn et al., 1982; Hanski, 1992; Sproule et al., 2002; Arndt et al., 2008). Komatiite-associated Ni-Cu sulfide deposits are hosted mainly by AUK (e.g., Kambalda: Lesher, 1989; Thompson: Layton-Matthews et al., 2007) and less commonly by ADK (e.g., Forrestania: Perring et al., 1996; Maggie Hays: Heggie et al., 2012), arguably resulting from AUK being more abundant than ADK.

The currently accepted model for the origin of komatiite-associated Ni-Cu-(PGE) sulfide deposits (e.g., Lesher et al., 1984; Lesher, 1989; Lesher and Keays, 2002; Barnes, 2006; Arndt et al., 2008; Lesher and Barnes, 2009; Fiorentini et al., 2012; Konnunaho et al., 2015; Perring, 2015; Le Vaillant et al., 2016; Gole and Barnes, 2020; Staude et al., 2022) involves the following processes: i) generation of voluminous high-temperature komatiitic magma, generally accepted to be derived from a mantle plume; ii) emplacement as dynamic systems, such as high-flux lava channels, channelized sills or dikes , or chonoliths, iii) thermomechanical erosion of S-bearing crustal rocks , with assimilation of immiscible sulfide xenomelts; iv) concentration and upgrading of Ni-Cu-(PGE) contents of sulfide xenomelts through exchange with the magma;

and v) preservation from erosion and post-magmatic processes.,. Mantle source/residue compositions, depths/pressures of melting, and precise degrees of melting do not appear to affect the genesis of Ni-Cu-(PGE) deposits (e.g., Lesher, 1989; Lesher and Stone, 1996; Sproule et al., 2002; Barnes, 2006; Barnes and Fiorentini, 2012). On the other hand, komatiite flow facies defined by variations in the degree of internal differentiation and olivine accumulation are critical for the genesis and location of Ni-Cu-(PGE) deposits in komatiitic flow fields (Lesher et al., 1984; Lesher, 1989; Lesher and Keays, 2002; Arndt et al., 2008; Lesher and Barnes, 2009; Gole and Barnes, 2020).

The assimilation of S from host rocks is a critical feature for the origin of magmatic Ni-Cu-(PGE) deposits (Lesher, 1989; Barnes, 2006; Li and Ripley, 2009; Keays and Lightfoot, 2010; Lightfoot et al., 2012; Ripley and Li, 2013; Robertson et al., 2015; Le Vaillant et al., 2016; Lesher, 2017). In many komatiite-associated deposits, physical evidence for the incorporation of S from the local country rocks is matched with distinctive S isotope and S/Se ratio signatures, thus providing compelling evidence for the addition of external S (Lesher and Groves, 1986; Lesher and Burnham, 2001; Lesher 2017). The highly S-undersaturated nature of komatiitic magmas requires an input of external sulfur to generate economic Ni-Cu-(PGE) sulfide orebodies, being the most efficient and direct process leading to S saturation (e.g., Lesher and Burnham, 2001; Keays and Lightfoot, 2010; Ripley and Li, 2013). Sulfur assimilation from country rocks into mafic-ultramafic magmas can be accomplished by several different processes , all of them dependent on the sulfide saturation state of the magma and the amount of S in the country rocks: (i) complete dissolution of all available S, which can occur when the magma is sufficiently hot and unsaturated in sulfide (ii) devolatilization of country rocks, with or without other volatiles and low-melting components, which usually partially extracts the S from country rocks, and (iii) partial melting of country rocks forming xenomelt bubbles that coexist with the magma without being dissolved in it. Several studies support that partial melting of country rocks is the fastest and most efficient process for adding crustal S to mantellic magmas (e.g., Robertson et al. 2015; Lesher 2017; Virtanen et al. 2021 and 2024).

The Boa Vista deposit is located within the 2.7-2.9 Ga Crixás greenstone belt in Brazil. The nickel-copper sulfide mineralization occurs within interlayered mafic and ultramafic metavolcanic rocks with minor interflow metasediments. It is an example of Ni-Cu sulfide mineralization associated with aluminum-depleted komatiite (ADK) (Costa JR et al., 1997; Ferreira Filho and Lesher, 2001). Although previous studies provided a preliminary description of the Boa Vista deposit, including the characterization of the associated komatiites as ADK (Costa JR et al., 1997; Ferreira Filho and Lesher, 2001), a robust geological and petrological characterization of the Ni-Cu-(PGE) ore and associated komatiites has not yet been published. Particularly lacking are detailed lithogeochemical and sulfur isotopic data for the ores and komatiites. These data provide information about the ore-forming processes and volcanological features of the komatiitic flows, critical for interpreting the physical processes leading to sulfide segregation and deposition.

This paper combines new and previously published geological, volcanological, petrographic, whole-rock geochemical, and S isotopic data for komatiites and associated rocks from the Boa Vista deposit region, and an unmineralized segment of the Crixás greenstone belt. The compiled geochemical database, including Te, As, Bi and Sb, (TABS) and PGE, allowed us to improve geological and genetic models for the Boa Vista deposit and provide additional criteria for regional exploration of Ni-Cu-(PGE) sulfide deposits.

1.2. OVERVIEW OF THE GOIÁS MASSIF AND CRIXÁS GREENSTONE BELT GEOLOGY

The Boa Vista deposit is associated with komatiites of the Crixás greenstone belt in the Crixás-Goiás domain of the Goiás Massifin central Brazil (e.g., Costa Jr et al., 1997; Borges et al., 2021a.) The Goiás Massif comprises a complex collage of distinct Archean and Paleoproterozoic terranes amalgamated by successive orogenic and accretional cycles (Cordeiro and Oliveira, 2017). During the Archean-Paleoproterozoic the massif made up the western boundary of the São Francisco-Congo paleocontinent (Pimentel, 2016; Filgueiras et al., 2020; Sabóia et al., 2020). The Goiás Massif was subdivided by Cordeiro and Oliveira (2017) into four tectonic domains (**Fig. 2**): i) the Almas-Conceição do

Tocantins Domain, (e.g., Fuck et al. 2014; Martins-Ferreira et al., 2020); ii) the Cavalcante-Arraias Domain, (e.g., Cuadros et al., 2017); iii) the Campinorte Domain, (e.g., Giustina et al., 2009); and iv) the Crixás-Goiás Domain, the oldest crustal fragment of the Goiás Massif, which comprises an association of Archean TTG and Archean-Paleoproterozoic greenstone belts (e.g., Borges et al., 2021a).

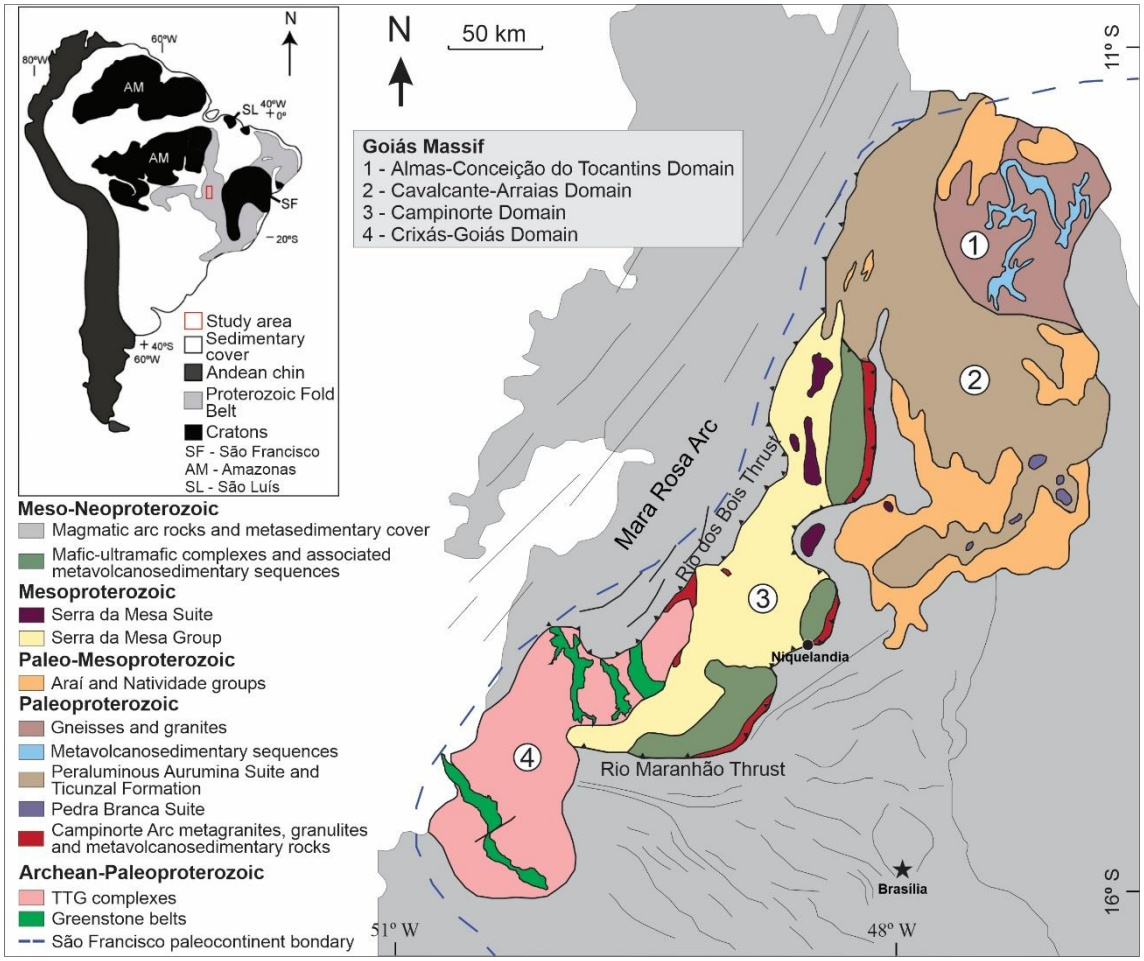

Figure 2 Regional geology of the Goiás Massif. The insert indicates the location of the Goiás Massif within the South American tectonic framework. (modified from Cordeiro and Oliveira, 2017).

The Crixás-Goiás Domain comprises five Archean-Paleoproterozoic (2.9-2.1 Ga) (Borges et al., 2017, 2020a and 2020b) greenstone belts (Crixás, Guarinos, Pilar de Goiás, Faina, and Serra de Santa Rita) and six Archean TTG complexes (Hidrolina, Moquém, Caiamar, Anta, Caiçara, and Uvá complexes) (**Fig. 3A**). The TTG complexes include polycyclic phases of magmatic pulses. (3.1–2.7 Ga) (Jost et al., 2013). The greenstone belts occur as synformal keels surrounded by TTG complexes (e.g., Queiroz et al., 2008). The basal sequences of these greenstone belts consist predominantly of metavolcanic rocks, which

are overlain by a sequence of predominantly metasedimentary rocks (e.g., Queiroz et al., 2008).

The Crixás greenstone belt (**Fig 3B and C**) is a 30 km long NW-trending volcanic-sedimentary sequence metamorphosed to greenschist to lower amphibolite facies. It is bordered by the Meso-Neoarchean Anta and Caiamar TTG complexes, except to the north, where rocks of the Neoproterozoic Mara Rosa Magmatic Arc overthrust the older units. The geology, stratigraphy, geochronology and tectonic setting of the Crixás greenstone belt are described and discussed in several previous studies (e.g., Jost and Oliveira, 1991; Jost et al., 2019; Borges et al., 2021a; and references therein), and just a brief overview is presented in here.

The lower unit of the Crixás greenstone belt (Córrego Alagadinho Formation in **Fig. 3B-C**) consists of of metamorphosed ultramafic rocks (e.g., serpentinite, talc-tremolite-serpentine schist) and minor metachert, and metamorphosed banded iron formations. The ultramafic rocks have primary volcanic structures and textures locally preserved, including spinifex textured flows (e.g., Sabóia and Teixeira 1983). The lower unit is overlain by metabasalts (e.g., greenschist, amphibolite) of the Rio Vermelho Formation (**Fig. 3C**). Primary magmatic features, including pillow lavas and phenocrysts, are locally preserved. Interlayered komatiitic and basaltic volcanic rocks occur in the northwestern portion of the belt (Costa Jr. et al., 1997), indicating a gradational upward transition from ultramafic to mafic volcanic rocks. The upper unit (Ribeirão das Antas Formation) consists of graphite schist and dolomite lenses (**Fig 3B-C**), overlain by rhythmically graded-bedded metagraywackes associated with minor meta-andesite lenses and metadiorite bodies (Ribeirão Córrego Geral Formation in **Fig. 3C**). The Mina Inglesa Sequence, located in the northern portion of the greenstone belt (**Fig. 3C**), is interpreted as an allochthonous unit consisting mainly of ultramafic metavolcanics (e.g., serpentinite and talc-chlorite schist).

The greenstone belt sequence underwent several deformational events, resulting in a complex structural framework (e.g., Jost et al., 2019, and references therein). The age of the lower mafic-ultramafic units is poorly constrained, with

available results suggest an Archean (ca. 2.7-2.9 Ga) age for the komatiitic magmatism (Arndt et al., 1989; Fortes et al., 2003).

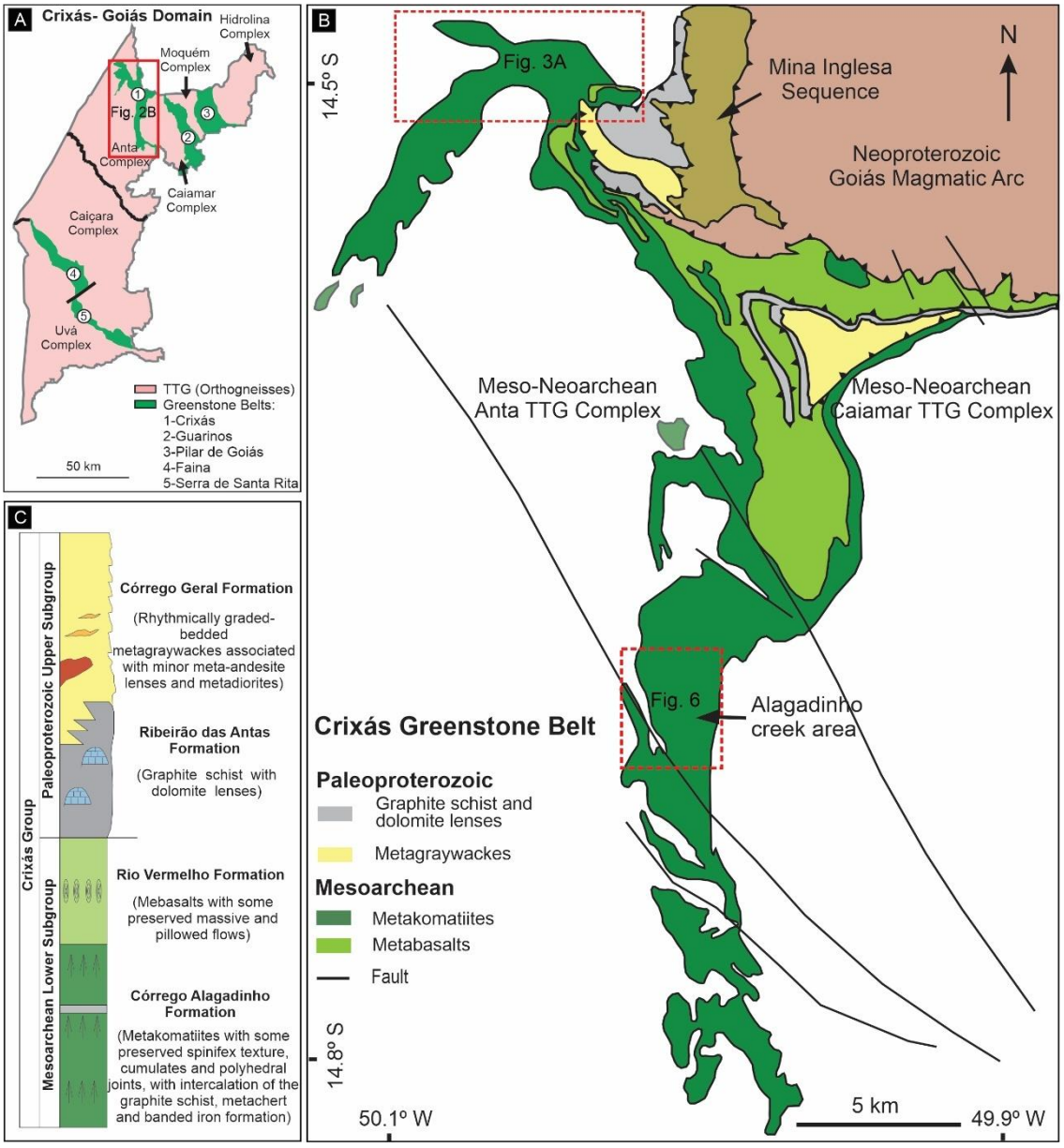

Figure 3 Geological features of the Crixás greenstone belt. (A) Main components of the Goiás-Crixás domain (modified from Jost et al., 2010). (B) Geological map of the Crixás greenstone belt (modified from Jost et al., 2019). Dashed rectangles indicate the location of Figures 3A and 6. (C) Schematic stratigraphic column of the Crixás greenstone belt (modified from Jost et al., 2019; Borges et al., 2021a).

1.3. GEOLOGY OF THE BOA VISTA DEPOSIT

The geology of the Boa Vista (BV) deposit area is described in detail by Costa JR et al. (1997), and only a brief updated overview is presented here. The E-W-trending sequence of metakomatiites and metabasalts are surrounded by poorly exposed tonalitic gneiss of the TTG Complex (Fig. 4A). Metakomatiites are

mainly massive serpentinite and ultramafic schists, the latter consisting of variable proportions of talc + chlorite, + serpentine, tremolite and magnetite. The mafic rocks are greenschists composed of actinolite + albite + chlorite with accessory epidote, quartz, biotite, titanite, and magnetite. Minor interlayered metasedimentary rocks consist of 2-3 meters-thick metamorphosed banded iron formation, metachert, and sulfide-bearing (pyrrhotite + chalcopyrite) graphite schist. Interlayered metamorphosed komatiitic and basaltic flows is a common feature of the supracrustal sequence of the Boa Vista area (Costa JR. et al., 1997). The supracrustal rocks underwent several major deformational events (e.g., Jost et al., 2019), including regional tight to isoclinal folds associated with the predominant metamorphic foliation generally parallel to the primary bedding. Geological contacts between the Boa Vista segment with the tonalitic gneiss (TTG Complex) and the metasedimentary unit of the greenstone belt to the east are considered thrust faults (e.g., Jost et al., 2019). A schematic interpretative section of the sequence of volcanic rocks illustrates the close association of ultramafic and mafic volcanic lithologies and interlayered metasedimentary rocks (**Fig. 4B**).

Following the first description of komatiites in the Crixás greenstone belt by Sabóia and Teixeira (1980), several studies investigated their volcanic structures and textures (e.g., Saboia and Teixeira, 1983), their lithogeochemical and isotopic composition (e.g., Arndt et al., 1989; Fortes et al., 2003; Ferreira Filho and Lesher, 2001; Kuyumjian and Jost, 2006; Borges et al., 2021a), and the volcanological and petrological features of the Boa Vista komatiite associated Ni-Cu sulfide deposit (e.g., Costa JR. et al., 1997; Ferreira Filho and Lesher, 2001). These studies indicate that the komatiites in the Crixás greenstone belt belong to the Al-depleted type (ADK) (e.g., Ferreira Filho and Lesher, 2001; Kuyumjian and Jost, 2006) and have Archean ages of ca. 2.7-2.9 Ga (e.g., Arndt et al., 1989; Fortes et al., 2003). Volcanological and chemical features of the Boa Vista Ni-Cu deposit indicate that sulfide mineralization resulted from segregation and concentration of an immiscible sulfide liquid from a channelized komatiitic lava flow within interlayered mafic and ultramafic flows (e.g., Costa JR. et al., 1997; Ferreira Filho and Lesher, 2001). These studies indicate that the Ni-Cu sulfide body occurs at the contact of olivine adcumulates with underlying basaltic

lavas. A geophysical model based on airborne electromagnetic surveys and borehole electromagnetics (VTEM and BHEM) indicates that the sulfide orebody is broadly concordant with the host ultramafic rocks and plunges 60-70° toward 340° (Henrique et al., 2009).

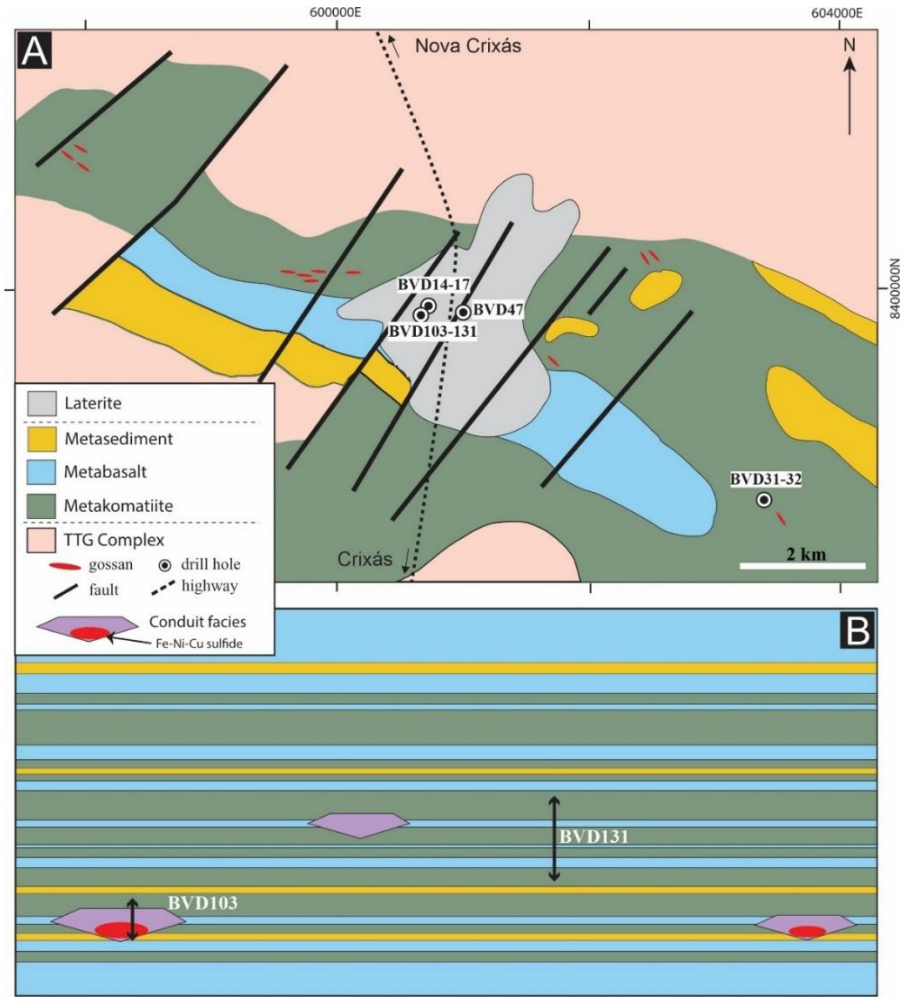

Figure 4(A) Local geology of the Boa Vista deposit area (modified from Costa Jr. et al., 1997). (B) Simplified interpretative schematic section through the volcanic pile of the Boa Vista area. Strip logs of drill cores BVD-131 and BVD-103 illustrate unmineralized and mineralized domains, respectively. To use the 350m of extension of BVB131 as scale in B.

1.4. SAMPLING AND ANALYTICAL METHODS

Fifty-six unmineralized komatiites (22 from the Boa Vista deposit and 34 from the Alagadinho Creek area), six representative Ni-Cu-(PGE) ores from the Boa Vista deposit, and three representative country-rock samples from the Crixás greenstone belt were collected from outcrops and diamond drill cores. Seventeen representative Ni-Cu sulfide ores in the Boa Vista deposit were collected for geochemical analyses of trace elements. Mineralogical, petrographic, and

textural description of these samples were undertaken on polished sections in the Instituto de Geociências at Universidade de Brasília and in the Departamento de Geociências at Universidade Federal do Amazonas.

Whole-rock lithogeochemical analyses were undertaken in the Central Analytical Facility and the Ontario Geoscience Laboratories at the Laurentian University campus in Sudbury, Ontario. Samples were crushed in a low-Cr steel jaw crusher, cleaned with Killarney quartzite, opened, brushed, and vacuumed between samples. Pulverization was done in agate balls. Major elements (Si, Ti, Al, Fe, Mn, Mg, Ca, Na, K, and P) were determined by wavelength dispersive X-ray fluorescence spectrometry (WD-XRFS), transition elements (Sc, Cr, V, Co, Ni, Cu, and Zn) were determined by a combination of WD-XRFS and atomic absorption spectrophotometry, and selected trace elements (Cs, Rb, Sr, Y, Zr, Hf, REE, Nb, Ta, Th, and U) were determined by inductively-coupled plasma mass spectrometry after a HF-$HClO_4$-HCl-HNO digestion. All data have been recalculated to 100% on a volatile-free basis with total Fe as FeO.

Whole-rock lithogeochemical data for drill cores BVD103 (89 samples) and BVD131 (355 samples) and BV ore (6 samples) were carried out at ALS Chemex and provided by Votorantim Metals for this study. After sample preparation at ALS Chemex they follow a sequential digestion with HF-$HClO_4$-HCl-HNO. The residue was dissolved with dilute HCl and was analyzed by inductively coupled plasma-atomic emission spectrometry (ICP-AES).

For isotope analysis of sulfides, polished mounts of 8 samples selected from petrographic studies were prepared and cleaned in an ultrasonic bath. Pyrrhotite, pentlandite, and chalcopyrite crystals from sulfide ore with different textures, and pyrrhotite and chalcopyrite from sulfide-bearing graphitic schist, were selected for isotopic analyses using a petrographic microscope. In situ ^{34}S-32S isotope analyses of pentlandite, chalcopyrite, and pyrrhotite were performed in the Geochronology Laboratory at Universidade de Brasília using a Finnigan Neptune MC-ICP-MS coupled with a New Wave UP 213 laser ablation system, with a beam size of the 100 µm, lasers energy of 53%, at 10 Hz frequency). IAEA-S1 and IAEA-S2 (Coplen and Krouse, 1998; Ding et al., 2001; Qi and Coplen, 2003) were used as external calibration standards and NBS-123 (chalcopyrite)

was used as an internal standard. The results are presented as ‰ $\delta^{34}S$, relative to Vienna Canyon Diablo Troilite with $^{34}S/^{32}S$ V-CDT = 0.044162589 (Skrzypek and Dunn, 2020). Routine precision is ± 0.1 to 0.5 ‰.

1.5. RESULTS

1.5.1. Komatiite volcanogenic facies description

The facies description and interpretation were based on Lesher and Keays (2002 and references therein) and Gole and Barnes (2020), following the widely accepted nomenclature proposed by Lesher and Keays (2002). Notwithstanding the metamorphic and tectonic partial obliteration of primary magmatic features in the Crixás greenstone belt, three distinct facies of komatiite flows have been identified within low-strain zones in the Boa Vista and Alagadinho Creek areas (**Fig. 5**): 1) differentiated non-cumulate (DNC) flows, 2) undifferentiated non-cumulate (UNC) flows, and 3) undifferentiated cumulate (UC) flows. The characterization of the komatiite facies of the Boa Vista area is based upon drill core descriptions and the geological setting presented in previous studies (e.g., Costa JR et. al., 1997). They include three komatiitic facies:

DNC facies in the Boa Vista area consist of thin (< 5 m), differentiated, non-cumulate flows (**Fig. 5**) characterized by (from top to base) fine-grained flow-top breccias, thick (1.0-1.8 m) spinifex-textured zones that grade downwards from fine random olivine spinifex texture to coarse platy olivine spinifex texture, and relatively thin (1.5-2.0 m) olivine cumulate zones. Olivine plates in spinifex-textured rocks are pseudomorphosed into fine-grained aggregates serpentine ± chlorite ± talc ± tremolite, with rims outlined by fine-grained magnetite. The interstitial matrices between Ol plates are replaced by tremolite, chlorite, carbonate, and magnetite, with few pseudomorphosed radiating pyroxene crystals. Euhedral olivine in cumulate zones is pseudomorphosed into fine-grained aggregates of serpentine ± talc ± chlorite ± magnetite, which is enveloped by a matrix of serpentine, talc, tremolite, chlorite, carbonate, and magnetite. Primary chromite in spinifex and cumulate zones has been replaced by magnetite. DNC flows were described only in drill cores of the eastern portion of the Boa Vista area (see BVD31-32 in **Fig. 4**).

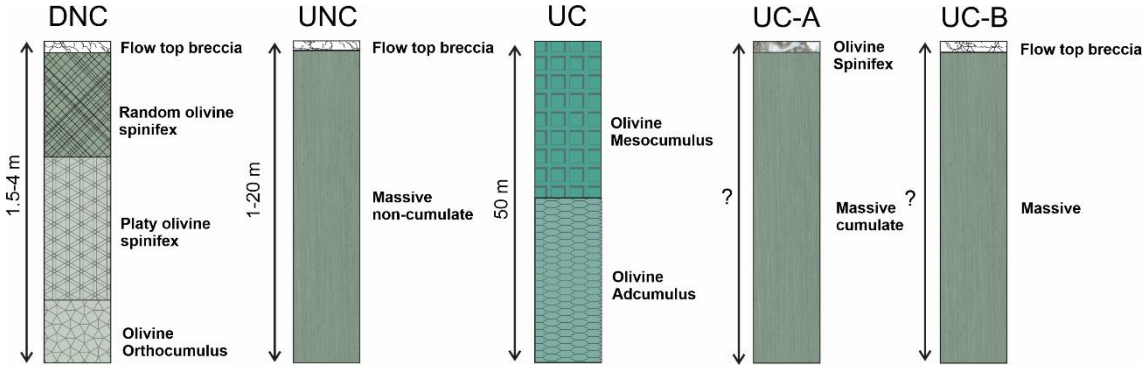

Figure 5 Schematic structures, dimensions, and textures interpreted of komatiite flow in the Boa Vista deposit area (DNC, UNC, and UC) and Alagadinho creek area (DNC, UC-A and UC-B). Komatiite flow facies after Lesher et al. (1984; see also Lesher & Keays; 2002; Arndt et al. 2008): DNC = differentiated non-cumulate flow, UNC = undifferentiated non-cumulate flow, UC = undifferentiated cumulate flow.

UNC facies in the Boa Vista area consist of undifferentiated, non-cumulate flows (**Fig. 5**) with variable thickness (1-20 m). These flows massive flows consist mainly of randomly oriented aggregates of fine- to medium-grained prismatic to acicular tremolite. The rock is a tremolitite with minor amounts of talc - chlorite and carbonate. Except for fine-grained flow-top breccias, observed in drill cores in the western (BVD22) and eastern (BVD31-32) portions of the Boa Vista area, these flows don't have primary magmatic textures preserved. Although they lack evidence of an extrusive origin (e.g., polyhedral jointing: see Arndt et al. 1989), their association with DNC flows suggests that UNC units may also be extrusive.

UC facies in the Boa Vista area consist of up to 50 m thick undifferentiated olivine cumulate flows (**Fig. 5**) without a distincive flow top. kwith. Adcumulate to mesocumulate textures consist of olivine pseudomorphs replaced by serpentine ± magnetite, in a matrix of fine-grained tremolite-talc-serpentine, and minor chlorite and carbonate. UC facies characterize the intercepts closely associated with the Boa Vista Ni-Cu-(PGE) mineralization and interpreted as a lava conduit facies.

The characterization of the komatiite facies of the Alagadinho Creek area is based upon a detailed map of the (ultramafic zone) UZ of the Crixás greenstone belt (see **Fig. 3B and 6**). The mapped area contains the best-preserved komatiites of the Crixás greenstone belt, including the outcrop of thin spinifex-textured flows on the Alagadinho creek described in previous studies. The area was mapped along a 100 m spaced E-W grid established for geophysical

exploration, providing the first flow facies map of komatiites in the Crixás greenstone belt. This map improved the understanding of the komatiitic flows and allowed sampling of different komatiite facies over a larger area (**Fig. 6**). The mapped area consists mainly of metamorphosed ultramafic rocks with variably preserved magmatic textures. Metamafic lithotypes occur as very minor scattered in situ blocks of greenschist or massive fine-grained actinolite-chlorite-plagioclase rocks. Within domains where primary textures are preserved, three different N-S trending komatiitic facies were mapped (**Fig. 6**). The continuity of these facies cannot be followed in areas where ultramafic schists, consisting of variable proportions of serpentine, talc, chlorite, tremolite, and magnetite, occur. Several facing criteria (e.g., flow-top breccias, gradations from fine random spinifex to coarse platy spinifex, contacts between platy spinifex and cumulates) indicate that the sequence is overturned and follows the regional N-S tectonic trend with a moderate dip to the west. Three distinct facies of komatiite flows are present in the Alagadinho Creek area:

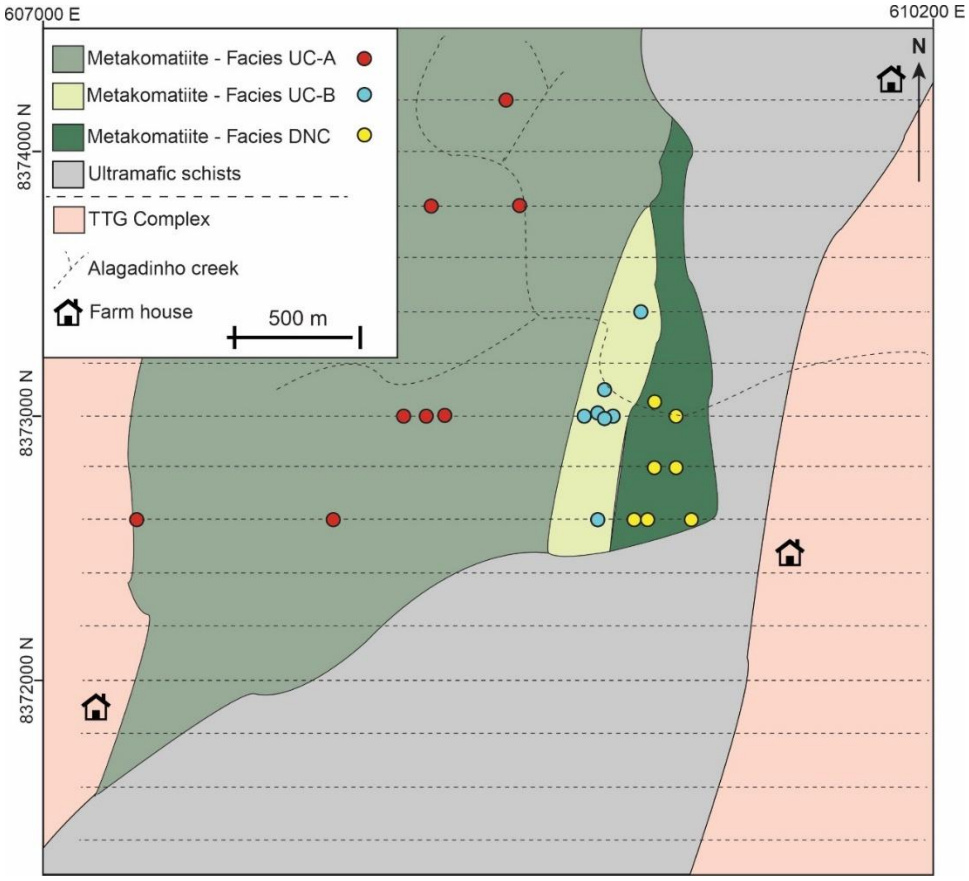

Figure 6 Local geology of the Alagadinho Creek area. Circles indicate the location of samples from different komatiites facies with lithochemical analyses. The coordinator system is the Universal Translate of Mercator (UTM).

DNC facies flows in the Alagadinho Creek area occur in a 1600 m long (N-S) domain in the eastern part of the mapped region (**Fig. 6**). DNC facies consist of thin flows (1-2 m) with a lower cumulate zone that is about the same thickness as the overlying spinifex zone (**Fig. 6 and 7A**). The upper spinifex zone grades downward from thin fine-grained flow top breccias through fine random spinifex to coarse-grained platy spinifex (**Fig. 6**). Primary magmatic textures are well preserved, including relics of skeletal quench Cpx crystals pseudomorphosed to tremolite between olivine blades (**Fig. 7B**), but primary minerals are pervasively altered to fine-grained aggregate of serpentine, tremolite, magnetite, with minor talc and chlorite. The cumulate zones have orthocumulate textures (**Fig. 7C**) characterized by euhedral olivine pseudomorphs replaced for serpentine and magnetite, within a fine-grained matrix consisting of serpentine and tremolite, with minor talc, chlorite, and magnetite.

UC facies flows in the Alagadinho Creek area are subdivided in two subtypes based on distinct internal features (**Fig. 5**). UC-A facies flows are the most abundant in the Alagadinho Creek area (**Fig. 6**), consisting predominantly of thick massive polyhedrally-jointed cumulate komatiite (**Fig. 7D)** with minor spinifex-textured zones. Precise thickness of individual massive flows are difficult to define, but their characteristics suggest interlayered undifferentiated to weakly differentiated sheet flows. The massive domains of the flows consist mainly of pseudomorphs of olivine replaced by fine-grained aggregates of serpentine and minor magnetite, within a fine-grained matrix of serpentine, tremolite, chlorite, magnetite, carbonate, and talc. UC-B facies flows are similar to the UC-A but lacks the upper spinifex-textured zone (**Fig. 5).** Different from the UC-A facies, spinifex texture occurs only as minor veins (up to few cm) crosscutting the massive flow. The thickness of the UC-B flows is also poorly constrained. However, a few thin (< 10 cm) brecciated zones, similar to the flow-top breccias in the Boa Vista deposit area, are interpreted as flow tops.

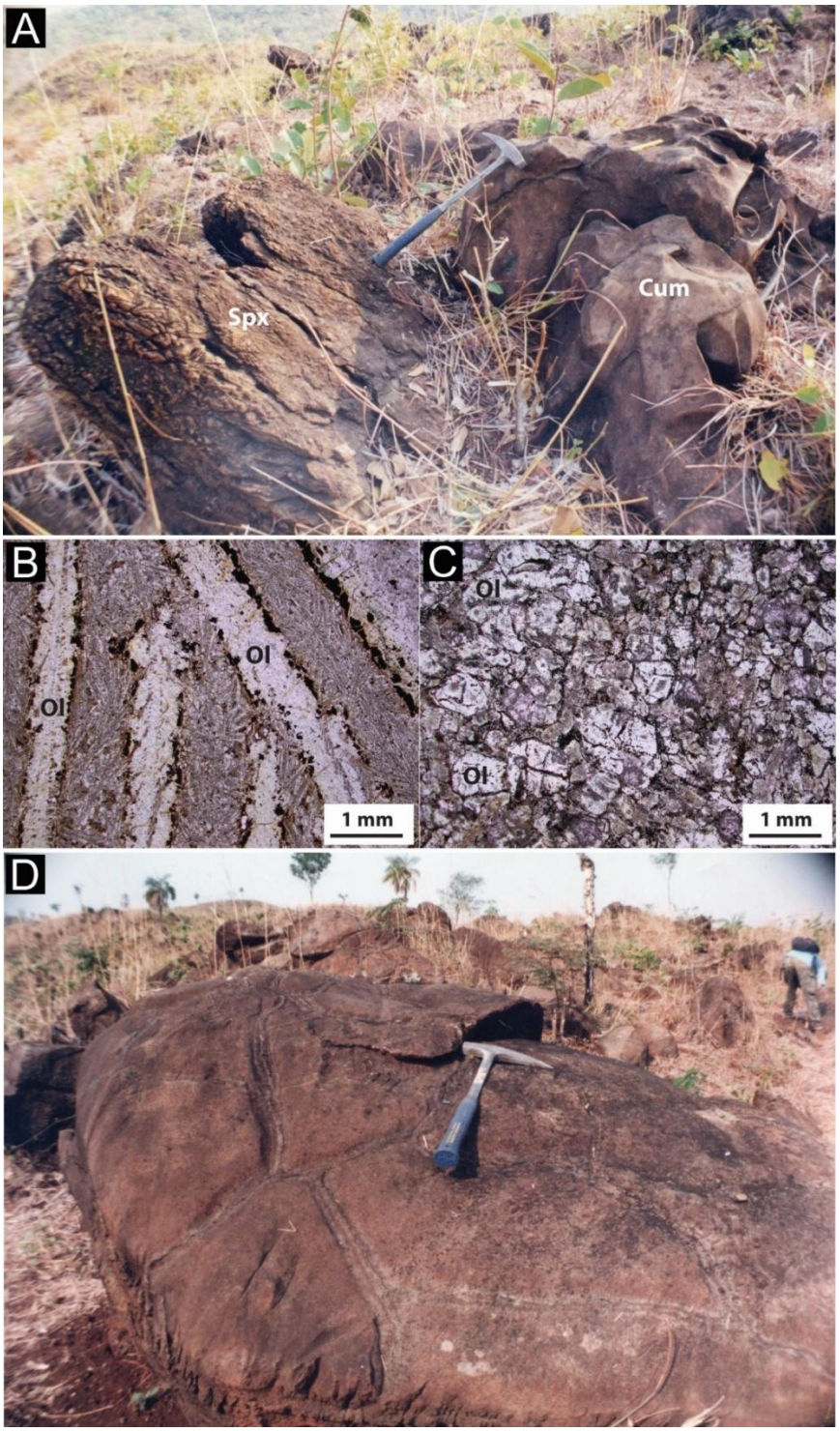

Figure 7: Komatiites in the Alagadinho Creek area. (A). Typical outcrop of thin differentiated, non-cumulate flows (DNC) consisting of a lower massive cumulate zone (Cum) and an upper spinifex-textured zone (Spx). (B) Photomicrograph of platy olivine spinifex texture in DNC facies. Former olivine blades (Ol) have been pseudomorphically replaced by serpentine and magnetite; interstitial quench pyroxene and glass have been replaced by chlorite, tremolite, talc, and magnetite. (C) Photomicrograph of massive mesocumulate texture in DNC facies. Former euhedral-subhedral olivine (Ol) has been pseudomorphically replaced by serpentine and magnetite; the fine-grained interstitial matrix has been replaced by chlorite, tremolite, talc, and magnetite. (D) Boulders of polyhedrally-jointed massive serpentinite in UC-A facies.

1.5.2. **Sulfide Mineralization**

The Boa Vista Ni-Cu deposit has been previously described by Costa JR et al. (1997) and this section has a brief geological and petrographic context for the new geochemical results of this study. The Ni-Cu sulfide mineralization of the Boa Vista deposit occurs within interlayered mafic and ultramafic flows (**Fig. 4B**). A representative drill hole profile intercepting the unmineralized stratigraphic sequence of the Boa Vista area (**Fig. 8A**), shows the complex interlayering of volcanic rocks with variable compositions, including basalt, basaltic komatiites and komatiites. Although the primary volcanic stratigraphic sequence was folded, thrusted, and partially disrupted by later granitic intrusions, interlayering of different types of volcanics is supported by primary structures and textures within low strain zones.

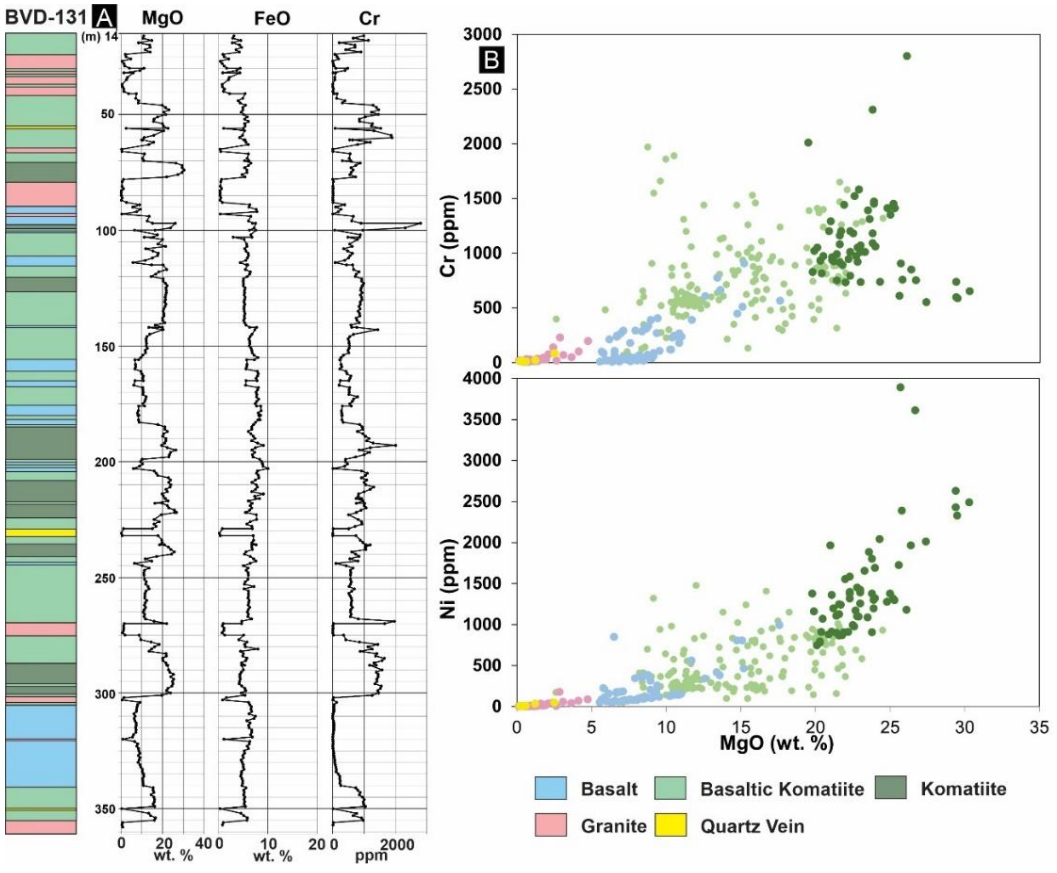

Figure 8 (A) Strip log of drill core BVD-131 through the Boa Vista deposit and MgO, FeO, and Cr geochemical profiles. (B) Binary diagrams of MgO vs. Cr and Ni for all data of the drill core BVD-131. (Data from Votorantim Metals internal reports.)

Therefore, compositional variations throughout drill holes in the Boa Vista area (e.g., MgO, FeO, Cr in **Fig. 8A**) indicate a flow field consisting of successive

flows of variable compositions, as schematically represented in Figure 3B. The plots of MgO vs Cr and MgO vs Ni (**Fig. 8B**) show the expected fractionation trends from basaltic to komatiitic compositions, as indicated by MgO contents ranging from 5 to 30 wt.%. The compositional range in Figure 8A consists of samples with highly variable textures, including komatiites with cumulate textures as well as massive serpentinites and serpentine-talc schists, and should not be interpreted as consisting just of rocks representative of liquid compositions.

The Ni-Cu orebodies of the Boa Vista deposit occur as variably sheared and altered intercepts of massive to disseminated sulfides.The main orebody, intercepted in a extensively drilled region covered by lateritic crust (e.g., BVD14-22 in **Fig. 4A**), is up to 2 m thick and extends for up to 300 m along strike. A minor orebody, located ~12 km southeast of the main one (e.g., BVD31-32 in **Fig. 4A**), is < 1 m thick and up to 10 meters long. Small lenses with Ni-Cu sulfides occur scattered along the komattitic trend of the Boa Vista, commonly closely associated with gossans (**Fig. 4A**).

A representative drill hole profile intercepting the mineralized stratigraphic sequence of the Boa Vista deposit (**Fig. 9**), illustrates the complex distribution of Ni-Cu sulfides within interlayered mafic (basalt and komatiitic basalt) and ultramafic (komatiite) flows. The complex distribution of the orebodies partially results from folding, shearing and partial remobilization of Ni-Cu sulfides. Nevertheless, the common location of the orebodies along contact zones between komatiite and basalts, together with intercepts where semi-massive to matrix ore at the base progressively change upwards to disseminated ore (see Costa JR et al., 1997 for a schematic section and photos of the ore), are consistent with the primary magmatic structure schematically represented in Figure 3B.

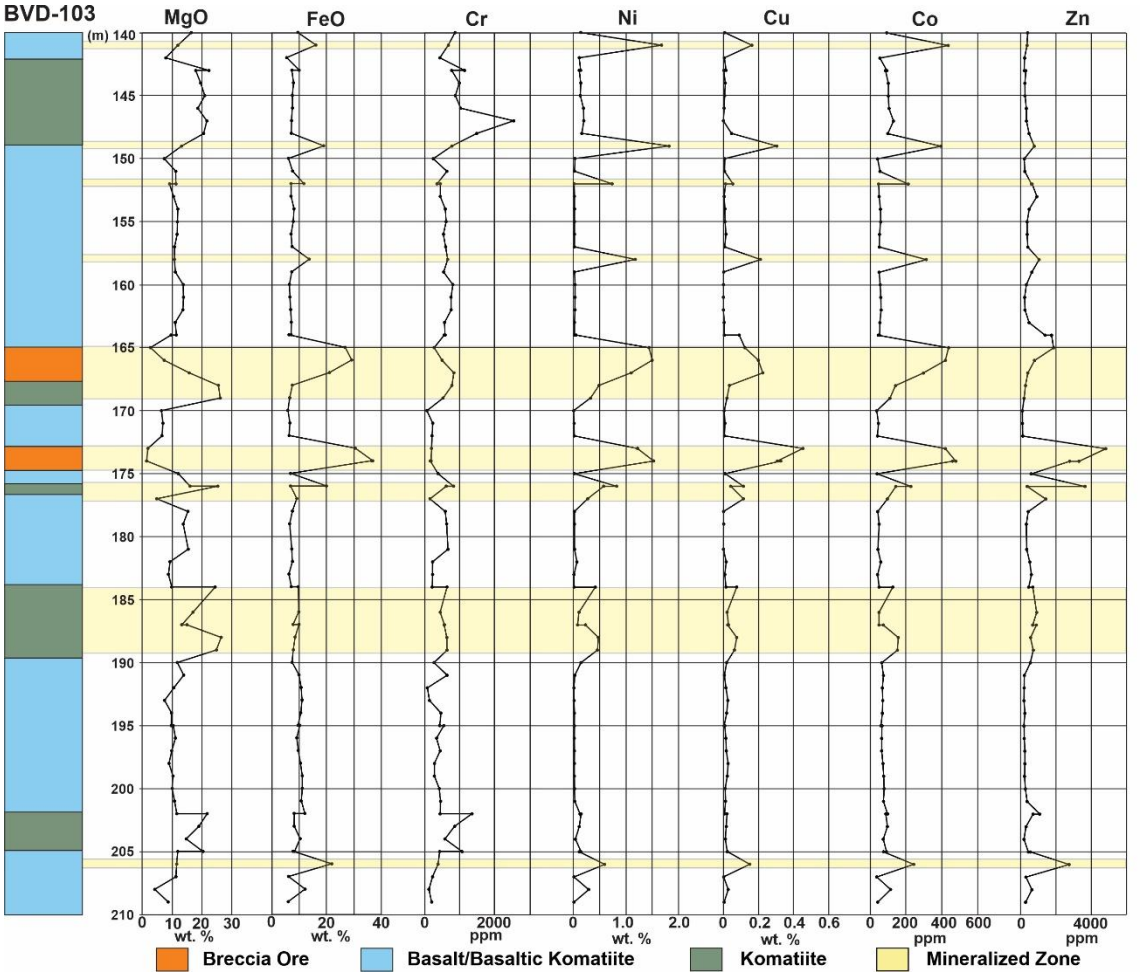

Figure 9 Strip log of drill core BVD-103. and MgO, FeO, Cr, Ni, Cu, Co, and Zn geochemical profiles. See Fig. 4 for the location of drill hole BVD-103. Data from Votorantim Metals internal reports.

Sulfide ore consists predominantly of matrix ore breccia with minor massive to semi-massive ore. Matrix ore breccia (**Fig. 10A-G**) consists of a sulfide-rich groundmass with variable amounts of irregular fragments of serpentinite and talc schist, as well as minor fragments of metasedimentary rocks, including graphite schists and metachert. The modal percent of sulfides in the groundmass is variable but commonly within the 30-65% range. Sulfides consist mainly of pyrrhotite (> 70 vol. %) and pentlandite (**Fig. 10B-E-F),** with minor and highly variable proportions of chalcopyrite (**Fig. 10E**) and sphalerite (**Fig. 10B**). Sulfide-rich rocks within extensively sheared zones have tectonic foliation and consist mainly of pyrrhotite and up to 20% of euhedral pyrite crystals (**Fig. 10D).**

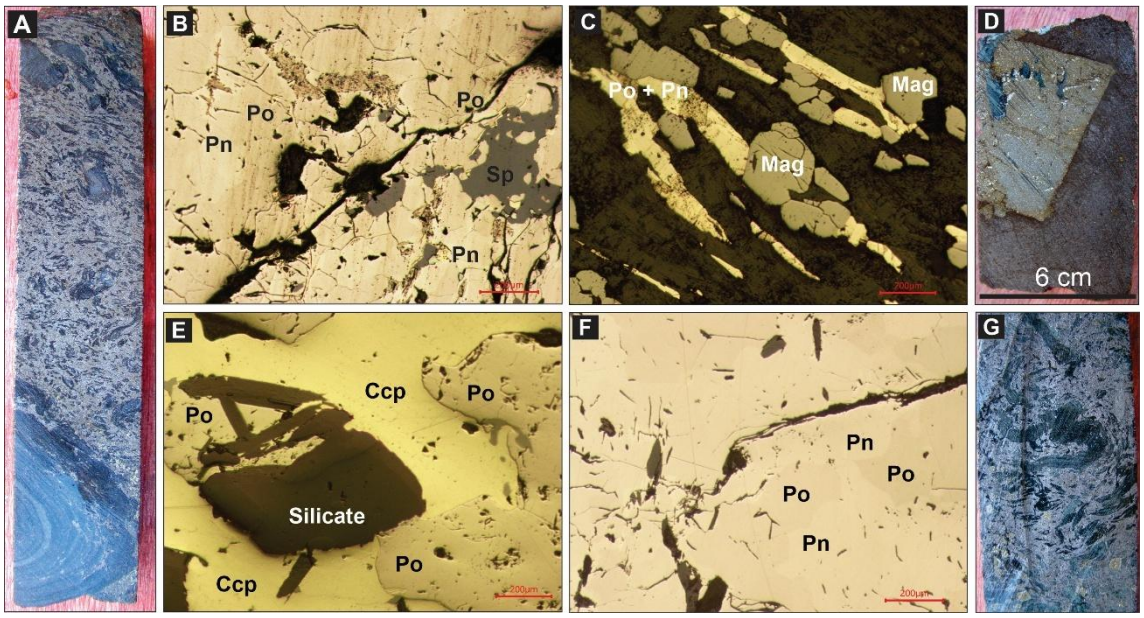

Figure 10 (A, and G) Drill core samples of sulfide matrix ore breccia. Both samples consist of irregular fragments of serpentinite and talc schist within a sulfide-rich groundmass. In A shows a large fragment of folded metasedimentary rock. The core is 4 cm wide. B, E and F) Photomicrographs of sulfide-rich groundmass in matrix ore samples.). Sulfides consist of Po and Pn (B and F) with minor associated Ccp (E) and Sp (B). The scale bar is 200 mm. C) Photomicrograph of foliated stringer disseminated Po-Pn-Mag). D) Core sample of remobilized ore consisting of Po and euhedral Py crystals. Mag – Magnetite, Ccp– Chalcopyrite, Pn – Pentlandite, Po – Pyrrhotite, Py – Pyrite; Sp – Sphalerite.

A plot of Primitive mantle-normalized metals in sulfide matrix ore breccia samples (**Fig. 11**) shows that the ores are enriched in Bi-Se-Sb-Pb-Mo-Cu-Ni-Co-Zn and generally have lower abundances of Au-PGE-Cr. The sulfides are enriched in Cu-Ni-Co relative to Pd-Pt-Rh-Ru-Ir-Os. For some trace elements, the variation is more than ten times each other, such as Se, Pb, Rh, Zn, and Cr.

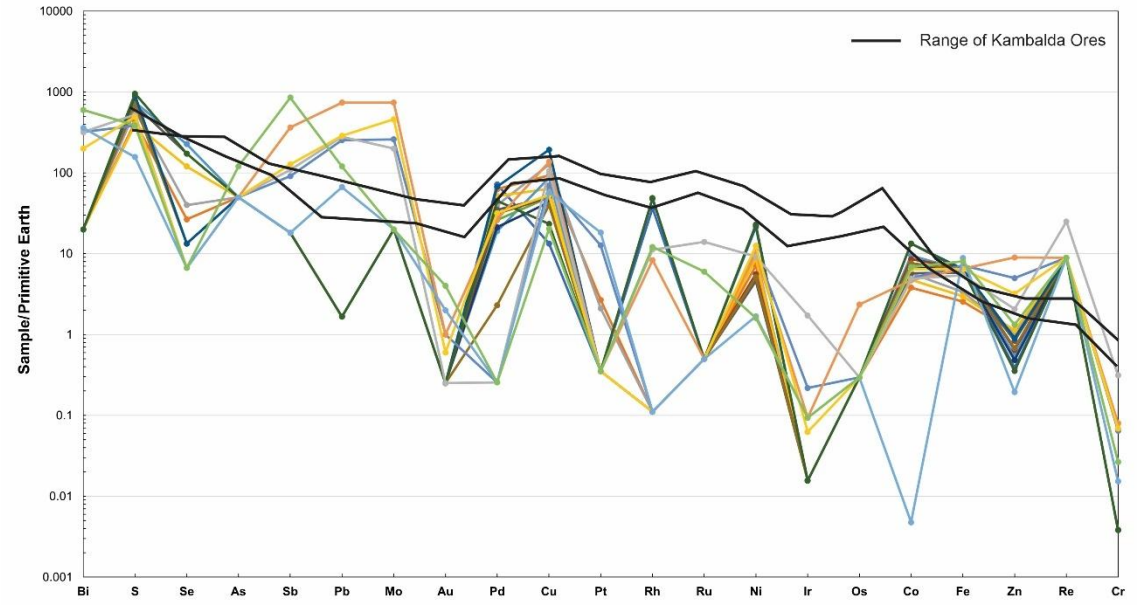

Figura 11 Multi-element diagrams of trace-element composition of primary and secondary base-metal sulfides (whole sample) analyzed by LA- ICP-MS, from matrix breccia ore samples from Boa Vista Ni-Cu-(PGE) sulfide deposit. Primitive Mantle normalization after McDonough and Sun, (1995).

1.5.3. Whole-Rock Geochemistry

The major and trace element compositions of 30 komatiites from the Boa Vista area and 24 from the Alagadinho Creek area are in the supplementary material spreadsheet file. The samples exhibit variable degrees of hydration, carbonation, and sulfidation (imprecisely measured by loss-on-ignition) depending on the degree of alteration and original composition (more for cumulates, less for spinifex). Hence, for comparison and plotting, the compositions of major and minor elements have been normalized to 100% volatile-free. The data from ATW9 and B+21 (Arndt, 1989 and Borges et al., 2021a, respectively) are described and interpreted by DNC and UC-A facies in the Alagadinho Creek area.

Plots of MgO vs selected major elements and minor/trace elements grouped by location and volcanic facies illustrate the main geochemical characteristics of the komatiites (**Fig. 12).** MgO contents vary between 21 and 41 wt.%, with spinifex-textured komatiites ranging up to 35% MgO and cumulate komatiites ranging up to 41% MgO. Most elements exhibit some degree of scatter, but in general, elements that are compatible in olivine (Ni-Co) (increase with increasing Mg content and elements that are incompatible in olivine (Ti-Si-Ca-Cr) decrease with increasing MgO. UC samples are enriched in Al and

depleted in Fe-Ti relative to other samples with similar Mg contents but similar Ca contents. Fe decreases slightly with increasing Mg, with the highest Mg and lowest Fe samples. Spinifex-textured komatiites have higher Si-Ca-Ti and lower Mg-Ni-Co-Cu-Zn than cumulate komatiites. A carbonate-talc schist developed by shearing komatiites from the UC facies has lower Si and higher Fe contents (sample BVD14-118.80 in supplementary material spreadsheet file).

Additional differences between different komatiite facies are evident in mantle-normalized incompatible element patterns (**Fig. 13**). Where UC-A facies komatiites in the Alagadinho Creek area are depleted in Th-LREE > MREE > HREE-Al with variably positive U and Ti anomalies, and negative Nb and Al anomalies (**Fig. 13A**). UC-B and DNC facies komatiites in the Alagadinho Creek area have relatively flat Th-Nb-LREE-MREE profiles, most with variably negative Zr-Hf anomalies, and are depleted in HREE relative to MREE with negative Al anomalies (Fig. **13A-B**).

DNC, UNC, and UC facies komatiites at the Boa Vista area (**Fig. 13C**) have Zr-Hf-REE-Y abundances that are ~1-10 times primitive mantle – lower in olivine cumulates and higher in spinifex-textured rocks. Lu contents in UC facies cumulates are below the lower limit of detection. Several samples of UNC facies exhibit pronounced negative Eu anomalies. Sample (BVD14-118.80) has higher LREE contents than others in UC facies. Some samples exhibit unexpected negative La ± Zr-Hf ± Ti anomalies and unexpected positive Nb-Sm anomalies.

DNC facies samples have negative Nb-Ce-Zr anomalies and positive U-La-Sm anomalies. UC-B facies samples have a substantial range of variation compared with chondrite, highlighting the Th-U-Nb-Zr-Gd. The differences observed between DNC facies between samples are associated with the variation of the composition of rocks, a group more primitive (cumulate texture – black line with quadrate) and others no (spinifex texture - gray line) (Figs. **13B and C**). Half of the samples from DNC facies exhibit negative Ce anomalies. Samples from the UC facies have lower REE contents and La/Yb ratios.

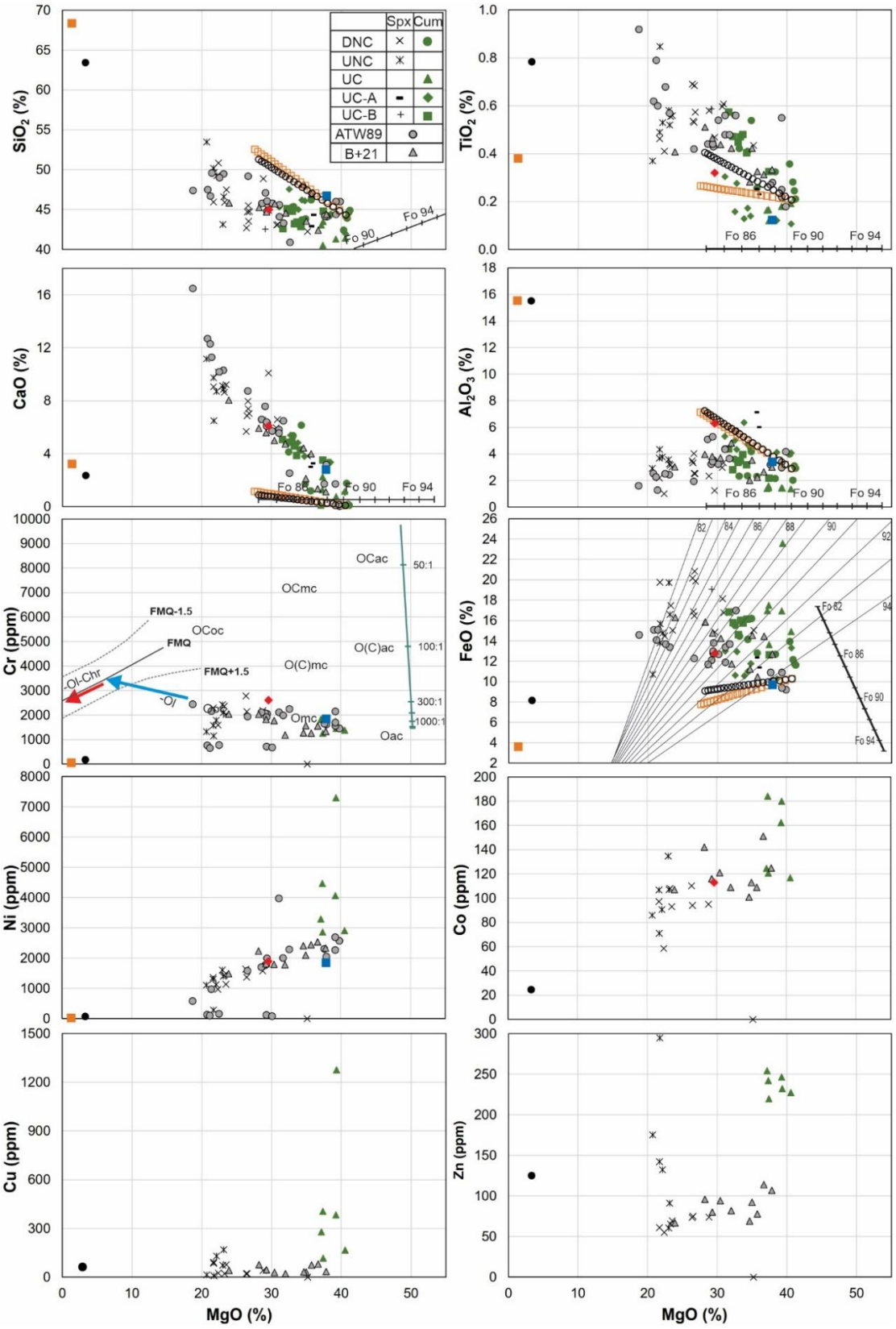

Figure 12 Volatile-free major, minor, and trace element compositional variations of Crixás komatiites (data from Arndt 1989 – gray circle, Borges et al. 2021B – gray triangle, and this study - the other symbols). Also plotted are compositional variations of Archean relict igneous komatiitic olivine (Si-Mg-Fe by stoichiometry, others estimated from data in Lesher, 1989 and Arndt et al., 2008). The field of olivine cumulates, non-cotectic olivine-(chromite) cumulates, and cotectic olivine-chromite cotectic cumulates (Lesher and Stone, 1996; Barnes, 1998), and the chromite

saturation surface at FMQ (Murck and Campbell 1986). O = olivine; C = Chromite; oc = orthocumulate; mc = mesocumulate; ac = adcumulate/ Spx = spinifex; Cum = Cumulate. In the Cr vs MgO diagram, the red line is Chr-saturated liquids, and the blue line is Chr-undersaturated liquids. All information about AFC models is in Table 2. The initial AFC modeling was done using sample KT161H from the DNC facies. The black circle represents the average of graphite schist (N=15) from Borges et al., 2021B. The orange square is the TTG average composition from Martin et al, 2005 (TTG <3 Ga.) The red diamond is an Alexo AUK sample (M662) from Arndt, 1986. The blue square is a Barberton ADK average of the cumulate samples (N=10) from Stiegler et al., 2012.

The whole-rock data on the different rock facies in the mineralized sequence of the Boa Vista deposit, including drill core data, contribute to the possible interactions between magma and country rocks. By thermomechanical erosion, the assimilation of sulfur and metal into the magma and forming the ore sulfide. Arndt et al. (1989) and Kuyumjian and Jost (2006) summarized that the komatiite from Crixás greenstone belts has confused and complex geochemistry. The AFC models in **Fig. 12** show that between the two candidates for assimilation, graphite schist and TTG complex (basement), where the first has a better correlation with the data, particularly for Ti-Fe, for the other elements, both could be the contaminant. Another aspect is that all data was compared with a typical AUK (Alexo - red diamond) and ADK (Barberton - blue square) (references and other information are in the legend of **Fig. 12**). The AFC models were made by the EasyMELTS modeling software that was used to test how Crixás komatiite crystallizing and assimilating two different country rocks. The model's conditions were equal; all parameters are described in Table 1. The EasyMELTS is a Graphic User Interface (GUI) of MELTS and was designed to model the cooling and crystallization of melt bodies (Smith & Asimow, 2005). The software relies on thermodynamics to determine a liquid’s composition as it cools and the solid phases crystallize at each cooling step, including assimilation. The MELTS model version used was MELTS_v1.0x, and whole-rock of the major elements of the initial composition (KT-161H) and country rocks assimilated are detailed in supplementary material.

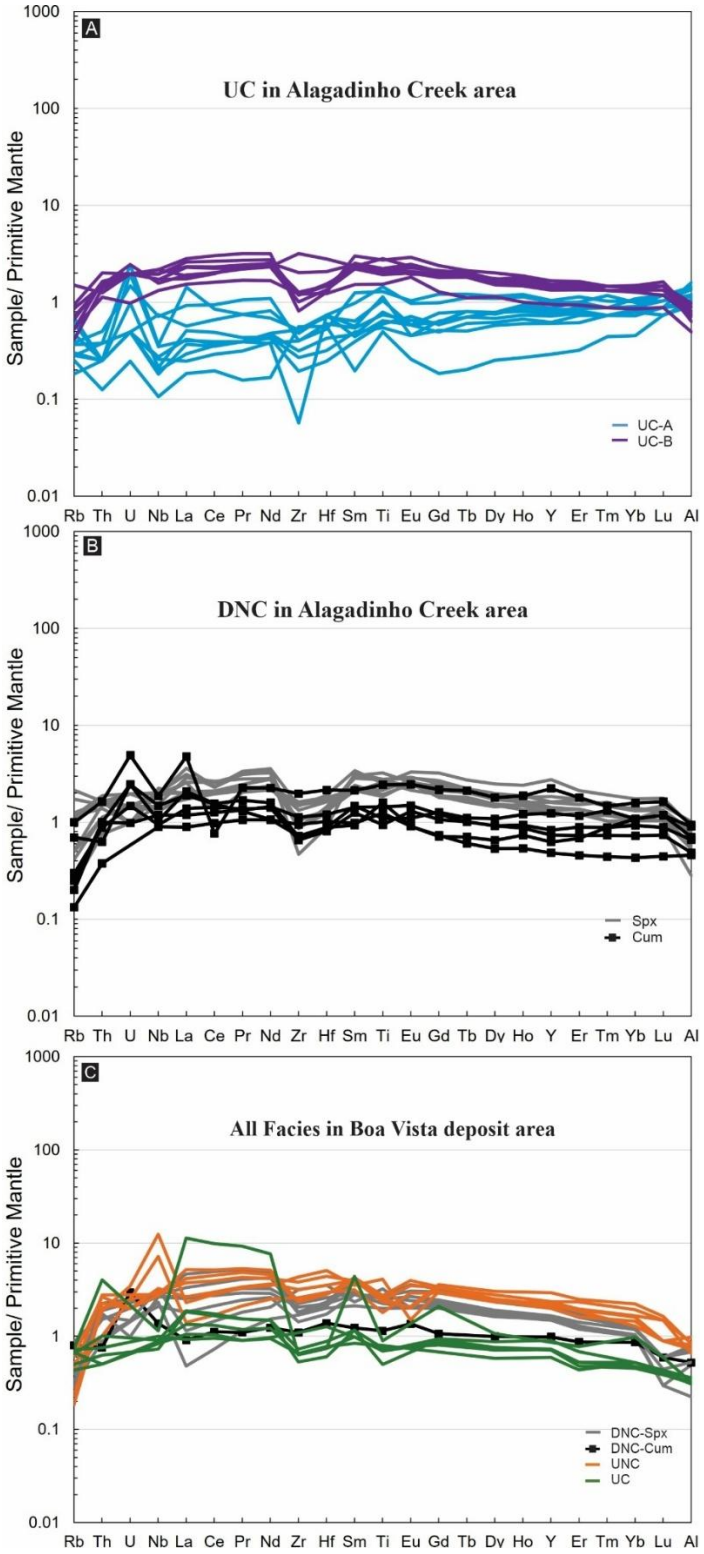

Figure 13 Extended incompatible element patterns for different facies of komatiites of the Crixás greenstone belt. Primitive mantle normalization values from McDonough and Sun (1995).

Table 1 All parameters used in the EasyMELTS to create the AFC models.

Parameters	**Information**
Initial temperature (Cº)	1800
Pressure (bar)	1000
Calculation Mode	Isothermal
fO_2	QFM
Number of steps	20
The increment between steps (T Cº)	-20
The increment between steps (P bar)	0
Fractionated phases	Solids
temperature of assimilation (Cº)	1800
Mass/step	2.5
Solid phases	Olivine, clinopyroxene, orthopyroxene, spinel, feldspar, and hornblende

1.5.4. Sulfur isotopes

Boa Vista sulfides (Table 2) range mainly between +16‰ and +18.5 ‰ δ^{34}SV-CDT (**Fig. 14A-B**) with no systematic variation for samples from different ore types or with distinct ore tenors. Tenor is a widely used term in studies of magmatic sulfide deposits to indicate metal abundance to 100 percent sulfide (i.e., the metal content when recalculated to 100% sulfides (Naldrett, 1989). In addition, different sulfides (i.e., Pn and Po) in ore samples have the same compositional range. The graphite schist δ^{34}SV-CDT ranges between +30 and +34‰, with no systematic variation for different sulfides (i.e., Po and Ccp).

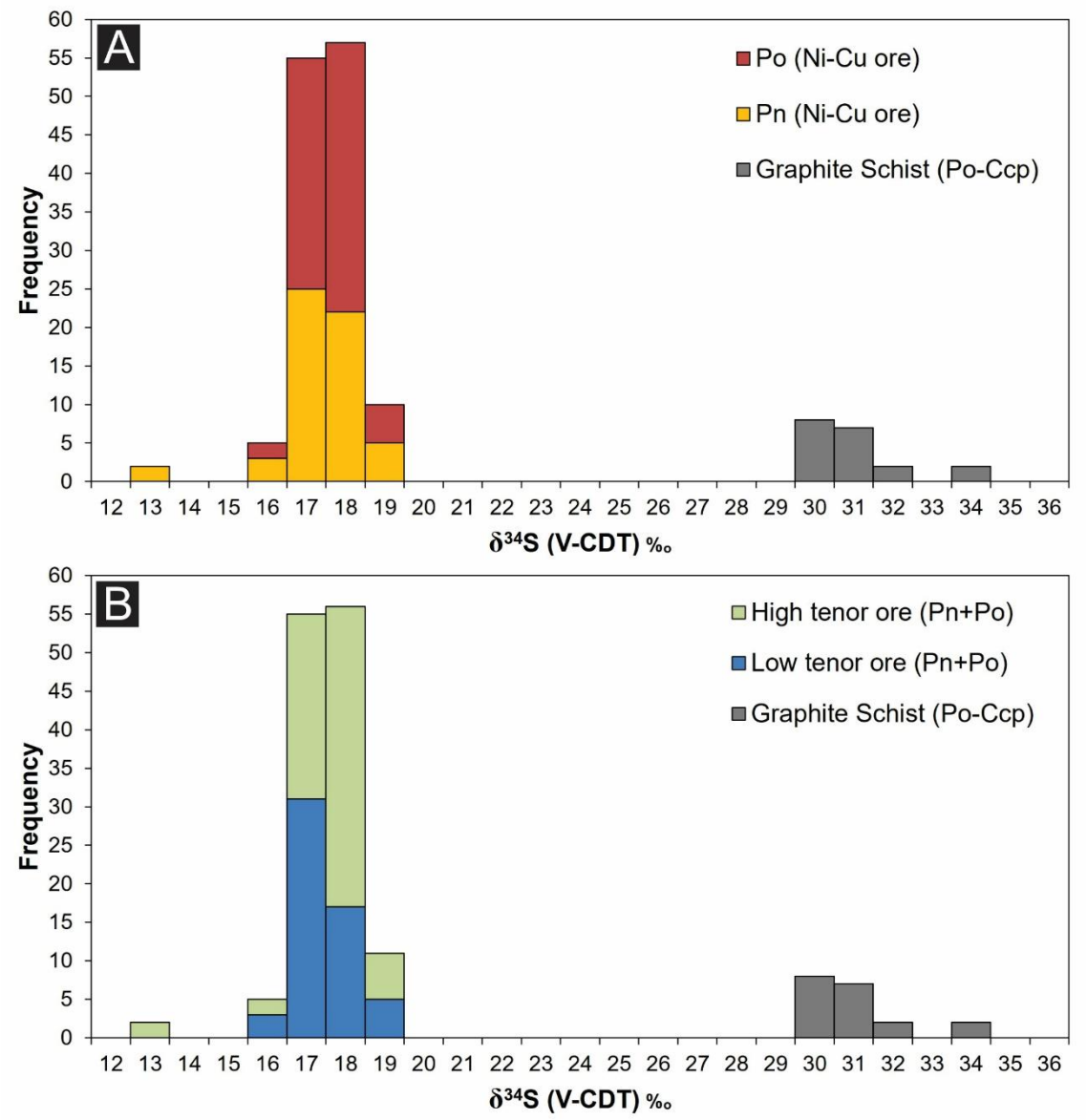

Figure 14 (A) Histograms of δ34S values for the Boa Vista Ni-Cu deposit separated by mineral, compared to graphite schist country rocks; and (B) Histograms of δ34S values for the Boa Vista Ni-Cu deposit separated by tenor, comparing with graphite schist country rocks.

Table 2 Representative sulfur isotope data from the Boa Vista deposit.

Sample ID..	Drill hole	Mether DH.	Lithology	Sulfide Texture	Mineral	$\delta^{34}S$ (‰V-CDT)
PCX-BIV-46,5	PCX-BIV	46.50	Graphite schist	-	Po + Cpy	30.33
BVD31-32,7	BVD- 31	32.70	Sulfide	semimassive	Pn	17.36
BVD31-33,26	BVD- 31	33.36	Sulfide	Matrix breccia	Pn	18.42
BVD31-42,15	BVD- 31	42.15	Sulfide	Matrix breccia	Pn	17.53
BVD14-47,77	BVD-14	47.77	Sulfide	Matrix breccia	Pn	18.06
BVD22-114,71	BVD- 22	114.71	Sulfide	Matrix breccia	Pn	17.51
BVD22-114,87	BVD- 22	114.87	Sulfide	Matrix breccia	Pn	16.96
BVD22-115	BVD- 22	115.00	Sulfide	Matrix breccia	Pn	18.16

1.1. DISCUSSION

1.1.1. Evidence for crustal contamination and S assimilation

In the Boa Vista deposit, komatiitic flows are interlayered with sulfide-bearing graphite schist, interpreted as metamorphosed black shales. This is a distinctively different geological feature compared to the Crixás GB's southern part (Alagadinho Creek area). The BVD-103 Drill hole profile (**Fig. 9**) shows a positive correlation between Ni, Cu, Co, and Zn content, showing that they are associated. High Zn content, including sphalerite. It is not so common in komatiite-associated Ni-Cu-(PGE) sulfide deposits. Low-MgO Zn-bearing sedimentary rocks are typical contaminants in Kambalda (Bavinton, 1981). Cowden (1988) has also suggested that the anomalously high Zn content of the flank streams may be due to the assimilation of Zn-enriched sediments between the streams. The UC and UNC have up to Zn contents (220–300 ppm) (**Fig. 12**), but only UC has Ni-Cu ore. So, the Zn positive anomalies combined with adcumulus channelized/conduit flow facies (high MgO content) and geochemistry correlate with sulfide ore, which has a high Zn content. The sphalerite was not found in the graphite schist.

The nature and timing of contamination can be identified through its distribution (Lesher et al., 2001): if all lavas in a sequence are contaminated, it likely occurred at the source; if contamination varies systematically through the sequence, it probably occurred during ascent through the crust, and if contamination is restricted to specific flows or individual parts of flows, contamination probably occurred during emplacement. The spread observed in binary diagrams (**Fig. 12**) reflects the different flow and textures, including olivine

cumulus and spinifex. However, Si-Ti-Ca-Fe-Zn has a substantial spread, evidencing some contamination and mobilization.

Part of these elements combined with REE-Zr-Nb (**Fig. 13**) are immobile and should not vary so much from each other in a group of cogenetic rocks. Komatiites contaminated by the continental crust or by clastic sedimentary rocks are enriched in Th-U-LREE relative to MREE-HREE and less enriched in Nb-Ta-Ti relative to elements of similar compatibility (Jochum et al. (1991). The diagram (La/Sm)N vs. (Th/Yb)N (**Fig. 15A**) compares Crixás komatiite with graphite schist as a contaminant. The results are that the komatiite has clues of crustal contamination (e.g. $(La/Sm)_N > 1.2$), the ample spread evidence that there is a range level of crustal contamination. However, several samples of UNC facies exhibit pronounced negative Eu anomalies (**Fig. 13**), reflecting the mobility of Eu^{2+} during hydrothermal alteration and regional metamorphism (e.g., Lesher and Stone, 1996; Arndt et al., 2008), All of the patterns are irregular to varying degrees, reflecting mobilization of even the least-mobile elements during serpentinization, amphibolitization, and chloritization. Then, the effects of metamorphism cannot be excluded (Arndt et al., 1989).

In comparison with Barberton and Alexo, both are komatiite with evidence of crustal contamination of the felsic and andesitic rock, respectively (Barberton, e.g., Robin-Popieul et al., 2012; Grosch and Slama, 2021; Lowe, 2024) (Alexo, e.g., Houlé et al., 2012). The comparison with Crixás komatiite, including the Boa Vista deposit area, showed that both are similar (**Fig. 12**). To Barberton, the average of the cumulate komatiite and Alexo was selected as a sample with high MgO, indicative of cumulate facie. In general, the contamination of the Crixás komatiite is not uniform in all flow and facies.

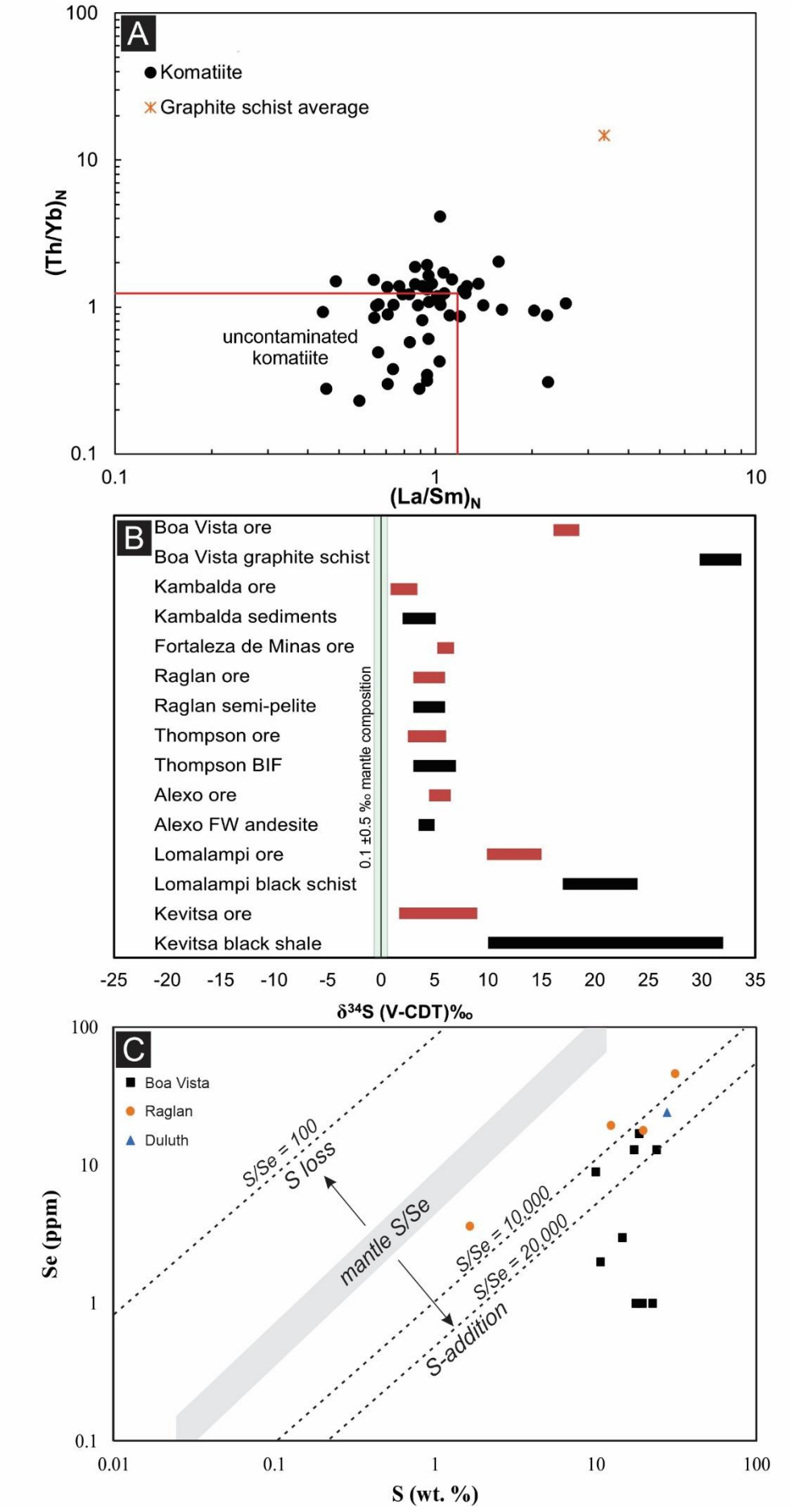
A
Komatiite
Graphite schist average
uncontaminated komatiite
(Th/Yb)N
(La/Sm)N
100
10
1
0.1
0.1
1
10
B
Boa Vista ore
Boa Vista graphite schist
Kambalda ore
Kambalda sediments
Fortaleza de Minas ore
Raglan ore
Raglan semi-pelite
Thompson ore
Thompson BIF
Alexo ore
Alexo FW andesite
Lomalampi ore
Lomalampi black schist
Kevitsa ore
Kevitsa black shale
0.1 ±0.5 ‰ mantle composition
-25 -20 -15 -10 -5 0 5 10 15 20 25 30 35
δ34S (V-CDT)‰
C
Boa Vista
Raglan
Duluth
S/Se = 100
S loss
mantle S/Se
S/Se = 10,000
S/Se = 20,000
S-addition
Se (ppm)
S (wt. %)
100
10
1
0.1
0.01
0.1
1
10
100

Figure 15 (A)$^{34}S/^{32}S$ isotopic data for selected komatiite-hosted Ni-Cu deposits, Ni-Cu sulfide deposits ores, and S-bearing country rocks (see also Lesher (2017) and Ripley and Li (2017). Data source: Fortaleza de Minas: Choudhuri et al. (1997); Alexo: Naldrett (1966); Raglan: Lesher et al. (1999); Kambalda: Donnelly et al. (1978); Thompson: Bleeker and Macek, 1996; Lomalamp: Törmänen et al. (2016); Kevitsa: Luolavirta (2018). (B) S and Se binary diagram of the Boa Vista ore deposit, the mantle domain S/Se values are from Queffurus and Barnes (2015); (C) Plot of PM-normalized La/Sm and Th/Yb data for all outcrop komatiite samples aimed at evaluating contamination between komatiite magma and country rocks (graphite schist average from Borge et al., 2021B) (after Piña et al., 2012). Primitive Mantle normalization after McDonough and Sun (1995).

Reduced sulfur would have been the stable ionic species in the water throughout the Archean period (Farquhar et al., 2000, 2002). When S2− is the dominant fluid species, S2− becomes stable (high pH and low f(O_2)), then the δ34S value of the precipitating sulfides would be slight to highly positive (e.g., sulfides in a carbon-rich reducing layer) (Sharp, 2017). Monster et al. (1979) demonstrated that the divergence of sulfur isotope ratios in sediments happened between 3.1 and 2.8 billion years ago. By the middle of the Archean, the $\delta^{34}S$ values ranged from −20 to +20‰, including black shales. Compared with other komatiite-hosted Ni-Cu sulfide deposits, the Boa Vista deposit has distinctively high positive $\delta^{34}S$ (**Fig. 15B**), explained by the country rock values of 30–33‰. The very positive $\delta^{34}S$ signature of country rock and Ni-Cu sulfide ore suggests that the assimilation of graphite schist was critical for the origin of the deposit.

Results from the Boa Vista and other komatiite-associated Ni-Cu-(PGE) sulfide deposits (16–19) indicate that the highest $\delta^{34}S$ values occur in komatiite-associated deposits that assimilated black shales or graphite schist like the Paleoproterozoic Kevitsa and Lamolampi deposits (Luolavirta, 2018; Törmänen et al., 2016 respectively) located in the Baltic-Slavic craton (**Fig. 15B**). The positive and similar $\delta^{34}S$ signatures of ore and their respective country rocks in Kambalda, Thompson, Alexo, and Reglan is a distinctive feature also identified in the Boa Vista deposit. However, in the BV deposit, the $\delta^{34}S$ signature is very high, more than all, and the graphite schist, too. The difference between them is nearly 13; it is not expected. However, knowing that the initial composition of the sulfide of magmatic origin is close to 0 (Chaussidon et al. (1989), it makes sense to mix two isotopic signatures and have an intermediate value.

The S/Se ratio in Ni-Cu deposits and the source of sulfur can vary depending on the deposit's geology (Queffurus and Barnes, 2015). However, sulfur can generally be derived from several sources, including migrating sulfide-

rich hydrothermal fluids, sulfide-rich sedimentary rocks, sulfide-rich igneous rocks, and sulfide-rich magmatic fluids. In some Ni-Cu deposits, sulfur may come from multiple sources (Queffurus and Barnes, 2014). The S/Se ratio has long been used to trace the S source and constrain the role of crustal contamination in triggering sulfide saturation, including syn- and post-magmatic processes in Ni-Cu-(PGE) sulfide deposits (Smith et al., 2016). The S/Se mantle ratio ranges from 2500 to 4500, and, therefore, contents out of this range can be associated with the addition of S from crustal sources, S loss, or Se gain.

The S/Se ratio of the massive sulfide recalculated to 100% sulfides of the Boa Vista deposit (>10,000) indicates that S is derived from an external crustal source. When comparing Boa Vista, Raglan and Duluth, three examples of Ni-Cu-(PGE) sulfide deposits that have semi-pelite and black-shale country rocks, they all have high S/Se ratio close to 9000–10,000, consistent with an external S source (Samalens et al., 2017; Yao and Mungall, 2021 respectively) (**Fig. 15C**). Kambalda ores with an average S/Se ratio of 9430 (Cowden et al., 1986) and Thompson ore with S/Se of 12,800 (Bleeker and Macek, 1996), both interpreted as resulting from S assimilation of an external source, have S/Se ratio very similar to the Boa Vista deposit.

1.1.2. Characteristic features and classification of the Boa Vista Ni-Cu deposit

The spatial correlation and difference between the Boa Vista deposit and Alagadinho Creek areas (**Fig. 5-7**) showed similarity and variation of the komatiite volcanic flows, with adcumulus conduit/channelized flow typically of the komatiitic volcanic/subvolcanic environment. The strong positive correlation between MgO and Ni contents (**Fig. 8, Fig. 12**) indicates the role of olivine fractionation/accumulation. In contrast, decreasing Cr with increasing Mg in most magnesian rocks indicates that olivine was the only phase on the liquidus during the formation of the cumulate komatiites (e.g., Lesher and Stone, 1996; Barnes et al., 2023). About Cr content is consistent with the komatiites reaching saturation in chromite during fractionation (Murck and Campbell, 1986; Lesher and Stone, 1996; Barnes, 1998). Ti exhibits a similar trend. Some spinifex-textured komatiites in the Crixás belt contain as much as 35% MgO, indicating

that some olivine accumulated and expelled trapped liquid (e.g., Lesher et al., 1981). This is not so common in komatiites; this content of MgO, in general, is associated with olivine cumulate facies (Arndt et al., 2008.).

There are many mineralized zones, including expressive sulfide matrix ore breccia (**Fig. 9**). The geological ore framework is characterized by spatial correlation with the channelized/conduit adcumulate facies of the komatiite and intercalation of graphite schist. The ore has mainly sulfide matrix ore breccia texture and restricted semi-massive and disseminated textures, consisting of Po + Pn ± Cpy (**Fig. 10**), are preserved, indicating that sulfide mineralization accumulated at the basal contact of conduit facies metakomatiites overlying metabasalts and interlayered with graphite schist. The sulfide matrix ore breccia shown assimilation of the metasediment (i.e., clast in the lower left corner in **Fig. 10A**) and ductile deformed clasts of metasediment 'swimming' in the sulfides ore.

The mineralization is variably deformed and mobilized along shear zones (**Fig. 10A and 10C**). Barnes et al. (2018) argue that based on the nature of silicate-sulfide contacts and the nature of the silicate inclusions, semi-massive sulfide ores and sulfide matrix ore breccia can be subdivided into magmatic and tectonic breccias. One of these, tectonic “Durchbewegung” breccias, forms in the solid state by deformation when developing a concordant foliation in silicate and sulfide components, including folded ore. By this definition, only the stringer ore texture (foliated sulfide) (**Fig. 10C**) is a tectonic ore but not breccia. Many structures, including euedric py, typically a recrystallization product, are found only in mobilized and deformed ore. Six new trace geochemistry data of sulfide matrix ore breccias samples from the southeastern orebody (drill core BVD31) and one sample of mobilized ore (drill core BVD43) were integrated with eleven data samples of sulfide matrix ore breccia from the main orebody (drill cores BVD14-22-103) (Costa JR et al., 1997) (**Fig. 11**). This data show a considerable geochemistry variation in the ore. The multi-element distribution observed in Fig. 11 shows a partial similarity with the range of Kambalda ores but, at the same time, presents an extensive range of content ranging from 2 to almost 500 times. Elements like Se, Sb, Pb, Pd, Pt, Ir, and Cr are in the extensive range. It can be explained by the difference in the texture of ore, variation in the amount of silicate xenoliths present, and mobilization of some elements. Another recent argument

is that the multi-stage crystallization of sulfide, precisely the monosulfide solid solution (MSS), can explain the observed variations in major and trace elements. (Staude et al., 2022). The ranges for sulfide mineral and tenors (**Fig. 14B**) show slight variation between mineral ore and tenor. For that, it was calculated the tenors of the ore, then the $\delta^{34}S$ signature and sulfide mineralogy were separated and compared using different tenors as criteria. So, the $\delta^{34}S$ isotopic signature was not affected by the change of the mineral and tenor of the ore. The range of $\delta^{34}S$ values for our samples (13–19‰) is distinctively lower than the country-rock values, suggesting that crustal sulfide xenomelts were partially shifted toward mantle S isotopic compositions by effective silicate liquid: sulfide liquid mass ratios (R factors) (see Lesher and Burnham, 2001). The R factor modeling was defined by Campbell and Naldrett (1979). It is a metal mass balance in magmatic ore deposits, indicating the final and initial concentrations of metal in the silicate liquid and the final and initial concentrations of metal in the sulfide melt (all data about the R factor model is in supplementary material).

All samples of the Boa Vista deposit appear to have formed at R factor between 300 and 400 (**Fig. 16**), thus limiting the shift toward mantle isotopic compositions. Barnes et al. (2012) estimated an R factor between 100 and 350 for komatiite-associate Ni-Cu-sulfide deposit. Virnes et al. (2023) also showed that using in situ S isotopes and Pd contents of pentlandite in the Mount Keith MKD5 orebody could estimate an R factor between 200 and 400. The Kambalda ore sulfide shows R factor values of around 100–500 (Lesher and Campbell, 1993), similar to the Boa Vista deposit. The estimated R factor values for komatiitic Ni sulfide deposits come from comparatively low PGE tenors of 500–3000 ppb for Pd (Barnes, 2006; Barnes et al., 2012). This suggests that the Pd content and spread (Fig. 16) are associated with a post-magmatic process, including mobilization. The discrepancy in the calculation of the R factor can be explained by decoupling sulfur with other elements during the ore-forming process (Staude et al., 2024).

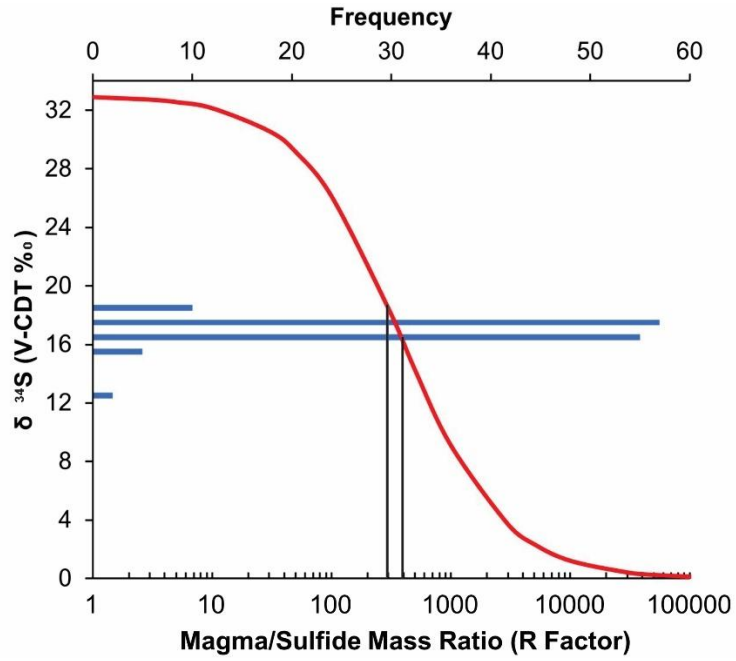

Figura 16: R factor versus $\delta^{34}S$ histogram (blue bars) for 129 mineralized analyses from the Boa Vista deposit. Modeled variations in $\delta^{34}S$ with varying magma: sulfide mass ratio (red line) has been calculated for a magma containing 0.1 % S with 0 ‰ $\delta^{34}S$ equilibrating with a sulfide xenomelt (derived from country-rock sulfidic graphitic schist) containing 38% S with 33‰ $\delta^{34}S$). (For interpretation of the references to color in this figure legend, the reader is referred to the Web version of this article.)

Metal100 contains the specific element in 100% sulfide (**Fig. 17**), showing that the main ore body has systematically higher Ni100 values. However, the range is lower than many other deposits of this type (e.g., Kambalda: Lesher and Campbell, 1993). The Cu100 values are more variable than Pd and Co. When comparing Ni100 vs. Metal100 (Fig. 16), two clusters of samples are controlled by Ni tenor. The R factor models were generated using Equation number 5 and variations in Lesher and Burnham (2001), it was modeled three different curves for different conditions: R factor Y0 = 0 for barren sulfide incorporated by magma, R factor Y0 > 0 for metal-bearing sulfide incorporated by magma, and R factor Y0 = X0 for Sulfide exsolved from magma. In Ni-Co-Zn-Cu, the sample overlaps or is next to the red curve (R factor Y0 > 0), indicating a metal-bearing sulfide incorporated by the magma process (Lesher and Burnham, 2001). For the Pd diagram, the spread is significant.

The Boa Vista ore has variable Ni tenors (5–8.5% and ±2%), Ni/Cu ratios (1:10 and 1:5; see supplementary material), and low PGE tenors (Fig. 16, Fig. 17A), indicating that there may be different parts of the ore body reflecting different stages of ore formation (Staude et al., 2022). Two different tenors are

associated with a variably efficient mineralization process. Barnes et al. (2017) reveal that the typical Ni/Cu ratios are 20:1 and 4:1 in ores linked to komatiites and komatiitic basalts, respectively. In addition, primitive high-T komatiites contain very high Ni and low Cu compared to more fractionated mafic magmas, which have lower Ni/Cu ratios. It is a direct result of parent magma compositions or extensive fractionation of the parental magma. The equilibration of sulfide liquid and olivine exhibits a positive dependency of Kd on sulfide liquid Ni + Cu concentration, as well as fO2, resulting in a crucial nonlinearity in the connection between sulfide and olivine-saturated silicate liquid compositions that proportionally increase the Ni/Cu ratios (Barnes et al., 2013). Zn is a contaminant and has no association with Ni-Cu-(PGE) sulfide. A geochemical profile through the volcanic rocks and mineralized horizons intercepted in drill core BVD-103 (Fig. 8) a waited highlights the higher Fe-Ni-Cu-Co contents in the mineralized horizons and that some, but not all, of the horizons are also enriched in Zn. The Cr does not have any positive correlation with the ore zone.

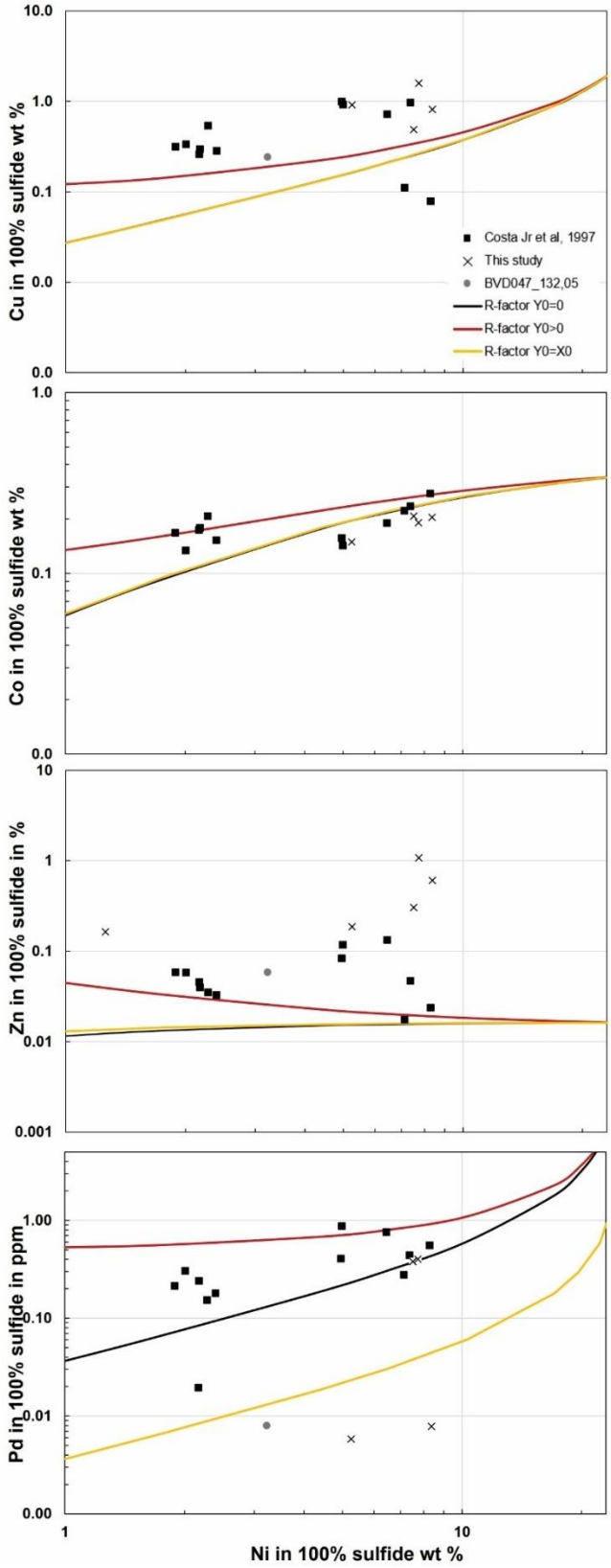

Figure 17 Co100, Cu100, Pd100, and Zn100, all vs Ni100 in Boa Vista ores. R-factor (magma: sulfide) models generated using Eq 5 in Lesher and Burnham (2001) using XoNi = 1700 ppm, XoCo = 115ppm, XoCu = 45 ppm, XoPd = 6 ppb, XoZn = 65 ppm; YoNi = 2000 ppm, YoCo = 1000 ppm, YoCu = 1000 ppm, YoPd = 500 ppb, YoZn = 1000 ppm; and DSul/SilNi = 150, DSul/SilCo = 30, DSul/SilCu = 600, DSul/SilPd= 30,000, DSul/SilZn = 2.5. (Barnes et al. 2017).

Initial magma composition adapted from Lesher and Arndt (1995). All data is disponible in the supplementary material.

The patterns in Fig. 12 reflect the possible pyroxenitic sources (PGE < Cu-Ni-Co) like Pechenga and are similar to most Chinese Ni-Cu-(PGE) deposits (Lu et al., 2019) and/or sulfide retention/segregation (PGE ≪ Cu < Ni < Co). The mobilization process reduced the Ni and Cu tenors and the REE contents but did not change the Ni/Cu ratio (see BVD047_132.05 sample in **Fig. 18A–B**). The unmineralized BVD131 drill hole has low Ni/Cr and Ni/Ti ratios (**Fig. 18C**), consistent with the absence of channel flow facies coherent with the low PGE tenors (**Fig. 18A**). Although the BV deposit shares some similarities with deposits from the Kambalda field, the lower tenor and small volume suggest a significantly smaller and less dynamic flow environment. **Fig. 18A–B** suggest that the increasing MSS accumulation was the primary process for forming the BV deposit.

However, it was not enough to generate a significant volume of sulfide, and the mantle source was a little enriched by Ni and Cu; another point is the variable and low R factor, 10–100, suggests mobilization of the metals contents. The plot of the Crixás data in this diagram (**Fig. 18C**) shows that only the UC facies belong to the sulfide bearing-cumulates domain, precisely the BVD14–118.80 sample that has sulfide. The plot in **Fig. 18C** shows too that the UC, including the BVD14–118.80 sample (green filled circle), have high Ni/Cr and Ni/Ti ratios, both indicating sulfide-bearing cumulates, possibly by thermomechanical erosion of intercalated S-rich graphite schist.

This general framework is common in many komatiite-associated Ni-Cu-(PGE) sulfide deposits worldwide (e.g., Barnes, 2006; Collins et al., 2012). The integration and compilation of our results showed that the Boa Vista Ni-Cu deposit is the result of a complex interplay of volcanic, sedimentary, and post-magmatic processes, with basal/contact into the adcumulus olivine channelized/conduit facies flow. Primary volcanic-sedimentary processes include the deposition and formation of the black shale, komatiitic volcanism, thermomechanical erosion with assimilation of sulfur-bearing crustal rocks, sulfide liquid immiscible (SLI) formation, and segregation. The post-mineralization processes are complex and include deformation, metamorphism, and some level of hydrothermal alteration

through time. All these aspects indicate that the Boa Vista deposit belongs to magmatic type 1 or contact type (e.g., Kambalda) and the restricted mobilized ore type 5 along the shear zones (e.g., Thompson) (Barnes, 2006; Lesher and Keays, 2002).

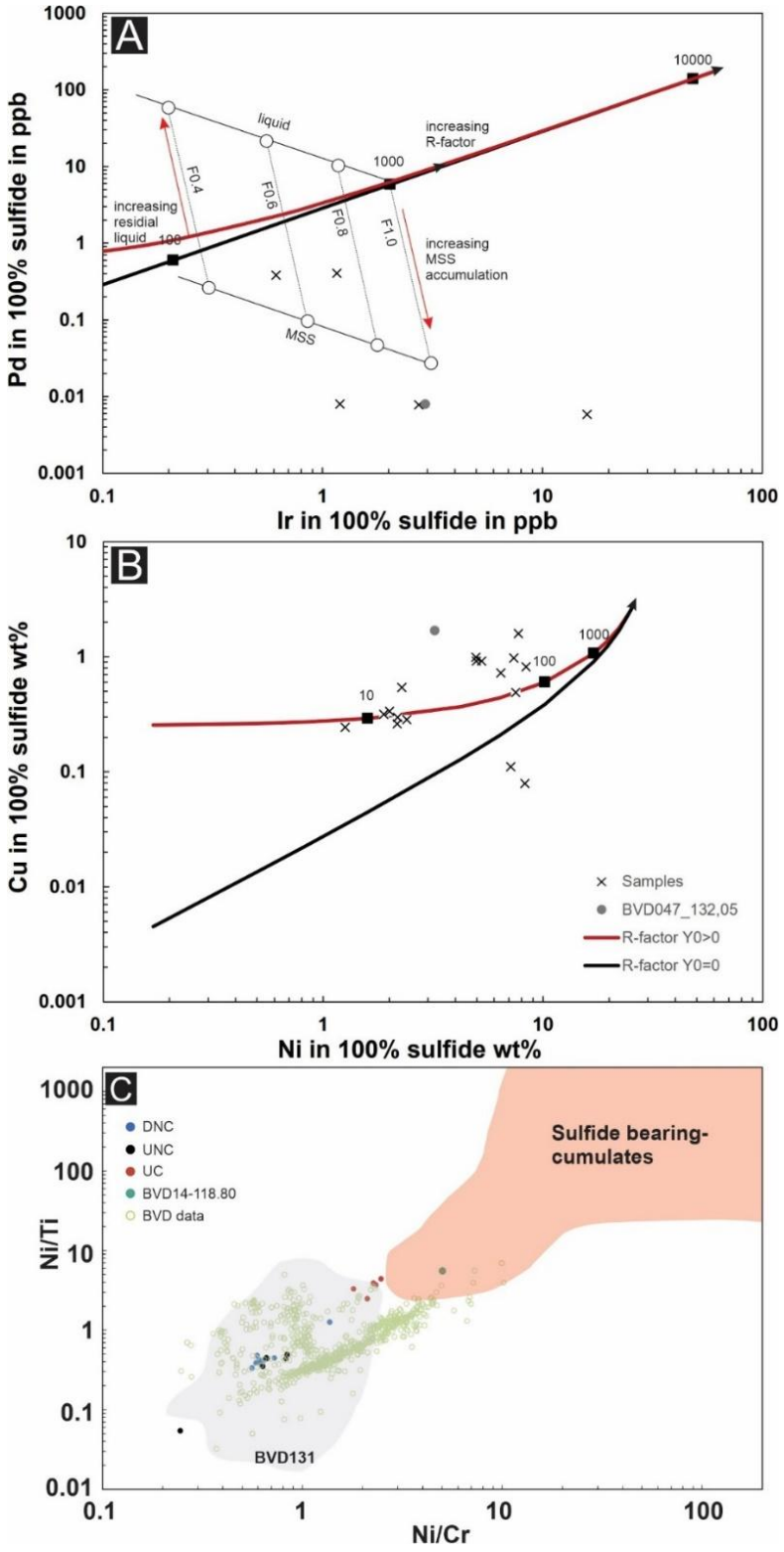

Figure 18 (A and B) Modeled variation of Ir vs Pd and Ni vs Cu in 100% sulfide in Boa Vista ore with varying magma: sulfide mass ratio (R factor: open squares) and fractional crystallization of monosulfide solid solution from sulfide liquid (open circles). F = fraction of sulfide liquid. The R factor model parameters are the same as in Figure 13, including X_0Ir = 2.1 ppb, Y_0Ir = 0, and D_{Sul}/Sil_{Pd} = 30,000. (C) A binary diagram of the Ni/Cu and Ni/Ti ratio of the Boa Vista rocks, sulfide-bearing cumulate camp is from Le Vaillant et al., (2016).

1.1.3. Implications for Exploration

The Alagadinho Creek and Boa Vista deposit areas have two significant geological differences. The accumulation of channelized flow facies (UC) and interlayered graphite schist within the volcanic pile is restricted to the Boa Vista area (**Fig. 5 and 6**). These features are critical for the origin of magmatic sulfides associated with komatiites and explain why Ni-Cu sulfides occur in the Boa Vista area but not in the Alagadinho Creek area. Based on these geochemical features, high ratios of Ni/Ti and Ni/Cr (**Fig. 18C**) are helpful for the detection of sulfide segregation in mafic to ultramafic systems are susceptible indicators for sulfide fractionation and extraction (Fiorentini et al., 2010; Heggie et al., 2013; Konnunaho et al., 2015; Le Vaillant et al., 2016; Makkonen et al., 2017). Other Ni exploration criteria for Ni-Cu-(PGE) sulfide deposits is the Ni depletion or enrichment in igneous olivine and/or pyroxene minerals and their host rocks (e.g., Lesher and Stone, 1996; Barnes and Fiorentini, 2012; Barnes et al., 2023 and references therein).

Geochemical features connected with these differences may be used as an exploration guide for exploring new targets of Ni-Cu komatiite-associated sulfide deposits in Crixás and other greenstone belts in central Brazil. Lavas with high Mg contents are hotter and have a lower viscosity, leading to a higher degree of channelization/conduit environment. To properly evaluate the potential of channelized/conduit flow facies to host sulfide deposits, it is necessary to understand the facies and flow architecture, including spatial relationships with sulfur-bearing country rock.

1.2. CONCLUSIONS

Based on the results and discussions presented in this research, it is possible to conclude the following about the Boa Vista Ni-Cu deposit and its relationship with the Crixás greenstone belt.

1. The Boa Vista Ni-Cu deposit shows all requirements for the formation of sulfide deposits associated with komatiites: (1) Channel/conduit flow facies; (2) Sulfur-rich country-rock; (3) Assimilation of the embedding rock; (4) Segregation and accumulation of sulfide liquid. These requirements are not present in the south-central portion of the Crixás greenstone belt.

2. The heavy δ34S isotopic signatures of Ni-Cu ores (16–19) and country-rock graphite schists (30–34) and very high S/Se ratios (>10,000) suggest that the ore has a mix of the mantellic and an external S source, and that the graphite schist was the origin of the external S source for the Boa Vista deposit. The whole-rock geochemistry, including AFC models, also suggests that graphite schist was assimilated.

3. The Boa Vista Ni-Cu deposit is a Type I (basal contact) deposit, variably deformed and mobilized along shear zones. The deposit contains a spatial variation of the metal tenors. The ore comprises Po + Pn ± Ccp within sulfide matrix ore breccia, local tectonic stringer ore, and rare semi-massive and disseminated ores. The relatively low grades of the ores are attributable to relatively low metal tenors, which is consistent with a magma: sulfide ratio (R factor) < 600.

4. High Ni-Zn- MgO contents resulting from sulfur-bearing sedimentary rocks associated with adcumulate channelized flow facies provide the best geochemical exploration guide to be used to identify potential targets for komatiite-associated Ni-Cu-(PGE) sulfide deposits in the Crixás and other greenstone belts in central Brazil

Acknowledgments

This study was financed in part by the Coordenação de Aperfeiçoamento de Pessoal de Nível Superior - Brasil (CAPES) - Finance Code 001. Analytical facilities at the University of Brasília (UnB) provided additional support for this research. Cesar F. Ferreira Filho is a Research Fellow of CNPq (Conselho Nacional de Desenvolvimento Científico e Tecnológico - Processo 303132/2022-1) and acknowledges the continuous support through research grants and scholarships for his Research Groups. Analytical facilities at the University Federal do Amazonas (UFAM) provided additional support for this research. Other collaborative reviewers and researchers, in special for Carl Michael Lesher have provided important comments on a draft of the paper.

REFERENCES

Arndt, N.T., 1986. Differentiation of komatiite flows. J. Petrol. 27, 279–301. https://doi. org/10.1093/petrology/27.2.279.

Arndt, N.T., Teixeira, N.A., White, W.M., 1989. Bizarre geochemistry of komatiites from the Crixás greenstone belt, Brazil. Contrib. Mineral. Petrol. 101, 187–197. https:// doi.org/10.1007/BF00375305.

Arndt, N.T., Lesher, C.M., Barnes, S.J., 2008. Komatiite. Cambridge University Press, New York, p. 488. https://doi.org/10.1017/CBO9780511535550.

Barnes, S.J., 1998. Chromite in komatiites, 1. Magmatic controls on crystallization and composition. J. Petrol. 39 (10), 1689–1720. https://doi.org/10.1093/petroj/ 39.10.1689.

Barnes, S.J., 2006. Komatiite-hosted nickel sulfide deposits: geology, geochemistry, and genesis. Komatiite-hosted nickel sulfide deposits: geology. Geochemistry, and Genesis 51–97. https://doi.org/10.5382/sp.13.03.

Barnes, S.J., Fiorentini, M.L., 2012. Komatiite magmas and sulfide nickel deposits: a variably endowed archean terranes comparison. Econ. Geol. 107, 755–780. https:// doi.org/10.2113/econgeo.107.5.755.

Barnes, S.J., Fiorentini, M.L., Fardon, M.C., 2012. Platinum group element and nickel sulfide ore tenors of the Mount Keith nickel deposit, Yilgarn Craton, Australia. Miner. Deposita 47, 129–150. https://doi.org/10.1007/s00126-011-0348-5.

Barnes, S.J., Godel, B., Gürer, D., Brenan, J.M., Robertson, J., Paterson, D., 2013. Sulfide- olivine Fe-Ni exchange and the origin of anomalously Ni-rich magmatic sulfides. Econ. Geol. 108, 1971–1982. https://doi.org/10.2113/econgeo.108.8.1971.

Barnes, S.J., Holwell, D.A., Le Vaillant, M., 2017. Magmatic sulfide ore deposits. Elements 13, 89–95. https://doi.org/10.2113/gselements.13.2.89.

Barnes, S.J., Staude, S., Le Vaillant, M., Pi˜ na, R., Lightfoot, P.C., 2018. Sulfide-silicate textures in magmatic Ni-Cu-(PGE) sulfide ore deposits: massive,

semi-massive and sulfide-matrix breccia ores. Ore Geol. Rev. 101, 629–651. https://doi.org/10.1016/j. oregeorev.2018.08.011. ISSN 0169-1368.

Barnes, S.J., Yao, Z. Sen, Mao, Y.J., Jesus, A.P., Yang, S., Taranovic, V., Maier, W.D., 2023. Nickel in olivine as an exploration indicator for magmatic Ni-Cu sulfide deposits: a data review and re-evaluation. Am. Mineral. 108, 1–17. https://doi.org/ 10.2138/am-2022-8327.

Bavinton, O.A., 1981. The nature of sulfidic metasediments at Kambalda and their broad relationships with associated ultramafic rocks and nickel ores. Econ. Geol. 76, 1606–1628. https://doi.org/10.2113/gsecongeo.76.6.1606.

Bleeker, W., Macek, J., 1996. Evolution of the Thompson nickel belt, Manitoba: setting of Ni-Cu deposits in the western part of the Circum Superior boundary zone. Joint Annual Meeting, Winnipeg, Manitoba, URL:. https://www.manitoba.ca/iem/info/l ibmin/gacmac/guidebook_a1.pdf.

Borges, C.C.A., Toledo, C.L.B., Silva, A.M., Chemale, F., Jost, H., Lana, C. de C., 2017. Geochemistry and isotopic signatures of metavolcanic and metaplutonic rocks of the Faina and Serra de Santa Rita greenstone belts, Central Brazil: Evidences for a Mesoarchean interoceanic arc. Precambr. Res. 292, 350–377. https://doi.org/ 10.1016/j.precamres.2017.02.017.

Borges, C.C.A., Toledo, C.L.B., Silva, A.M., Kirk, J., Ruiz, J., Chemale, F., Souza, R.G., Santos, B.A., Campos, M.P., Campos, L.M., Santos, A.M., 2021a. Archean to Paleoproterozoic evolution of the Crixás greenstone belt, Central Brazil: insights from two contrasting assemblies of metaigneous rocks. Lithos 404–405, 106493. https://doi.org/10.1016/j.lithos.2021.106493.

Borges, C.C.A., Toledo, C.L.B., Silva, A.M., Chemale, F., dos Santos, B.A., Figueiredo, F.L., Zacchi, ´ E.N.P., 2021b. Unraveling a hidden Rhyacian magmatic arc through the provenance of metasedimentary rocks of the Crix´ as greenstone belt, Central Brazil. Precambr. Res. 353. https://doi.org/10.1016/j.precamres.2020.106022.

Campbell, I.H., Naldrett, A.J., 1979. The influence of silicate: sulfide ratios on the geochemistry of magmatic sulfides. Econ. Geol. 74, 1503–1506. https://doi.org/ 10.2113/gsecongeo.74.6.1503.

Chaussidon, M., Albaréde, F., Sheppard, S.M.F., 1989. Sulphur isotope variations in the mantle from ion microprobe analyses of micro-sulphide inclusions. Earth Planet Sci. Lett. 92 (2), 144–156. https://doi.org/10.1016/0012-821X(89)90042-3. ISSN 0012- 821X.

Choudhuri, A., Iyer, S.S., Krouse, H.R., 1997. Sulfur isotopes in komatiite-hosted ni-cu sulfide deposits from the Morro do ferro greenstone belt, southeastern Brazil. Int. Geol. Rev. 39, 230–238. https://doi.org/10.1080/00206819709465269.

Collins, J.E., Hagemann, S.G., McCuaig, T.C., Frost, K.M., 2012. Structural controls on sulfide mobilization at the high-grade flying fox Ni-Cu-(PGE) sulfide deposit, Forrestania greenstone belt, western Australia. Econ. Geol. 107, 1433–1455. https:// doi.org/10.2113/econgeo.107.7.1433.

Coplen, T.B., Krouse, H.R., 1998. Sulfur isotope data consistency improved. Nature 392, 32. https://doi.org/10.1038/32080. Cordeiro, P.F. de O., Oliveira, C.G. de, 2017. The Goi´ as Massif: implications for a pre-Columbia 2.2–2.0 Ga continent-wide amalgamation cycle in central Brazil. Precambr. Res. 298, 403–420. https://doi.org/10.1016/j.precamres.2017.06.021.

Costa, J.R.C.N., Ferreira Filho, C.F., Araujo, G.A.O.S.M., Lopes, R.O., 1997. Geology and geochemistry of the Boa Vista nickel sulfide deposit, Crix´as greenstone belt, Central Brazil. Rev. Bras. Geociencias 27, 365–376. https://doi.org/10.25249/0375- 7536.1997365376.

Cowden, A., 1988. Emplacement of komatiite lava flows and associated nickel sulfides at Kambalda, Western Australia. Econ. Geol. 83, 436–442. https://doi.org/10.2113/ gsecongeo.83.2.436.

Cowden, A., Donaldson, M.J., Naldrett, A.J., Campbell, I.H., 1986. Platinum-group elements and gold in the komatiite-hosted Fe-Ni-Cu sulfide

deposits at Kambalda, Western Australia. Econ. Geol. 81, 1226–1235. https://doi.org/10.2113/ gsecongeo.81.5.1226.

Cuadros, F.A., Botelho, N.F., R A, Fuck, Dantas, E.L., 2017. The peraluminous Aurumina Granite Suite in central Brazil: an example of mantle-continental crust interaction in a Paleoproterozoic cordilleran hinterland setting? Precambr. Res. 299, 75–100. https://doi.org/10.1016/j.precamres.2017.07.029.

Ding, T., Valkiers, S., Kipphardt, H., De Biévre, P., Taylor, P.D.P., Gonfiantini, R., Krouse, R., 2001. Calibrated sulfur isotope abundance ratios of three IAEA sulfur isotope reference materials and V-CDT with reassessment of the atomic weigh to sulfur. Geochem. Cosmochim. Acta 65, 2433–2437. https://doi.org/10.1016/S0016- 7037(01)00611-1.

Donnelly, T.H., Lambert, I.B., Oehler, D.Z., Hallberg, J.A., Hudson, D.R., Smith, J.W., et al., 1978. A reconnaissance study of stable isotope ratios in Archaean rocks from the Yilgarn Block, Western Australia. J. Geol. Soc. Aust. 24, 409–420.

Farquhar, J., Bao, H., Thiemens, M., 2000. Atmospheric influence of Earth's earliest sulfur cycle. Science 289, 756–758.

Farquhar, J., Wing, B.A., McKeegan, K.D., Harris, J.W., Cartigny, P., Thiemens, M.H., 2002. Mass-independent sulfur of inclusions in diamonds and sulfur recycling on early Earth. Science 298, 2369–2372.

Ferreira-Filho, C.F., Lesher, C.M., 2001. The komatiite-associated Ni-sulfide deposit of Boa Vista, Brazil. 4th International Archean Symposium Extended Abstracts, Theme Five - Mineralization, AGSO Record 2001/37 429–431. URL: https://ecat.ga.gov.au/ geonetwork/dashboard/api/records/a05f7892-b633-7506-e044-00144fdd4fa6.

Filgueiras, B. de C., Oliveira, C.G. de, Sousa, I.M.C. de, Cordeiro, P., 2020. Further evidence of Rhyacian arc magmatism in the basement of the Brasília Belt, western São Francisco pericraton. J. S. Am. Earth Sci. 103, 102739. https://doi.org/10.1016/ j.jsames.2020.102739.

Fiorentini, M., Barnes, S.J., Lesher, C.M., Keays, R.R., Burnham, O.M., 2010. PGE geochemistry of komatiites, komatiitic basalts, basalts. Econ. Geol. 105, 795–823.

Fiorentini, M., Beresford, S., Barley, M., Duuring, P., Bekker, A., Rosengren, N., Cas, R., Hronsky, J., 2012. District to camp controls on the genesis of komatiite-hosted nickel sulfide deposits, agnew-wiluna greenstone belt, western Australia: insights from the multiple sulfur isotopes. Econ. Geol. 107 (5), 781–796. https://doi.org/10.2113/ econgeo.107.5.781.

Fortes, P.T.F.O., Martins, Pimentel M., Ventura Santos, R., Luiz, Junges S., 2003. Sm-Nd studies at Mina III gold deposit, Crix´as greenstone belt, central Brazil: implications for the depositional age of the upper metasedimentary rocks and associated Au mineralization. J. S. Am. Earth Sci. 16, 503–512. https://doi.org/10.1016/j. jsames.2003.07.001.

Fuck, R.A., Dantas, E.L., Pimentel, M.M., Botelho, N.F., Armstrong, R., Laux, J.H., Junges, S.L., Soares, J.E., Praxedes, I.F., 2014. Paleoproterozoic crust-formation and reworking events in the Tocantins Province, central Brazil: A contribution for Atlantica supercontinent reconstruction. Precambrian Research 244, 53–74. https:// doi.org/10.1016/j.precamres.2013.12.003.

Giustina, M.E.S.D., de Oliveira, C.G., Pimentel, M.M., de melo, L.V., R A, Fuck, Dantas, E. L., Buhn, B., 2009. U-pb and Sm-Nd Constraints on the Nature of the Campinorte Sequence and Related Palaeoproterozoic Juvenile Orthogneisses, Tocantins Province, Central Brazil, vol. 323. Geological Society Special Publication, pp. 255–269. https://doi.org/10.1144/SP323.12.

Gole, M.J., Barnes, S.J., 2020. The association between Ni-Cu-(PGE) sulfide and Ni-Co lateritic ores and volcanic facies within the komatiites of the 2.7 Ga East Yilgarn Craton Large Igneous Province, Western Australia. Ore Geol. Rev. 116, 103231. https://doi.org/10.1016/j.oregeorev.2019.103231. ISSN 0169-1368.

Grosch, E.G., Slama, J., 2021. On the volcanic architecture, petrology, and geodynamic setting of the 3.48 Ga Barberton komatiite suite, South Africa. S. Afr. J. Geol. 124 (2), 343–352. https://doi.org/10.25131/sajg.124.0036.

Hanski, E.J., 1992. Petrology of the Pechenga ferropicrites and cogenetic, Ni-bearing gabbro-wehrlite intrusions, Kola Peninsula, Russia. Geol. Surv. Fin. Bull. 367, 192.

Heggie, G.J., Fiorentini, M.L., Barnes, S.J., Barley, M.E., 2012. Maggie Hays Ni deposit: Part 2. Nickel mineralization and the spatial distribution of PGE ore-forming signatures in the Maggie Hays Ni system, lake Johnston greenstone belt, western Australia. Econ. Geol. 107, 797–816. https://doi.org/10.2113/econgeo.107.5.797

Heggie, G.J., Barnes, S.J., Fiorentini, M.L., 2013. Application of lithogeochemistry in the assessment of nickel- sulfide potential in komatiite belt from northern Finland and Norway. Bull. Geol. Soc. Finland 85 (1–2), 107–126. https://doi.org/10.17741/ BGSF/85.2.001.

Henrique, E., Oliveira, S.B., Fruchting, A., Boniatti, J.H., Oliveira, G.D., 2009. Aplicação conjunta dos métodos eletromagnéticos aéreo (VTEM) e de furo na pesquisa de níquel sulfetado em Goiás. SEG Global Meeting Abstracts 1090–1096. https://doi. org/10.1190/sbgf2009-235.

Houlé, M.G., Lesher, C.M., Davis, P.C., 2012. Thermomechanical erosion and genesis of komatiite-associated Ni-Cu-(PGE) mineralization at the Alexo mine, Abitibi greenstone belt, Ontario. Mineral. Deposita 47 (1–2), 105–128. https://doi.org/ 10.1007/s00126-011-0371-6.

Jahn, B.-m., Gruau, G., Glikson, A.Y., 1982. Komatiites of the Onverwacht Group, S. Africa: REE geochemistry, Sm/Nd age and mantle evolution. Contrib. Mineral. Petrol. 80, 25–40. https://doi.org/10.1007/BF00376732.

Jochum, K.P., Arndt, N.T., Hofmann, A.W., 1991. Nb-Th-La in komatiites and basalts: constraints on komatiite petrogenesis and mantle evolution. Earth Planet Sci. Lett. 107, 272–289. https://doi.org/10.1016/0012-821X(91)90076-T.

Jost, H., De Oliveira, A.M., 1991. Stratigraphy of the greenstone belts, Crixás region, Goiás, central Brazil. J. S. Am. Earth Sci. 4, 201–214. https://doi.org/10.1016/0895- 9811(91)90031-F.

Jost, H., Chemale, F., Dussin, I.A., Tassinari, C.C.G., Martins, R., 2010. A U-Pb zircon Paleoproterozoic age for the metasedimentary host rocks and gold mineralization of the Crix´ as greenstone belt, Goiás, Central Brazil. Ore Geol. Rev. 37, 127–139. https://doi.org/10.1016/j.oregeorev.2010.01.003.

Jost, H., Junior, F.C., R A, Fuck, Dussin, I.A.ˆ O., 2013. Uvá complex, the oldest orthogneisses of the archean-paleoproterozoic terrane of Central Brazil. J. S. Am. Earth Sci. 47, 201–212. https://doi.org/10.1016/j.jsames.2013.07.002.

Jost, H., Hofmann Apollo, J.F., Weber, W., Salles, R., dos, R., Marques, J.C., Massucatto, A.J., Costa, D.A., Araújo dos Santos, B., 2019. Stratigraphic update, paleotectonic, paleogeographic, and depositional environments of the Crixás Greenstone Belt, Central Brazil. J. S. Am. Earth Sci. 96, 102329. https://doi.org/ 10.1016/j.jsames.2019.102329.

Keays, R.R., Lightfoot, P.C., 2010. Crustal sulfur is required to form magmatic Ni-Cu sulfide deposits: evidence from chalcophile element signatures of Siberian and Deccan Trap basalts. Miner. Deposita 45, 241–257. https://doi.org/10.1007/ s00126-009-0271-1

Konnunaho, J., Halkoaho, T., Hanski, E., T¨ orm¨ anen, T., 2015. Chapter 3.2 - komatiite- hosted Ni-Cu-(PGE) deposits in Finland. In: Wolfgang D, Maier, Lahtinen, Raimo (Eds.), Hugh O'Brien, Mineral Deposits of Finland. Elsevier, pp. 93–131. https://doi. org/10.1016/B978-0-12-410438-9.00004-2. ISBN 9780124104389.

Kuyumjian, R.M., Jost, H., 2006. Low- and high-alumina komatiites of Goi´as, Central Brazil. J. S. Am. Earth Sci. 20, 315–326. https://doi.org/10.1016/j. jsames.2005.11.003.

Layton-Matthews, D., Lesher, C.M., Burnham, O.M., Liwanag, J., Halden, N.M., Hulbert, L., et al., 2007. Magmatic Ni–Cu–platinum group element

deposits of the Thompson Nickel Belt. In: Goodfellow, W.D. (Ed.), Mineral Deposits of Canada: a Synthesis of Major Deposit Types, District Metallogeny, the Evolution of Geological Provinces, and Exploration Methods. Geological Association of Canada Special Publication, vol. 5. Geological Association of Canada, Mineral Deposits Division, Ottawa, Ont, pp. 409–432.

Le Vaillant, M., Fiorentini, M.L., Barnes, S.J., 2016. Review of lithogeochemical exploration tools for komatiite-hosted Ni-Cu-(PGE) deposits. J. Geochem. Explor. 168, 1–19. https://doi.org/10.1016/j.gexplo.2016.05.010.

Lesher, C.M., 1989. Komatiite-associated nickel sulfide deposits. Ore deposition associated with magmas: Rev. Econ. Geol. 4, 45–101. https://doi.org/10.5382/ Rev.04.05. Lesher, C.M., 2017. Roles of xenomelts, xenoliths, xenocrysts, xenovolatiles, residues, and skarns in the genesis, transport, and localization of magmatic Fe-Ni-Cu-(PGE) sulfides and chromite. Ore Geol. Rev. 90, 465–484. https://doi.org/10.1016/j. oregeorev.2017.08.008.

Lesher, C.M., Arndt, N.T., 1995. REE and Nd isotope geochemistry, petrogenesis and volcanic evolution of contaminated komatiites at Kambalda, Western Australia. Lithos 34, 127–157. https://doi.org/10.1016/0024-4937(95)90017-9.

Lesher, C.M., Barnes, S.J., 2009. Komatiite-associated Ni-Cu-(PGE) deposits. In: Li, C., Ripley, E.M. (Eds.), Magmatic Ni-Cu-(PGE) Deposits: Genetic Models and Exploration. Geological Publishing House of China, Beijing, pp. 27–101.

Lesher, C.M., Burnham, O.M., 2001. Multicomponent elemental and isotopic mixing in Ni-Cu-(PGE) ores at Kambalda, Western Australia. Can. Mineral. 39, 421–446. https://doi.org/10.2113/gscanmin.39.2.421.

Lesher, C.M., Campbell, I.H., 1993. Geochemical and fluid dynamic modelling of composi- tional variations in Archean komatiite-hosted nickel sulfide ores in Western Australia. Econ. Geol. 88, 804–816. Lesher, C.M., Groves,

D.I., 1986. Controls on the formation of komatiite-associated nickel-copper sulfide deposits. In: Friedrich, G.H. (Ed.), Geology and Metallogeny of Copper Deposits. Springer Verlag, Berlin. https://doi.org/10.1007/978-3-642- 70902-9_4.

Lesher, C.M., Keays, R.R., 2002. In: Cabri, L.J. (Ed.), The Geology, Geochemistry, Mineralogy, and Mineral Beneficiation of the Platinum-Group Elements, 54. Canadian Institute of Mining, Metallurgy and Petroleum, Special, pp. 579–617.

Lesher, C.M., Stone, W.E., 1996. Exploration geochemistry of komatiites. In: Wyman, D. (Ed.), Igneous Trace Element Geochemistry: Applications for Massive Sulphide Exploration, vol. 12. Geological Association of Canada, Short Course Notes, pp. 153–204.

Lesher, C.M., Lee, R.F., Groves, D.I., Bickle, M.J., Donaldson, M.J., 1981. Geochemistry of komatiites from Kambalda, Western Australia: I. Chalcophile element depletion - a consequence of sulfide liquid separation from komatiitic magmas. Econ. Geol. 76, 1714–1728. https://doi.org/10.2113/gsecongeo.76.6.1714.

Lesher, C.M., Arndt, N.T., Groves, D.I., 1984. Genesis of komatiite- associated nickel sulphide deposits at Kambalda, Western Australia: a distal volcanic model. In: Buchanan, D.L., Jones, M.J. (Eds.), Sulphide Deposits in Mafic and Ultramafic Rocks. Institution of Mining and Metallurgy, London, pp. 70–80.

Lesher, C.M., Barnes, S.-J., Gillies, S.L., Ripley, E.M., 1999. Ni-Cu-(PGE) sulphides in the raglan block. In: Lesher, C.M. (Ed.), Komatiitic Peridotite-Hosted Fe-Ni-Cu-(PGE) Sulphide Deposits in the Raglan Area, Cape Smith Belt, New Qu´ ebec. Guidebook Series 2, Mineral Exploration Research Centre. Laurentian University, Sudbury, pp. 177–184.

Lesher, C.M., Burnham, O.M., Keays, R.R., Barnes, S.J., Hulbert, L., 2001. Trace-element geochemistry and petrogenesis of barren and ore-associated komatiites. Can. Mineral. 39, 673–696. https://doi.org/10.2113/gscanmin.39.2.673.

Li, C., Ripley, E.M., 2009. Sulfur contents at sulfide-liquid or anhydrite saturation in silicate melts Empirical equations and example applications. Econ. Geol. 104, 405–412. https://doi.org/10.2113/gsecongeo.104.3.405.

Lightfoot, P.C., Keays, R.R., Evans-Lamswood, D., Wheeler, R., 2012. S saturation history of Nain Plutonic Suite mafic intrusions: origin of the Voisey's Bay Ni-Cu-Co sulfide deposit, Labrador, Canada. Miner. Deposita 47, 23–50. https://doi.org/10.1007/ s00126-011-0347-6.

Lowe, D.R., 2024. Onverwacht group, Barberton greenstone belt, South Africa: 300 m.y. development of a paleoarchean stagnant lid. GSA Bulletin. https://doi.org/10.1130/ B37573.1.

Lu, Y., Lesher, C.M., Deng, J., 2019. Geochemistry and genesis of magmatic Ni–Cu–(PGE) and PGE–(Cu)–(Ni) deposits in China. Ore. Geol. Rev. 107, 863–887.

Luolavirta, K., 2018. Magmatic Evolution of the Kevitsa Igneous Complex, Northern Finland, and its Relation to the Associated Ni-Cu-(PGE) Mineralization. University of Oulu, Thesis, p. 68. Oulu Mining School, P.O. Box 3000, FIN-90014 Oulun yliopisto, Finland. URL: https://www.researchgate.net/publication/333508201_Magmatic_evolution_of_the_Kevitsa_igneous_complex_northern_Finland_and_its_relation_to_the_ associated_Ni-Cu-PGE_mineralization.

Makkonen, H.V., Halkoaho, T., Konnunaho, J., Rasilainen, Kontinen, A., Eilu, P., 2017. Ni-(Cu-PGE) deposits in Finland – geology and exploration potential. Ore Geol. Rev. 90 (2017), 667–696. https://doi.org/10.1016/j.oregeorev.2017.06.008. ISSN 0169- 1368.

Martin, H., Smithies, R.H., Rapp, R., Moyen, J.-P., Champion, D., 2005. An overview of adakite, tonalite– trondhjemite–granodiorite (TTG), and sanukitoid: relationships and some implications for crustal evolution. Lithos 79, 1–24. https://doi.org/ 10.1016/j.lithos.2004.04.048.

Martins-Ferreira, M.A.C., Dias, A.N.C., Chemale, F., Campos, J.E.G., Seraine, M., Novais- Rodrigues, E., 2020. Multi-stage crustal accretion by magmatic flare-up and quiescence intervals in the western margin of the

S˜ãoo Francisco Craton: U-Pb-Hf and geochemical constraints from the Almas Terrane. Gondwana Res. 85, 32–54. https:// doi.org/10.1016/j.gr.2020.04.005.

McDonough, W.F., Sun, S.s., 1995. The composition of the Earth. Chem. Geol. 120, 223–253. https://doi.org/10.1016/0009-2541(94)00140-4.

Monster, J., Appel, P.W.U., Thode, H.G., Schidlowski, M., Carmichael, C.M., Bridgwater, D., 1979. Sulfur isotope studies in early Archaean sediments from Isua, West Greenland: implications for the antiquity of bacterial sulfate reduction. Geochem. Cosmochim. Acta 43, 405–413. https://doi.org/10.1016/0016-7037(79) 90205-9.

Murck, B.W., Campbell, I.H., 1986. The effect of temperature, oxygen fugacity, and melt composition on the behaviour of chromium in basic and ultrabasic melts. Geochem. Cosmochim. Acta 50, 1871–1887. https://doi.org/10.1016/0016-7037(86)90245-0.

Naldrett, A.J., 1966. The role of sulphurization in the genesis of iron-nickel sulphide deposits of the Porcupine District, Ontario. Can. Inst. Mining Metal. Trans. 69, 147–155.

Naldrett, A.J., 1989. Magmatic Sulfide Deposits. Oxford Monographs on Geology and Geophysics No. 14. Vii + 186. Oxford University Press, New York, Oxford. https:// doi.org/10.1017/S001675680001400X. ISBN 0 19 505119 X. Geological Magazine. 1990;127(2):188-188.

Nesbitt, R.W., Sun, S.-S., Purvis, A.C., 1979. Komatiites: geochemistry and genesis. Can. Mineral. 17, 165–186. URL: https://rruff.geo.arizona.edu/doclib/cm/vol17/CM1 7_165.pdf.

Perring, C.S., 2015. Volcanological and structural controls on mineralization at the Mount Keith and Cliffs komatiite-associated nickel sulfide deposits, Agnew-Wiluna belt, Western Australia-implications for ore genesis and targeting. Econ. Geol. 110, 1669–1695.

Perring, C.S., Barnes, S.J., Hill, R.E.T., 1996. Geochemistry of komatiites from Forrestania, southern cross province, western Australia: evidence for

crustal contamination. Lithos 37, 181–197. https://doi.org/10.1016/0024-4937(95)00036- 4.

Pimentel, M.M., 2016. The tectonic evolution of the Neoproterozoic Brasília Belt, central Brazil: a geochronological and isotopic approach. Brazilian Journal of Geology 46, 67–82. https://doi.org/10.1590/2317-4889201620150004.

Pina, R., Gervilla, F., Ortega, L., Lunar, R., 2012. Geochemical constraints on the origin of the Ni–Cu sulfide ores in the tejadillas prospect (cortegana igneous complex, SW Spain). Resour. Geol. 62, 263–280. https://doi.org/10.1111/j.1751- 3928.2012.00194.x.

Qi, H.P., Coplen, T.B., 2003. Evaluation of the 34S/32S ratio of Soufre de Lacq elemental sulfur isotopic reference material by continuous flow isotope-ratio mass spectrometry. Chem. Geol. 199, 183–187. https://doi.org/10.1016/S0009-2541(03) 00075-5.

Queffurus, M., Barnes, S.J., 2014. Selenium and sulfur concentrations in country rocks from the Duluth Complex, Minnesota, USA: implications for the formation of the Cu- Ni-PGE sulfides. Econ. Geol. 109, 785–794. https://doi.org/10.2113/ econgeo.109.3.785.

Queffurus, M., Barnes, S.J., 2015. A review of sulfur to selenium ratios in magmatic nickel-copper and platinum-group element deposits. Ore Geol. Rev. 69, 301–324. https://doi.org/10.1016/j.oregeorev.2015.02.019.

Queiroz, C.L., Jost, H., Silva, L.C., McNaughton, N.J., 2008. U-Pb SHRIMP and Sm-Nd geochronology of granite-gneiss complexes and implications for the evolution of the Central Brazil Archean Terrain. J. S. Am. Earth Sci. 26, 100–124. https://doi.org/ 10.1016/j.jsames.2007.07.007.

Ripley, E.M., Li, C., 2013. Sulfide saturation in mafic mag- mas: is external sulfur required for magmatic Ni-Cu- (PGE) ore deposits. Econ. Geol. 108 (1), 45–58. https://doi.org/10.2113/econgeo.108.1.45.

Ripley, E.M., Li, C., 2017. A review of the application of multiple s isotopes to magmatic Ni-Cu-(PGE) deposits and the significance of spatially variable

Δ33S Values. Econ. Geol. 112 (4), 983–991. https://doi.org/10.2113/econgeo.112.4.983.

Robertson, J., Ripley, E.M., Barnes, S.J., Li, C., 2015. Sulfur liberation from country rocks and incorporation in mafic magmas. Econ. Geol. 110, 1111–1123. https://doi.org/ 10.2113/econgeo.110.4.1111.

Robin-Popieul, C.C.M., Arndt, N.T., Chauvel, C., Byerly, G.R., Sobolev, A.V., Wilson, A., 2012. A new model for Barberton komatiites: deep critical melting with high melt retention. J. Petrol 53, 2191–2229.

Sabóia, L.A., Teixeira, N.A., 1980. Lavas ultrab´asicas da unidade basal do Greenstone Belt de Crixás (GO): Uma nova classe de rochas ultram´ aficas no Estado de Goiás. Rev. Bras. Geociencias 10, 28–42. URL: http://bjg.siteoficial.ws/1980/n1/saboia. pdf.

Sabóia, L.A., Teixeira, N.A., 1983. Ultramafic flows of the Crixas greenstone belt, Goias - Brazil. Precambr. Res. 22, 23–40. https://doi.org/10.1016/0301-9268(83)90057-8.

Sabóia, A.M., de Oliveira, C.G., Dantas, E.L., Cordeiro, P., Scandolara, J.E., Rodrigues, J. B., de Sousa, I.M.C., 2020. The Siderian crust (2.47–2.3 Ga) of the Goiás Massif and its role as a building block of the Sao Francisco paleocontinent. Precambr. Res. 350, 105901. https://doi.org/10.1016/j.precamres.2020.105901.

Samalens, N., Barnes, S.-J., Sawyer, E.W., 2017. The role of black shales as a source of sulfur and semimetals in magmatic nickel-copper deposits: example from the Partridge River Intrusion, Duluth Complex, Minnesota, USA. Ore Geol. Rev. 81, 173–187. https://doi.org/10.1016/j.oregeorev.2016.09.030.

Sharp, Z.D., 2017. Principles of Stable Isotope Geochemistry 385. https://doi.org/ 10.25844/h9q1-0p82.

Skrzypek, G., Dunn, P.J.H., 2020. Absolute isotope ratios defining isotope scales used in isotope ratio mass spectrometers and optical isotope instruments. Rapid Commun. Mass Spectrom. 34, 1–5. https://doi.org/10.1002/rcm.8890.

Smith, P.M., Asimow, P.D., 2005. Adiabat_1ph: a new public front-end to the MELTS, pMELTS, and pHMELTS models: adiabat_1PH front-end. G-cubed 6 (2). https://doi. org/10.1029/2004GC000816.

Smith, J.W., Holwell, D.A., McDonald, I., Boyce, A.J., 2016. The application of S isotopes and S/Se ratios in determining ore-forming processes of magmatic Ni-Cu-(PGE) sulfide deposits: a cautionary case study from the northern Bushveld Complex. Ore Geol. Rev. 73, 148–174. https://doi.org/10.1016/j.oregeorev.2015.10.022.

Sproule, R.A., Lesher, C.M., Ayer, J.A., Thurston, P.C., Herzberg, C.T., 2002. Spatial and temporal variations in the geochemistry of komatiites and komatiitic basalts in the Abitibi greenstone belt (Precambrian Research (2002) 115 (153-186)). Precambr. Res. 126, 169–172. https://doi.org/10.1016/S0301-9268(03)00219-5.

Staude, S., Oelze, M., Markl, G., 2022. Multi-stage sulfide evolution of the Moran Ni sulfide ore, Kambalda, Western Australia: insights into the dynamics of ore forming processes of komatiite-hosted deposits. Miner. Deposita 57, 889–909. https://doi. org/10.1007/s00126-021-01060-5.

Staude, S., Martin, L.A., Aleshin, M., et al., 2024. The multiple sulfur isotope architecture of the Kambalda nickel camp, Western Australia. Miner. Deposita 59, 505–518. https://doi.org/10.1007/s00126-023-01223-6.

Stiegler, M.T., Cooper, M., Byerly, G.R., Lowe, D.R., 2012. Geochemistry and petrology of komatiites of the pioneer ultramafic complex of the 3.3Ga Weltevreden formation, Barberton greenstone belt, South Africa. Precambr. Res. 212–213, 1–12. https://doi. org/10.1016/j.precamres.2012.04.017.

Tormanen, T., Konnunaho, J.P., Hanski, E., Moilanen, M., Heikura, P., 2016. The paleoproterozoic komatiite-hosted PGE mineralization at Lomalampi, central Lapland greenstone belt, northern Finland. Miner. Deposita 51, 411–430. https://doi.org/ 10.1007/s00126-015-0615-y.

Virnes, A.B., Fiorentini, M.L., Barnes, S.J., Caruso, S., Martin, L.A.J., Aleshin, M., Schoneveld, L.E., Roberts, M.P., Masurel, Q., Thebaud, N., 2023.

Decoupling of sulfur isotope signatures from platinum group elements in komatiite-hosted ore systems: evidence from the Mount Keith MKD5 Ni-(Co-Cu) deposit, western Australia. Econ. Geol. 118 (8), 1813–1834. https://doi.org/10.5382/econgeo.5030.

Virtanen, V.J., Heinonen, J.S., Molnár, F., et al., 2021. Fluids as primary carriers of sulphur and copper in magmatic assimilation. Nat. Commun. 12, 6609. https://doi. org/10.1038/s41467-021-26969-3.

Virtanen, V.J., Heinonen, J.S., Marki, L., et al., 2024. Sedimentary and metamorphic processes priming black shale for magmatic assimilation of sulfur: an example from the Virginia Formation, Minnesota, United States. Miner. Deposita. https://doi.org/ 10.1007/s00126-024-01268-1.

Yao, Z.-S., Mungall, J.E., 2021. Kinetic controls on the sulfide mineralization of komatiite-associated Ni-Cu-(PGE) deposits. Geochem. Cosmochim. Acta 305, 185–211. https://doi.org/10.1016/j.gca.2021.05.009.

Appendix A

Whole-rock geochemistry of the Crixás komatiite

Sample	BVD31 62.40	BVD31 83,15	BVD31 95.40	BVD31 122.80	BVD32 70.70	BVD32 92.18	BVD32 93.30	KT-161A
Rock	Tremolitite	Tremolitite	Tremolitite	Tremolitite	Tremolitite	Tremolitite	Tremolitite	Tremolite-serpentinite
SiO2 (wt. %)	50.82	45.95	47.48	45.90	44.71	42.67	48.88	42.25
TiO2 (wt. %)	0.41	0.46	0.56	0.56	0.54	0.69	0.58	0.43
Al2O3 (wt. %)	0.99	2.19	3.02	3.15	3.32	3.48	2.34	4.50
FeO (wt. %)	14.48	19.75	15.05	17.47	16.89	20.15	11.61	15.04
MnO (wt. %)	0.19	0.21	0.20	0.20	0.20	0.19	0.20	0.19
MgO (wt. %)	22.39	21.68	23.53	23.28	26.51	26.39	28.81	35.17
CaO (wt. %)	10.16	9.06	9.21	8.65	6.87	5.69	6.53	3.84
Na2O (wt. %)	0.52	0.68	0.93	0.73	0.92	0.69	1.02	0.06
K2O (wt. %)	0.01	0.01	0.01	0.01	0.01	0.01	0.01	0.00
P2O5 (wt. %)	0.01	0.02	0.02	0.04	0.02	0.03	0.02	0.02
LOI (wt. %)	4.12	4.40	4.36	5.90	7.94	7.54	7.27	11.38
Ce (ppm)	1.22	3.54	6.16	8.26	4.85	2.43	4.59	4.44
Cr (ppm)	1591.00	2287.10	2031.00	2361.20	2145.80	2783.90	2173.20	L.D.L.
Cs (ppm)	N.A.	0.04	0.01	0.02	0.06	0.05	0.06	0.19
Dy (ppm)	1.09	1.20	1.57	1.63	1.28	1.12	1.23	1.16
Er (ppm)	0.56	0.57	0.70	0.75	0.62	0.52	0.54	0.67
Eu (ppm)	0.31	0.32	0.47	0.55	0.41	0.31	0.37	0.38
Gd (ppm)	1.08	1.22	1.64	1.75	1.33	1.17	1.26	1.16
Hf (ppm)	0.57	0.49	0.60	0.66	0.73	1.00	0.63	0.38
Ho (ppm)	0.18	0.19	0.26	0.26	0.20	0.18	0.19	0.24
La (ppm)	0.31	1.17	2.15	3.00	1.64	0.74	1.73	1.86
Lu (ppm)	0.02	0.02	0.04	0.04	0.04	0.04	0.03	0.10
Nb (ppm)	1.53	1.37	1.83	1.83	1.74	2.10	1.76	1.01
Nd (ppm)	1.92	3.26	5.27	6.13	4.02	2.56	3.61	3.54
Pr (ppm)	0.29	0.62	1.04	1.32	0.83	0.46	0.74	0.71
Rb (ppm)	0.18	0.24	0.17	0.19	0.52	0.46	0.36	1.29
Sm (ppm)	0.86	1.14	1.53	1.67	1.19	0.95	1.14	0.98
Sr (ppm)	18.60	11.20	14.60	13.90	46.60	27.30	18.10	74.81
Ta (ppm)	0.08	0.07	0.10	0.10	0.10	0.13	0.10	0.08
Tb (ppm)	0.15	0.16	0.22	0.26	0.17	0.15	0.16	0.20
Th (ppm)	0.07	0.08	0.15	0.18	0.14	0.13	0.12	0.13
Tm (ppm)	L.D.L.	L.D.L.	0.03	0.03	0.02	L.D.L.	L.D.L.	0.11
U (ppm)	L.D.L.	L.D.L.	L.D.L.	L.D.L.	0.02	0.03	L.D.L.	0.04
V (ppm)	94.40	108.80	101.70	126.20	123.80	135.90	111.50	N.A.
Y (ppm)	6.58	6.98	8.58	8.79	7.11	6.40	6.84	6.90
Yb (ppm)	0.46	0.43	0.54	0.53	0.52	0.44	0.46	0.58
Zr (ppm)	17.74	14.95	18.48	18.96	23.63	33.16	21.58	10.85
Co (ppm)	58.40	97.20	93.00	107.90	94.00	110.20	95.00	N.A.
Cu (ppm)	25.30	85.50	76.80	22.30	21.20	22.20	42.60	N.A.
Ni (ppm)	969.80	1357.20	1136.90	1433.80	1374.30	1633.60	1571.80	N.A.
Sc (ppm)	14.70	22.30	22.50	21.10	22.90	29.70	23.20	N.A.
Zn (ppm)	54.90	61.00	69.50	65.30	74.90	73.40	73.90	N.A.

L.D.L. = Lower than detection limit

N.A. = not analyzed

KT-12A	KT-12B	KT-12C	KT-12D	KT-26A	KT-161E	BVD32 66.00
Tremolite-serpentinite	Tremolite-serpentinite	Tremolite-serpentinite	Tremolite-serpentinite	Serpentine-tremolitite	Serpentine-tremolitite	Serpentinite
43.13	44.74	43.52	43.06	45.52	44.89	46.24
0.61	0.57	0.68	0.60	0.53	0.47	0.26
3.33	2.51	2.55	2.97	4.04	1.25	2.32
16.77	19.85	20.84	18.15	16.48	14.86	12.81
0.21	0.19	0.18	0.20	0.18	0.19	0.17
30.89	26.83	26.71	30.71	26.66	29.59	35.66
6.59	7.04	7.38	5.96	7.97	10.09	1.21
0.12	0.17	0.17	0.12	0.20	0.16	1.31
0.01	0.02	0.01	0.00	0.01	0.00	0.01
0.03	0.06	0.05	0.07	0.07	0.00	0.01
8.82	5.25	6.02	8.90	4.97	9.59	11.10
3.84	3.48	3.53	4.35	3.95	3.29	1.87
L.D.L.	L.D.L.	L.D.L.	L.D.L.	L.D.L.	L.D.L.	1434.20
0.17	0.11	0.12	0.18	0.05	0.03	0.19
1.28	1.21	1.20	1.33	1.68	1.04	0.67
0.76	0.60	0.60	0.74	0.93	0.53	0.38
0.45	0.36	0.40	0.44	0.51	0.42	0.21
1.38	1.34	1.26	1.46	1.76	1.02	0.58
0.25	0.41	0.38	0.35	0.54	0.46	0.39
0.27	0.24	0.25	0.28	0.36	0.20	0.08
2.02	1.31	1.26	1.68	2.35	1.12	0.59
0.09	0.08	0.07	0.09	0.12	0.06	0.04
1.32	1.29	1.48	1.27	1.28	0.98	0.90
4.03	3.47	3.58	4.17	4.47	2.98	1.55
0.80	0.62	0.62	0.79	0.85	0.54	0.28
0.70	0.75	0.70	0.67	0.31	0.14	0.48
1.30	1.16	1.23	1.27	1.38	0.91	0.50
110.73	25.55	53.49	77.81	24.75	204.41	L.D.L.
0.09	0.09	0.11	0.12	0.09	0.06	0.04
0.22	0.21	0.20	0.22	0.27	0.18	0.06
0.15	0.13	0.11	0.13	0.12	0.06	0.06
0.10	0.08	0.08	0.10	0.13	0.07	L.D.L.
0.04	0.02	0.02	0.03	0.04	0.02	0.06
N.A.	N.A.	N.A.	N.A.	N.A.	N.A.	72.20
7.91	5.69	6.12	7.00	11.83	5.19	4.24
0.61	0.47	0.50	0.58	0.77	0.41	0.38
4.92	9.01	9.49	9.21	15.47	14.01	11.50
N.A.	N.A.	N.A.	N.A.	N.A.	N.A.	121.90
N.A.	N.A.	N.A.	N.A.	N.A.	N.A.	50.20
N.A.	N.A.	N.A.	N.A.	N.A.	N.A.	1966.50
N.A.	N.A.	N.A.	N.A.	N.A.	N.A.	13.30
N.A.	N.A.	N.A.	N.A.	N.A.	N.A.	97.30

KT-161D	KT-161F	KT-161G	KT-25B	KT-27	KT-161B	KT-161C
Tremolite-serpentinite	Tremolite-serpentinite	Tremolite-serpentinite	Serpentinite	Serpentinite	Tremolite-serpentinite	Serpentinite
44.85	43.71	45.41	43.86	44.66	44.25	43.94
0.56	0.41	0.42	0.54	0.25	0.32	0.28
3.61	2.36	2.35	4.19	3.12	2.16	2.03
15.55	14.17	14.47	16.22	11.75	12.70	12.18
0.23	0.18	0.18	0.15	0.17	0.16	0.17
32.49	34.32	33.13	34.86	41.03	38.25	40.80
4.15	6.16	5.37	1.74	0.19	3.36	1.77
0.09	0.09	0.09	0.05	0.02	0.06	0.02
0.00	0.00	0.00	0.00	0.00	0.00	0.00
0.04	0.02	0.02	0.01	0.00	0.01	0.01
8.09	10.98	8.93	9.74	11.63	11.71	12.65
2.12	3.43	3.52	1.28	2.62	2.12	1.64
L.D.L.	L.D.L.	L.D.L.	L.D.L.	L.D.L.	L.D.L.	L.D.L.
0.19	0.08	0.06	0.25	0.11	0.02	0.02
0.97	1.01	N.A.	1.21	0.73	0.62	0.36
0.60	0.55	0.52	0.79	0.51	0.32	0.20
0.33	0.40	0.38	0.38	0.17	0.23	0.14
1.05	0.98	1.01	1.18	0.69	0.66	0.40
0.48	0.37	0.51	0.61	0.25	0.34	0.29
0.23	0.20	0.22	0.28	0.18	0.13	0.08
1.66	1.25	1.34	3.10	1.35	0.77	0.58
0.09	0.07	0.08	0.11	0.08	0.05	0.03
1.19	0.85	0.96	1.23	0.69	0.78	0.59
2.70	2.85	2.84	2.83	1.99	1.82	1.33
0.52	0.58	0.56	0.58	0.43	0.34	0.27
1.04	0.30	0.25	0.60	0.42	0.12	0.08
0.84	0.86	0.88	0.87	0.60	0.58	0.40
15.51	139.74	122.54	3.43	13.54	60.27	72.22
0.09	0.07	0.08	0.09	0.05	0.06	0.04
0.16	0.17	0.16	0.21	0.11	0.10	0.06
0.12	0.09	0.09	0.13	0.05	0.08	0.03
0.08	0.07	0.08	0.10	0.09	0.05	0.03
0.03	0.03	0.03	0.10	0.05	0.02	0.01
L.D.L.	N.A.	N.A.	N.A.	N.A.	N.A.	N.A.
5.96	5.02	5.25	9.61	5.33	3.17	2.08
0.48	0.46	0.48	0.70	0.48	0.32	0.19
15.83	11.40	17.09	20.72	7.48	11.90	9.99
N.A.	N.A.	N.A.	N.A.	N.A.	N.A.	N.A.
N.A.	N.A.	N.A.	N.A.	N.A.	N.A.	N.A.
N.A.	N.A.	N.A.	N.A.	N.A.	N.A.	N.A.
N.A.	N.A.	N.A.	N.A.	N.A.	N.A.	N.A.
N.A.	N.A.	N.A.	N.A.	N.A.	N.A.	N.A.

‹T-161H	KT-162	BVD22 174.10	BVD22 177.25	BVD22 178.40	BVD22 184.20	BVD31 130.15	BVD32 78.52	BVD14 102.00
ɛrpentinite	Serpentinite	Tremolitite	Tremolitite	Tremolitite	Tremolitite	Tremolitite	Tremolitite	Serpentinite
44.91	42.44	53.49	49.22	50.17	49.67	43.14	46.59	43.48
0.21	0.36	0.37	0.53	0.49	0.85	0.58	0.52	0.12
2.94	4.01	2.90	3.77	3.68	4.34	3.58	3.25	1.46
11.64	13.96	10.71	14.78	13.81	15.69	19.73	16.58	13.64
0.16	0.20	0.23	0.17	0.16	0.24	0.21	0.20	0.11
41.18	40.33	20.70	22.13	21.69	21.75	23.01	23.15	37.39
0.11	0.08	11.16	8.72	9.73	6.50	9.12	8.87	2.25
0.02	0.02	0.39	0.63	0.23	0.89	0.59	0.82	1.53
0.00	0.00	0.01	0.01	0.01	0.01	0.01	0.01	0.01
0.00	0.00	0.03	0.03	0.04	0.06	0.03	0.01	0.01
11.35	11.03	3.57	4.98	4.90	5.02	6.92	5.20	17.60
2.40	2.58	2.82	6.61	4.98	4.73	8.62	7.52	2.78
L.D.L.	L.D.L.	1314.90	1782.10	1578.10	1148.30	2426.50	2105.30	1263.80
0.04	0.02	0.06	N.A.	N.A.	N.A.	0.05	0.02	0.06
0.62	0.44	1.57	1.87	2.04	1.61	1.66	1.69	0.51
0.39	0.30	0.86	1.02	1.09	0.71	0.84	0.81	0.21
0.20	0.14	0.45	0.31	0.32	0.23	0.61	0.54	0.14
0.58	0.39	1.59	1.80	1.94	1.63	1.84	1.81	0.50
0.23	0.25	0.84	1.25	1.00	1.43	0.80	0.80	0.17
0.14	0.11	0.30	0.36	0.39	0.26	0.28	0.29	N.A.
0.90	1.23	0.91	2.43	1.72	1.49	3.37	2.69	1.18
0.06	0.08	0.10	0.10	0.11	0.06	0.06	0.06	N.A.
0.62	0.98	4.72	1.94	2.14	8.16	1.84	1.80	0.48
1.77	1.34	3.14	5.18	4.55	4.38	6.39	5.72	1.85
0.35	0.33	0.54	1.09	0.86	0.84	1.35	1.23	0.39
0.18	0.15	0.31	0.11	0.11	0.14	0.26	0.37	0.30
0.51	0.38	1.28	1.60	1.62	1.43	1.73	1.59	0.47
18.07	17.79	29.70	26.00	30.40	19.90	33.00	62.00	37.10
0.33	0.07	0.26	0.10	0.11	0.30	0.11	0.10	0.03
0.10	0.07	0.22	0.27	0.30	0.23	0.24	0.24	N.A.
0.07	0.08	0.08	0.16	0.18	0.15	0.22	0.21	0.05
0.06	0.06	0.07	0.07	0.10	0.03	0.04	0.04	N.A.
0.03	0.05	0.05	0.05	0.04	0.07	N.A.	0.04	N.A.
N.A.	N.A.	103.50	119.20	105.70	119.60	140.50	124.80	30.70
3.57	2.70	9.96	10.12	12.61	8.57	8.92	9.41	3.05
0.41	0.48	0.73	0.85	0.98	0.64	0.71	0.57	0.20
6.88	7.56	27.10	40.10	33.30	45.57	24.95	24.41	5.59
N.A.	N.A.	90.50	106.70	70.90	134.70	107.00	L.D.L.	120.80
N.A.	N.A.	14.80	130.40	91.60	8.20	73.70	168.00	116.50
N.A.	N.A.	1104.10	1127.40	1306.40	281.20	1602.10	1398.80	2858.00
N.A.	N.A.	18.50	22.20	16.80	29.50	26.00	23.00	10.40
N.A.	N.A.	175.30	132.20	142.00	294.80	60.70	90.90	219.70

BVD14 105.40	BVD14 109.35	BVD14 110.55	BV0D14 114.3	BVD14 118.80	KT-54	KT-55
Serpentinite	Serpentinite	Serpentinite	Serpentinite	Carb-talc	Tremolite-serpentinite	Olivine-serpentinite
41.40	41.30	40.54	43.05	34.04	44.43	44.99
0.19	0.18	0.17	0.16	0.21	0.12	0.13
1.37	1.44	1.59	1.40	1.42	4.13	6.36
14.91	16.93	17.49	16.96	23.57	10.28	10.57
0.13	0.12	0.11	0.11	0.27	0.09	0.12
40.56	39.22	37.34	37.14	39.33	38.51	33.83
1.16	0.37	1.27	0.11	0.77	3.35	4.82
0.24	0.42	1.48	1.05	0.35	0.12	0.24
0.01	0.01	0.01	0.01	0.01	0.00	0.00
0.01	0.01	0.01	0.01	0.02	0.00	0.00
17.83	17.68	16.98	15.82	15.86	10.87	7.24
1.74	2.92	1.60	2.20	16.55	0.82	0.59
1378.00	1746.60	1807.90	1829.40	1454.80	L.D.L.	L.D.L.
0.07	0.13	0.12	0.09	0.10	0.07	0.07
0.39	0.48	0.59	0.51	0.72	0.39	0.53
0.19	0.23	0.30	0.23	0.34	0.27	0.44
0.08	0.06	0.07	0.03	0.19	0.07	0.11
0.37	0.44	0.51	0.46	1.14	0.28	0.32
0.22	0.25	0.36	0.21	0.21	0.09	0.07
N.A.	N.A.	N.A.	N.A.	0.05	0.09	0.14
0.68	1.21	0.60	0.87	7.29	0.33	0.24
N.A.	N.A.	N.A.	N.A.	0.04	0.06	0.08
0.55	0.60	0.66	0.58	0.75	0.14	0.12
1.18	1.86	1.21	1.52	9.57	0.55	0.53
0.23	0.39	0.23	0.30	2.35	0.11	0.10
0.26	0.39	0.43	0.40	0.44	0.18	0.28
0.34	0.47	0.40	0.40	1.79	0.20	0.16
17.10	2.00	18.90	N.A.	8.60	67.74	27.70
0.03	0.04	0.05	0.04	0.04	0.02	0.01
N.A.	N.A.	N.A.	N.A.	0.08	0.05	0.07
0.04	0.08	0.06	0.04	0.32	0.02	0.02
N.A.	N.A.	N.A.	N.A.	N.A.	0.05	0.06
N.A.	N.A.	N.A.	N.A.	N.A.	0.02	0.01
37.80	46.30	54.20	47.40	30.50	N.A.	N.A.
2.55	3.10	3.89	3.13	3.70	2.61	3.76
0.23	0.23	0.23	0.21	0.43	0.32	0.48
6.85	7.67	11.41	6.66	6.63	2.82	2.05
116.70	162.30	184.10	124.60	180.00	N.A.	N.A.
167.50	383.80	406.00	279.60	1276.00	N.A.	N.A.
2907.70	4069.50	4469.30	3294.90	7301.20	N.A.	N.A.
9.50	11.40	10.90	13.40	11.90	N.A.	N.A.
227.40	246.50	242.00	254.10	232.20	N.A.	N.A.

KT-56A	KT-56B	KT-75	KT-138B	KT-142B	KT-146	KT-70A
Tremolitite	Tremolite-serpentinite	Tremolite-serpentinite	Tremolitite	Tremolitite	Olivine-tremolitite	Serpentinite
45.31	45.28	46.08	41.96	47.54	46.21	42.89
0.30	0.28	0.14	0.11	0.16	0.17	0.25
5.33	4.33	4.39	4.07	5.02	4.71	7.13
12.98	12.94	11.77	13.30	10.62	11.00	12.37
0.14	0.12	0.15	0.14	0.17	0.15	0.12
31.09	32.76	34.77	40.59	32.52	34.35	35.42
5.89	5.39	3.80	1.07	4.80	4.35	3.00
0.25	0.18	0.09	0.09	0.23	0.16	0.04
0.00	0.00	0.00	0.00	0.00	0.00	0.00
0.00	0.02	0.00	0.00	0.00	0.00	0.01
5.92	7.01	7.38	7.57	6.27	8.38	9.33
1.11	1.58	0.60	0.33	0.49	0.63	0.66
L.D.L.	L.D.L.	L.D.L.	L.D.L.	L.D.L.	L.D.L.	L.D.L.
0.09	0.10	0.04	0.10	0.19	0.16	0.04
0.74	0.78	0.42	0.17	0.53	0.51	0.46
0.44	0.50	0.32	0.14	0.39	0.36	0.34
0.15	0.16	0.09	0.04	0.10	0.09	0.07
0.54	0.66	0.27	0.10	0.33	0.34	0.35
0.21	0.15	0.21	0.16	0.17	0.12	0.21
0.17	0.18	0.10	0.04	0.12	0.13	0.11
0.37	0.60	0.19	0.12	0.16	0.27	0.26
0.07	0.08	0.05	0.05	0.08	0.06	0.06
0.49	0.47	0.13	0.07	0.17	0.18	0.23
1.02	1.37	0.47	0.21	0.48	0.59	0.60
0.19	0.27	0.10	0.04	0.08	0.10	0.10
0.17	0.23	0.11	0.15	0.41	0.36	0.17
0.40	0.51	0.18	0.08	0.22	0.19	0.23
55.12	79.20	50.34	7.18	21.43	17.23	13.89
0.05	0.04	0.09	0.01	0.03	0.02	2.55
0.11	0.12	0.06	0.02	0.07	0.08	0.07
0.03	0.04	0.02	0.01	0.02	0.02	0.02
0.08	0.07	0.05	0.03	0.06	0.05	0.05
0.01	0.03	0.01	N.A.	0.01	0.01	0.04
N.A.	N.A.	N.A.	N.A.	N.A.	N.A.	N.A.
4.29	4.51	2.67	1.25	3.34	3.27	3.11
0.44	0.45	0.35	0.20	0.40	0.37	0.36
5.03	4.24	0.60	5.91	4.20	3.31	5.50
N.A.	N.A.	N.A.	N.A.	N.A.	N.A.	N.A.
N.A.	N.A.	N.A.	N.A.	N.A.	N.A.	N.A.
N.A.	N.A.	N.A.	N.A.	N.A.	N.A.	N.A.
N.A.	N.A.	N.A.	N.A.	N.A.	N.A.	N.A.
N.A.	N.A.	N.A.	N.A.	N.A.	N.A.	N.A.

KT-70B	KT-06	KT-08B	KT-09	KT-10	KT-19B
Tremolite-serpentinite	Tremolite-serpentinite	Olivine-serpentinite	Olivine-tremolitite	Tremolite-serpentinite	Olivine-tremolitite
44.34	43.45	43.24	42.86	44.82	42.63
0.23	0.48	0.47	0.40	0.33	0.57
6.02	3.96	3.49	3.19	2.20	4.38
11.41	15.76	16.04	16.15	12.63	16.84
0.12	0.26	0.27	0.29	0.21	0.24
35.72	33.64	33.26	34.18	37.38	31.61
3.27	3.89	4.59	4.30	3.53	5.10
0.03	0.13	0.19	0.20	0.16	0.24
0.00	0.00	0.02	0.02	0.01	0.03
0.00	0.02	0.03	0.01	0.01	0.05
9.50	7.21	5.34	4.64	6.06	5.34
1.43	3.89	4.43	3.38	2.71	5.08
L.D.L.	L.D.L.	L.D.L.	L.D.L.	L.D.L.	L.D.L.
0.03	0.05	0.04	0.05	0.03	0.08
0.53	1.09	1.17	1.02	0.77	1.36
0.38	0.62	0.69	0.59	0.41	0.72
0.09	0.30	0.38	0.31	0.28	0.45
0.42	1.06	1.13	0.98	0.70	1.30
0.20	0.42	0.42	0.38	0.35	0.36
0.13	0.23	0.27	0.22	0.15	0.28
0.93	1.51	1.69	1.24	1.00	1.83
0.07	0.10	0.10	0.08	0.06	0.10
0.24	1.30	1.28	1.04	0.87	1.43
0.86	3.13	3.42	2.91	2.10	3.97
0.19	0.62	0.69	0.56	0.43	0.81
0.22	0.40	0.57	0.52	0.32	0.90
0.26	0.92	1.03	0.90	0.62	1.22
15.11	41.78	60.54	59.76	46.34	81.29
0.04	0.09	0.09	0.08	0.06	0.10
0.08	0.18	0.19	0.18	0.11	0.21
0.03	0.13	0.16	0.12	0.09	0.10
0.06	0.10	0.10	0.09	0.06	0.10
0.05	0.04	0.04	0.05	0.02	0.04
N.A.	N.A.	N.A.	N.A.	N.A.	N.A.
3.56	6.11	6.55	5.73	4.09	7.15
0.39	0.64	0.62	0.56	0.38	0.62
5.48	13.39	12.43	10.68	12.71	8.57
N.A.	N.A.	N.A.	N.A.	N.A.	N.A.
N.A.	N.A.	N.A.	N.A.	N.A.	N.A.
N.A.	N.A.	N.A.	N.A.	N.A.	N.A.
N.A.	N.A.	N.A.	N.A.	N.A.	N.A.
N.A.	N.A.	N.A.	N.A.	N.A.	N.A.

KT-28	KT-46	KT-19A
Tremolite-serpentinite	Tremolite-serpentinite	Olivine-tremolitite
45.14	44.81	42.54
0.47	0.45	0.59
2.81	3.38	3.61
15.78	14.64	19.07
0.18	0.21	0.28
32.18	32.95	29.12
4.87	4.92	6.41
0.10	0.11	0.28
0.00	0.00	0.02
0.04	0.01	0.00
8.16	7.24	3.96
3.32	3.77	3.40
L.D.L.	L.D.L.	L.D.L.
0.04	0.03	0.04
1.17	1.14	1.19
0.66	0.61	0.69
0.35	0.32	0.36
1.16	1.08	1.15
0.59	0.44	0.79
0.26	0.24	0.25
1.13	1.49	1.21
0.10	0.09	0.11
1.14	1.13	1.43
3.16	2.96	2.93
0.60	0.57	0.56
0.25	0.32	0.43
1.00	0.90	0.96
63.46	69.07	91.92
0.08	0.07	0.10
0.20	0.19	0.19
0.11	0.13	0.12
0.09	0.09	0.10
0.04	0.04	0.04
N.A.	N.A.	N.A.
6.16	5.99	6.37
0.59	0.59	0.66
21.36	12.45	33.42
N.A.	N.A.	N.A.
N.A.	N.A.	N.A.
N.A.	N.A.	N.A.
N.A.	N.A.	N.A.
N.A.	N.A.	N.A.

BVD103 data geochemistry

Sample ID.	23896	23897	23898	149260	23899	23900	23902	23903	23904
depth_from	88.07	89.07	90.22	91.22	91.71	92.71	93.21	118.09	119.09
depth_to	89.07	90.22	91.22	91.71	92.71	93.21	94.21	119.09	119.82
MgO (%)	9.47	24.10	25.70	22.80	23.20	20.40	22.10	10.35	14.75
Ni (%)	0.042	0.429	0.153	0.141	0.109	0.556	0.123	0.028	0.070
Cu (%)	0.016	0.049	0.016	0.031	0.007	1.710	0.016	0.016	0.016
Fe (%)	10.10	9.32	8.75	8.12	10.75	11.25	9.13	10.80	10.20
S (%)						1.33			
Co (ppm)	79	113	74	103	68	110	93	73	75
Cr (ppm)	363	990	854	1020	1120	1110	1090	457	633
Zn (ppm)	142	176	194	228	196	236	211	167	427
Pd (ppm)		0.054				0.42			
Pt (ppm)		0.21				0.01			
Ag (ppm)	0.7	0.6	0.25	0.25	0.25	13.9	0.25	0.25	0.25
Au (ppm)		0.002				0.024			

23905	23906	23907	23908	23909	149262	149263	149266	149267	149268
119.82	120.45	140.31	141.31	142.22	143.22	143.76	144.63	145.35	146.28
120.45	121.45	141.31	142.22	143.22	143.76	144.63	145.35	146.28	147.28
16.00	22.90	16.45	11.95	7.89	22.40	17.95	19.60	21.00	18.65
0.151	0.126	0.143	1.680	0.113	0.142	0.114	0.143	0.135	0.194
0.063	0.022	0.009	0.163	0.006	0.016	0.003	0.011	0.008	0.005
14.85	9.21	9.50	16.10	5.44	10.00	7.34	7.93	7.49	7.52
176	124	93	437	55	94	86	102	102	106
712	1170	868	676	439	1140	773	990	877	1030
2750	461	386	354	212	197	283	233	240	311
			0.185						
			0.141						
2.3	0.6	0.25	0.25	0.7	0.7	0.25	0.25	0.25	0.25
0.005			0.002						

149270	23910	23911	23912	23913	23914	23915	149271	149272	149273
147.28	148.30	149.30	150.36	151.36	152.09	152.65	153.65	154.65	155.65
148.3	149.3	150.36	151.36	152.09	152.65	153.65	154.65	155.65	156.65
21.70	20.60	13.20	7.38	11.25	11.30	9.14	10.50	11.95	11.80
0.200	0.164	1.820	0.033	0.024	0.739	0.018	0.021	0.025	0.024
0.001	0.047	0.305	0.008	0.007	0.055	0.013	0.005	0.009	0.010
7.20	7.15	18.95	6.10	7.57	11.70	7.03	7.03	8.11	7.84
131	99	396	42	56	213	48	51	58	59
2540	1490	780	247	636	356	450	448	593	614
318	470	765	198	228	605	647	911	473	356
0.25	1.3	1.7	0.5	0.25	0.25	0.25	0.25	0.25	0.25

149274	23916	23917	23918	149275	149276	149277	149278	149279	23919
156.65	157.59	158.59	159.13	160.13	161.13	162.13	163.13	164.00	164.74
157.59	158.59	159.13	160.13	161.13	162.13	163.13	164	164.74	165.74
11.70	10.85	10.80	11.10	13.75	13.85	13.65	11.05	11.45	9.65
0.024	0.022	1.180	0.023	0.034	0.033	0.032	0.024	0.023	0.053
0.015	0.008	0.212	0.002	0.001	0.001	0.001	0.006	0.006	0.091
7.02	7.38	13.65	7.28	6.42	6.63	6.86	7.16	7.05	6.28
									0.75
53	52	314	51	57	60	62	55	53	46
539	602	658	545	807	754	760	569	587	561
361	392	1040	624	313	214	240	467	1380	1750
0.25	0.25	0.25	0.25	0.25	0.25	0.25	0.25	0.25	0.25

23920	23922	23923	23924	24318	24319	149281	23926	23927	23928
165.74	166.50	167.51	168.46	169.46	170.90	171.90	172.61	173.61	174.11
166.5	167.51	168.46	169.46	170.9	171.9	172.61	173.61	174.11	174.63
2.73	7.32	15.75	25.60	26.20	6.43	6.93	6.60	1.87	1.42
1.440	1.500	1.100	0.489	0.329	0.008	0.015	0.019	1.220	1.530
0.123	0.200	0.225	0.035	0.021	0.005	0.010	0.007	0.454	0.308
26.80	29.20	21.10	7.51	6.54	5.85	6.63	6.31	30.50	36.90
439	421	298	142	111	37	47	41	421	479
274	501	835	781	530	67	235	214	199	189
1865	781	395	265	189	86	90	115	4840	3310
0.25	1	0.7	0.25	0.25	0.25	0.25	0.25	2.5	0.5

23929	23930	23931	23932	23933	23934	149282	23935	23936	23937
174.63	175.45	176.21	176.91	177.93	178.57	179.57	181.03	182.03	183.03
175.45	176.21	176.91	177.93	178.57	179.57	181.03	182.03	183.03	184.03
1.48	12.10	16.05	25.40	4.83	15.30	13.75	15.45	9.28	8.76
1.520	0.021	0.824	0.576	0.272	0.023	0.022	0.025	0.070	0.014
0.328	0.011	0.115	0.042	0.115	0.002	0.002	0.001	0.016	0.009
36.50	6.83	19.95	6.85	9.13	7.49	6.52	7.29	7.53	6.25
461	39	228	144	97	43	51	44	60	42
166	386	828	618	156	591	629	668	229	228
2780	589	3650	365	1425	419	315	335	508	599
1.6	0.5	1.3	1	0.8	0.25	1.5	0.25	0.25	0.25

23938	23939	23940	23941	23942	23943	23944	23945	149283	149284
184.03	184.81	186.11	187.10	187.77	188.56	189.56	190.83	191.83	192.83
184.81	186.11	187.1	187.77	188.56	189.56	190.83	191.83	192.83	193.4
9.88	24.50	17.05	13.25	15.00	26.50	24.90	11.75	13.90	10.60
0.017	0.419	0.108	0.083	0.233	0.477	0.459	0.146	0.030	0.013
0.015	0.077	0.022	0.030	0.025	0.077	0.064	0.019	0.006	0.015
7.15	9.66	9.82	7.76	9.92	8.48	7.86	7.41	9.91	10.75
51	127	50	50	74	158	153	65	75	69
217	641	446	566	558	635	644	271	644	82
446	683	901	678	885	553	708	538	202	190
	0.066								
	0.055								
0.25	0.25	0.25	0.25	0.6	0.5	0.25	0.7	0.25	0.25
	0.002								

149285	23947	23948	23949	149286	149289	149290	149291	149293	23950
193.40	194.00	195.00	195.50	196.50	197.50	198.50	199.50	200.50	201.05
194	195	195.5	196.5	197.5	198.5	199.5	200.5	201.05	202.05
7.46	9.83	9.71	10.40	11.15	9.88	8.96	10.30	10.05	10.85
0.015	0.021	0.019	0.021	0.018	0.021	0.020	0.021	0.025	0.029
0.026	0.019	0.005	0.009	0.015	0.017	0.028	0.023	0.011	0.013
11.05	10.60	9.59	10.25	9.12	9.69	10.45	11.15	11.15	10.80
71	69	61	67	65	65	72	76	79	75
140	466	433	547	342	446	283	282	420	457
179	230	172	186	192	230	230	209	259	358
		0.015							
		0.006							
0.25	0.25	14.6	0.25	0.25	0.25	0.25	0.25	0.6	0.25
		0.017							

23951	23952	149294	149295	149296	23953	23954	23955	23956	23957
202.05	202.61	203.61	204.61	205.20	205.92	206.92	207.49	208.82	209.36
202.61	203.61	204.61	205.2	205.92	206.92	207.49	208.82	209.36	210.36
11.60	21.80	19.00	14.75	20.40	11.90	11.55	11.30	4.17	8.67
0.129	0.150	0.115	0.040	0.148	0.114	0.597	0.014	0.293	0.014
0.007	0.021	0.017	0.012	0.023	0.024	0.151	0.002	0.028	0.005
12.05	8.20	8.19	10.35	8.32	7.75	21.90	6.11	12.15	5.97
98	88	97	74	92	75	244	37	115	43
443	1350	853	580	1070	429	384	227	126	202
1075	695	294	177	422	540	2750	289	629	267
0.25	0.25	0.25	0.25	0.25	0.25	1.7	0.25	0.25	0.25
								0.0025	

BVD31 data geochemistry

Sample	208470	208471	208472	208473	208474	208475	208476	208477	208478
depth_from	15.09	16.00	17.00	18.00	19.00	20.00	21.00	22.00	23.21
depth_to	16.00	17.00	18.00	19.00	20.00	21.00	22.00	23.21	24.00
MgO (%)	10.95	10.6	14.8	8.4	13.8	14.05	11.65	14	2.11
Al2O3 (%)	8.46	9.54	9.73	9.98	10.35	10.4	10.6	10.75	11.85
FeO (%)	3.17	2.95	4.59	2.86	4.35	4.71	3.61	4.29	0.94
MnO (%)	0.0695	0.0687	0.133	0.0693	0.138	0.145	0.105	0.118	0.0262
CaO (%)	1.51	1.96	4.69	0.52	2.09	2.2	2.53	2.27	0.53
K2O (%)	1.14	1.41	0.56	0.64	1.14	1.31	0.75	0.67	1.35
Na2O (%)	0.84	1.34	0.6	0.78	0.4	0.46	1.13	0.18	2.25
TiO2 (%)	0.18	0.2	0.17	0.11	0.19	0.24	0.23	0.2	0.04
Ni (%)	0.037	0.030	0.048	0.010	0.027	0.027	0.018	0.037	0.004
Cu (%)	0.0013	0.0007	0.0028	0.0006	0.0047	0.0134	0.0004	0.0006	0.0006
S (%)									
Co (ppm)	37	33	49	20	43	45	31	43	5
C (ppm)	989	656	1140	214	711	712	419	907	76
V (ppm)	74	73	113	69	134	140	119	109	13
Zn (ppm)	52	50	68	44	75	85	64	69	10
Zr (ppm)	36	71	16	29	13	13	19	18	40
As (ppm)	2.5	2.5	2.5	2.5	2.5	2.5	5	5	2.5
Ag (ppm)	0.25	0.25	0.25	0.25	0.25	0.25	0.25	0.25	0.25

208481	208482	208483	208484	208485	208486	208487	208488	208489	208492
24.00	25.00	26.00	27.00	28.00	29.00	29.49	30.16	31.11	31.91
25.00	26.00	27.00	28.00	29.00	29.49	30.16	31.11	31.91	33.33
2.42	4.75	0.55	1.45	1.82	4.13	11.1	9.02	1.42	5.9
11.95	12.15	12.2	12.25	12.55	13.1	13.35	13.85	14	14.05
1.2	2.13	0.47	0.82	1.23	1.72	4.45	3.75	0.92	4.38
0.0284	0.0504	0.0092	0.0167	0.031	0.0458	0.142	0.107	0.0196	0.15
0.4	1.73	0.44	1.19	1.55	1.7	2.98	2.89	0.97	5.86
0.58	1.86	0.87	0.93	0.94	1.56	2.51	1.62	1.34	1.81
0.74	3.06	5.04	4.33	4.82	3.52	1.17	1.41	2.34	2.53
0.06	0.21	0.05	0.07	0.12	0.14	0.41	0.28	0.06	0.53
0.005	0.009	0.000	0.001	0.002	0.007	0.022	0.017	0.001	0.008
0.0019	0.0032	0.0026	0.0025	0.0089	0.0016	0.0003	0.0022	0.0035	0.009
7	15	2	5	7	14	38	32	5	33
139	195	6	20	42	102	484	397	19	100
23	61	8	16	43	53	145	118	17	202
14	33	4	9	14	29	94	67	12	93
12	45	39	42	36	43	15	12	34	18
2.5	2.5	2.5	2.5	2.5	2.5	2.5	2.5	2.5	2.5
0.25	0.25	0.25	0.25	0.25	0.25	0.25	0.25	0.25	0.25

3493	208494	208495	208496	208497	208498	208499	208500	208503	208504
33.33	34.63	36.00	37.00	38.00	39.00	40.00	40.59	42.00	43.00
34.63	36.00	37.00	38.00	39.00	40.00	40.59	42.00	43.00	44.00
3.1	2.61	0.55	0.74	1.37	1.4	3.65	7.37	7.1	8.56
14.1	14.1	14.15	14.2	14.25	14.25	14.3	14.4	14.4	14.5
2.27	2.07	0.82	0.86	1.27	1.06	2.32	5.44	4.97	4.03
0.078	0.0696	0.0272	0.0245	0.0364	0.0289	0.0625	0.159	0.159	0.132
3.21	3.28	1.28	1.9	2.12	1.76	2.31	6.44	5.71	5.23
1.48	1.4	1.39	1.2	1.11	1.26	2.29	2.41	2.25	1.78
4.01	3.97	5.14	5.45	4.35	4.44	3.69	1.8	1.79	2.33
0.3	0.31	0.15	0.15	0.22	0.14	0.42	0.98	0.99	0.49
0.006	0.005	0.000	0.000	0.002	0.001	0.004	0.013	0.012	0.015
0.0052	0.0062	0.0037	0.0023	0.0021	0.001	0.0014	0.0159	0.0114	0.0057
18	19	3	3	8	4	12	37	33	34
68	67	5	5	33	13	49	142	128	396
94	89	12	16	48	22	96	293	290	147
56	115	63	50	60	31	81	106	105	134
38	42	65	65	46	67	53	24	14	41
2.5	2.5	2.5	2.5	2.5	5	2.5	2.5	2.5	2.5
0.25	0.25	0.25	0.25	0.25	0.25	0.25	0.25	0.25	0.25

3505	208506	208507	208508	208509	208510	208511	208512	208513	208514
44.00	45.00	46.00	47.00	48.00	49.00	50.00	51.00	52.00	53.00
45.00	46.00	47.00	48.00	49.00	50.00	51.00	52.00	53.00	54.00
8.34	19.85	21.4	23.1	20.5	21.6	17.6	15.95	15.65	19.95
14.6	14.65	14.65	14.75	14.75	14.8	14.8	14.8	14.85	14.9
4.43	5.51	4.98	4.99	4.66	5.15	5.88	5.4	6.13	5.37
0.134	0.155	0.161	0.169	0.138	0.146	0.137	0.128	0.115	0.147
6.65	5.54	7.82	8.37	6.38	7.02	5.48	5.43	3.67	6.44
1.99	1.06	0.33	0.03	0.1	0.08	1.1	1.08	2.53	1.07
2.1	0.14	0.14	0.13	0.09	0.13	0.84	1.14	0.79	0.15
0.43	0.21	0.11	0.06	0.06	0.06	0.25	0.3	0.44	0.22
0.016	0.058	0.081	0.089	0.083	0.081	0.047	0.045	0.038	0.069
0.0038	0.0019	0.0017	0.0045	0.005	0.0025	0.0042	0.0061	0.0092	0.0016
44	74	73	70	77	82	82	61	60	75
314	1290	1400	1470	1240	1460	1050	853	866	1270
176	157	133	125	126	145	162	144	171	161
244	132	76	73	65	81	107	140	126	77
30	10	7	6	5	7	13	26	32	5
2.5	2.5	2.5	2.5	2.5	2.5	2.5	2.5	2.5	2.5
0.25	0.25	0.25	0.25	0.25	0.25	0.25	0.25	0.25	0.25

208515	208516	208517	208518	208519	149069	149070	149071	149790	149791
54.00	55.00	55.72	56.72	58.00	59.42	60.42	60.92	61.92	62.94
55.00	55.72	56.72	58.00	59.42	60.42	60.92	61.92	62.94	64.04
20.4	22.7	2.51	20.5	15.75	11.15	9.95	10.5	15.7	13.4
14.9	14.95	15	15.05	15.05	15.05	15.15	15.2	15.2	15.25
5.43	5.14	1.11	5.31	4.89	4.35	5.21	5.44	5.61	6.09
0.148	0.161	0.0176	0.15	0.17					
6.42	7.49	0.73	6.59	10.15					
1.13	0.1	0.9	1.36	0.18					
0.28	0.12	5.15	0.59	0.73					
0.23	0.07	0.11	0.21	0.21					
0.066	0.081	0.005	0.064	0.064	0.058	0.027	0.022	0.038	0.025
0.0006	0.0009	0.0003	0.0002	0.0012	0.0022	0.0109	0.0082	0.0017	0.0085
75	78	9	78	72	80	59	58	66	61
1240	1530	83	1310	1860	1890	541	637	1200	795
164	139	22	162	172					
75	91	14	70	59	76	159	77	104	109
5	9	58	5	2.5					
2.5	2.5	2.5	2.5	2.5					
0.25	0.25	0.25	0.25	0.25	0.25	0.25	0.25	0.25	0.25

149792	149793	149794	149795	149796	149072	149073	149074	149075	149076
64.04	65.43	66.75	68.21	69.08	69.90	70.90	71.90	72.90	73.90
65.43	66.75	68.21	69.08	69.90	70.90	71.90	72.90	73.90	74.90
0.35	0.46	11.3	10.35	10.9	11.05	26.4	29.4	29.5	30.3
15.45	15.45	15.65	15.85	15.85	15.85	15.9	15.95	15.95	16.1
0.41	0.51	6.13	5.85	6.19	5.36	6.61	6.14	5.36	5.78
0.000	0.001	0.025	0.024	0.025	0.105	0.583	0.263	0.233	0.249
0.0006	0.0006	0.0101	0.0085	0.0092	0.0165	0.0518	0.0127	0.0096	0.0097
						1.33			
1	2	58	55	60	69	159	105	104	111
9	12	558	531	581	313	888	738	587	653
9	17	75	82	89	138	138	153	141	149
0.25	0.25	0.25	0.25	0.25	0.8	0.25	0.25	0.25	0.9

149077	149078	149079	149080	208520	208521	208522	208525	208526	208527
74.90	75.90	76.90	77.92	78.92	80.00	81.00	82.00	83.00	84.00
75.90	76.90	77.92	78.92	80.00	81.00	82.00	83.00	84.00	85.00
29.4	27.4	22	1.18	0.62	0.48	1.13	0.19	0.15	0.18
16.15	3.98	4.83	5.83	6.26	6.43	6.83	6.92	6.97	6.99
5.81	4.84	5.41	0.68	0.54	0.46	0.7	0.37	0.4	0.4
				0.0165	0.0138	0.0236	0.0142	0.0132	0.0139
				0.42	0.6	0.62	0.97	0.41	0.66
				4.79	2.85	3.62	3.37	4.64	3.29
				3.52	4.94	4.04	4.57	3.9	4.51
				0.04	0.04	0.04	0.04	0.05	0.05
0.243	0.201	0.156	0.002	0.001	0.001	0.001	0.000	0.000	0.000
0.0092	0.0077	0.0063	0.0004	0.0002	0.0017	0.0002	0.0011	0.0007	0.0003
113	96	92	2	1	1	1	0.5	1	1
598	551	731	11	30	13	15	12	17	18
				3	6	3	2	2	0.5
138	120	104	25	10	7	16	6	7	11
				26	45	53	45	26	55
				2.5	2.5	2.5	2.5	9	2.5
0.25	0.25	0.25	0.5	0.25	0.25	0.25	0.25	0.25	0.25

208528	208529	208530	208531	208532	208533	208534	208535	208536	208537
85.00	86.00	87.00	88.32	89.00	90.00	91.00	92.16	93.91	95.00
86.00	87.00	88.32	89.00	90.00	91.00	92.16	93.91	95.00	96.00
0.58	0.21	2.64	8.95	5.66	9.35	7.58	0.44	13.6	12.6
7	7.08	7.22	7.23	7.32	7.39	7.4	7.55	7.55	7.58
0.52	0.39	0.83	6.41	6.21	7.66	7.81	0.45	6.59	6.13
0.0189	0.0105	0.0221	0.164	0.15	0.189	0.179	0.0096	0.183	0.177
0.48	0.46	0.6	6.84	6.32	8.78	8.17	0.79	9.77	9.65
3.09	2.95	3.32	2.31	1	0.9	1.27	0.48	0.99	0.37
4.14	3.49	2.78	1.48	3.72	2.49	2.83	6.12	1.78	2.21
0.04	0.03	0.04	0.95	1.27	1.43	2.2	0.05	0.85	0.79
0.000	0.000	0.001	0.020	0.008	0.019	0.009	0.000	0.038	0.034
0.0002	0.0002	0.0001	0.0125	0.0215	0.0086	0.0096	0.0011	0.012	0.0083
0.5	1	2	46	37	52	48	2	62	54
10	14	17	388	99	269	179	10	662	608
1	1	2	187	197	222	190	2	260	252
15	4	11	98	87	141	117	5	93	96
45	34	47	8	11	8	12	34	2.5	2.5
2.5	2.5	2.5	2.5	2.5	2.5	2.5	2.5	2.5	2.5
0.25	0.25	0.25	0.25	0.25	0.25	0.25	0.25	0.25	0.25

208538	208539	208540	208542	208554	208555	208556	208557	208558	208541
96.00	96.80	98.00	99.93	110.28	111.00	112.00	113.00	114.00	99.04
96.80	98.00	99.04	101.17	111.00	112.00	113.00	114.00	114.72	99.93
15.2	26.1	23.8	6.53	17.6	15.1	11.7	5.79	14.75	16.45
7.69	7.73	7.88	8.04	8.59	8.64	8.64	8.87	8.9	7.97
6.93	7.55	7.27	7.63	6.13	5.9	5.57	4.44	5.71	6.3
0.199	0.173	0.176	0.205	0.192	0.178	0.167	0.113	0.158	0.208
9.75	4.85	6.77	7.46	8.47	7.92	7.32	3.83	6.77	12.05
0.45	0.01	0.01	0.37	1.8	1.64	0.8	1.16	2.37	0.07
1.55	0.02	0.03	4.64	0.78	1.88	3.47	6.49	2.12	0.53
0.8	0.37	0.4	1.25	0.46	0.49	1.01	1.27	0.74	0.61
0.046	0.118	0.091	0.006	0.099	0.081	0.056	0.023	0.080	0.040
0.0072	0.0039	0.0044	0.0327	0.0029	0.0176	0.0252	0.0308	0.0116	0.0116
69	119	106	55	72	67	56	34	65	69
904	2800	2310	72	563	508	389	83	446	962
237	100	112	235	123	134	165	144	125	173
102	92	81	120	94	90	81	62	88	101
2.5	2.5	2.5	5	59	68	68	117	74	2.5
2.5	7	2.5	2.5	2.5	2.5	2.5	2.5	2.5	5
0.25	0.25	0.25	0.25	0.25	0.25	0.25	0.25	0.25	0.25

208543	208544	208545	208546	208547	208550	208551	208552	208553	208559
101.17	102.00	102.84	103.95	105.00	106.00	107.00	108.00	109.00	114.72
102.00	102.84	103.95	105.00	106.00	107.00	108.00	109.00	110.28	116.00
17.5	15.7	11.2	20	17.8	21.5	11.9	15.35	17.95	20.2
8.06	8.19	8.28	8.3	8.31	8.37	8.43	8.54	8.55	8.92
6.58	6.81	3.04	5.24	5.73	5.8	5.39	5.62	6.05	5.97
0.168	0.176	0.0589	0.104	0.155	0.168	0.178	0.194	0.205	0.186
9.03	8.24	1.43	3.49	6.77	7.88	5.54	7.74	8.32	8.92
0.18	1.19	0.07	0.85	0.54	0.68	1.82	1.28	0.89	0.49
0.99	1.11	2.53	0.21	0.19	0.2	3.54	1.53	0.64	0.36
0.42	0.69	0.08	0.2	0.16	0.18	0.9	0.37	0.29	0.16
0.069	0.053	0.037	0.101	0.083	0.124	0.059	0.084	0.091	0.115
0.0051	0.0121	0.0002	0.0085	0.0173	0.0047	0.0301	0.0086	0.0024	0.0219
75	70	28	69	68	83	56	66	74	80
886	861	487	787	545	623	355	482	633	638
202	189	72	125	124	113	136	116	122	110
86	94	48	84	75	95	87	93	96	102
2.5	10	59	51	64	49	84	59	56	54
2.5	2.5	2.5	2.5	2.5	2.5	2.5	2.5	2.5	2.5
0.25	0.25	0.25	0.25	0.25	0.25	0.25	0.25	0.25	0.25

208560	208561	208562	208563	208564	208565	208566	208567	208568
116.00	117.00	118.00	119.00	120.00	121.00	122.00	123.00	124.00
117.00	118.00	119.00	120.00	121.00	122.00	123.00	124.00	125.00
22	18.25	16.7	14.45	20.3	20.3	21.4	22.2	21.6
8.94	8.95	8.98	9	9.02	9.05	9.09	9.13	9.15
5.49	6.5	6.33	5.86	5.12	5.07	5.13	5.11	5.43
0.181	0.196	0.185	0.179	0.148	0.147	0.1585	0.1635	0.1535
7.56	7.81	8.07	8.43	7.29	7.36	7.79	8.14	7.16
0.15	1.97	1.2	0.33	0.1	0.08	0.05	0.05	0.13
0.19	0.45	1.46	2.1	1.17	1.24	0.38	0.26	0.55
0.08	0.56	0.6	0.62	0.07	0.07	0.05	0.06	0.07
0.141	0.083	0.066	0.046	0.079	0.078	0.090	0.091	0.086
0.0146	0.005	0.006	0.009	0.0004	0.0001	0.0003	0.0001	0.0001
86	79	70	59	66	65	68	69	69
667	842	755	728	930	933	989	944	914
98	142	209	232	173	174	142	144	158
87	93	92	95	73	66	63	63	68
42	37	15	2.5	2.5	2.5	2.5	2.5	2.5
2.5	2.5	2.5	2.5	2.5	2.5	2.5	2.5	2.5
0.25	0.25	0.25	0.25	0.25	0.25	0.25	0.25	0.25

208569	208570	208571	208572	208573	208576	208577	208578	208579	208580
125.00	126.00	127.00	128.00	129.00	130.00	131.00	132.00	133.00	134.00
126.00	127.00	128.00	129.00	130.00	131.00	132.00	133.00	134.00	135.00
21.8	21.8	21.5	21.3	21.4	21.1	21.6	21.2	20.5	20.3
9.16	9.35	9.35	9.38	9.43	9.43	9.43	9.47	9.51	9.55
5.32	5.32	5.27	5.43	5.32	5.2	5.39	5.22	5.19	5.26
0.1505	0.1455	0.155	0.158	0.151	0.1485	0.159	0.154	0.1455	0.147
7.06	6.65	7.46	7.54	7.13	7.03	7.61	7.75	6.99	7.19
0.18	0.28	0.24	0.25	0.27	0.21	0.23	0.29	0.25	0.13
0.55	0.69	0.52	0.46	0.73	0.67	0.5	0.64	0.84	1.35
0.07	0.07	0.07	0.07	0.07	0.07	0.07	0.08	0.1	0.08
0.087	0.088	0.088	0.089	0.089	0.085	0.085	0.085	0.080	0.075
0.00005	0.0001	0.00005	0.0001	0.0001	0.0001	0.0001	0.0001	0.0001	0.0008
72	70	72	71	69	71	72	69	67	66
893	940	889	927	934	884	885	846	873	812
158	158	154	150	158	152	152	148	158	173
67	67	65	67	67	64	67	65	66	65
2.5	2.5	5	2.5	2.5	2.5	2.5	2.5	2.5	2.5
2.5	2.5	2.5	2.5	2.5	2.5	2.5	2.5	2.5	2.5
0.25	0.25	0.25	0.25	0.25	0.25	0.25	0.25	0.25	0.25

208581	208582	208583	208584	208585	208586	208587	208588	208589	208590
135.00	136.00	137.00	138.00	139.00	140.00	141.00	141.84	142.81	144.00
136.00	137.00	138.00	139.00	140.00	141.00	141.84	142.81	144.00	145.00
20.6	20.7	20	20.1	21.1	16.5	19.95	13.4	20.2	13.8
9.55	9.56	9.56	9.58	9.68	9.69	9.7	9.75	9.84	9.84
5.41	5.3	5.32	5.15	5.36	5.6	6.35	7.77	7.42	6.83
0.1495	0.153	0.161	0.1495	0.153	0.157	0.201	0.223	0.1965	0.1695
7.17	7.53	8.13	7.43	7.29	6.77	9.09	8.54	7.7	8.49
0.32	0.16	0.11	0.12	0.08	0.55	0.16	0.37	0.02	0.07
1	0.78	0.95	1.23	0.8	0.85	0.28	2.11	0.19	2.14
0.1	0.08	0.09	0.08	0.07	0.31	0.27	0.92	0.63	0.8
0.079	0.081	0.077	0.073	0.083	0.080	0.115	0.042	0.086	0.041
0.0004	0.0001	0.009	0.0008	0.0105	0.0018	0.0327	0.0116	0.0137	0.0117
71	68	68	69	71	67	80	70	95	64
858	869	754	781	855	583	608	774	1440	668
169	163	183	173	170	122	120	183	147	245
69	66	61	63	70	82	92	111	91	87
2.5	2.5	2.5	2.5	2.5	40	38	8	2.5	5
2.5	5	2.5	2.5	2.5	2.5	2.5	2.5	2.5	2.5
0.25	0.25	0.25	0.25	0.25	0.25	0.25	0.25	0.25	0.25

208591	208592	208593	208594	208595	208598	208599	208600	208601	208602
145.00	146.00	147.00	148.00	149.00	150.00	151.00	152.00	153.00	154.00
146.00	147.00	148.00	149.00	150.00	151.00	152.00	153.00	154.00	155.00
12.5	12.05	12.2	12.3	12.15	12.7	11.65	11.85	10.45	9.63
9.94	9.97	9.97	9.97	9.98	9.99	10	10	10.05	10.1
6.44	6.2	6.34	6.38	6.29	6.66	6.77	6.86	7.24	8.01
0.1785	0.173	0.178	0.171	0.172	0.204	0.198	0.198	0.198	0.203
9.84	9.65	10.1	10.1	9.86	9.8	9.15	9.13	9.11	10.6
0.16	0.15	0.35	0.21	0.18	0.26	0.63	0.73	1.16	0.29
2.41	2.26	2.25	2.14	2.27	2.05	2.15	1.71	2.05	1.74
0.79	0.74	0.81	0.79	0.79	0.8	0.84	0.79	1.05	1.12
0.033	0.033	0.033	0.034	0.034	0.036	0.026	0.037	0.024	0.025
0.0059	0.008	0.0041	0.0068	0.0066	0.0084	0.0133	0.0077	0.0029	0.0296
57	54	56	58	55	59	57	62	61	64
547	494	525	528	539	526	492	520	347	275
250	238	246	249	244	236	246	242	269	290
99	101	100	88	86	96	93	95	104	103
2.5	2.5	2.5	2.5	2.5	5	5	6	20	7
2.5	2.5	2.5	2.5	2.5	2.5	2.5	2.5	2.5	2.5
0.25	0.25	0.25	0.25	0.25	0.25	0.25	0.25	0.25	0.25

208603	208604	208605	208606	208607	208608	208609	208610	208611	208612
155.00	155.68	157.00	158.00	159.00	160.35	161.00	162.00	163.00	164.00
155.68	157.00	158.00	159.00	160.35	161.00	162.00	163.00	164.00	164.59
8.47	6.68	6.96	7.11	6.67	9.63	9.98	10.8	10.45	10.7
10.1	10.15	10.15	10.2	10.2	10.2	10.2	10.25	10.3	10.3
7.28	5.74	5.84	5.74	5.6	7.93	8.08	7.97	7.69	7.85
0.177	0.155	0.156	0.152	0.147	0.205	0.216	0.221	0.222	0.229
9.28	8.87	9.06	8.92	9.08	11.45	11.1	11.2	11.5	11.95
0.47	0.83	1.02	1.2	0.92	0.24	0.23	0.25	0.2	0.28
1.94	2.94	2.45	2.16	2.68	1.25	1.6	1.83	1.62	1.5
0.96	0.59	0.59	0.57	0.57	1	0.98	0.94	0.9	0.86
0.014	0.017	0.018	0.018	0.018	0.017	0.022	0.030	0.028	0.028
0.0213	0.0076	0.0064	0.0085	0.0087	0.0169	0.0168	0.0154	0.0124	0.0117
57	49	51	49	46	66	67	77	73	75
228	243	268	290	236	426	461	583	552	523
271	168	174	169	167	248	230	219	209	216
94	80	87	83	78	110	112	115	113	120
17	26	25	24	19	5	8	6	6	7
2.5	2.5	2.5	2.5	2.5	2.5	2.5	2.5	2.5	2.5
0.25	0.25	0.25	0.25	0.25	0.25	0.25	0.25	0.25	0.25

208613	208614	208615	208616	208617	208618	208621	208622	208623	208624
164.59	166.00	167.24	168.00	169.00	170.00	171.00	172.00	173.00	174.00
166.00	167.24	168.00	169.00	170.00	171.00	172.00	173.00	174.00	175.00
6.77	6.17	10.45	10.55	10.7	10.55	12.1	11.85	11.4	10.5
10.3	10.45	10.45	10.6	10.65	10.8	11.1	11.15	11.15	11.2
5.65	5.53	8.12	7.97	7.7	7.81	7.74	8.16	7.77	7.47
0.154	0.148	0.217	0.226	0.235	0.214	0.2	0.205	0.207	0.208
8.96	9	11.9	11.75	10.85	10.9	11.35	12.2	11.5	12.15
1.08	1.13	0.4	0.4	0.57	0.35	0.41	0.19	0.36	0.23
2.59	2.62	1.5	1.82	2.01	2.2	1.51	2.04	1.91	2.24
0.58	0.6	0.92	0.92	0.91	0.95	0.89	0.99	0.94	0.93
0.018	0.016	0.026	0.029	0.035	0.032	0.056	0.044	0.043	0.041
0.0084	0.0096	0.0096	0.0156	0.0128	0.0159	0.0102	0.0114	0.0127	0.0103
49	45	73	72	72	73	87	82	79	77
245	210	546	527	533	515	799	667	626	550
169	164	224	214	215	217	199	219	212	206
82	78	119	130	107	120	107	103	124	143
16	18	7	5	2.5	6	6	6	6	6
2.5	2.5	2.5	2.5	2.5	2.5	2.5	2.5	2.5	2.5
0.25	0.25	0.25	0.25	0.25	0.25	0.25	0.25	0.25	0.25

208625	208626	208627	208628	208629	208630	208631	208632	149082	149083
175.00	175.97	177.00	178.00	179.00	179.56	181.00	181.65	182.32	183.32
175.97	177.00	178.00	179.00	179.56	181.00	181.65	182.32	183.32	184.00
11.35	8.54	8.37	7.93	8.66	8.21	8.47	8.49	8.79	17.75
11.2	11.2	11.5	11.55	11.55	11.55	11.65	11.7	11.75	11.8
7.77	8.59	8.67	8.12	8.55	8.2	8.43	8.01	7.55	7.14
0.212	0.181	0.195	0.182	0.203	0.212	0.208	0.2		
11.6	9.91	10.45	10.35	10.7	12.5	12.2	11.95		
0.2	0.36	0.33	0.36	0.47	0.3	0.27	0.27		
2.09	3.07	2.82	3.06	2.7	2.87	2.41	2.56		
0.92	1.24	1.21	1.19	1.19	1.21	1.21	1.23		
0.041	0.038	0.036	0.034	0.038	0.037	0.038	0.039	0.039	0.098
0.0161	0.0181	0.0145	0.0145	0.017	0.0122	0.0123	0.0161	0.0149	0.0122
75	77	76	72	77	76	75	78	79	96
602	316	284	290	309	296	301	303	334	865
202	217	210	211	213	216	214	216		
138	125	136	126	162	159	134	136	140	244
6	19	15	15	14	13	16	15		
2.5	2.5	2.5	2.5	2.5	2.5	2.5	2.5		
0.25	0.25	0.25	0.25	0.25	0.25	0.25	0.25	1.5	0.8

149084	149085	149086	149087	149088	149089	149090	149091	149092	149093
184.00	185.00	186.00	187.00	188.00	189.00	190.00	191.00	192.00	193.00
185.00	186.00	187.00	188.00	189.00	190.00	191.00	192.00	193.00	194.00
21.1	21.1	22.3	20.5	20.1	21.6	21.6	21	19.5	22.3
11.85	11.95	11.95	12	12.05	12.1	12.1	12.15	12.15	12.2
6.78	6.8	6.09	6.58	7.1	7.45	6.72	7.97	9.13	7.52
0.091	0.136	0.140	0.107	0.075	0.113	0.125	0.197	1.090	0.138
0.0072	0.0111	0.0086	0.0059	0.0032	0.012	0.0099	0.0269	0.184	0.0105
								2.98	
90	101	93	97	92	102	87	108	269	95
938	962	792	973	1050	1160	1080	1290	2010	1200
168	153	153	181	215	246	194	273	501	418
0.25	0.25	0.6	0.25	0.25	0.25	0.25	0.9	6	0.25

149094	149095	149096	149097	149098	149799	149800	149801	149802	149803
194.00	195.00	196.00	197.00	198.22	199.22	200.64	201.88	202.88	203.70
195.00	196.00	197.00	198.22	199.22	200.64	201.88	202.88	203.70	204.63
26.4	23.8	23.3	23	10.15	9.41	10.35	8.95	5.88	15.95
12.25	12.3	12.35	12.35	12.4	12.45	12.5	12.5	12.55	12.55
6.81	7.36	6.89	7.03	8.36	8.78	8.98	9.02	10.07	7.97
0.197	0.180	0.166	0.126	0.026	0.026	0.034	0.032	0.012	0.079
0.011	0.0113	0.009	0.0144	0.0202	0.0192	0.0151	0.0194	0.0346	0.011
113	115	105	99	78	74	78	76	73	96
849	1180	1010	734	412	405	479	386	18	921
536	444	439	724	230	238	179	181	168	115
0.7	0.9	0.25	0.5	3.3	0.25	0.25	0.25	0.5	0.25

149805	149099	149100	149101	149102	149104	149105	149106	149107	149108
204.63	205.89	206.89	207.89	208.89	209.89	210.89	211.89	212.89	213.49
205.89	206.89	207.89	208.89	209.89	210.89	211.89	212.89	213.49	214.50
16.95	17.65	22.8	23.8	23	24	23.6	21.7	22.3	19.8
12.55	12.65	12.8	12.8	12.85	12.9	13.05	13.1	13.45	13.55
7.73	8.12	8.24	7.51	6.81	7.72	7.89	7.52	6.76	9.13
0.092	0.087	0.110	0.138	0.139	0.132	0.189	0.124	0.159	0.138
0.015	0.0129	0.0087	0.0137	0.0099	0.0185	0.0338	0.0269	0.0349	0.0432
100	100	97	107	101	103	140	105	110	198
1110	1050	921	1090	1010	1060	1310	1200	1010	828
92	128	195	260	165	349	361	474	704	2270
0.25	0.6	0.25	0.6	0.25	0.25	0.25	0.25	0.25	2.5

149109	149110	149111	149112	149806	149113	149114	149115	149116	149117
214.50	215.00	215.50	216.00	217.00	217.45	218.45	219.45	220.45	221.45
215.00	215.50	216.00	217.00	217.45	218.45	219.45	220.45	221.45	221.97
20.4	21.2	21.4	22.7	16.35	19.9	22.3	23	25.7	26.7
13.65	14.05	14.1	14.2	15.05	15.55	4.5	9.69	9.86	10.95
7.35	7.59	8.32	6.06	6.87	6.79	6.47	6.74	6.37	5.5
0.091	0.120	0.111	0.117	0.078	0.116	0.132	0.143	0.389	0.361
0.0226	0.0381	0.0281	0.0161	0.0016	0.0128	0.01	0.0091	0.0304	0.0315
								0.41	0.61
89	92	114	96	85	99	101	103	141	124
814	924	749	972	757	1020	1010	1070	906	753
1500	1040	1990	1720	190	171	131	129	130	118
0.6	1	0.7	0.6	0.25	1.2	0.6	0.25	0.25	0.25

149118	208633	208634	208635	208636	208637	208638	208639	208640	208643
221.97	222.97	224.00	225.00	226.00	227.00	228.00	228.74	230.00	231.00
222.97	224.00	225.00	226.00	227.00	228.00	228.74	230.00	231.00	231.64
25.8	19.4	15.95	18.4	15.95	16.95	15.1	1.23	0.2	0.61
11.1	11.4	12	12.2	12.55	12.55	12.6	12.65	12.65	12.65
5.78	7.72	7.77	6.48	5.8	6.79	6.91	0.84	0.25	0.44
	0.191	0.235	0.1715	0.166	0.1505	0.1665	0.0159	0.005	0.0084
	3.49	10.15	6.2	6.34	2.89	5.36	0.34	0.52	0.53
	0.24	0.47	1	1.02	0.53	1.29	0.34	0.12	0.08
	0.73	0.96	1.26	2.4	0.65	0.35	4.41	8.4	9.57
	0.65	0.81	0.32	0.26	0.23	0.54	0.03	0.01	0.01
0.239	0.071	0.055	0.062	0.054	0.043	0.067	0.004	0.001	0.001
0.0138	0.006	0.0124	0.001	0.0014	0.0005	0.0139	0.0013	0.0004	0.0004
111	80	81	77	67	65	76	5	1	3
758	511	813	928	936	718	521	21	10	8
	155	186	155	154	154	160	10	1	3
133	285	178	249	218	174	114	14	3	11
	56	6	19	23	32	30	2.5	2.5	6
	2.5	2.5	2.5	2.5	2.5	5	2.5	2.5	2.5
0.25	0.25	0.25	0.25	0.25	0.25	0.25	0.25	0.25	0.25

149118	208633	208634	208635	208636	208637	208638	208639	208640	208643
221.97	222.97	224.00	225.00	226.00	227.00	228.00	228.74	230.00	231.00
222.97	224.00	225.00	226.00	227.00	228.00	228.74	230.00	231.00	231.64
25.8	19.4	15.95	18.4	15.95	16.95	15.1	1.23	0.2	0.61
11.1	11.4	12	12.2	12.55	12.55	12.6	12.65	12.65	12.65
5.78	7.72	7.77	6.48	5.8	6.79	6.91	0.84	0.25	0.44
	0.191	0.235	0.1715	0.166	0.1505	0.1665	0.0159	0.005	0.0084
	3.49	10.15	6.2	6.34	2.89	5.36	0.34	0.52	0.53
	0.24	0.47	1	1.02	0.53	1.29	0.34	0.12	0.08
	0.73	0.96	1.26	2.4	0.65	0.35	4.41	8.4	9.57
	0.65	0.81	0.32	0.26	0.23	0.54	0.03	0.01	0.01
0.239	0.071	0.055	0.062	0.054	0.043	0.067	0.004	0.001	0.001
0.0138	0.006	0.0124	0.001	0.0014	0.0005	0.0139	0.0013	0.0004	0.0004
111	80	81	77	67	65	76	5	1	3
758	511	813	928	936	718	521	21	10	8
	155	186	155	154	154	160	10	1	3
133	285	178	249	218	174	114	14	3	11
	56	6	19	23	32	30	2.5	2.5	6
	2.5	2.5	2.5	2.5	2.5	5	2.5	2.5	2.5
0.25	0.25	0.25	0.25	0.25	0.25	0.25	0.25	0.25	0.25

;	149127	149128	149129	149807	149808	149809	149810	149811	149812
..75	242.75	243.85	244.88	245.88	246.48	247.65	248.63	250.30	251.52
:.75	243.85	244.88	245.88	246.48	247.65	248.63	250.30	251.52	252.40
..65	14.8	6.52	10.3	13.55	11.3	11	11.05	11.35	12.2
13.5	13.6	13.8	13.8	13.9	14	14.05	14.1	14.35	14.75
'.14	7.61	6.45	5.05	6.03	5.67	6.02	6.09	5.99	5.46
)41	0.072	0.085	0.030	0.025	0.023	0.025	0.023	0.023	0.029
)82	0.0173	0.0293	0.0176	0.0179	0.0068	0.011	0.0092	0.0079	0.0088
68	93	77	52	59	54	59	57	58	58
552	809	106	434	649	574	580	573	571	601
137	191	565	645	134	146	170	206	186	148
0.6	1.1	0.25	0.9	0.25	0.25	0.25	0.25	0.25	0.25

149130	149131	149132	208648	208649	208650	208651	208652	208653	208654
252.40	253.40	254.40	255.40	256.00	257.00	258.00	259.00	260.00	261.00
253.40	254.40	255.40	256.00	257.00	258.00	259.00	260.00	261.00	262.00
11.9	13	13.5	12	11.55	11.5	11.45	12.4	11.65	11.3
14.85	14.85	15.4	15.5	16.05	17.6	18.6	18.8	20.4	33.9
5.29	7.21	5.23	6.15	6.13	6.13	6.02	6.26	6.17	6.05
			0.219	0.234	0.222	0.1955	0.212	0.223	0.2
			7.72	8.37	8.06	8.99	7.69	8.57	8.95
			1.34	1.35	1.3	1.15	1.03	1.25	0.78
			1.69	1.81	1.7	1.53	1.2	1.65	1.67
			0.53	0.52	0.51	0.51	0.52	0.53	0.51
0.027	0.148	0.032	0.024	0.023	0.022	0.023	0.022	0.023	0.022
0.0114	0.0336	0.0029	0.0085	0.008	0.0098	0.0066	0.0062	0.0056	0.0072
56	84	58	57	57	57	54	55	57	55
574	528	694	610	521	559	600	612	595	590
			206	209	207	207	212	220	211
101	547	296	219	158	163	108	112	172	118
			2.5	2.5	2.5	2.5	2.5	2.5	2.5
			2.5	2.5	2.5	2.5	2.5	2.5	2.5
0.6	1.5	0.25	0.25	0.25	0.25	0.25	0.25	0.25	0.25

208655	208656	208657	208658	208659	208660	208661	208662	208663	208664
262.00	263.00	264.00	265.00	266.00	267.00	268.00	269.00	269.56	270.50
263.00	264.00	265.00	266.00	267.00	268.00	269.00	269.56	270.50	271.00
11.85	11.2	10.7	11.35	11.15	11.75	15.95	22	1.61	1.25
4.21	4.34	6.44	6.65	6.8	6.86	6.89	6.91	6.93	7.68
6.38	6.06	5.9	6.09	6	6.75	4.76	4.71	1.02	0.86
0.205	0.1835	0.1785	0.1805	0.1815	0.153	0.209	0.161	0.0454	0.0312
9.02	9.19	9.4	8.68	8.46	5.18	15.75	10.9	4.5	2.47
0.83	0.41	0.49	0.54	0.62	0.93	0.31	0.01	2.15	2.16
1.45	1.54	1.6	1.63	1.54	0.79	0.25	0.07	6.75	6.95
0.54	0.51	0.51	0.51	0.49	0.4	0.17	0.07	0.16	0.14
0.023	0.022	0.021	0.022	0.022	0.037	0.070	0.094	0.003	0.001
0.0065	0.0062	0.0143	0.0093	0.0085	0.0163	0.0041	0.0022	0.0002	0.0002
59	56	55	58	55	74	74	71	8	4
630	579	570	596	570	818	1970	1660	29	14
216	209	208	203	198	292	173	191	20	15
141	96	105	86	98	736	92	86	28	23
2.5	2.5	2.5	2.5	2.5	2.5	2.5	2.5	136	102
8	2.5	2.5	2.5	2.5	18	2.5	2.5	2.5	2.5
0.25	0.25	0.25	0.25	0.25	0.25	0.25	0.25	0.25	0.25

208665	208666	208667	208670	208671	208672	208673	208674	208675	208676
271.00	272.00	273.00	274.00	274.68	276.00	277.00	278.00	279.00	280.00
272.00	273.00	274.00	274.68	276.00	277.00	278.00	279.00	280.00	281.00
1.37	1.2	0.8	1.94	8.74	9.58	14.5	18.4	16.2	14.7
8.08	8.16	8.25	9.01	9.05	9.65	9.72	9.8	9.86	
1.18	1.15	0.78	1.32	5.15	4.16	5.81	5.37	5.48	8.01
0.0446	0.0429	0.0253	0.0417	0.116	0.101	0.151	0.191	0.154	0.142
1.81	1.06	0.64	2.1	3.32	4.38	5.56	9.22	6.19	4.12
2.67	2.33	1.63	2.57	3.05	1.11	1.53	0.33	0.89	2.3
7	5.45	4.69	5.3	1.16	1.55	0.9	0.3	0.63	0.16
0.18	0.19	0.13	0.24	0.49	0.3	0.34	0.13	0.32	0.47
0.001	0.001	0.001	0.002	0.018	0.019	0.043	0.069	0.057	0.070
0.0003	0.0003	0.0006	0.0004	0.0036	0.0007	0.0062	0.0029	0.005	0.0334
4	3	1	6	42	38	63	67	72	98
15	10	8	28	350	424	859	1440	1130	1260
16	13	9	27	162	115	179	120	160	168
32	29	17	32	103	85	139	146	164	293
106	98	67	109	27	44	10	9	13	19
2.5	5	2.5	7	2.5	2.5	2.5	2.5	2.5	14
0.25	0.25	0.25	0.25	0.25	0.25	0.25	0.25	0.25	0.25

208677	208678	208679	208680	208681	208682	208683	208684	208685	208686
281.00	282.00	283.00	284.00	285.00	286.00	287.00	287.82	289.00	290.00
282.00	283.00	284.00	285.00	286.00	287.00	287.82	289.00	290.00	291.00
13.6	21.7	21.8	20.1	20.2	21.6	22.1	22.5	22.9	23.5
10.57									
4.52	5.08	4.96	5.81	5.55	4.73	5.37	4.73	5.11	4.68
0.0861	0.145	0.151	0.168	0.172	0.164	0.154	0.146	0.152	0.145
3.38	7.81	8.21	8.36	8.35	9.1	7.62	8.02	7.89	7.69
0.84	0.01	0.01	0.2	0.16	0.01	0.01	0.005	0.005	0.005
0.58	0.07	0.07	0.19	0.18	0.11	0.07	0.04	0.04	0.04
0.18	0.05	0.05	0.11	0.1	0.05	0.11	0.11	0.15	0.12
0.050	0.091	0.090	0.097	0.090	0.093	0.084	0.099	0.110	0.109
0.0109	0.0049	0.0011	0.0001	0.00005	0.0001	0.0011	0.0032	0.0042	0.0037
51	79	77	87	80	72	77	75	85	77
877	1410	1370	1650	1580	1320	1390	1180	1580	1390
106	130	127	137	141	120	137	97	117	98
118	70	64	76	77	66	59	47	51	48
18	2.5	2.5	2.5	2.5	2.5	2.5	2.5	2.5	2.5
2.5	2.5	2.5	2.5	2.5	2.5	2.5	2.5	2.5	2.5
0.25	0.25	0.25	0.25	0.25	0.25	0.25	0.25	0.25	0.25

208687	208688	208689	208690	208691	208692	208695	208696	208697	208698
291.00	292.00	293.00	294.00	295.00	296.00	297.00	298.00	299.00	300.22
292.00	293.00	294.00	295.00	296.00	297.00	298.00	299.00	300.22	301.42
25.2	23.9	25.3	24.8	25	24.5	22.6	21.9	23.9	19.55
		7.75							
4.4	4.37	4.45	4.31	4.25	4.75	5.39	5.56	4.64	5.43
0.0904	0.122	0.114	0.0997	0.11	0.0936	0.146	0.145	0.104	0.163
3.66	7.25	5.33	4.55	5.71	4.25	7.01	6.63	4.23	7.22
0.005	0.005	0.005	0.005	0.005	0.005	0.01	0.08	0.01	1.4
0.01	0.01	0.01	0.01	0.01	0.03	0.05	0.08	0.04	0.16
0.11	0.09	0.12	0.12	0.07	0.1	0.13	0.07	0.04	0.15
0.132	0.130	0.130	0.128	0.138	0.132	0.098	0.091	0.120	0.074
0.0035	0.0059	0.0056	0.0055	0.0044	0.0058	0.0025	0.0019	0.0036	0.001
82	84	83	76	80	90	85	78	81	72
1450	1450	1410	1410	1350	1550	1520	1440	1470	1260
102	101	101	100	96	109	140	140	106	136
51	45	47	46	45	50	54	61	63	111
2.5	2.5	2.5	2.5	2.5	2.5	2.5	2.5	2.5	12
2.5	2.5	2.5	2.5	2.5	2.5	2.5	2.5	2.5	2.5
0.25	0.25	0.25	0.25	0.25	0.25	0.25	0.25	0.25	0.25

208699	208700	208701	208702	208703	208704	208705	208706	208707	208708
301.42	302.00	303.38	304.50	305.00	306.00	307.00	308.00	309.00	310.00
302.00	303.38	304.50	305.00	306.00	307.00	308.00	309.00	310.00	311.00
1.49	0.61	9.15	8.05	7.77	7.55	7.42	6.23	6.85	6.37
14.15									
1.66	0.88	6.17	6.34	6.71	6.61	6.75	6.22	7.51	7.24
0.0245	0.0205	0.156	0.155	0.168	0.165	0.172	0.16	0.172	0.172
1.29	1.83	8.94	9.92	9.54	9.16	9.83	8.67	9.34	9.21
2.19	0.92	1.05	0.3	0.26	0.21	0.19	0.16	0.21	0.33
3.73	4	2.18	1.73	2.24	2.58	2.72	2.38	2.6	2.26
0.24	0.1	0.72	0.75	0.79	0.82	0.79	0.84	0.94	1.01
0.002	0.001	0.010	0.008	0.008	0.008	0.008	0.006	0.006	0.005
0.0109	0.006	0.0057	0.0068	0.0146	0.0156	0.0172	0.0056	0.0013	0.0061
5	2	47	48	49	48	49	46	51	49
28	13	131	54	44	50	46	18	7	5
23	9	259	265	275	274	279	271	319	333
35	18	100	71	73	69	66	55	58	56
100	41	5	5	5	2.5	6	7	6	8
2.5	5	2.5	2.5	2.5	2.5	2.5	2.5	2.5	2.5
0.25	0.25	0.25	0.25	0.25	0.25	0.25	0.25	0.25	0.25

208709	208710	208711	208712	208713	208714	208717	208718	208719	208720
311.00	312.00	313.00	314.00	315.00	316.00	317.00	318.00	319.44	320.18
312.00	313.00	314.00	315.00	316.00	317.00	318.00	319.44	320.18	321.00
6.7	7.28	7.3	7.07	7.25	7.18	6	5.55	0.92	6.55
5.77	6.44	6.16	6.23	6.78	6.76	6.55	6.89	1.16	6.37
0.147	0.158	0.152	0.155	0.177	0.179	0.163	0.158	0.0322	0.178
7.19	9.63	9.53	10.5	9.74	9.86	11	10.7	2.8	9.54
0.82	0.25	0.22	0.32	0.31	0.29	0.24	0.42	1.05	0.77
2.54	2.5	2.56	2.38	2.46	2.23	1.25	1.13	4.4	1.87
0.68	0.78	0.78	0.75	0.77	0.82	0.84	0.9	0.18	0.76
0.006	0.007	0.008	0.007	0.008	0.007	0.006	0.005	0.001	0.007
0.0046	0.0057	0.009	0.0008	0.0082	0.0063	0.0112	0.0121	0.0022	0.004
41	45	42	45	52	49	45	50	6	42
33	45	46	45	44	30	17	8	11	18
234	279	276	270	276	289	293	301	41	279
60	54	45	50	72	63	53	54	15	77
10	6	5	5	7	6	7	6	54	7
2.5	2.5	2.5	2.5	2.5	2.5	2.5	2.5	2.5	2.5
0.25	0.25	0.25	0.25	0.25	0.25	0.25	0.25	0.25	0.25

208721	208722	208723	208724	208725	208726	208727	208728	208729	208730
321.00	322.00	323.00	324.00	325.00	326.00	327.00	328.00	329.00	330.00
322.00	323.00	324.00	325.00	326.00	327.00	328.00	329.00	330.00	331.00
8.04	7.6	8.45	8.57	9.02	8.37	9.13	8.73	8.2	9.14
		14.93							
6.28	5.85	6.13	5.28	5.32	4.98	5.05	4.67	4.88	5.04
0.176	0.167	0.183	0.148	0.145	0.139	0.143	0.132	0.134	0.142
9.75	10.9	10.95	10.7	11.35	11.85	11.75	11.6	12.2	12.8
1.02	0.7	0.54	0.42	0.42	0.23	0.19	0.17	0.18	0.18
1.99	1.99	2.48	2.12	2.49	2.2	2	1.91	1.83	1.65
0.61	0.54	0.62	0.62	0.54	0.46	0.43	0.42	0.45	0.45
0.009	0.009	0.009	0.010	0.010	0.010	0.012	0.011	0.010	0.012
0.0106	0.0156	0.0133	0.0019	0.0079	0.0082	0.01	0.0028	0.0077	0.0096
46	45	50	45	44	40	44	41	43	43
17	10	15	29	39	42	57	70	69	87
248	230	254	230	224	197	195	176	197	198
99	78	81	71	50	46	52	42	43	48
6	5	2.5	2.5	2.5	2.5	2.5	2.5	2.5	2.5
2.5	2.5	2.5	2.5	2.5	2.5	2.5	2.5	2.5	2.5
0.25	0.25	0.25	0.25	0.25	0.25	0.25	0.25	0.25	0.25

208731	208732	208733	208734	208735	208736	208739	208740	208741	208742
331.00	332.00	333.00	334.00	335.00	336.00	337.00	338.00	339.00	340.20
332.00	333.00	334.00	335.00	336.00	337.00	338.00	339.00	340.20	341.00
9.54	10.3	10.25	10.85	11	10.4	10.5	10.6	10.85	15.45
5.06	5.21	4.72	4.69	4.58	4.8	4.97	4.93	4.8	5.61
0.139	0.143	0.132	0.136	0.136	0.135	0.1395	0.1415	0.1405	0.173
11.9	11.75	12.1	11.4	11.55	11.9	11.6	11	11.4	12.3
0.35	0.46	0.56	0.74	0.41	0.31	0.38	0.47	0.53	0.21
1.96	1.71	1.67	2.14	2.13	2.12	2.37	2.44	2.5	1.09
0.47	0.43	0.4	0.4	0.37	0.36	0.37	0.35	0.37	0.4
0.012	0.014	0.013	0.014	0.016	0.014	0.014	0.014	0.015	0.022
0.0067	0.0089	0.0051	0.0021	0.003	0.0052	0.0082	0.0096	0.0089	0.0128
44	48	45	44	45	41	44	45	44	58
105	119	118	179	236	228	244	240	266	739
203	198	187	184	173	170	176	173	175	227
53	57	50	58	56	60	63	65	65	78
2.5	2.5	2.5	2.5	2.5	2.5	2.5	2.5	2.5	2.5
2.5	2.5	5	2.5	2.5	2.5	2.5	2.5	5	2.5
0.25	0.25	0.25	0.25	0.25	0.25	0.25	0.25	0.25	0.25

208743	208744	208745	208746	208747	208748	208749	208750	208751	208752
341.00	342.00	343.00	344.00	345.00	346.00	347.00	348.00	349.49	351.03
342.00	343.00	344.00	345.00	346.00	347.00	348.00	349.49	351.03	352.00
15.45	15.8	14.55	15.8	16.15	16.05	15.4	16.2	0.35	13.35
					8.37				
5.15	5.27	5.16	5.39	5.25	5.35	5.24	5.49	0.39	4.61
0.165	0.176	0.1625	0.1725	0.174	0.1745	0.1705	0.186	0.0099	0.154
12.05	12.35	12.1	13	12.5	12.55	12.75	12.65	1.66	10.5
0.14	0.18	0.28	0.17	0.26	0.28	0.2	0.39	0.37	0.68
1.01	1.14	1.52	1.03	0.97	1	0.98	0.9	6.19	2.05
0.36	0.36	0.36	0.37	0.36	0.38	0.37	0.37	0.03	0.33
0.022	0.022	0.021	0.023	0.023	0.023	0.023	0.024	0.000	0.019
0.0035	0.0039	0.0051	0.0066	0.0025	0.0018	0.0037	0.0031	0.0157	0.0012
49	52	50	52	50	52	51	53	1	43
802	879	852	950	1010	981	988	1050	19	769
199	207	200	210	207	219	216	212	4	181
73	71	66	68	69	74	71	94	8	86
2.5	2.5	7	2.5	2.5	2.5	2.5	2.5	17	15
2.5	2.5	5	2.5	2.5	2.5	2.5	2.5	2.5	2.5
0.25	0.25	0.25	0.25	0.25	0.25	0.25	0.25	0.25	0.25

208753	208754	208755	208766	208756	208757	208760	208761	208762	208763
352.00	353.00	354.00	363.11	355.08	356.00	357.00	358.00	359.00	360.00
353.00	354.00	355.08	363.94	356.00	357.00	358.00	359.00	360.00	361.00
14.2	16.6	16.05	19.55	0.8	0.5	0.87	0.67	1.74	0.89
									15.12
5.15	5.91	5.8	6.98	1.05	0.87	1.27	1.06	3.14	1.46
0.1835	0.208	0.211	0.226	0.0281	0.024	0.0339	0.0269	0.0904	0.0387
13.5	11.65	11.7	8.91	2.27	2.11	1.94	1.72	6.12	2.96
0.58	1.1	0.8	4.92	1.47	1.18	1.96	2.57	5.94	2.07
0.79	0.65	0.64	0.91	4.35	3.29	3.35	3.12	11.4	4.34
0.35	0.44	0.41	0.49	0.2	0.18	0.26	0.22	0.71	0.31
0.020	0.024	0.022	0.029	0.001	0.000	0.001	0.000	0.001	0.001
0.0015	0.0003	0.0012	0.0016	0.0007	0.0008	0.0005	0.0004	0.0008	0.0004
45	53	51	69	3	1	4	2	10	3
653	920	977	1070	25	16	25	14	42	18
191	236	218	202	17	12	19	15	49	22
138	181	182	250	29	27	52	43	146	59
2.5	2.5	2.5	17	70	57	85	68	189	89
2.5	2.5	2.5	2.5	2.5	2.5	2.5	2.5	2.5	2.5
0.25	0.25	0.25	0.25	0.25	0.25	0.25	0.25	0.25	0.25

208764	208765	208767	208768	208769
361.00	362.00	363.94	365.00	366.00
362.00	363.11	365.00	366.00	366.99
1.12	1.33	0.43	0.13	2.87
1.38	1.24	0.53	0.46	1.76
0.0394	0.0342	0.0361	0.0977	0.0922
2.48	1.52	0.54	0.81	2.45
2.52	2.5	3	2.74	2.03
4.03	3.89	3.9	5.51	3.86
0.3	0.26	0.04	0.03	0.21
0.001	0.001	0.001	0.000	0.018
0.002	0.0008	0.0008	0.0023	0.0055
4	3	1	1	19
17	16	15	15	229
22	18	2	0.5	41
54	46	22	13	119
99	92	15	40	54
2.5	2.5	2.5	2.5	2.5
0.25	0.25	0.25	0.25	0.25

	149127	149128	149129	149807	149808	149809	149810	149811	149812
.75	242.75	243.85	244.88	245.88	246.48	247.65	248.63	250.30	251.52
.75	243.85	244.88	245.88	246.48	247.65	248.63	250.30	251.52	252.40
.65	14.8	6.52	10.3	13.55	11.3	11	11.05	11.35	12.2
13.5	13.6	13.8	13.8	13.9	14	14.05	14.1	14.35	14.75
.14	7.61	6.45	5.05	6.03	5.67	6.02	6.09	5.99	5.46
041	0.072	0.085	0.030	0.025	0.023	0.025	0.023	0.023	0.029
082	0.0173	0.0293	0.0176	0.0179	0.0068	0.011	0.0092	0.0079	0.0088
68	93	77	52	59	54	59	57	58	58
552	809	106	434	649	574	580	573	571	601
137	191	565	645	134	146	170	206	186	148
0.6	1.1	0.25	0.9	0.25	0.25	0.25	0.25	0.25	0.25

)	149131	149132	208648	208649	208650	208651	208652	208653	208654
.40	253.40	254.40	255.40	256.00	257.00	258.00	259.00	260.00	261.00
.40	254.40	255.40	256.00	257.00	258.00	259.00	260.00	261.00	262.00
.1.9	13	13.5	12	11.55	11.5	11.45	12.4	11.65	11.3
14.85	14.85	15.4	15.5	16.05	17.6	18.6	18.8	20.4	33.9
.29	7.21	5.23	6.15	6.13	6.13	6.02	6.26	6.17	6.05
			0.219	0.234	0.222	0.1955	0.212	0.223	0.2
			7.72	8.37	8.06	8.99	7.69	8.57	8.95
			1.34	1.35	1.3	1.15	1.03	1.25	0.78
			1.69	1.81	1.7	1.53	1.2	1.65	1.67
			0.53	0.52	0.51	0.51	0.52	0.53	0.51
027	0.148	0.032	0.024	0.023	0.022	0.023	0.022	0.023	0.022
114	0.0336	0.0029	0.0085	0.008	0.0098	0.0066	0.0062	0.0056	0.0072
56	84	58	57	57	57	54	55	57	55
574	528	694	610	521	559	600	612	595	590
			206	209	207	207	212	220	211
101	547	296	219	158	163	108	112	172	118
			2.5	2.5	2.5	2.5	2.5	2.5	2.5
			2.5	2.5	2.5	2.5	2.5	2.5	2.5
0.6	1.5	0.25	0.25	0.25	0.25	0.25	0.25	0.25	0.25

208655	208656	208657	208658	208659	208660	208661	208662	208663	208664
262.00	263.00	264.00	265.00	266.00	267.00	268.00	269.00	269.56	270.50
263.00	264.00	265.00	266.00	267.00	268.00	269.00	269.56	270.50	271.00
11.85	11.2	10.7	11.35	11.15	11.75	15.95	22	1.61	1.25
4.21	4.34	6.44	6.65	6.8	6.86	6.89	6.91	6.93	7.68
6.38	6.06	5.9	6.09	6	6.75	4.76	4.71	1.02	0.86
0.205	0.1835	0.1785	0.1805	0.1815	0.153	0.209	0.161	0.0454	0.0312
9.02	9.19	9.4	8.68	8.46	5.18	15.75	10.9	4.5	2.47
0.83	0.41	0.49	0.54	0.62	0.93	0.31	0.01	2.15	2.16
1.45	1.54	1.6	1.63	1.54	0.79	0.25	0.07	6.75	6.95
0.54	0.51	0.51	0.51	0.49	0.4	0.17	0.07	0.16	0.14
0.023	0.022	0.021	0.022	0.022	0.037	0.070	0.094	0.003	0.001
0.0065	0.0062	0.0143	0.0093	0.0085	0.0163	0.0041	0.0022	0.0002	0.0002
59	56	55	58	55	74	74	71	8	4
630	579	570	596	570	818	1970	1660	29	14
216	209	208	203	198	292	173	191	20	15
141	96	105	86	98	736	92	86	28	23
2.5	2.5	2.5	2.5	2.5	2.5	2.5	2.5	136	102
8	2.5	2.5	2.5	2.5	18	2.5	2.5	2.5	2.5
0.25	0.25	0.25	0.25	0.25	0.25	0.25	0.25	0.25	0.25

208665	208666	208667	208670	208671	208672	208673	208674	208675	208676
271.00	272.00	273.00	274.00	274.68	276.00	277.00	278.00	279.00	280.00
272.00	273.00	274.00	274.68	276.00	277.00	278.00	279.00	280.00	281.00
1.37	1.2	0.8	1.94	8.74	9.58	14.5	18.4	16.2	14.7
8.08	8.16	8.25	9.01	9.05	9.65	9.72	9.8	9.86	
1.18	1.15	0.78	1.32	5.15	4.16	5.81	5.37	5.48	8.01
0.0446	0.0429	0.0253	0.0417	0.116	0.101	0.151	0.191	0.154	0.142
1.81	1.06	0.64	2.1	3.32	4.38	5.56	9.22	6.19	4.12
2.67	2.33	1.63	2.57	3.05	1.11	1.53	0.33	0.89	2.3
7	5.45	4.69	5.3	1.16	1.55	0.9	0.3	0.63	0.16
0.18	0.19	0.13	0.24	0.49	0.3	0.34	0.13	0.32	0.47
0.001	0.001	0.001	0.002	0.018	0.019	0.043	0.069	0.057	0.070
0.0003	0.0003	0.0006	0.0004	0.0036	0.0007	0.0062	0.0029	0.005	0.0334
4	3	1	6	42	38	63	67	72	98
15	10	8	28	350	424	859	1440	1130	1260
16	13	9	27	162	115	179	120	160	168
32	29	17	32	103	85	139	146	164	293
106	98	67	109	27	44	10	9	13	19
2.5	5	2.5	7	2.5	2.5	2.5	2.5	2.5	14
0.25	0.25	0.25	0.25	0.25	0.25	0.25	0.25	0.25	0.25

208677	208678	208679	208680	208681	208682	208683	208684	208685	208686
281.00	282.00	283.00	284.00	285.00	286.00	287.00	287.82	289.00	290.00
282.00	283.00	284.00	285.00	286.00	287.00	287.82	289.00	290.00	291.00
13.6	21.7	21.8	20.1	20.2	21.6	22.1	22.5	22.9	23.5
10.57									
4.52	5.08	4.96	5.81	5.55	4.73	5.37	4.73	5.11	4.68
0.0861	0.145	0.151	0.168	0.172	0.164	0.154	0.146	0.152	0.145
3.38	7.81	8.21	8.36	8.35	9.1	7.62	8.02	7.89	7.69
0.84	0.01	0.01	0.2	0.16	0.01	0.01	0.005	0.005	0.005
0.58	0.07	0.07	0.19	0.18	0.11	0.07	0.04	0.04	0.04
0.18	0.05	0.05	0.11	0.1	0.05	0.11	0.11	0.15	0.12
0.050	0.091	0.090	0.097	0.090	0.093	0.084	0.099	0.110	0.109
0.0109	0.0049	0.0011	0.0001	0.00005	0.0001	0.0011	0.0032	0.0042	0.0037
51	79	77	87	80	72	77	75	85	77
877	1410	1370	1650	1580	1320	1390	1180	1580	1390
106	130	127	137	141	120	137	97	117	98
118	70	64	76	77	66	59	47	51	48
18	2.5	2.5	2.5	2.5	2.5	2.5	2.5	2.5	2.5
2.5	2.5	2.5	2.5	2.5	2.5	2.5	2.5	2.5	2.5
0.25	0.25	0.25	0.25	0.25	0.25	0.25	0.25	0.25	0.25

EasyMETLS database from graphite schist AFC model

			Liquid composition wt%											
Index	T (C)	P (bar)	m (assim	SiO2	TiO2	Al2O3	Fe2O3	FeO	MnO	MgO	CaO	Na2O	K2O	P2O5
0	1800	1000	0	44.33	0.21	2.90	1.35	10.28	0.16	40.65	0.11	0.02	0.00	0.00
1	1780	1000	2.5	44.84	0.22	3.22	1.33	10.19	0.16	39.74	0.17	0.08	0.05	0.00
2	1760	1000	5	45.32	0.24	3.52	1.32	10.11	0.16	38.87	0.22	0.13	0.10	0.01
3	1740	1000	7.5	45.78	0.25	3.81	1.31	10.04	0.15	38.04	0.27	0.18	0.15	0.01
4	1720	1000	10	46.22	0.26	4.08	1.30	9.96	0.15	37.25	0.32	0.23	0.19	0.02
5	1700	1000	12.5	46.64	0.27	4.34	1.29	9.89	0.15	36.50	0.37	0.28	0.24	0.02
6	1680	1000	15	47.05	0.28	4.60	1.28	9.83	0.15	35.78	0.41	0.32	0.28	0.02
7	1660	1000	17.5	47.43	0.30	4.84	1.27	9.76	0.15	35.08	0.45	0.36	0.32	0.03
8	1640	1000	20	47.80	0.31	5.07	1.27	9.70	0.15	34.42	0.50	0.40	0.36	0.03
9	1620	1000	22.5	48.16	0.32	5.29	1.26	9.64	0.15	33.78	0.54	0.44	0.39	0.03
10	1600	1000	25	48.50	0.33	5.50	1.25	9.58	0.15	33.17	0.57	0.48	0.43	0.03
11	1580	1000	27.5	48.83	0.33	5.70	1.25	9.53	0.15	32.59	0.61	0.52	0.46	0.04
12	1560	1000	30	49.14	0.34	5.90	1.24	9.47	0.15	32.02	0.65	0.55	0.50	0.04
13	1540	1000	32.5	49.44	0.35	6.09	1.24	9.42	0.14	31.48	0.68	0.59	0.53	0.04
14	1520	1000	35	49.74	0.36	6.27	1.23	9.37	0.14	30.95	0.71	0.62	0.56	0.05
15	1500	1000	37.5	50.02	0.37	6.45	1.23	9.32	0.14	30.45	0.74	0.65	0.59	0.05
16	1480	1000	40	50.29	0.38	6.62	1.23	9.27	0.14	29.96	0.77	0.68	0.61	0.05
17	1460	1000	42.5	50.55	0.38	6.78	1.22	9.22	0.14	29.49	0.80	0.71	0.64	0.05
18	1440	1000	45	50.80	0.39	6.94	1.22	9.18	0.14	29.04	0.83	0.74	0.67	0.05
19	1420	1000	47.5	51.05	0.40	7.09	1.22	9.13	0.14	28.60	0.86	0.76	0.69	0.06
20	1400	1000	50	51.28	0.40	7.24	1.22	9.09	0.14	28.17	0.88	0.79	0.72	0.06

EasyMETLS database from TTG AFC model

Index	T (C)	P (bar)	m (assim)	SiO2	TiO2	Al2O3	Fe2O3	FeO	MnO	MgO	CaO	Na2O	K2O	P2O5
0	1800	1000	0	44.33	0.21	2.90	1.35	10.28	0.16	40.65	0.11	0.02	0.00	0.00
1	1780	1000	2.5	44.93	0.21	3.21	1.33	10.10	0.16	39.70	0.19	0.13	0.05	0.00
2	1760	1000	5	45.50	0.22	3.51	1.31	9.92	0.15	38.79	0.26	0.24	0.10	0.01
3	1740	1000	7.5	46.04	0.22	3.79	1.29	9.76	0.15	37.92	0.33	0.35	0.14	0.01
4	1720	1000	10	46.56	0.22	4.06	1.28	9.60	0.15	37.09	0.39	0.45	0.18	0.01
5	1700	1000	12.5	47.06	0.23	4.31	1.26	9.45	0.15	36.30	0.46	0.54	0.22	0.02
6	1680	1000	15	47.54	0.23	4.56	1.25	9.30	0.14	35.55	0.52	0.63	0.26	0.02
7	1660	1000	17.5	47.99	0.23	4.80	1.23	9.16	0.14	34.82	0.58	0.72	0.30	0.02
8	1640	1000	20	48.43	0.24	5.02	1.22	9.03	0.14	34.13	0.63	0.80	0.34	0.03
9	1620	1000	22.5	48.85	0.24	5.24	1.21	8.90	0.14	33.46	0.69	0.88	0.37	0.03
10	1600	1000	25	49.25	0.24	5.45	1.20	8.78	0.14	32.82	0.74	0.96	0.40	0.03
11	1580	1000	27.5	49.63	0.25	5.65	1.18	8.66	0.13	32.21	0.79	1.04	0.43	0.03
12	1560	1000	30	50.00	0.25	5.84	1.17	8.55	0.13	31.62	0.83	1.11	0.46	0.03
13	1540	1000	32.5	50.36	0.25	6.02	1.17	8.44	0.13	31.05	0.88	1.17	0.49	0.04
14	1520	1000	35	50.70	0.25	6.20	1.16	8.33	0.13	30.50	0.92	1.24	0.52	0.04
15	1500	1000	37.5	51.04	0.26	6.37	1.15	8.23	0.13	29.97	0.97	1.30	0.55	0.04
16	1480	1000	40	51.36	0.26	6.54	1.14	8.13	0.13	29.46	1.01	1.37	0.57	0.04
17	1460	1000	42.5	51.66	0.26	6.70	1.13	8.03	0.13	28.97	1.05	1.42	0.60	0.05
18	1440	1000	45	51.96	0.26	6.85	1.13	7.94	0.12	28.50	1.08	1.48	0.62	0.05
19	1420	1000	47.5	52.25	0.26	7.00	1.12	7.85	0.12	28.04	1.12	1.54	0.65	0.05
20	1400	1000	50	52.53	0.27	7.14	1.12	7.76	0.12	27.59	1.16	1.59	0.67	0.05

Geochemistry of ore of the Boa vista Ni-Cu-PGE sulfide deposit

Samples	Ore type	Fe %	S %	Ni %	Cu %	Co ppm	Zn ppm	Ni/ Cu
BVD22-115,00	Matrix breccia ore	40.40	19.10	4.20	0.04	1400	120	105.00
BVD22-114,39	Matrix breccia ore	16.00	10.70	1.40	0.28	400	330	5.00
BVD22-114,27	Matrix breccia ore	21.10	14.60	1.90	0.38	600	320	5.00
BVD22-114,13	Matrix breccia ore	18.60	10.00	1.70	0.19	500	350	8.95
BVD31-23,83	Matrix breccia ore	39.10	18.60	1.10	0.26	1000	170	4.23
BVD31-24,60	Matrix breccia ore	37.40	18.40	0.90	0.15	800	280	6.00
BVD31-26,30	Matrix breccia ore	40.60	17.70	1.10	0.13	700	150	8.46
BVD31-26,30A	Matrix breccia ore	41.10	19.50	1.10	0.15	900	200	7.33
BVD31-32,70	Matrix breccia ore	36.50	17.30	0.90	0.15	600	260	6.00
BVD31-33,26	Matrix breccia ore	39.40	17.80	1.00	0.12	800	210	8.34
BVD14-47,77	Matrix breccia ore	40.20	22.50	4.40	0.58	1400	280	7.59
BVD14-65,22	Matrix breccia ore	39.00	23.90	4.50	0.07	1400	110	64.29
BVD103_178,46	Matrix breccia ore	44.81	9.61	2.14	0.21	521	1550	10.24
BVD103_177,75	Matrix breccia ore	40.91	9.71	2.00	0.41	492	2790	4.88
BVD103_167,20	Matrix breccia ore	34.03	13.10	1.81	0.32	513	640	5.75
BVD103_166,25	Matrix breccia ore	40.19	12.30	2.45	0.16	675	990	15.41
BVD047_132,05	Matrix breccia ore	55.55	3.92	0.33	0.17	0.03	60	1.91
BVD047_131,90	Matrix breccia ore	50.43	9.69	0.32	0.06	717	410	5.16

Os ppb	Ir ppb	Ru ppb	Rh ppb	Pt ppb	Pd ppb	Re ppb	Au ppb	Cr ppm	Se ppm
B.D.L.	B.D.L.	B.D.L.	33	B.D.L.	282	-	B.D.L.	-	1
B.D.L.	B.D.L.	B.D.L.	B.D.L.	19	245	-	B.D.L.	-	2
B.D.L.	B.D.L.	B.D.L.	B.D.L.	15	156	-	B.D.L.	-	3
B.D.L.	B.D.L.	B.D.L.	B.D.L.	B.D.L.	201	-	B.D.L.	-	9
B.D.L.	B.D.L.	B.D.L.	B.D.L.	B.D.L.	74	-	B.D.L.	-	17
B.D.L.	B.D.L.	B.D.L.	B.D.L.	B.D.L.	102	-	B.D.L.	-	1
B.D.L.	B.D.L.	B.D.L.	B.D.L.	B.D.L.	83	-	B.D.L.	-	1
B.D.L.	B.D.L.	B.D.L.	B.D.L.	B.D.L.	122	-	B.D.L.	-	1
B.D.L.	B.D.L.	B.D.L.	B.D.L.	B.D.L.	137	-	B.D.L.	-	13
B.D.L.	B.D.L.	B.D.L.	B.D.L.	B.D.L.	9	-	B.D.L.	-	1
B.D.L.	B.D.L.	B.D.L.	43	B.D.L.	263	-	B.D.L.	-	1
B.D.L.	B.D.L.	B.D.L.	44	B.D.L.	176	-	B.D.L.	-	13
B.D.L.	0.7	B.D.L.	B.D.L.	90	B.D.L.	B.D.L.	1	170	-
8	0.3	B.D.L.	7.5	B.D.L.	104	B.D.L.	1	210	-
B.D.L.	5.5	70	10.1	B.D.L.	B.D.L.	7	B.D.L.	820	-
B.D.L.	0.2	B.D.L.	B.D.L.	B.D.L.	124	B.D.L.	0.6	180	-
B.D.L.	0.3	B.D.L.	B.D.L.	130	B.D.L.	B.D.L.	2	40	-
B.D.L.	0.3	30	10.9	B.D.L.	B.D.L.	B.D.L.	4	70	-

Ag ppm	W ppm	V ppm	As ppm	Mo ppm	Sn ppm	Bi ppm	Sb ppm	Pb ppm	Reference
-	-	-	-	-	-	-	-	-	Costa JR, et al 1997
-	-	-	-	-	-	-	-	-	Costa JR, et al 1997
-	-	-	-	-	-	-	-	-	Costa JR, et al 1997
-	-	-	-	-	-	-	-	-	Costa JR, et al 1997
-	-	-	-	-	-	-	-	-	Costa JR, et al 1997
-	-	-	-	-	-	-	-	-	Costa JR, et al 1997
-	-	-	-	-	-	-	-	-	Costa JR, et al 1997
-	-	-	-	-	-	-	-	-	Costa JR, et al 1997
-	-	-	-	-	-	-	-	-	Costa JR, et al 1997
-	-	-	-	-	-	-	-	-	Costa JR, et al 1997
-	-	-	-	-	-	-	-	-	Costa JR, et al 1997
-	-	-	-	-	-	-	-	-	Costa JR, et al 1997
B.D.L.	2	67	B.D.L.	13	3	0.8	0.5	38	This study
1	3.9	81	B.D.L.	37	3	1.5	2	111	This study
1	4.1	98	B.D.L.	10	7	0.8	0.6	42	This study
B.D.L.	3.9	85	B.D.L.	23	2	0.5	0.7	43	This study
B.D.L.	B.D.L.	28	B.D.L.	B.D.L.	B.D.L.	0.9	B.D.L.	10	This study
B.D.L.	5	37	6	B.D.L.	B.D.L.	1.5	4.7	18	This study

B.D.L. = below detection limit

- not analyzed

100% Sulfide calculus of Boa vista deposit

	Analysis							
	%	%	%	%	%	ppm	ppm	ppm
Samples	S	Fe	Ni	Cu	Co	Pd	Ir	Zn
BVD103_178,46	9.61	44.81	2.14	0.21	0.05	0.00	0.70	1550.00
BVD103_177,75	9.71	40.91	2.00	0.41	0.05	0.10	0.30	2790.00
BVD103_167,20	13.10	34.03	1.81	0.32	0.05	0.00	5.50	640.00
BVD103_166,25	12.30	40.19	2.45	0.16	0.07	0.12	0.20	990.00
BVD047_131,90	9.69	50.43	0.32	0.06	0.00	0.00	0.30	410.00
BVD047_132,05	3.92	55.55	0.33	0.17	0.07	0.00	0.30	60.00
BVD22-115,00	19.10	40.40	4.20	0.04	0.14	0.28		120.00
BVD22-114,39	10.70	16.00	1.40	0.26	0.04	0.25		330.00
BVD22-114,27	14.60	21.10	1.90	0.38	0.06	0.16		320.00
BVD22-114,13	10.00	18.60	1.70	0.19	0.05	0.20		350.00
BVD31-23,83	18.60	39.10	1.10	0.26	0.10	0.07		170.00
BVD31-24,60	18.40	37.40	0.90	0.15	0.08	0.10		280.00
BVD31-26,30	17.70	40.60	1.10	0.13	0.07	0.08		150.00
BVD31-26,30A	19.50	41.10	1.10	0.15	0.09	0.12		200.00
BVD31-32,70	17.30	36.50	0.90	0.15	0.06	0.14		260.00
BVD31-3326	17.80	39.40	1.00	0.12	0.08	0.01		210.00
BVD14-47,77	22.50	40.20	4.40	0.58	0.14	0.26		280.00
BVD14-65, 22	23.90	39.00	4.50	0.07	0.14	0.18		110.00

Normative Mineralogy

% Ccp	% Pn	% Po	% Mag	% Sulfide Only
0.604	5.6	19.3		25.6
1.18	5.3	19.4		25.8
0.91	4.8	28.8		34.4
0.46	6.5	25.7		32.6
0.18	0.83	24.0		25.0
0.50	0.87	8.9		10.2
0.116	11.1	39.5		50.7
0.75	3.7	23.7		28.1
1.10	5.0	32.2		38.3
0.55	4.5	21.4		26.4
0.75	2.90	44.6		48.3
0.43	2.37	44.8		47.6
0.375	2.9	42.6		45.9
0.43	2.9	47.2		50.5
0.43	2.4	42.0		44.8
0.35	2.6	43.1		46.1
1.68	11.60	46.4		59.7
0.20	11.86	51.1		63.1

100% Sulfides with Fe by Difference

% S_{100}	% Fe_{100}	% Ni_{100}	% Cu_{100}	% Co_{100}	ppm Pd_{100}	ppm Ir_{100}	ppm Zn	% Zn	% Total
37.6	*53.0*	8.4	0.8	0.20	0.01	2.74	6061.38	0.61	100.6
37.6	*52.9*	7.7	1.6	0.19	0.40	1.16	10799.97	1.08	101.1
38.0	*55.6*	5.3	0.9	0.15	0.01	15.97	1858.61	0.19	100.2
37.7	*54.0*	7.5	0.5	0.21	0.38	0.61	3038.26	0.30	100.3
38.7	*59.8*	1.3	0.2		0.01	1.20	1638.72	0.16	100.2
38.3	*56.1*	3.2	1.7	0.70	0.02	2.93	585.67	0.06	100.1
37.7	*53.7*	8.3	0.1	0.28	0.56		236.72	0.02	
38.1	*55.9*	5.0	0.9	0.14	0.87		1174.57	0.12	
38.1	*55.8*	5.0	1.0	0.16	0.41		834.64	0.08	
37.9	*54.8*	6.4	0.7	0.19	0.76		1325.99	0.13	
38.5	*58.4*	2.3	0.5	0.21	0.15		352.25	0.04	
38.6	*59.0*	1.9	0.3	0.17	0.21		587.78	0.06	
38.6	*58.6*	2.4	0.3	0.15	0.18		326.71	0.03	
38.6	*58.8*	2.2	0.3	0.18	0.24		395.73	0.04	
38.6	*58.9*	2.0	0.3	0.13	0.31		580.19	0.06	
38.6	*58.8*	2.2	0.3	0.17	0.02		455.27	0.05	
37.7	*53.7*	7.4	1.0	0.23	0.44		469.33	0.05	
37.9	*54.7*	7.1	0.1	0.22	0.28		174.21	0.02	

R factor calculus data about Boa Vista ore

R-factor Y_0=0	Komatiite					
	Co	**Ni**	**Cu**	**Pd**	**Ir**	**Zn**
	ppm	ppm	ppm	ppb	ppb	ppm
Xo	115	1700	45	6	2.1	65
	%	%	%	ppm	ppm	%
Yo	0	0	0	0	0	0
$D_{Sul/Sil}$	30	150	600	30,000	30,000	2.5

	Y_f					
R	**Co (%)**	**Ni (%)**	**Cu (%)**	**Pd (ppm)**	**Ir (ppm)**	**Zn (%)**
1	0.01	0.17	0.00	0.01	0.00	0.0046
3	0.03	0.50	0.01	0.02	0.01	0.0089
5	0.05	0.82	0.02	0.03	0.01	0.0108
10	0.09	1.59	0.04	0.06	0.02	0.0130
30	0.17	4.25	0.13	0.18	0.06	0.0150
50	0.22	6.38	0.21	0.30	0.10	0.0155
100	0.27	10.20	0.39	0.60	0.21	0.0159
300	0.31	17.00	0.90	1.78	0.62	0.0161
500	0.33	19.62	1.23	2.95	1.03	0.0162
1000	0.33	22.17	1.69	5.81	2.03	0.0162
3000	0.34	24.29	2.25	16.36	5.73	0.0162
5000	0.34	24.76	2.41	25.71	9.00	0.0162
10000	0.34	25.12	2.55	45.00	15.75	0.0162
30000	0.34	25.37	2.65	90.00	31.50	0.0162
50000	0.34	25.42	2.67	112.50	39.38	0.0162
100000	0.34	25.46	2.68	138.46	48.46	0.0162
300000	0.34	25.49	2.69	163.64	57.27	0.0162
500000	0.34	25.49	2.70	169.81	59.43	0.0162
1000000	0.34	25.50	2.70	174.76	61.17	0.0162
3000000	0.34	25.50	2.70	178.22	62.38	0.0162
5000000	0.34	25.50	2.70	178.93	62.62	0.0162
10000000	0.34	25.50	2.70	179.46	62.81	0.0162

R-factor $Y_0>0$

Komatiite

	Co	Ni	Cu	Pd	Ir	Zn
	ppm	ppm	ppm	ppb	ppb	ppm
Xo	115	1700	45	6	2.1	65
	%	%	%	ppm	ppm	%
Yo	0.1	0.2	0.1	0.5	0	0.1
$D_{Sul/Sil}$	30	150	600	30,000	30,000	2.5

Y_f

R	Co (%)	Ni (%)	Cu (%)	Pd (ppm)	Ir (ppm)	Zn (%)
1	0.11	0.37	0.10	0.51	0.00	0.0761
3	0.12	0.70	0.11	0.52	0.01	0.0543
5	0.14	1.02	0.12	0.53	0.01	0.0442
10	0.16	1.78	0.14	0.56	0.02	0.0330
30	0.22	4.42	0.22	0.68	0.06	0.0227
50	0.25	6.53	0.30	0.80	0.10	0.0202
100	0.29	10.32	0.47	1.10	0.21	0.0183
300	0.32	17.07	0.97	2.28	0.62	0.0169
500	0.33	19.66	1.28	3.44	1.03	0.0167
1000	0.34	22.20	1.73	6.29	2.03	0.0165
3000	0.34	24.30	2.27	16.82	5.73	0.0163
5000	0.34	24.76	2.42	26.14	9.00	0.0163
10000	0.34	25.13	2.55	45.38	15.75	0.0163
30000	0.34	25.37	2.65	90.25	31.50	0.0163
50000	0.34	25.42	2.67	112.69	39.38	0.0163
100000	0.34	25.46	2.68	138.58	48.46	0.0163
300000	0.34	25.49	2.69	163.68	57.27	0.0163
500000	0.34	25.49	2.70	169.84	59.43	0.0163
1000000	0.34	25.50	2.70	174.77	61.17	0.0163
3000000	0.34	25.50	2.70	178.22	62.38	0.0163
5000000	0.34	25.50	2.70	178.93	62.62	0.0163
10000000	0.34	25.50	2.70	179.46	62.81	0.0163

R-factor $Y_0=X_0$		Komatiite				
	Co	Ni	Cu	Pd	Ir	Zn
	ppm	ppm	ppm	ppb	ppb	ppm
Xo	115	1700	45	6	2.1	65
	%	%	%	ppm	ppm	%
Yo	0.015	0.17	0.0045	0.006	0.0021	0.0065
$D_{Sul/Sil}$	30	150	600	30,000	30,000	2.5

	Y_f					
R	**Co (%)**	**Ni (%)**	**Cu (%)**	**Pd (ppm)**	**Ir (ppm)**	**Zn (%)**
1	0.02	0.34	0.01	0.00	0.00	0.01
3	0.04	0.67	0.02	0.00	0.00	0.01
5	0.06	0.99	0.03	0.00	0.00	0.01
10	0.09	1.75	0.05	0.01	0.00	0.01
30	0.18	4.39	0.13	0.02	0.01	0.02
50	0.22	6.50	0.21	0.03	0.01	0.02
100	0.27	10.30	0.39	0.06	0.02	0.02
300	0.31	17.06	0.90	0.18	0.06	0.02
500	0.33	19.65	1.23	0.30	0.10	0.02
1000	0.34	22.20	1.69	0.58	0.20	0.02
3000	0.34	24.29	2.25	1.64	0.57	0.02
5000	0.34	24.76	2.41	2.57	0.90	0.02
10000	0.34	25.13	2.55	4.50	1.58	0.02
30000	0.34	25.37	2.65	9.00	3.15	0.02
50000	0.34	25.42	2.67	11.25	3.94	0.02
100000	0.34	25.46	2.68	13.85	4.85	0.02
300000	0.34	25.49	2.69	16.36	5.73	0.02
500000	0.34	25.49	2.70	16.98	5.94	0.02
1000000	0.34	25.50	2.70	17.48	6.12	0.02
3000000	0.34	25.50	2.70	17.82	6.24	0.02
5000000	0.34	25.50	2.70	17.89	6.26	0.02
10000000	0.34	25.50	2.70	17.95	6.28	0.02

Sulfur isotope all data from ore of the Boa Vista Ni-Cu-PGE sulfide deposit

Sample	Standard 1	Standard 2	1s SD 32/34S	2s SD 32/34S	Error 1s absolute	Error 2s absolute	Error 1s ‰	Error 2s ‰	1s SD 34/32S	2s SD 34/32S	‰CDT	δ^{34}S ‰V-CDT
PCX-BIV-46,5												
003_po	001_123		21.97	21.97	0.01	0.03	0.59	1.18	0.05	0.05	10.79	30.73
004_po	001_123		21.97	21.97	0.01	0.02	0.53	1.07	0.05	0.05	10.74	30.67
008_po	006_cpyp		21.98	21.98	0.01	0.02	0.56	1.12	0.05	0.05	10.21	30.13
009_po	006_cpyp		21.97	21.97	0.01	0.02	0.55	1.10	0.05	0.05	10.51	30.44
013_po	011_123		21.98	21.98	0.01	0.02	0.40	0.79	0.05	0.05	10.22	30.14
014_po	011_123		21.98	21.98	0.01	0.02	0.51	1.01	0.05	0.05	10.24	30.16
018_po	016_cpyp		21.97	21.97	0.01	0.02	0.50	1.00	0.05	0.05	10.75	30.68
019_po	016_cpyp		21.97	21.97	0.01	0.02	0.55	1.10	0.05	0.05	10.66	30.60
023_po	021_123		21.91	21.91	0.02	0.04	0.99	1.98	0.05	0.05	13.71	33.70
024_po	021_123		21.91	21.91	0.02	0.05	1.06	2.11	0.05	0.05	13.58	33.57
028_po	026_cpyp		21.98	21.97	0.01	0.03	0.62	1.25	0.05	0.05	10.50	30.43
029_po	026_cpyp		21.97	21.97	0.01	0.03	0.60	1.19	0.05	0.05	10.71	30.65
033_po	031_123		21.99	21.99	0.02	0.03	0.71	1.41	0.05	0.05	9.88	29.80
034_po	031_123		21.99	21.98	0.02	0.03	0.69	1.38	0.05	0.05	10.15	30.07
039_po	036_123	037_cpyp	21.77	21.76	0.01	0.02	0.43	0.85	0.05	0.05	20.25	40.37
040_po	036_123	042_123	21.96	21.96	0.01	0.02	0.45	0.89	0.05	0.05	11.30	31.24
044_cpy	042_123		21.94	21.94	0.02	0.04	0.80	1.61	0.05	0.05	12.01	31.97
045_cpy	042_123		21.94	21.94	0.02	0.03	0.71	1.42	0.05	0.05	12.23	32.20
049_cpy	047_cpyp		21.97	21.97	0.02	0.04	0.91	1.83	0.05	0.05	10.92	30.86
050_cpy	047_cpyp		21.97	21.98	0.02	0.04	0.85	1.70	0.05	0.05	10.47	30.40
BVD31-33,26												
003_po	001_123		22.24	22.24	0.01	0.02	0.45	0.91	0.04	0.04	-1.42	18.28
004_po	001_123		22.23	22.23	0.01	0.02	0.42	0.84	0.04	0.04	-1.23	18.47
008_po	006_pnp		22.23	22.23	0.01	0.01	0.30	0.59	0.04	0.04	-1.23	18.47
009_po	006_pnp		22.23	22.23	0.01	0.01	0.24	0.48	0.04	0.04	-1.32	18.38
013_po	011_123		22.24	22.24	0.01	0.02	0.49	0.97	0.04	0.04	-1.42	18.28
014_po	011_123		22.24	22.24	0.01	0.02	0.46	0.92	0.04	0.04	-1.40	18.30
018_po	016_pnp		22.23	22.23	0.01	0.02	0.35	0.71	0.04	0.04	-1.07	18.63
019_po	016_pnp		22.23	22.23	0.01	0.01	0.33	0.67	0.04	0.04	-1.06	18.65
023_cpy	021_123		22.24	22.24	0.01	0.03	0.67	1.34	0.04	0.04	-1.56	18.14
024_cpy	021_123		22.24	22.25	0.01	0.02	0.48	0.96	0.04	0.04	-1.80	17.89
029_pn	026_pnp		22.23	22.23	0.01	0.01	0.26	0.53	0.04	0.04	-1.20	18.50
030_pn	026_pnp		22.23	22.23	0.01	0.01	0.27	0.55	0.04	0.04	-1.20	18.50
BVD31-32,7												
003_pn	001_pnp		22.25	22.25	0.01	0.02	0.34	0.69	0.04	0.04	-1.89	17.79
004_pn	001_pnp		22.25	22.25	0.01	0.02	0.55	1.09	0.04	0.04	-2.01	17.67
008_po	006_pnp		22.25	22.25	0.01	0.02	0.34	0.69	0.04	0.04	-2.10	17.59
009_po	006_pnp		22.25	22.25	0.01	0.01	0.32	0.64	0.04	0.04	-2.18	17.50
013_pn	011_123		22.25	22.25	0.01	0.02	0.54	1.07	0.04	0.04	-2.15	17.53
014_pn	011_123		22.25	22.25	0.01	0.03	0.59	1.18	0.04	0.04	-2.00	17.68
018_po	016_123		22.26	22.26	0.01	0.02	0.52	1.05	0.04	0.04	-2.44	17.23
019_po	016_123		22.25	22.25	0.01	0.03	0.58	1.15	0.04	0.04	-2.22	17.46
023_pn	021_pnp		22.25	22.25	0.01	0.02	0.42	0.85	0.04	0.04	-1.90	17.79
024_pn	021_pnp		22.25	22.25	0.01	0.02	0.41	0.83	0.04	0.04	-1.89	17.79
028_po	026_pnp		22.26	22.26	0.01	0.03	0.60	1.20	0.04	0.04	-2.23	17.45
029_po	026_pnp		22.25	22.25	0.01	0.03	0.65	1.29	0.04	0.04	-2.10	17.58
033_pn	031_123		22.25	22.25	0.02	0.03	0.78	1.56	0.04	0.04	-2.03	17.66
034_pn	031_123		22.26	22.26	0.02	0.04	0.81	1.62	0.04	0.04	-2.44	17.23
038_po	036_123		22.25	22.25	0.02	0.03	0.76	1.52	0.04	0.04	-2.20	17.48
039_po	036_123		22.26	22.25	0.01	0.02	0.47	0.95	0.04	0.04	-2.20	17.48
044_pn	042_123	048_123	22.26	22.26	0.01	0.02	0.51	1.02	0.04	0.04	-2.34	17.33
045_pn	042_123	048_123	22.25	22.25	0.01	0.02	0.51	1.03	0.04	0.04	-2.20	17.47
044_pn	041_pnp	047_pnp	22.26	22.26	0.01	0.02	0.39	0.77	0.04	0.04	-2.35	17.33
045_pn	041_pnp	047_pnp	22.26	22.25	0.01	0.02	0.52	1.05	0.04	0.04	-2.18	17.50
050_po	047_pnp		22.26	22.26	0.01	0.03	0.59	1.19	0.04	0.04	-2.56	17.12
051_po	047_pnp		22.26	22.27	0.01	0.02	0.40	0.81	0.04	0.04	-2.69	16.98
050_po	048_123		22.26	22.26	0.03	0.06	1.43	2.87	0.04	0.04	-2.32	17.36
051_po	048_123		22.26	22.26	0.03	0.06	1.38	2.77	0.04	0.04	-2.49	17.18

BVD31-42,15

003_po	001_123		22.23	22.23	0.01	0.03	0.58	1.17	0.04	0.04	-1.12	18.58
004_po	001_123		22.22	22.22	0.02	0.03	0.69	1.39	0.05	0.05	-0.75	18.96
008_po	006_cpyp		22.25	22.25	0.02	0.03	0.78	1.56	0.04	0.04	-2.17	17.51
009_po	006_cpyp		22.25	22.24	0.02	0.03	0.76	1.52	0.04	0.04	-1.76	17.93
013_pn	011_123		22.25	22.26	0.01	0.03	0.57	1.14	0.04	0.04	-2.33	17.34
014_pn	011_123		22.26	22.26	0.02	0.03	0.74	1.47	0.04	0.04	-2.41	17.26
018_pn	016_cpyp		22.25	22.25	0.02	0.03	0.70	1.41	0.04	0.04	-2.22	17.46
019_pn	016_cpyp		22.25	22.26	0.02	0.03	0.70	1.40	0.04	0.04	-2.28	17.39
023_po	021_123		22.26	22.26	0.01	0.03	0.59	1.18	0.04	0.04	-2.43	17.25
024_po	021_123		22.26	22.26	0.01	0.03	0.62	1.25	0.04	0.04	-2.32	17.35
028_po	026_cpyp		22.26	22.26	0.01	0.03	0.65	1.30	0.04	0.04	-2.31	17.37
029_po	026_cpyp		22.26	22.26	0.01	0.03	0.62	1.24	0.04	0.04	-2.29	17.39
033_pn	031_123		22.26	22.26	0.01	0.02	0.49	0.97	0.04	0.04	-2.50	17.17
034_pn	031_123		22.26	22.26	0.01	0.02	0.35	0.69	0.04	0.04	-2.48	17.19
038_pn	036_cpyp		22.26	22.26	0.02	0.03	0.76	1.51	0.04	0.04	-2.45	17.23
039_pn	036_cpyp		22.26	22.25	0.02	0.03	0.71	1.41	0.04	0.04	-2.21	17.47
044_po	041_123	047_123	22.26	22.26	0.01	0.02	0.44	0.89	0.04	0.04	-2.55	17.12
045_po	041_123	047_123	22.27	22.27	0.01	0.02	0.45	0.91	0.04	0.04	-2.80	16.86
044_po	042_cpyp	048_cpyp	22.26	22.26	0.01	0.02	0.47	0.94	0.04	0.04	-2.50	17.18
045_po	042_cpyp	048_cpyp	22.27	22.27	0.01	0.02	0.43	0.85	0.04	0.04	-2.85	16.82
050_pn	047_123		22.28	22.28	0.01	0.03	0.59	1.17	0.04	0.04	-3.17	16.49
051_pn	047_123		22.27	22.27	0.01	0.03	0.58	1.16	0.04	0.04	-3.05	16.61
050_pn	048_cpyp		22.29	22.29	0.01	0.02	0.55	1.09	0.04	0.04	-3.61	16.04
051_pn	048_cpyp		22.28	22.28	0.01	0.02	0.49	0.98	0.04	0.04	-3.37	16.29

BVD14-47,77

003_po	001_123		22.24	22.24	0.01	0.02	0.51	1.02	0.04	0.04	-1.56	18.14
004_po	001_123		22.25	22.25	0.01	0.02	0.44	0.88	0.04	0.04	-2.21	17.47
008_po	006_pnp		22.23	22.23	0.01	0.02	0.39	0.78	0.04	0.04	-1.25	18.45
009_po	006_pnp		22.24	22.24	0.01	0.02	0.39	0.78	0.04	0.04	-1.44	18.25
013_po	011_pnp		22.24	22.24	0.01	0.02	0.40	0.80	0.04	0.04	-1.44	18.25
014_po	011_pnp		22.24	22.24	0.01	0.02	0.36	0.72	0.04	0.04	-1.58	18.11
018_pn	016_pnp		22.24	22.24	0.01	0.01	0.32	0.65	0.04	0.04	-1.67	18.02
019_pn	016_pnp		22.25	22.25	0.01	0.01	0.28	0.56	0.04	0.04	-1.84	17.84
024_po	022_pnp		22.24	22.24	0.01	0.01	0.31	0.62	0.04	0.04	-1.71	17.98
025_po	022_pnp		22.25	22.25	0.01	0.02	0.35	0.69	0.04	0.04	-1.94	17.74
024_po	021_123		22.24	22.24	0.01	0.03	0.65	1.30	0.04	0.04	-1.54	18.15
025_po	021_123		22.24	22.24	0.01	0.03	0.63	1.25	0.04	0.04	-1.62	18.07

BVD22-114,71

003_pn	001_123		22.26	22.26	0.01	0.02	0.47	0.93	0.04	0.04	-2.49	17.18
004_pn	001_123		22.26	22.26	0.01	0.02	0.46	0.92	0.04	0.04	-2.25	17.42
008_po	006_123		22.26	22.26	0.01	0.02	0.45	0.89	0.04	0.04	-2.56	17.11
009_po	006_123		22.26	22.26	0.01	0.02	0.42	0.84	0.04	0.04	-2.38	17.29
014_pn	011_pnp	018_pnp	22.24	22.24	0.01	0.02	0.38	0.75	0.04	0.04	-1.68	18.01
015_pn	011_pnp	018_pnp	22.25	22.25	0.01	0.01	0.30	0.60	0.04	0.04	-1.89	17.80
014_pn	012_123	017_123	22.25	22.25	0.01	0.02	0.46	0.92	0.04	0.04	-2.13	17.56
015_pn	012_123	017_123	22.25	22.26	0.01	0.02	0.37	0.74	0.04	0.04	-2.24	17.44
019_po	017_123		22.26	22.26	0.01	0.02	0.45	0.89	0.04	0.04	-2.28	17.39
020_po	017_123		22.26	22.26	0.01	0.02	0.37	0.74	0.04	0.04	-2.35	17.33
024_pn	022_pnp		22.25	22.25	0.01	0.02	0.48	0.96	0.04	0.04	-2.07	17.61
025_pn	022_pnp		22.25	22.25	0.01	0.01	0.32	0.64	0.04	0.04	-1.98	17.71
029_po	027_pnp		22.25	22.25	0.01	0.02	0.39	0.78	0.04	0.04	-2.11	17.57
030_po	027_pnp		22.25	22.25	0.01	0.02	0.49	0.99	0.04	0.04	-1.91	17.78
034_pn	032_123		22.26	22.26	0.01	0.03	0.63	1.25	0.04	0.04	-2.45	17.22
035_pn	032_123		22.26	22.26	0.01	0.02	0.47	0.93	0.04	0.04	-2.31	17.36
039_po	037_123		22.26	22.26	0.01	0.02	0.44	0.88	0.04	0.04	-2.31	17.36
040_po	037_123		22.25	22.26	0.01	0.02	0.43	0.86	0.04	0.04	-2.25	17.43
044_pn	042_pnp		22.25	22.25	0.01	0.02	0.40	0.80	0.04	0.04	-2.01	17.68
045_pn	042_pnp		22.25	22.25	0.01	0.02	0.38	0.76	0.04	0.04	-1.93	17.75
049_po	047_pnp		22.25	22.25	0.01	0.02	0.36	0.73	0.04	0.04	-1.95	17.73
050_po	047_pnp		22.25	22.25	0.01	0.01	0.33	0.66	0.04	0.04	-1.83	17.86

BVD22-114,87

003_po	001_cpyp		22.25	22.25	0.02	0.04	0.82	1.63	0.04	0.04	-1.88	17.81
004_po	001_cpyp		22.25	22.25	0.01	0.03	0.61	1.22	0.04	0.04	-1.84	17.85
008_po	006_123		22.27	22.27	0.02	0.04	0.80	1.61	0.04	0.04	-3.01	16.66
009_po	006_123		22.27	22.27	0.02	0.03	0.73	1.46	0.04	0.04	-2.89	16.77
013_pn	011_cpyp		22.26	22.26	0.01	0.03	0.63	1.25	0.04	0.04	-2.57	17.10
014_pn	011_cpyp		22.26	22.26	0.02	0.03	0.70	1.39	0.04	0.04	-2.41	17.26
018_pn	016_123		22.27	22.27	0.01	0.03	0.62	1.24	0.04	0.04	-2.87	16.80
019_pn	016_123		22.26	22.27	0.02	0.03	0.72	1.44	0.04	0.04	-2.75	16.92
023_po	021_cpyp		22.26	22.26	0.02	0.04	0.86	1.73	0.04	0.04	-2.34	17.34
024_po	021_cpyp		22.25	22.25	0.01	0.03	0.60	1.20	0.04	0.04	-2.16	17.52
028_po	026_123		22.27	22.27	0.02	0.04	0.84	1.69	0.04	0.04	-3.01	16.65
029_po	026_123		22.28	22.28	0.02	0.04	0.87	1.75	0.04	0.04	-3.18	16.48
033_pn	031_cpyp		22.37	22.36	0.02	0.04	0.99	1.97	0.04	0.04	-6.97	12.61
034_pn	031_cpyp		22.36	22.36	0.02	0.04	0.96	1.91	0.04	0.04	-6.73	12.86
038_pn	036_123		22.27	22.27	0.01	0.02	0.46	0.92	0.04	0.04	-2.86	16.81
039_pn	036_123		22.27	22.27	0.01	0.02	0.46	0.92	0.04	0.04	-2.93	16.74
044_po	041_123	047_123	22.28	22.28	0.01	0.03	0.59	1.17	0.04	0.04	-3.14	16.52
045_po	041_123	047_123	22.28	22.28	0.01	0.01	0.32	0.63	0.04	0.04	-3.21	16.45
050_pn	048_cpyp		22.26	22.26	0.02	0.03	0.69	1.38	0.04	0.04	-2.64	17.03
051_pn	048_cpyp		22.26	22.26	0.01	0.02	0.55	1.09	0.04	0.04	-2.58	17.09

BVD22-115

003_po	001_123		22.24	22.24	0.01	0.02	0.56	1.12	0.04	0.04	-1.76	17.93
004_po	001_123		22.24	22.24	0.01	0.03	0.59	1.18	0.04	0.04	-1.76	17.93
008_pn	006_123		22.24	22.24	0.01	0.02	0.48	0.96	0.04	0.04	-1.45	18.24
009_pn	006_123		22.24	22.24	0.01	0.03	0.58	1.15	0.04	0.04	-1.53	18.16
013_po	011_pnp		22.24	22.24	0.01	0.03	0.66	1.32	0.04	0.04	-1.59	18.10
014_po	011_pnp		22.24	22.24	0.01	0.03	0.58	1.17	0.04	0.04	-1.71	17.98
018_pn	016_pnp		22.23	22.23	0.01	0.01	0.32	0.65	0.04	0.04	-1.04	18.66
019_pn	016_pnp		22.24	22.24	0.01	0.02	0.53	1.06	0.04	0.04	-1.56	18.14
023_po	021_123		22.23	22.24	0.01	0.02	0.53	1.06	0.04	0.04	-1.39	18.30
024_po	021_123		22.23	22.23	0.01	0.02	0.54	1.08	0.04	0.04	-1.12	18.58
028_pn	026_123		22.23	22.23	0.01	0.02	0.40	0.80	0.04	0.04	-1.00	18.71
029_pn	026_123		22.22	22.22	0.01	0.02	0.45	0.90	0.04	0.04	-0.82	18.89
033_po	031_pnp		22.25	22.25	0.01	0.02	0.46	0.91	0.04	0.04	-1.78	17.91
034_po	031_pnp		22.24	22.24	0.01	0.01	0.33	0.65	0.04	0.04	-1.69	18.00
038_pn	036_pnp		22.24	22.24	0.01	0.01	0.24	0.48	0.04	0.04	-1.40	18.29
039_pn	036_pnp		22.24	22.24	0.00	0.01	0.22	0.44	0.04	0.04	-1.53	18.16
044_po	041_123	047_123	22.24	22.24	0.01	0.02	0.46	0.92	0.04	0.04	-1.36	18.33
045_po	041_123	047_123	22.23	22.23	0.01	0.01	0.32	0.65	0.04	0.04	-1.27	18.43
050_pn	048_pnp		22.22	22.22	0.01	0.01	0.23	0.46	0.05	0.04	-0.76	18.95
051_pn	048_pnp		22.23	22.23	0.01	0.01	0.26	0.52	0.04	0.04	-0.93	18.77

2. CAPÍTULO 2

The role of banded iron formations as a source of sulfur and semimetals in komatiite-associated Ni-Cu-PGE deposits: Example from the Fortaleza de Minas deposit, Brazil.

The role of banded iron formations as a source of sulfur and semimetals in komatiite-associated Ni-Cu-PGE deposits: Example from the Fortaleza de Minas deposit, Brazil.

Tiago F. A. Maia[1,2], Cesar F. Ferreira Filho[1]

[1]Programa de pós-graduação em geologia, Instituto de Geociências, Universidade de Brasília, Brasília-DF, 70910-900, Brazil

[2]Departamento de Geociências, Universidade Federal do Amazonas, 69080-900, Brazil

Abstract

The Fortaleza de Minas Ni-Cu-PGE deposit is described as a deposit associated with a highly fractionated ponded komatiite flow. New data for Fortaleza de Minas ore and footwall banded iron formation, including geological, petrographic description, trace-geochemistry, and sulfur isotope, are integrated into this study to understand how the external source of the S, semimetals, as well as the particular association that the deposit has with the highly fractionated ponded komatiite flow. Our results showed that the orebody occurs in contact with sheared talc schist, and at the BIF footwall, the ore in direct contact with BIF is breccia ore, followed by the matrix (net-texture) and disseminated ore, through the trace-geochemistry and sulfur isotope confirmed that the banded iron formation is an external source of S and semimetal. A weak positive correlation was observed with Se and Te, Se, As, and Bi, and good Ni-Cu with Te, Se, and Bi. Multi-element plots normalized by the primitive mantle showed that the ore has higher sulfide ore contents than those for host rocks in the Fortaleza de Minas deposit. The $\delta^{34}S$ values for sulfide ore samples show a narrow compositional range bracketed between +6.1 and +6.5‰, and the $\delta^{34}S$ values for samples of BIF have a compositional +9.5‰. The R factor was calculated with results 150-400. Additional discussions were made regarding the envelope highly fractionated ponded flow and the Fortaleza de Minas Ni-Cu-PGE deposit, where the R factor, high Cr content, and the presence of association with the ore sulfide cannot happen. We propose that there was a combination and superposition of two different environments, one with a conduit/channeled flow at first and other ponded flow facies (lava lake) at last.

Keywords: Banded Iron formations, komatiite, sulfur isotope, pounded flow facies

2.1. INTRODUCTION

The genetic model for the origin of magmatic sulfide deposits requires the existence of an immiscible sulfide liquid as the collector of Ni-Cu-PGE from the mafic-ultramafic magma (e.g., Naldrett, 2004; Robertson et al., 2015; Barnes et al., 2016; Lesher, 2017). However, as the initial concentration of S of mantle magmas is commonly low, an external source of S is demanded to form large magmatic sulfide deposits (e.g., Ripley and Li, 2013; Lesher, 2017). It is now widely accepted that world-class magmatic Ni-Cu-PGE deposits (e.g., Kambalda, Noril'sk, Pechenga, Raglan, Sudbury, Thompson, Voisey's Bay) were derived by assimilation of S-bearing country rocks during lava/magma emplacement in the crust (e.g., Lesher et al., 1984; Barnes and Lightfoot, 2005; Arndt et al., 2008; Keays and Lightfoot, 2010; Ripley and Li, 2013; Barnes et al., 2016; Staude et al., 2017; Staude et al., 2022).

Distinct types of country rocks are thought to be the external source of S for magmatic Ni-Cu-PGE deposits, including black shales (e.g., Kambalda, Raglan, Duluth), banded iron formation (BIF) (e.g., Thompson, Langmuir), evaporites (Noril'sk-Talnakh) and paragneiss (Voisey's Bay). Samalens et al. (2017) and Lesher (2017) pointed out that sulfur is not the only element that could be derived from assimilated country rocks in Ni-Cu-PGE magmatic sulfides. Samalens et al. (2017), for example, investigated the Partridge River Intrusion (Duluth Complex), where Ni-Cu sulfide mineralization occurs close to the intrusion basal contact with S-rich black shales enriched in TABS (Te, As, Bi, Sb). The authors provided physical and geochemical evidence indicating that contamination of mafic magmas by black shales originated sulfide melts enriched in chalcophile metals (e.g., Ni, Cu, Co, PGE) and semi-metals (e.g. TABS). Their results indicate that assimilation of additional elements derived from country impacts the composition of magmatic sulfide deposit, providing potential fingerprints for the contaminants. In several komatiite-associated deposits, physical and geochemical evidence for assimilation of S from closely associated country rocks is supported by S isotope data (Lesher, 1989; Keays and Lightfoot, 2010; Houlé et al., 2012; Ripley and Li, 2013). In addition, combining different types of isotopes have been used to distinguish between different external

sources, leading to possible local to district-scale controls on komatiite-hosted Ni-Cu-PGE deposits (e.g., Fiorentini et al., 2012; Hiebert et al., 2016).

The Fortaleza de Minas Ni-Cu-PGE deposit is South America's largest komatiite-associated Ni-Cu-PGE deposit (Brenner et al. 1990; Brenner, 2006). It is associated with the Archean Morro do Ferro greenstone belt, near the southwestern edge of the São Francisco Craton in Brazil. The total global resource of the deposit is on the order of 10 Mt with an average grade of 2.5% Ni, 0.40 % Cu, 500 ppm Co, and 0.7 g/t Pt, Pd, Au (Brenner, 2006). Nickel production lasted from 1998 to 2013 when mining and processing were discontinued. Previous studies of the Fortaleza de Minas (FM) deposit indicate some remarkable features. The footwall of the orebody consists of sulfide-bearing banded iron formation (BIF), thus providing an appropriate site for investigating the assimilation of BIF by the komatiitic magma as the possible source of S and TABS for the Ni-Cu ore.

More intriguing, however, the FM deposit is located at the base of a fractionated sequence consisting of basal olivine cumulates, clinopyroxene cumulates, and upper gabbro. This fractionated sequence was interpreted by Brenner (2006) as a distal fractionated ponded flow similar to Fred's flow in Munro Township (Arndt, 1977), a scenario that does not provide a turbulent flow along magma conduits necessary to form high-grade Ni-Cu-PGE deposits such as FM. In this study, we use new petrographic, lithochemical, and S isotope data, along with a review of previous geological-geochemical studies of the FM deposit (Brenner et al., 1990; Marchetto, 1990; Choudhuri et al., 1997; Brenner, 2006; Almeida et al., 2007), to investigate and discuss the relative importance of assimilation of the BIF host rocks for the origin of the FM deposit, as well as the constraints for crustal assimilation and metal enrichment in ponded komatiitic flow facies.

2.2. REGIONAL SETTING

2.2.1. Campos Gerais Domain

The Fortaleza de Minas deposit occurs within the Campos Gerais Domain (CGD) in the southwest of the São Francisco Craton (SFC) in Brazil (**Fig. 19**). The SFC is a Brazilian (Neoproterozoic) crustal block within the South

American platform, with records of a complex geodynamic evolution since the Paleoarchean (Almeida et al., 2000; Barbosa et al., 2020; Oliveira et al., 2020). The CGD follows the geological evolution of the southern SFC and their segments reworked during the Neoproterozoic Brasiliano-PanAfrican orogeny, with a Mesoarchean to Statherian (3.1–1.7 Ga) crustal evolution, interpreted as a westward extension of the cratonic terrain (Pinheiro et al., 2021). The CGD consists of variably migmatized orthogneisses, metatonalites, and metagranitoids (i.e., Campos Gerais Complex) associated with metamorphosed supracrustal sequences and mafic-ultramafic rocks. The latter are grouped into several tectonic blocks, including Petúnia and Mumbuca segments and Morro do Ferro greenstone belt (**Fig. 19**). They consist of variable associations of mafic-ultramafic rocks intercalated with metasedimentary rocks, juxtaposed along major NW-SE trending fault systems (Turbay et al. 2013; Pinheiro et al. 2021).

The Campos Gerais Domain has tectonic contact with younger metasedimentary sequences belonging to the Ediacaran Passos nappe system and the Criogenian—Ediacaran Andrelândia nappe system (**Fig. 19**; Pinheiro et al. 2021). Mafic–ultramafic magmatic events recognized in the CGD include typical Archean greenstone belt sequences (Teixeira et al. 1987; Brenner et al. 1990) and tectonic segments interpreted as ophiolites (Lima, 2017).

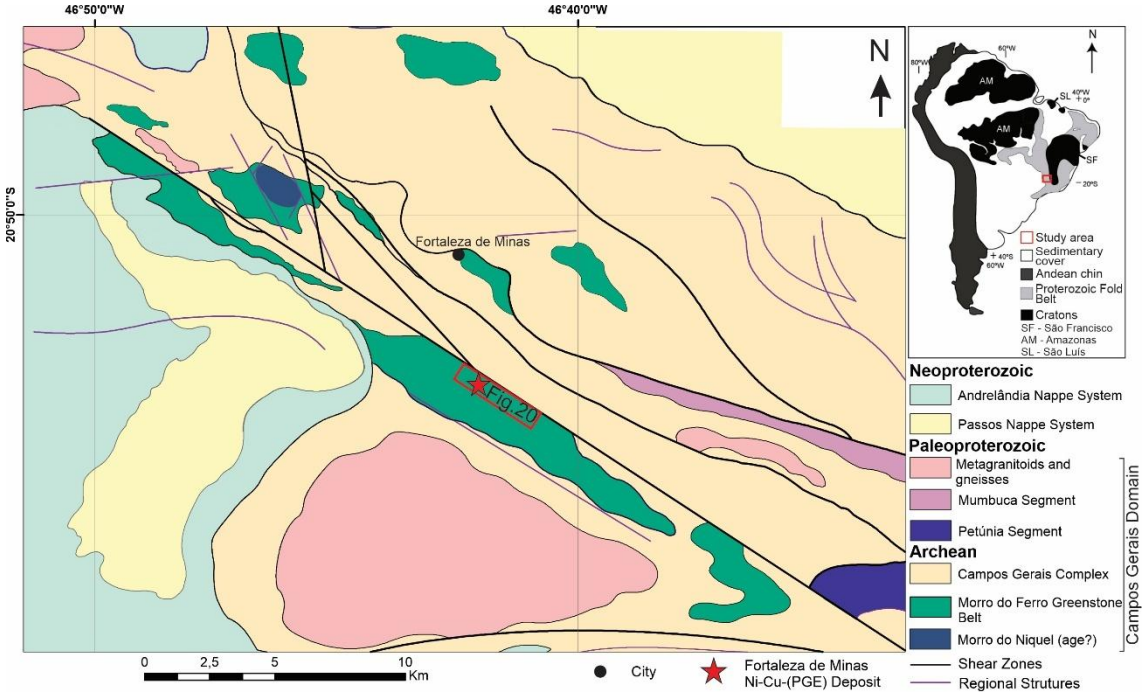

Figure 19 Regional Geological map of the Morro do Ferro Greenstone Belt region (modified from Pinheiro et al., 2021).

2.2.2. Morro do Ferro greenstone belt

The Morro do Ferro greenstone belt is an Archean supracrustal sequence overprinted by younger tectonism and metamorphism (Szabo, 1996; Pinheiro et al., 2021). The greenstone belt segment close to the Fortaleza de Minas Ni-Cu-PGE deposit (**Fig. 20**) consists of metamorphosed komatiitic flows interlayered with metabasalts and metasediments (Teixeira et al., 1987; Brenner et al., 1990). Komatiites include spinifex-textured and layered flows, the latter consisting of basal olivine cumulate (metamorphosed dunite) followed by metapyroxenite and metagabbro. Komatiitic flows are commonly interlayered with metamorphosed BIF, metachert, and graphite schist (Teixeira et al., 1987; Brenner et al., 1990; Brenner, 2006) (**Fig. 20**). The age of the komatiites is constrained by a Sm-Nd isochron (2,863±65 Ma; Pimentel and Ferreira Filho, 2002). The Morro do Niquel is a distinctive serpentinite body that hosts a mined-out Ni laterite deposit. It consists mainly of extensively serpentinized massive dunite (olivine and chromite adcumulate) that has been interpreted as an exhumed mantle portion of a Neoproterozoic ophiolite (Lima et al., 2021) or as Archean serpentinite plugs or lower-level sills (Teixeira et al., 1987).

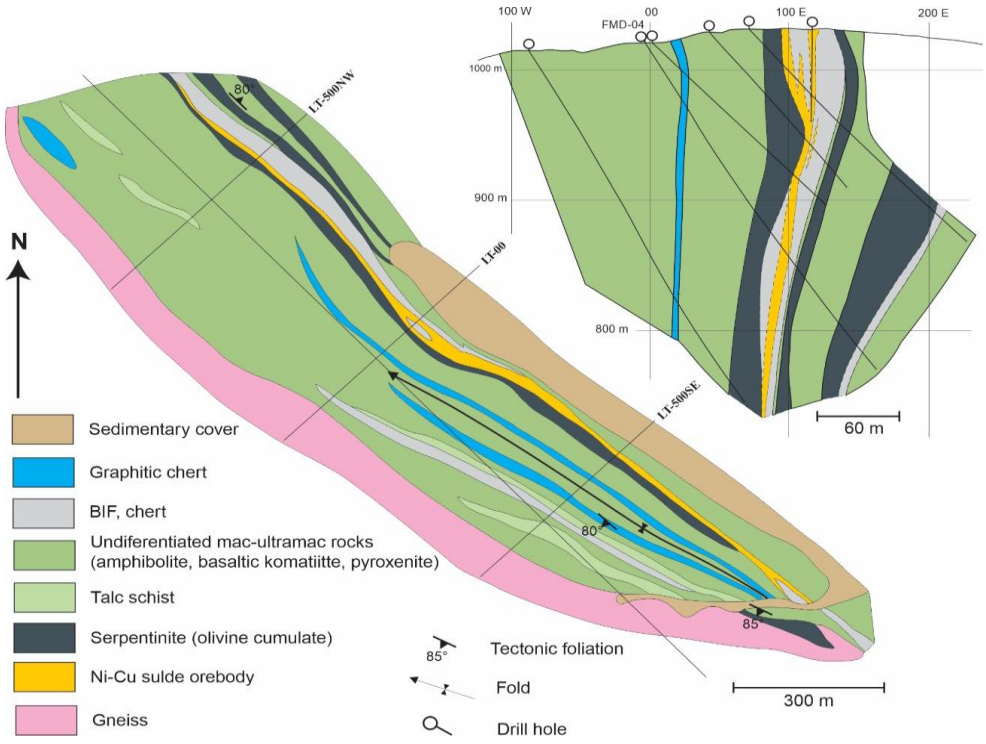

Figure 20 Geological map of the Fortaleza de Minas deposit into the Morro do Ferro greenstone belt segment. The geological section (indicated by LT-00) follows the orientation of the exploration grid indicated in the map. The map and section are partially based on Brenner et al. (1990) and Brenner (2006).

2.2.3. Fortaleza de Minas Ni-Cu-PGE deposit

The Fortaleza de Minas Ni-Cu-PGE deposit (FM), also named the O´ Toole deposit, is associated with komatiitic rocks of the Archean Morro do Ferro Greenstone Belt (Brenner *et al*., 1990). The stratigraphic sequence close to the FM deposit consists of different types of komatiitic flows interlayered with minor metasediments, including metamorphosed BIF and chert (**Fig. 21**). The geology of this sequence occurs along a NW trending sub-vertical syncline structure that was detailed following intensive drilling and mapping carried out for mineral exploration (**Fig. 20**). Although primary structures and textures are variably preserved in the volcanic rocks, their mineral assemblages are predominantly metamorphic and consist of parageneses of the upper greenschist to lower amphibolite facies. The sulfide orebody with a broadly tabular shape extends for 1.5 km along strike with an average width of 5 m. Mineral resources of 6 Mt with an average grade of 2.5% Ni, 0.40 % Cu, 500 ppm Co, and 0.7 g/t Pt+Pd+Au are indicated to a downdip extension of 500 m (Brenner, 2006).

Four cycles of flow units, each one composed of an upward sequence of olivine cumulate (serpentinite), clinopyroxenite (tremolitite), and gabbro (amphibolite), characterize the volcanic pile close to the FM deposit (Brenner *et al*., 1990). This sequence of flow units separated by banded iron formations is a distinctively different stratigraphic feature within the Morro do Ferro greenstone belt (Brenner *et al*., 1990). Brenner (2006) interpreted the cyclic units as a sequence of highly fractionated flows originated in ponded lava lakes.

The Ni-Cu-PGE sulfide orebody of the FM deposit overlies a thick banded iron formation located at the bottom of the upper cycle (**Fig. 21**). The flow unit overlying the orebody consists of serpentinite (average thickness of 13 m), followed by clinopyroxenite (about 15 m thick) and gabbro (about 20 m thick) (Fig. 3). The serpentinite is an olivine and chromite cumulate with meso- to adcumulate texture indicated by olivine pseudomorphs. The clinopyroxenite has a predominantly adcumulate texture indicated by euhedral clinopyroxene variably altered to tremolite, talc, and minor chlorite. The gabbro consists mainly of a metamorphic assemblage of amphibole, plagioclase, and epidote with partially preserved gabbroic texture. The contact between serpentinite (olivine cumulate) and clinopyroxenite (Cpc cumulate) is sharp, whereas the contact between

clinopyroxenite and gabbro is gradational and indicated by interstitial plagioclase at the contact zone. Although this stratigraphic sequence is recognized throughout the extension of the orebody, tectonic overprint results in disruption and/or extensive alteration of the orebody and host rocks, commonly indicated by sheared rocks and abundant talc schists. Extensive remobilization of the sulfide ore along shear zones is suggested by sulfide mineralization contained within footwall chert and BIF (Brenner, 1990; see section in **Fig. 21**).

A detailed description of the sulfide ore is provided by Brenner *et al*. (1990) and Brenner (2016), and the following is a summary focused on the best-preserved sections of the orebody. The least-deformed portions of the sulfide orebody consist of massive to semi-massive breccia ore overlain by matrix and disseminated sulfides (**Fig. 21**). The breccia ore occurs at the lower contact with BIF and comprises rounded or angular fragments of serpentinite, talc schist and BIF within a sulfide-rich groundmass. Matrix ore comprises irregular aggregates of fine-grained serpentine or olivine pseudomorphs in a continuous matrix of sulfide. The matrix ore grades upward into a disseminated ore comprising sulfides interstitial to the host serpentinite. The thickness of the different types of ore is highly variable as the sequence is commonly sheared and disrupted. Sulfide (vol.%) and Ni (wt.%) contents are variable for each ore type, with average contents of sulfides ranging from 20% in disseminated ore and 60% in breccia ore, whereas Ni contents range from about 1% up to 4%. Sulfides consist predominantly of pyrrhotite, pentlandite, and chalcopyrite, at a recalculated ratio of 65:30:5, with no significant variation observed for different ore types. Magnetite, cobaltite, gersdorffite, and platinum group minerals occur as minor minerals associated with sulfides.

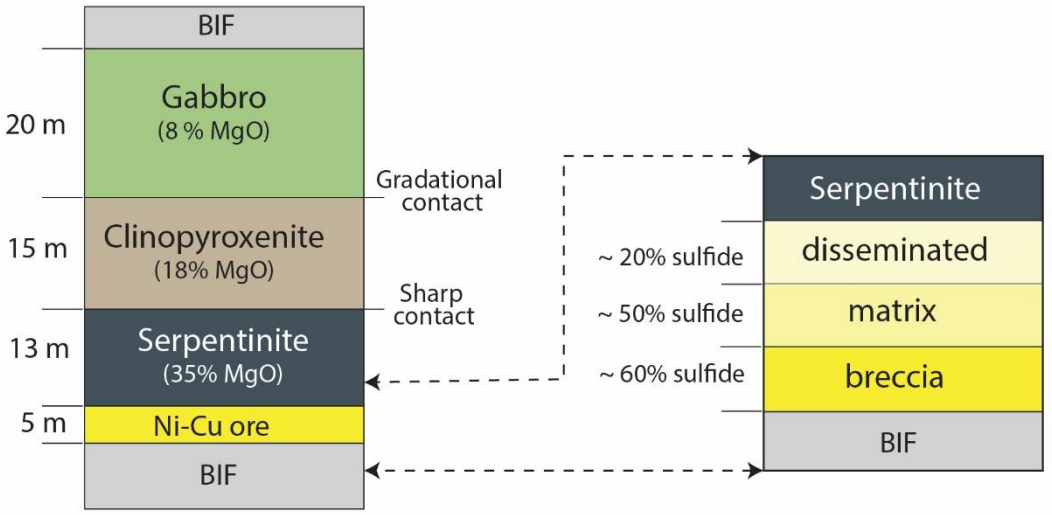

Figure 21Schematic stratigraphic column of the flow unit (or upper cycle) overlying the Ni-Cu-PGE orebody. The average contents of MgO for each rock type and sulfide for each ore type are indicated. Modified from Brenner et al. (1990) and Brenner (2006).

2.3. MATERIALS AND METHODS

2.3.1. Sample selection and trace elements geochemical analyses

Twelve unweathered drill core samples were selected for petrographic studies, geochemical analyses of Se and TABS (Te, As, Bi, Sb), and sulfur isotope analyses. These samples are representative of different types of Ni-Cu-PGE ore and host rocks of the FM deposit. Petrographic studies using optical microscopy (reflected and transmitted light) were carried out at the Federal University at Amazonas (UFAM) and the University of Brasília (UnB). Sample preparation for geochemical analyses includes crushing, quartering, and grinding to the 200-mesh fraction. Powdered fractions were digested by aqua regia and analyzed for trace elements by ICP-MS at ALS Geochemistry Laboratory in Goiania – Brazil. The analytical errors and limited detection of the elements are very low.

2.3.2. Sulfur isotope analyses

The same twelve samples were weighed into tin capsules and the sulfur isotopic composition was measured using a MAT 253 Stable Isotope Ratio Mass Spectrometer coupled to a Costech ECS 4010 Elemental Analyzer. The standard calibration samples used were NBS127 and IAEA-SO-6 (20.2 and -34.0 of the $\delta^{34}S$ ‰ respectively). The $\delta^{34}S$ values were calculated by normalizing the $^{34}S/^{32}S$

ratios in the sample to that in the Vienna Canyon Diablo Troilite (V-CDT) international standard. Values are reported using the delta (δ) notation in units of permille (‰) and are reproducible to 0.2‰. Sample preparation and chemical analyses were carried out at the Isotope Research Center, Queen's University, Canada.

2.4. RESULTS

2.4.1. Geology and petrography of the ore

Detailed sampling of the orebody and host rocks was conducted in the open pit and underground mine. Sampling sites are representative of the best-preserved portions of the orebody. The stratigraphic sequence of typical ore types of the FM deposit (**Fig. 21**) is indicated by the E to W sequence of breccia ore, matrix ore, and disseminated ore shown in our detailed maps of the sub-vertical orebody (**Fig. 22**). The footwall BIF occurs in the open pit sampling site. In contrast, the orebody footwall contact occurs with sheared talc schist at the underground sampling site. From a total of 19 samples collected at the 953 m level in the open pit and eight samples collected at the 1,100 m level in the underground mine (**Fig. 22**), seven samples of Ni-Cu-PGE sulfide ore and two samples of BIF were selected for geochemical studies. Three samples of host rocks, including two BIF and one graphitic chert, were collected in drill hole FMD04, which has a representative intercept of the orebody. Table 4 has a summary of the samples selected for geochemical studies. The following provides a brief description of the selected samples.

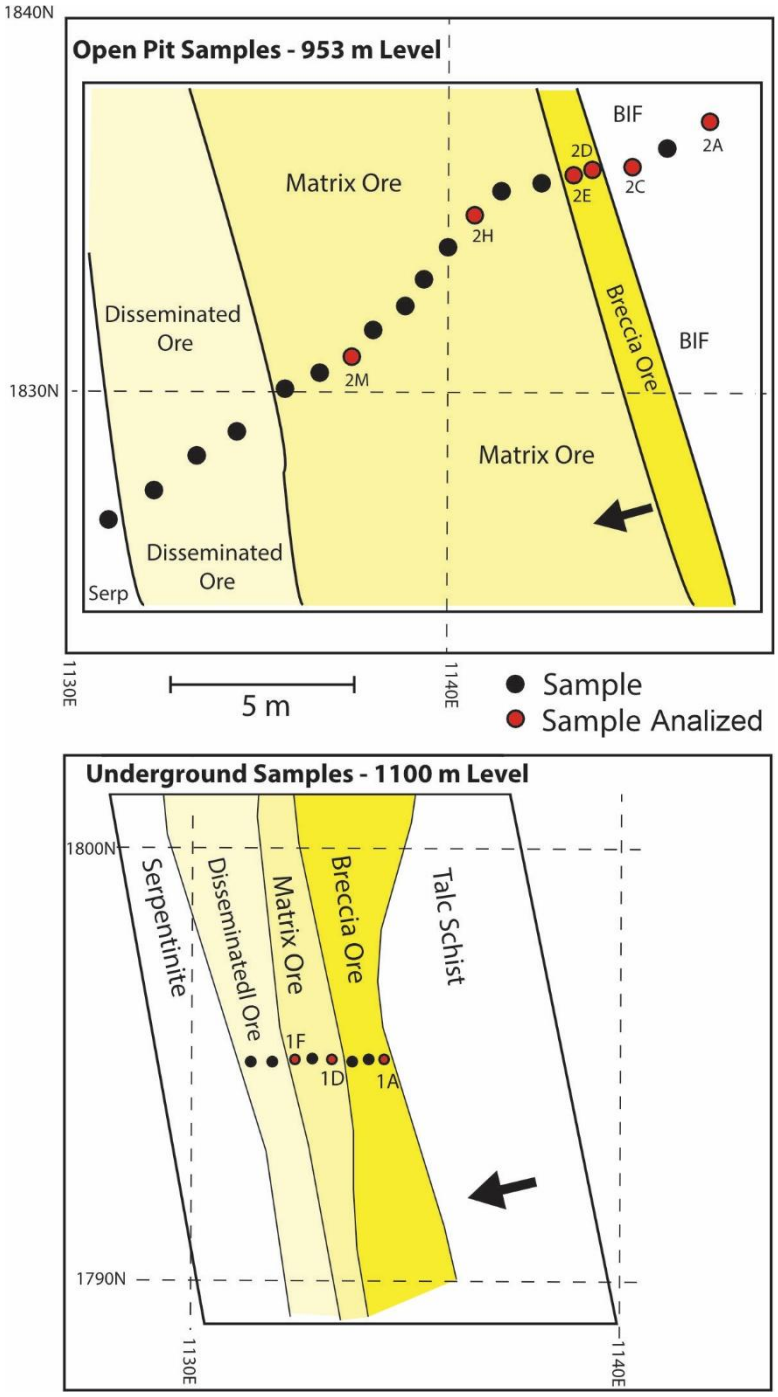

Figure 22 Detailed map of the orebody and location of samples selected for geochemical and isotopic studies. See Table 4 for a brief description of samples indicated by a red dot. Arrows indicate the facing. The maps follow the orientation of the exploration grid indicated in Figure 20.

Samples of banded iron formation (**Fig. 23A and B**) are foliated rocks consisting mainly of amphibole-rich bands and minor magnetite- or quartz-rich bands. Amphibole-rich bands have nematoblastic texture consisting of prismatic fine- to medium-grained colorless to pale-green amphiboles (hornblende-actinolite). Magnetite (Mag) occurs as fine-grained euhedral to subhedral crystals or annealed aggregates (**Fig. 23C and D**). The graphitic chert is a fine-grained

rock with granoblastic texture, consisting mainly of quartz and minor oriented graphite. Both BIF and graphitic schist have minor (< 5%) disseminated sulfides consisting of Pyrite (Py)+Po and minor Ccp (**Fig. 23C and D**).

Samples of breccia ore (**Fig. 23E**) consist of a sulfide-rich groundmass with variable amounts (up to 30%) of serpentinite, talc schist, and BIF/chert fragments. Fragments of up to a few centimeters in size are commonly rounded and elongated parallel to the foliation. The groundmass (**Fig. 23F**) consists of euhedral to rounded fine- to medium-grained (up to 1-2 mm) magnetite (~5%) within a granoblastic aggregate of sulfides (~95%). Sulfides occur as fine-grained crystals (< 0.5 mm) with polygonal contacts, consisting of Po (~60% of the sulfide fraction), Pn (~30%) and unevenly distributed Ccp (~10%).

Samples of matrix ore (Fig. 5G) consist of variable amounts of sulfides (up to 60%) enveloping irregular domains or olivine pseudomorphs consisting of fine-grained aggregates of serpentine and magnetite. Sulfides have texture and composition similar to those described in the breccia ore, occurring as fine-grained aggregates of Po+Pn and minor Ccp, enveloping rounded fine- to medium-grained magnetite crystals (**Fig. 23H**).

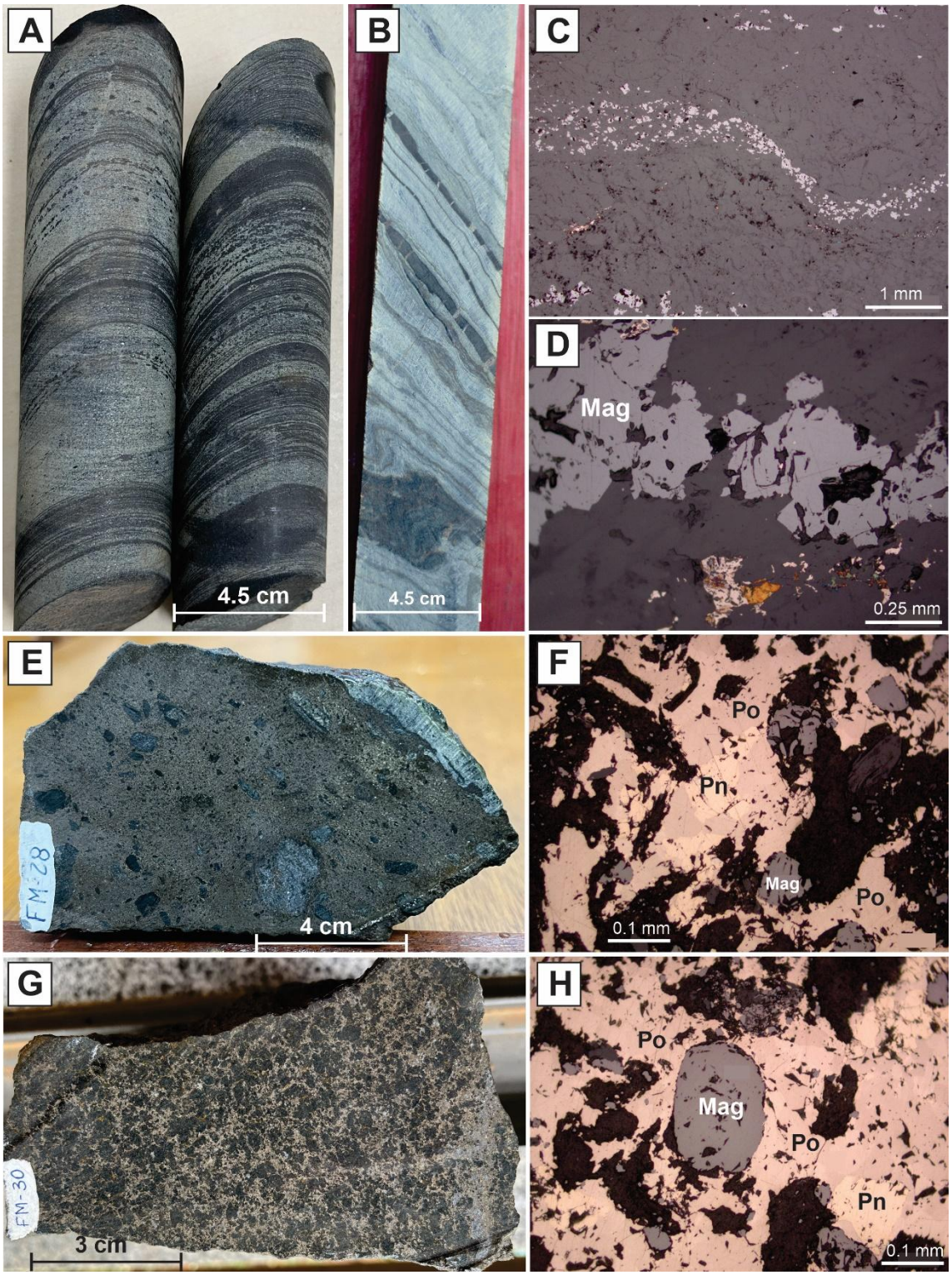

Figure 23 Representative photos and photomicrographs of selected samples. (A) Drill core sample of BIF consisting of magnetite-rich (dark color) interlayered with quartz and amphibole-rich (light color) bands. (B) Drill core sample of BIF consisting of thin magnetite-rich bands (dark color). Note deformational features (folded bands and pull-apart structures) and minor sulfides (yellowish color). Sulfides are disseminated or remobilized within pull-apart structures. (C) and (D) Photomicrographs showing folded thin magnetite-rich bands. Note minor disseminated sulfides (yellow or rusted colors). (E) Hand sample of breccia ore. Fragments of serpentinite, talc-schist, and BIF of variable sizes and shapes occur within a sulfide groundmass. (F) Photomicrograph of breccia ore. Sulfides consist of fine-grained Po and Pn. Note minor euhedral to subhedral disseminated magnetite. (G) Hand sample of matrix ore. Olivine pseudomorphs

replaced by fine-grained aggregates of serpentine and magnetite (dark color) are enveloped by sulfides. (H) Photomicrograph of matrix ore. Sulfides consist of fine-grained Po and Pn. Note euhedral magnetite crystals with rounded faces.

2.4.2. TABS-Ni-Cu geochemistry

The contents of TABS, Se, Cu, and Ni of 10 sulfide ore samples and two samples of BIF footwall rocks from the Fortaleza de Minas deposit are available in **Table 3**. Binary plot diagrams for these elements show the main geochemical characteristics of the Fortaleza de Minas ore and its footwall rocks (**Fig. 24**). Plots of Se vs TABS show variable contents and generally scattered distribution for most of the elements, with contents for sulfide ore samples distinctively higher than those from host rocks (**Fig. 24A-D**). The sulfide ore samples show strong positive correlation between Se and Te (r = 0.85), moderate positive correlation between Se and Bi (r = 0.49), and are mainly uncorrelated with As and Sb (**Fig. 24A-D**). The contents for Sc in sulfide ore samples (Sc < 0.28 ppm) are distinctively lower than Te (up to 8.41 ppm), As (up to 33.9 ppm), and Bi (up to 2.72 ppm). The sample of host graphitic chert has very low contents for Se and TABS (**Table 3**). Another point is that the ore samples have, in general, more contents that BIF and graphitic chert samples, independent of the element.

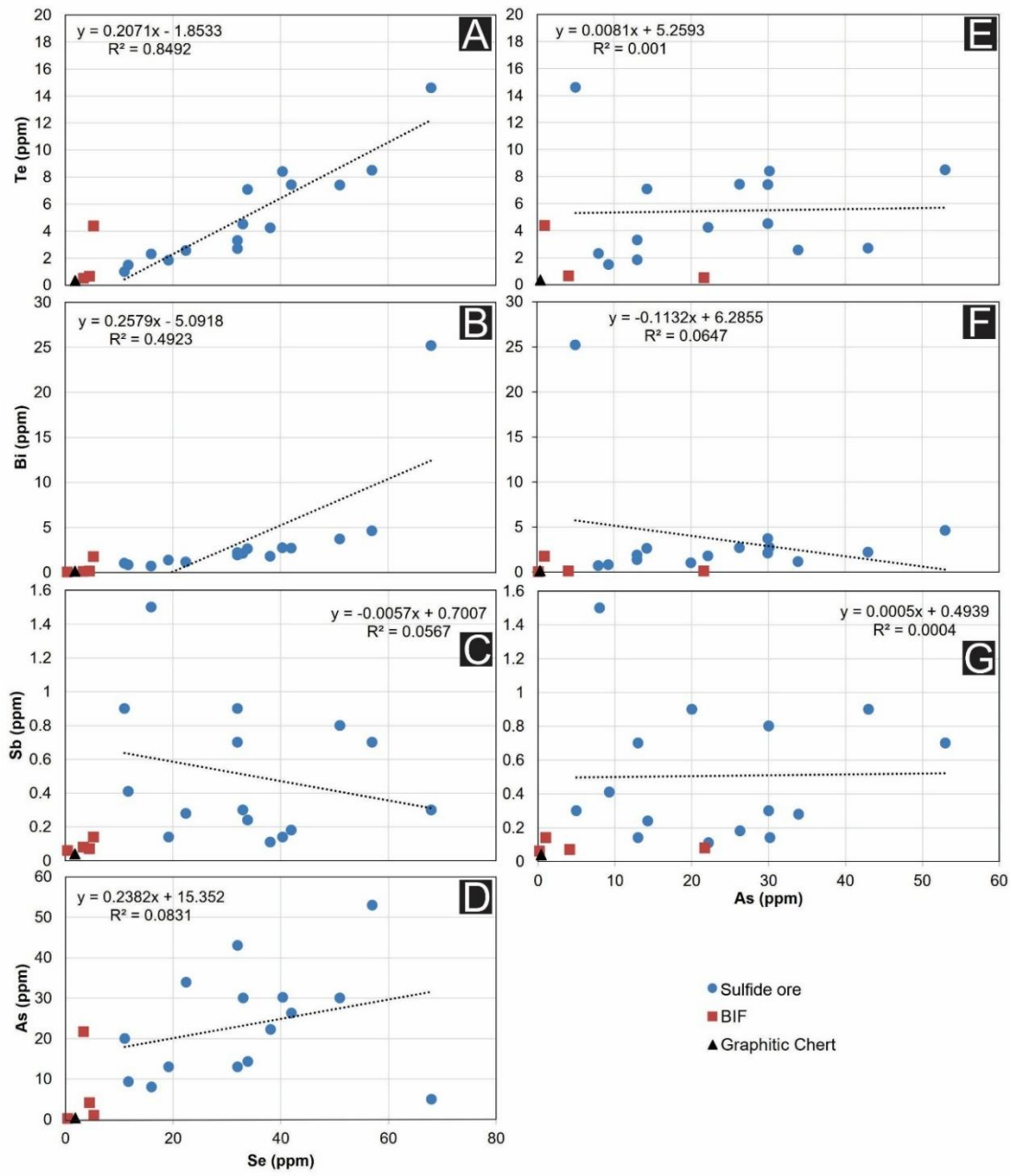

Figure 24 Binary TABS + Se diagrams. See Table 3 for the Fortaleza de Minas data. Linear regression was made by sulfide ore samples from Fortaleza de Minas.

The correlation between different TABS in the sulfide ore samples is generally weak, as illustrated by plots of As versus Te-Bi-Sb (**Fig. 24E-F-G**). When comparing the As vs. others TABS plot (**Fig. 24E-G**), the variation in the contents is more evident, but there is still no positive correlation. Already, the other samples have more variable ratios. Plots of Ni and Cu contents with TABS + Se show strong to moderate positive correlations, except for Sb (**Fig. 25**). For ore and BIF (2A sample see **Table 3**) of the Fortaleza de Minas deposit (**Fig. 25**) demonstrate that all contents of the elements are upper in ore sulfide than BIF.

The Ni and Cu have some positive correlation with TABS + Se, except for the Sb (**Fig. 25B and G**).

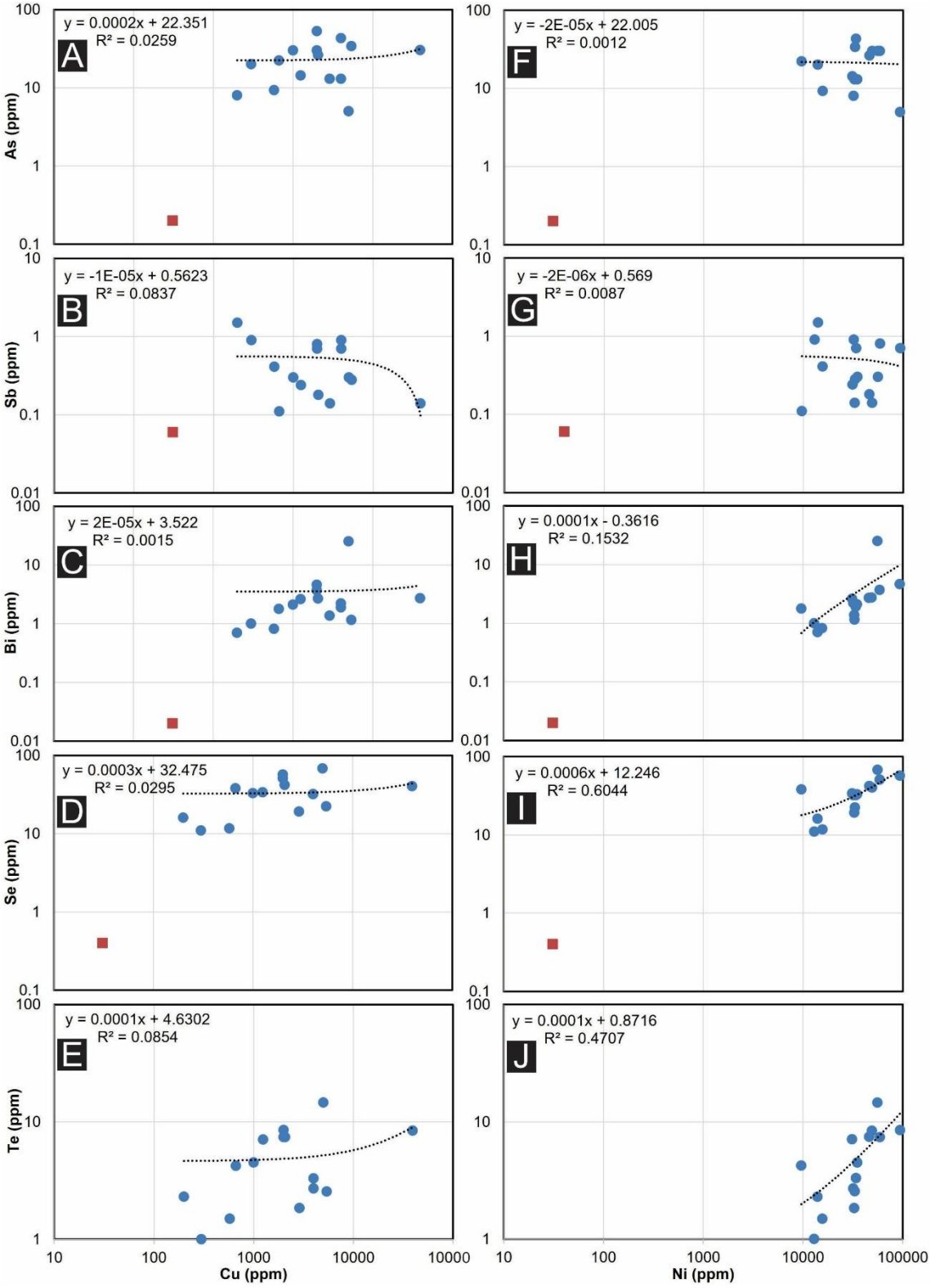

Figure 25 Binary diagrams of TABS + Se vs. Cu and Ni. See Fig. 20 for legends. Linear regression was made by sulfide ore samples from Fortaleza de Minas.

The primitive mantle-normalized TABS + Se diagram (**Fig. 26**) enhances the higher sulfide ore contents compared with those for host rocks in the Fortaleza de Minas deposit. The overall shape of the TABS + Se profile is similar to that of the average Kambalda ore, including a distinctive negative anomaly for Sb.

Table 3 Geochemistry analysis of Fortaleza de Minas Ni-Cu-(PGE) ore samples, BIF and Graphitic Chert.

Samples	Rock type	Ore type	As	Sb	Bi	Se	Te	Cu
			ppm	ppm	ppm	ppm	ppm	ppm
1A	Sulfide ore	Brecciated	26.3	0.18	2.69	42	7.43	2076
1D	Sulfide ore	Matrix (Net-texture)	14.3	0.24	2.61	33.9	7.07	1251
1F	Sulfide ore	Matrix (Net-texture)	9.3	0.41	0.82	11.7	1.49	578
2A	BIF	-	0.2	0.06	0.02	0.4	0.01	31
2C	BIF	BIF-hosted	1	0.14	1.74	5.3	4.37	-
2D	Sulfide ore	Breccia	22.2	0.11	1.78	38.1	4.23	667
2E	Sulfide ore	Breccia	30.2	0.14	2.72	40.4	8.41	39382
2H	Sulfide ore	Matrix (Net-texture)	13	0.14	1.37	19.2	1.84	2891
2M	Sulfide ore	Matrix (Net-texture)	33.9	0.28	1.15	22.4	2.55	5415
FMD04-55,50	Graphitic Chert	-	0.4	0.05	0.13	1.8	0.34	-
FMD04-181,30	BIF	-	4.1	0.07	0.12	4.5	0.63	-
FMD04-180,85	BIF	-	21.7	0.08	0.11	3.4	0.49	-
1	Sulfide ore	discordant veins	53	0.7	4.6	57	8.5	2000
2	Sulfide ore	discordant veins	5	0.3	25.2	68	14.6	5000
3	Sulfide ore	brecciated	30	0.8	3.7	51	7.4	2000
4	Sulfide ore	brecciated	30	0.3	2.1	33	4.5	1000
5	Sulfide ore	net-textured	13	0.7	1.9	32	3.3	4000
6	Sulfide ore	net-textured	43	0.9	2.2	32	2.7	4000
7	Sulfide ore	interstitial	8	1.5	0.7	16	2.3	200
8	Sulfide ore	Stringer (foliated)	20	0.9	1	11	1	300

(-) not analyzed or not applied.

Analyses from this paper except for 1-8 samples (Almeida et al. 2007).

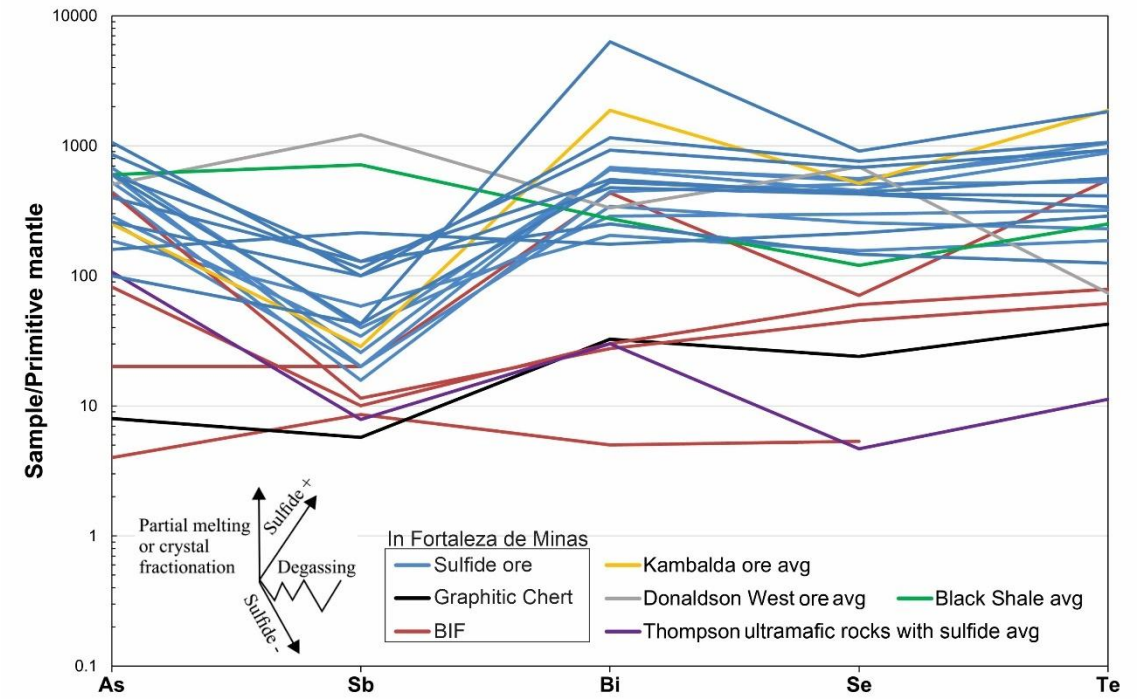

Figure 26 Multi-element plots for TABS + Se, normalized by the primitive mantle. The data for Kambalda are from Lesher and Keays (2002) and references therein, for Donaldson West from Dillon-Leitch et al. (1986), Thompson from McClenaghan et al. (2011) and for average black shale from Ketris and Yudovich (2009). All data were normalized by primitive mantle from Lyubetskaya and Korenaga (2007).

2.4.3. Sulfur isotope

The sulfur isotope data for the Fortaleza de Minas ore samples, BIF, and graphitic chert (**Table 4**) are represented in **Figure 27**. The $\delta^{34}S$ values for sulfide ore samples show a narrow compositional range bracketed between +6.1 and +6.5‰. These values overlap with the interval reported by Choudhuri et al. (1997) for the sulfide ore (i.e., +5.70 and +6.83‰). The $\delta^{34}S$ values for samples of BIF have a compositional range bracket between +9.5‰, whereas one sample of a graphitic chert has a $\delta^{34}S$ value of +6.7‰. The sample 2C (see **Table 4)** has +5.9‰ and it is BIF-hosted sulfide, so the $\delta^{34}S$ signature is of the ore.

When comparing all data obtained it is possible to infer that the BIF and the graphitic chert can be the S-source for the Fortaleza de Minas Ni-Cu-(PGE) sulfide deposit. But the geological context is when the important part of the ore is spatially related to the BIF, including a type of ore which is hosted into the BIF. All these aspects contribute to discarding the graphitic chert as a main S-source of the ore.

Table 4 ^{34}S isotope data from Fortaleza de Minas ore and the country rocks.

Sample ID	$\delta^{34}S$ ‰ (V-CDT)	Sulfides	Type of Rock
1A	6.5	Po>Pn>Ccp	Sulfide ore
1D	6.4	Pn>Po>Ccp	Sulfide ore
1F	6.2	Po>Pn>Ccp	Sulfide ore
2C	5.9	Po>Ccp	BIF-hosted ore
2D	6.5	Po>Pn>Ccp	Sulfide ore
2H	6.3	Po>Pn>Ccp	Sulfide ore
2M	6.2	Po>Ccp>Pn	Sulfide ore
2E	6.1	Po>Ccp>Pn	Sulfide ore
FMD04_55_50	6.7	Po	Graphitic Chert
FMD04_181_30	9.5	Ccp>Pn>Po	BIF
FMD04_180_85	9.5	Po>Pn>Ccp	BIF

2.5. DISCUSSION

2.5.1. Sulfur source

Most of the Ni-Cu-PGE deposits have $\delta^{34}S$ values that differ from the mantle and are similar or close to their sulfide-bearing host rocks (see Lesher, 2017). This is particularly relevant for komatiite-associated deposits, where the stratigraphic relationship between sulfide-bearing sediments and Ni-Cu mineralized komatiite flows is commonly well-known (Lesher, 2017). The $\delta^{34}S$ values for Ni-Cu sulfide ore show a positive association with sulfur-bearing rocks from several komatiite-associated deposits, as indicated in Figure 27. The remarkably close and/or overlapping $\delta^{34}S$ values for several deposits, as well as very positive $\delta^{34}S$ values for sulfide ore associated with black shales, support previous interpretations that the S in these deposits results from the incorporation of crustal S from nearby crustal sources (e.g., Ripley and Li, 2013; Lesher, 2017). In addition, these data indicate that S was assimilated from different types of crustal rocks, including black shales and BIF.

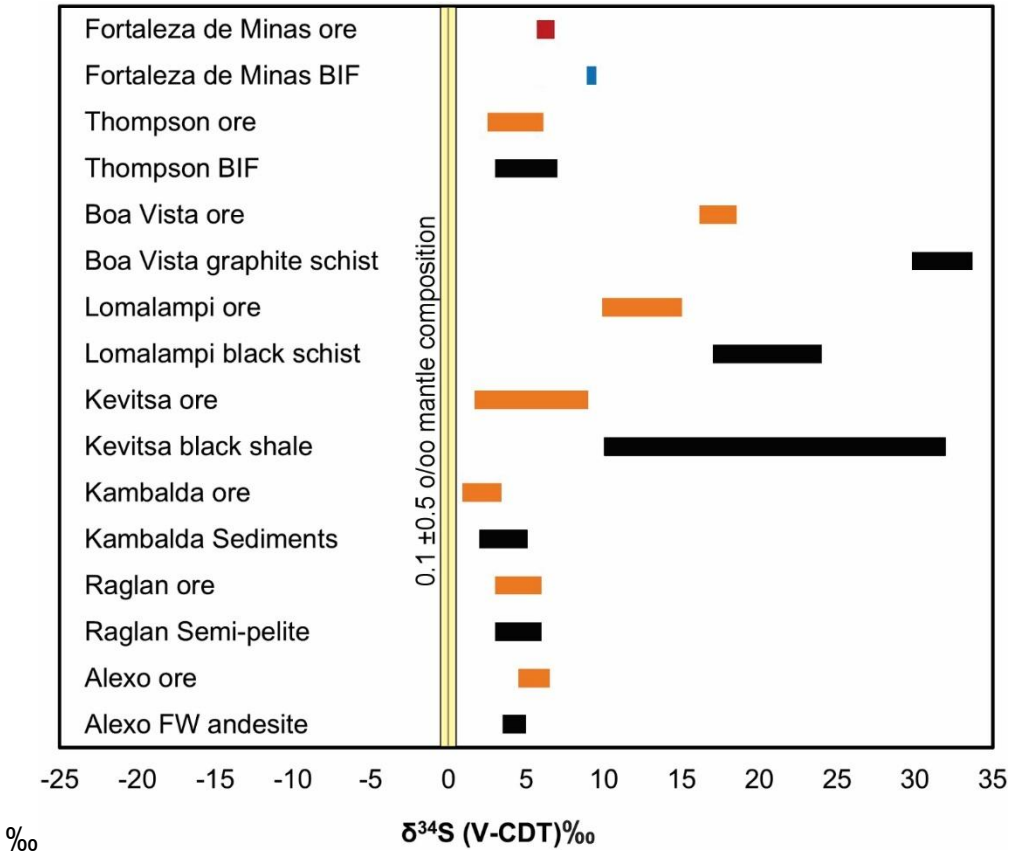

Figure 27 $^{34}S/^{32}S$ isotopic data for selected komatiite-associated Ni-Cu ores and S-bearing country rocks (see also Lesher (2017) and Ripley and Li, (2013). Data sources: Fortaleza de Minas: Choudhuri et al. (1997) and this study; Boa Vista: Maia et al., (submitted); Alexo: Naldrett (1966); Raglan: Lesher et al. (1999); Kambalda: Donnelly et al. (1978); Thompson: Bleeker and Macek (1996); Lomalamp: Törmänen et al. (2016); Kevitsa: Luolavirta (2018).

The $\delta^{34}S$ values for sulfide ore and host rocks of the Fortaleza de Minas deposit (**Fig. 27**) obtained in our study support the interpretation that sulfide-bearing BIF leads to the origin of the. Assimilation of host BIFs is also indicated as an external S-source for komatiite-associated Ni-Cu-(PGE) deposits in Forrestiana (Perring et al., 1995), Thompson (Layton-Matthews et al., 2010), and Hart (Hiebert et al. 2016). Sulfur isotope results obtained for the Fortaleza de Minas deposit are consistent with geological evidence indicated by the sulfide ore located in contact with a thick BIF layer (**Fig. 27**), as well as fragments of BIF within the Ni-Cu sulfide-rich groundmass. Apart from the strong line of evidence provided by sulfur isotope values for the assimilation of crustal S in mafic-ultramafic magmas, they also provide a quantitative indicator of the assimilation process (Lesher and Burnham, 2001; Ripley and Li, 2013).

The process leading to metal tenor upgrade by reaction with a large volume of mantle-derived melts in magmatic Ni-Cu-PGE sulfides (i.e., R factor:

Campbell and Naldrettt, 1979), should be accompanied by sulfur isotope exchange between the crustal contaminated sulfide ore and sulfur of mantle origin with $\delta^{34}S$ values close to zero (Lesher and Burnham, 2001; Ripley and Li, 2013). This process limits the degree of isotopic evidence for crustal sulfur contamination recorded by the sulfide ore (Lesher et al., 1999; Lesher and Stone, 1996), may be modeled for different magma:sulfide mass ratios if the S isotopic composition of the crustal contaminant is known. Our model, using the isotopic composition of sulfides from the host BIF of the Fortaleza de Minas as the crustal contaminant, suggests that the isotopic composition of the sulfide ore results from isotopic exchange with mantle S at an R factor of ~150-200 (**Fig. 28**).

This is associated with the fact that in most mafic-ultramafic magmas more magnesian than MORB, the undepleted PGE signatures and negative pressure dependence on the solubility of S, indicate that they are unlikely to have been saturated in sulfide (Lesher & Groves 1986, Naldrett & Barnes 1986, Arndt et al. 2005), thus the incorporation of crustal S is considered to be an essential component in genetic models of magmatic Ni-Cu-(PGE) deposits (Lightfoot et al., 2012; Robertson et al., 2015). Aware of, when comparing $\delta^{34}S$ isotope data from Fortaleza de Minas ore, with the BIF of the footwall, and others Komatiite-associated sulfide deposit and magma associated (**Fig. 27**)

In Fortaleza de Minas deposit, the BIF has strong similarity with the Fortaleza de Minas ore $\delta^{34}S$ isotope signature. Another point is that Boa Vista ore has a similar $\delta^{34}S$ isotope range to other komatiite-associated deposits, with the BIF similar and a little more positive than another external S-source, except Boa Vista and Kevitsa. With the combination of the $\delta^{34}S$ isotope signature with the presence of BIF xenoliths, and BIF-hosted ore, it is possible to indicate the BIF is the external S-source of the Fortaleza de Minas ore.

The effective magma: sulfide mass ratios (R factors), are high enough when crustal sulfide xenomelts can be shifted toward mantle S isotopic compositions (Lesher and Burnham, 2001). This affirmation allows create diagrams like figure 28, that show the $\delta^{34}S$ values of most Fortaleza de Minas sulfides vary between 5.9‰ and 6.5‰. and the magma:sulfide mass ratios (R factors) required to produce the observed variations in Fortaleza de Minas sulfide sulfides are 150-200 (**Fig. 28**).

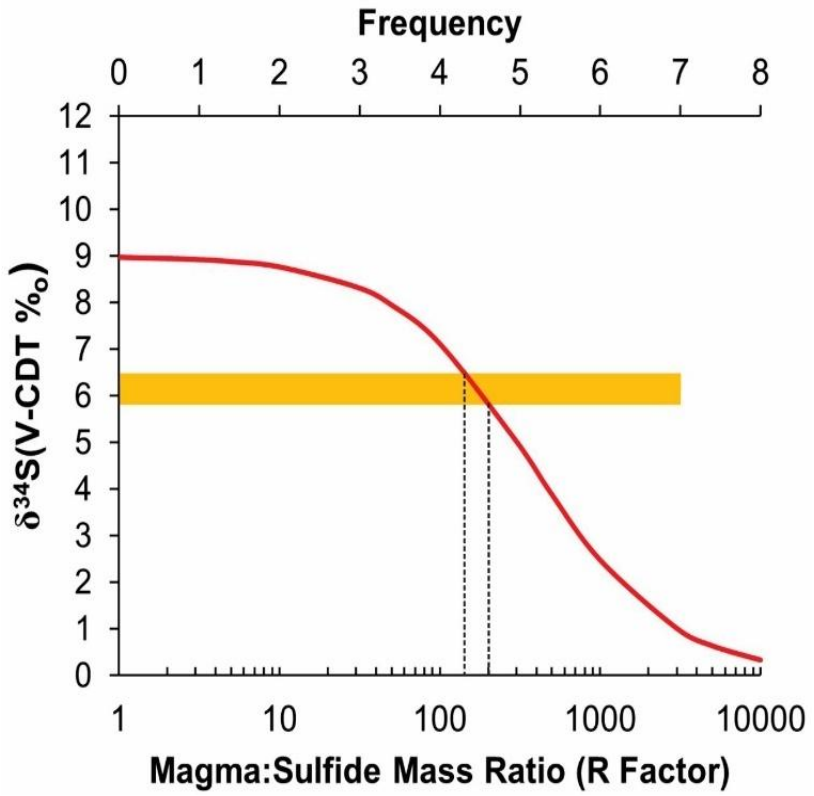

Figure 28 R factor versus $\delta^{34}S$ histogram (orange bar) for 7 mineralized analyses from the Fortaleza de Minas deposit. Variations in $\delta^{34}S$ with varying magma: sulfide ratios (R factors) have been calculated for a magma containing 0.1 % S with 0 ‰ $\delta^{34}S$ equilibrated with a sulfide xenomelts (derived from country-rock BIF) containing 38% S with 9‰ $\delta^{34}S$ (red line).

2.5.2. TABS + Se source

The process of assimilation of country rocks with different concentrations of TABS affects the composition of the silicate magma and, consequently, the composition and mineralogy of the sulfide ore originated from this magma. As a result, different contents of TABS in Ni-Cu-PGE sulfide deposits may be linked to the assimilation of different country rocks. As an example, the sulfide deposit of Ni-Cu-EGP from Limoeiro – Brazil (Mota-e-Silva et al., 2015) is enriched in Bi and Te, with a predominance of PGE bimutotelurides. On the other hand, in the Ni-Cu-PGE sulfide deposit of Santa Rita – Brazil (Barnes et al., 2011), TABS occur predominantly as tellurides associated with BMS (Knight et al., 2017).

In the Fortaleza de Minas ore has contents of Bi, Se, As, and Te significantly higher than those reported for primitive mantle (**Fig. 29**). Average values for the Fortaleza de Minas ore are about two (e.g., Bi, Se, As) to three (Te) orders of magnitude higher than primitive mantle. A similar geochemistry behavior is observed with contents of TABS+Se of the BIF average but with lower

content. Barnes and Mansur (2022) reported TABS + Se contents for Al-undepleted komatiites (AUK) between 2 and 3 times the primitive mantle. Assuming a similar composition for the Fortaleza de Minas the komatiite, the TABS are enriched about 30 and 50 times to the country rock and ore, respectively. The most important aspect here is the strong evidence that the BIF is a probable source of TABS + Se to the sulfide ore, where the BIF and the sulfide ore average have similar behavior when normalized by primitive mantle, highlighting the As. The high contents of As on the BIF caused a similar high content in the sulfide ore of the Boa Vista deposit.

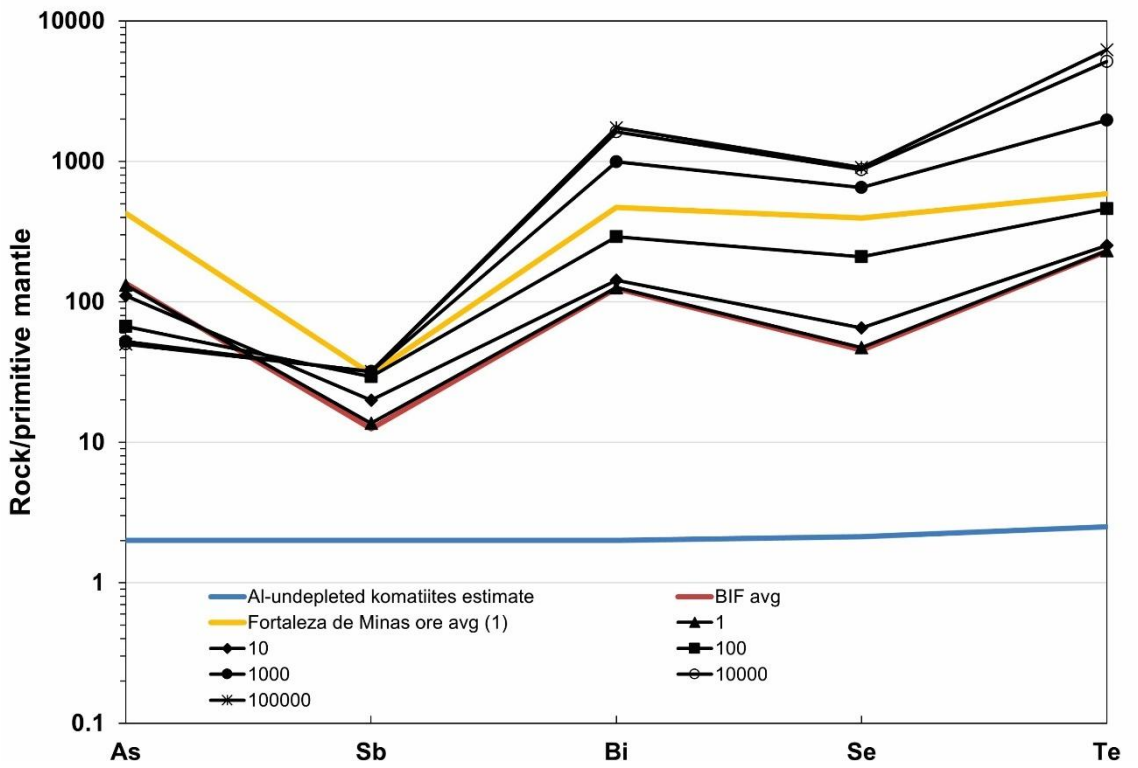

Figure 29 Primitive mantle-normalized plots of TABS + Se for average values of the Fortaleza de Minas sulfide ore and BIF host rocks. Composition models for assimilation of BIF by the komattite magma are calculated for different R-factors (magma:sulfide) models. The R-factor (magma:sulfide) models were generated using Eq 5 in Lesher and Burnham (2001). The data are XoAs = 0.1 pm, XoSb = 0.014 ppm, XoBi = 0.008 ppm, XoSe= 0.16 ppb, XoTe= 0.02 ppm from Al-undepleted komatiite estimate of the Barnes and Mansur (2022); YoAs= 6.75 ppm, YoSb = 0.09 ppm, YoBi = 0.5 ppm, YoSe= 3.4 ppb, YoTe = 1.83 ppm from BIF average from Fortaleza de Minas deposit; and DSul/SilAs = 150, DSul/SilSb= 30, DSul/SilBi = 600, DSul/SilSe = 105, DSul/SilTe =2550 from Barnes and Mansur, (2022). Primitive mantle is from Lyubetskaya and Korenaga (2007). (1) Data from this paper.

We applied the R-Factor (magma:sulfide) model (Lesher and Burnham, 2001) to estimate the amount of thermomechanical erosion of country BIF necessary to originate the content of TABS+Se of the Fortaleza de Minas ore. Our results indicate that the contents of Te, Bi, and Se are achieved with an R-

Factor between 100 and 400, whereas As contents would demand a higher R-Factor. Values for Te, Bi, and Se are consistent with those obtained using sulfur isotope date (**Fig. 29**), suggesting that an R Factor in the 100-400 provides a good estimate for the Fortaleza de Minas ore. 10, but not equal, mainly to As with R-Factor more high than of the others. Virnes et al., (2023), showed among several things that using in situ S isotopes and Pd contents of pentlandite in the Mount Keith MKD5 orebody, that was possible to estimate a R-factor between 100-400, similar too of the Barne et al., (2012) estimated (100-350). So, Fortaleza de minas orebody has an R-factor next to other komatiite-associated Ni-Cu-PGE sulfide deposits, like Mount Keith. In the Kambalda area, komatiite-associated massive sulfide ores have R factor values of around 100–500 (Lesher & Campbell 1993), another example is in the Raglan area, R factors have been estimated to be 300–1000 (Lesher et al., 1999). Estimated R factor values for komatiite-associated Ni-Cu sulfide deposits result from relatively low PGE tenors of 500 to 3000 ppb for Pd (Barnes, 2006a; Barnes et al., 2012). All data about the R factor models are in the supplementary material.

2.6. How does a Ni-Cu-PGE deposit originate in a ponded flow facies komatiite with high Cr content?

Overall, the ponded flow environment suggested for Fortaleza de Minas is not suitable for forming a Ni-Cu-PGE deposit (Hill, 2001; Lesher and Keays, 2002; Gole and Barnes, 2020). Knowing this, it is necessary to evaluate how the sulfide ore from Fortaleza de Minas was formed in this environment, whether the R factor is consistent with a ponded flow environment, and whether the presence of BIF as a host could explain/justify the formation of a Ni-Cu-PGE deposit in a ponded flow.

Fortaleza de Minas is a type 1(basal/contact) of the komatiite-associated Ni-Cu-PGE sulfide deposit (Hill, 2001; Lesher and Keays, 2002; Brenner, 2006). This implies that evidence for such structures is the presence of high MgO olivine cumulates and the absence of spinifex zones (not applicable for the Fortaleza de Minas highly fractionated flow), the presence of cumulate and massive textures in highly fractionated flows, the lateral changes to thinner sequences with spinifex

textures, evidence of thermomechanical erosion (lack of footwall BIF), and the presence of massive, matrix and disseminated ores in these troughs.

The ponded flow facies (lava lake) are characterized by the differentiates association of the cumulates and pyroxenitic-gabbroic/dolerite rocks, with relatively low MgO content compared to komatiites, were produced under calm conditions that underwent in situ fractionation (Hill, 2001; Ardnt et al. 2008; Gole and Barnes, 2020). Brenner (2006) argues that the Fortaleza de Minas deposit is an example of a komatiite-associated Ni-Cu-(PGE) deposit in highly fractionated ponded flows because it has all these characteristics and has high Cr content (>5000 ppm in olivine cumulate mineralized facies) and low Ni/Cr ratio. It is uncommon in this class of Ni-Cu-PGE sulfide deposit (Barnes, 2006; Barnes and Fiorentine, 2012; Barnes et al., 2013; Le Vaillant et al., 2016).

Efficient thermomechanical erosion is essential to assimilate the extensive sulfur content of country rocks (Robertson et al. 2015). It has a favorable specifical volcanic/subvolcanic environment, especially in conduit/channelized flow facies (Hill, 2001; Lesher and Keays, 2002; Barnes, 2006; Staude et al., 2017; Gole and Barnes, 2020). Ponded flow (lava lake) facies are not favorable to efficient thermomechanical erosion and subsequent formation of immiscible sulfide liquid after the crystallization of the Ni-Cu-PGE ore. The in-situ fractionation in ponded flow is caused by the ultra-low energy and flux of lava in a semi-closed system in a lava lake environment with calm conditions. These aspects are not good conditions for segregating the sulfide liquid. Another point is the R factor in a lava lake environment; it must be ultra-low. Different komatiite-associated Ni-Cu-PGE sulfide deposits were observed, particularly in Fortaleza de Minas of 100-400 (**Fig. 25 and 26**).

Chromite is least abundant in highly magnesian chrome-undersaturated lavas and most abundant in komatiites, as well as the textural and compositional strongly differentiated layered cumulate bodies like in ponded flow facies. Chromium is beneficial for evaluating them, as it reflects variations in the melt's temperature and oxygen fugacity (fO_2) (e.g., Barnes, 1998). However, parental melt compositions must be considered, as the reduced komatiitic melts become more oxidized with decreasing MgO content (Barnes, 1998; Barnes, 2006). The

assimilation of oxygen of the country rock rich in magnetite (Fe_2O_3), like BIF in the Fortaleza de Minas deposit, can have changed the oxygen fugacity(fO_2) into the komatiite melt, subsequently oxidized and created a condition to crystallized chromite in a volume a little higher than normal condition (absent or low Fe assimilation) (Barnes, 1998; Godel et al. 2013) in olivine cumulate mineralized zone like Fortaleza de Minas deposit.

To explain all these points together, it is necessary to think in a mixed model (**Fig. 30**). It must be a combination of conduit/channelize facies that is the olivine cumulus mineralized lower zone of the Fortaleza de Minas deposit in a first stage (**Fig. 30A-B**), and in the upper zone, a highly fractionated ponded flow facies (lava lake) in a last stage (**Fig. 30C-D**). Between both can occur a truncated, eroded, or uncovered, with facies change and decreased energy regime of the lava flow from lower to upper zones. This last aspect is critical to explaining the complete stratigraphy of the Fortaleza de Minas deposit. (**Fig. 30D**).

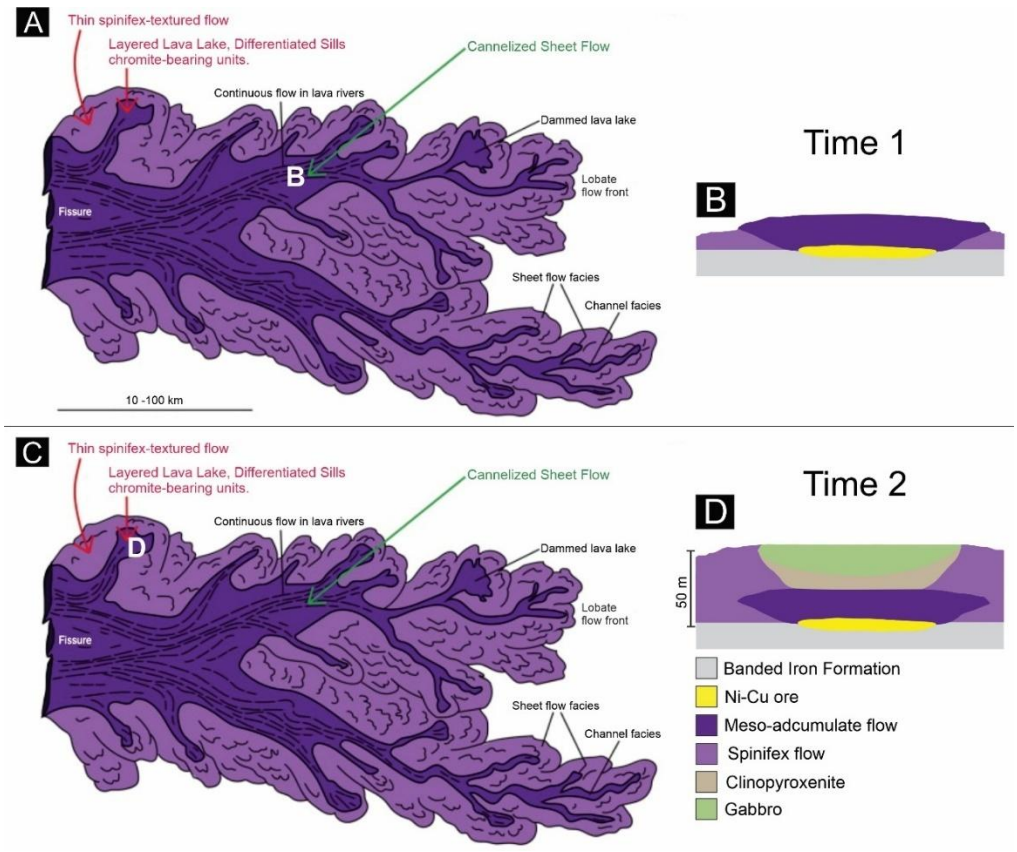

Figure 30 (A and C) Schematic komatiite flow facies in different subenvironments; (B and D) section of the channelized sheet flow and layered lava lake (ponded flow) environment respectively in different stages (time 1 and 2). Figure adapted after Gole and Barnes (2020).

2.7. CONCLUSION

The principal conclusions of this study can be summarized as follows:

(1) The $\delta^{34}S$ signatures of the sulfides of the Fortaleza de Minas orebody (+5.70 and +6.83‰) are consistent with the assimilation of the BIF (+9.5‰) that are embedded within the local stratigraphy.

(2) BIF is an important S + TABS + Se external source to the Ni-Cu-PGE sulfide deposits, and it was the source for the Fortaleza de Minas deposit.

(3) The Fortaleza de Minas deposit has a low R factor between 100-400 that is common in komatiite-associated Ni-Cu-PGE sulfide deposits.

(4) The ponded flow facies are not compatible with the R factor of the Fortaleza de Minas deposit, which has efficient thermomechanical erosion and Ni-Ci-PGE sulfide ore sulfide formation. There was a combination and superposition of two different environments, one with a conduit/channeled flow at first and other ponded flow facies (lava lake) at last.

(5) The high Cr content in the Fortaleza de Minas deposit can be explained by the assimilation of oxygen by the host BIF, which occasioned chromite crystallization.

Acknowledgments

This study was financed in part by the Coordenação de Aperfeiçoamento de Pessoal de Nível Superior - Brasil (CAPES) - Finance Code 001. Analytical facilities at the University of Brasília (UnB) provided additional support for this research. Cesar F. Ferreira Filho is a Research Fellow of CNPq (Conselho Nacional de Desenvolvimento Científico e Tecnológico - Processo 303132/2022-1) and acknowledges the continuous support through research grants and scholarships for his Research Groups. Analytical facilities at the University Federal do Amazonas (UFAM) provided additional support for this research. Other collaborative reviewers and researchers.

REFERENCES

Alexandre M. da C.F. 2000. Estudos Litoestruturais do Greestone Belt Morro do Ferro, entre a Faixa Mumbuca e a Faixa Morro do Ferro, Minas Gerais, e

suas implicações para a mineralizações sulfetadas: UNIVERSIDADE ESTADUAL DE CAMPINAS: 85 p.

Almeida C.M., Olivo G.R., Carvalho S.G. de 2007. The Ni-Cu-PGE sulfide ores of the komatiite-hosted Fortaleza de Minas deposit, Brazil: Evidence of hydrothermal remobilization. Canadian Mineralogist, **45**:751–773.

Almeida F.F.M. De, Brito Neves B.B. De, Dal Ré Carneiro C. 2000. The origin and evolution of the South American platform. Earth Science Reviews, **50**:77–111.

Arndt N.T., 1977. Thick, layered periodotite-gabbro lava flows in Munro Township, Ontario. Canadian Journal of Earth Sciences, 14, 2620–2637.

Arndt N.T., Lesher C.M., Czamanske G.K. 2005. Mantle-Derived Magmas and Magmatic Ni-Cu-(PGE) Deposits (J. W. Hedenquist, J. F. H. Thompson, R. J. Goldfarb, e J. P. Richards, Orgs.). One Hundredth Anniversary Volume, 5–23.

Arndt N.T., Lesher C.M., Barnes S.J. 2008. Komatiite (N. T. Arndt, Ed.). Komatiite, 295–327.

Barbosa N., Menezes Leal A.B., Debruyne D., Bastos Leal L.R., Barbosa N.S., Marinho M., Mercês L., Barbosa J.S., Koproski L.M. 2020. Paleoarchean to Paleoproterozoic crustal evolution in the Guanambi-Correntina block (GCB), north São Francisco Craton, Brazil, unraveled by U-Pb Geochronology, Nd-Sr isotopes and geochemical constraints. Precambrian Research, **340**:105614.

Barnes S.-J. 2016. Chalcophile Elements (S. I. P. S. Family, Org.). Archeological Geochemistry: A Comprehensive Reference Source on the Chemistry of the Earth, 1–11.

Barnes S.-J., Lightfoot P.C. 2005. Formation of Magmatic Nickel Sulfide Deposits and Processes Affecting Their Copper and Platinum Group Element Contents. Society of Economic Geologists, Inc. Economic Geology - One Hundredth Anniversary Volume, 179–213.

Barnes S.-J., Ripley E.M. 2016. Highly siderophile and strongly chalcophile

elements in magmatic ore deposits. Reviews in Mineralogy and Geochemistry, 81:725–774.

Barnes S.-J., Mansur E.T. 2022. Distribution of Te, As, Bi, Sb, and Se in Mid-Ocean Ridge Basalt and Komatiites and in Picrites and Basalts from Large Igneous Provinces: Implications for the Formation of Magmatic Ni-Cu-Platinum Group Element Deposits. Economic Geology; 117 (8): 1919–1933. doi: https://doi.org/10.5382/econgeo.4887

Barnes, S.J., 1998, Chromite in komatiites, 1. Magmatic controls on crystallization and composition: Journal of Petrology, v. 39, p. 1689–1720.

Barnes, S.J., 2006a, Komatiite-hosted nickel sulfide deposits: Geology, geochemistry, and genesis: Society of Economic Geologists Special Publication 13, p. 51–118.

Barnes, S.J., 2006b, Komatiites: Petrology, volcanology, metamorphism and geo chemistry: Society of Economic Geologists Special Publication 13, p. 13–49.

Barnes S.J., Osborne G.A., Cook D., Barnes L., Maier W.D., Godel B. 2011. The Santa Rita Nickel Sulfide Deposit in the Fazenda Mirabela Intrusion, Bahia, Brazil: Geology, Sulfide Geochemistry, and Genesis. Economic Geology; 106 (7): 1083–1110. doi: https://doi.org/10.2113/econgeo.106.7.1083

Barnes S.J., Fiorentini, M.L. 2012. Komatiite magmas and nickel sulfide deposits: A comparison of variably endowed Archean terranes: ECONOMIC GEOLOGY, v. 107, p. 755–780, doi:10.2113/econgeo.107.5.755.

Barnes, S.J., Fiorentini, M.L. & Fardon, M.C. 2012. Platinum group element and nickel sulphide ore tenors of the Mount Keith nickel deposit, Yilgarn Craton, Australia. Miner Deposita 47, 129–150. https://doi.org/10.1007/s00126-011-0348-5

Barnes, S.J., Heggie G.J., Fiorentini, M.L. 2013. Spatial Variation in Platinum Group Element Concentrations in Ore-Bearing Komatiite at the Long-Victor Deposit, Kambalda Dome, Western Australia: Enlarging the Footprint of Nickel Sulfide Orebodies. Economic Geology; 108 (5): 913–

933. doi: https://doi.org/10.2113/econgeo.108.5.913

Barnes S.J., Cruden A.R., Arndt N., Saumur B.M. 2016. The mineral system approach applied to magmatic Ni–Cu–PGE sulphide deposits. Ore Geology Reviews, **76**:296–316.

Bleeker W., Macek J. 1996. Evolution of the Thompson nickel belt, Manitoba: Setting of Ni-Cu deposits in the western part of the Circum Superior boundary zone. Joint Annual Meeting, Winnipeg, Manitoba, .

Brenner T.L. 2006.The Fortaleza De Minas Nickel, Copper and Platinoids Deposit : Ore Types , Tectonics and Volcanological Aspects a Jazida De Níquel , Cobre E Platinóides De Fortaleza De Minas : Aspectos Tectônicos , Vulcanológicos E Tipos De Minérios .: A Universidade Estadual Paulista Júlio de Mesquita Filho.

Brenner T.L., Teixeira N.A., Oliveira J.A.L., Franke N.D., Thompson J.F.H. 1990. The O'Toole nickel deposit, Morro do Ferro greenstone belt, Brazil. Economic Geology, **85**:904–920.

Campbell I.H., Naldrett A.J. 1979. The influence of silicate: sulfide ratios on the geochemistry of magmatic sulfides. Economic Geology, **74**:1503–1506. doi: https://doi.org/10.2113/gsecongeo.74.6.1503

Carvalho S.G. de, Brenner T.L. 2010. Depósito de Ni-Cu-Co-Au-EGP de Fortaleza de Minas, Minas Gerais. Modelos de depósitos de cobre do Brasil e sua resposta ao Intemperismo, 216.

Choudhuri A., Iyer S.S., Krouse H.R. 1997. Sulfur isotopes in komatiite-hosted ni-cu sulfide deposits from the morro do ferro greenstone belt, southeastern brazil. International Geology Review, **39**:230–238.

Dillon-Leitch H.C.H., Watkinson D.H., Coats C.J.A.1986. Distribution of platinum-group elements in the Donaldson West deposit, Cape Smith belt, Quebec. Econ Geol 81(5):1147–1158.

Donnelly, T.H., Lambert, I.B., Oehler, D.Z., Hallberg, J.A., Hudson, D.R., Smith, J.W., Bavinton, O.A., Golding, L., 1978. A reconnaissance study of stable isotopes ratios in Archaean rocks from the Yilgarn Block,

Western Australia. Geol. Soc. Australia J. 24, 409–420. Doi: doi.org/10.1080/00167617708728999

Gole M. J., Barnes S. J. 2020. The association between Ni-Cu-PGE sulfide and Ni-Co lateritic ores and volcanic facies within the komatiites of the 2.7 Ga East Yilgarn Craton Large Igneous Province, Western Australia, Ore Geology Reviews, Volume 116, 103231, ISSN 0169-1368,https://doi.org/10.1016/j.oregeorev.2019.103231.

Godel, B., Barnes, S.J., Gürer, D. et al. 2013. Chromite in komatiites: 3D morphologies with implications for crystallization mechanisms. Contrib Mineral Petrol 165, 173–189. https://doi.org/10.1007/s00410-012-0804-y

Grobler D.F., Brits J.A.N., Maier W.D., Crossingham A. 2019. Litho- and chemostratigraphy of the Flatreef PGE deposit, northern Bushveld Complex. Mineralium Deposita, 54:3–28.

Hiebert R.S., Bekker A., Houlé M.G., Wing B.A., Rouxel O.J. 2016. Tracing sources of crustal contamination using multiple S and Fe isotopes in the Hart komatiite-associated Ni–Cu–PGE sulfide deposit, Abitibi greenstone belt, Ontario, Canada. Mineralium Deposita, 51:919–935.

Hill, R.E.T., 2001, Komatiite volcanology, volcanological setting and primary geochemical properties of komatiite-associated nickel deposits: Geochemistry: Exploration, Environment, Analysis, v. 1, p. 365–381.

Houlé M.G., Lesher C.M., Davis P.C. 2012. Thermomechanical erosion at the Alexo Mine, Abitibi greenstone belt, Ontario: Implications for the genesis of komatiite-associated Ni-Cu-(PGE) mineralization. Mineralium Deposita, **47**:105–128.

Keays R.R., Lightfoot P.C. 2010. Crustal sulfur is required to form magmatic Ni-Cu sulfide deposits: Evidence from chalcophile element signatures of Ketris M.P., Yudovich Y.E. 2009. Estimations of Clarkes for Carbonaceous biolithes: World averages for trace element contents in black shales and coals. International Journal of Coal Geology, 78:135–148.Siberian and Deccan Trap basalts. Mineralium Deposita, **45**:241–257.

Knight R.D., Prichard H.M., Filho C.F.F. 2017. Evidence for as contamination and the partitioning of Pd into pentlandite and Co + platinum group elements into pyrite in the fazenda Mirabela intrusion, Brazil. Economic Geology, 112:1889–1912.

Layton-Matthews D., Lesher C.M., Burnham O.M., Hulbert L., Peck D.C.P., Golightly J.P., Keays D.R.R. 2010. Mineralization in the Thompson Nickel Belt, Manitoba. Exploration for Komatiite-Associated Ni-Cu-(PGE). Economic Geology – Special volume- Chapter 27. 517-538p.

Lesher, C.M., 1989, Komatiite-associated nickel sulfide deposits. Ore deposition associated with magmas: Reviews in Economic Geology, v. 4, p. 45−101. doi: https://doi.org/10.5382/Rev.04.05

Lesher, C.M., 2007. Ni-Cu-(PGE) deposits in the Raglan area, Cape Smith belt, New Quebec. In: Goodfellow, W.D. (Ed.), Mineral Deposits of Canada: A Synthesis of Major Deposit Types, District Metallogeny, the Evolution of Geological Provinces and Exploration Methods. Geological Association of Canada. Special Publication 5, pp. 351–387.

Lesher C.M. 2017. Roles of xenomelts, xenoliths, xenocrysts, xenovolatiles, residues, and skarns in the genesis, transport, and localization of magmatic Fe-Ni-Cu-PGE sulfides and chromite. Ore Geology Reviews, **90**:465–484.

Lesher, C. M., Groves, D. I. 1986. Controls on the formation of komatiite-associated nickel-copper sulfide deposits. In: G. H. Friedrich (ed.) Geology and Metallogeny of Copper Deposits. Berlin: Springer Verlag. doi https://doi.org/10.1007/978-3-642-70902-9_4:

Lesher, C.M., and Campbell, I.H., 1993, Geochemical and fluid dynamic modelling of compositional variations in Archean komatiite-hosted nickel sulfide ores in Western Australia: ECONOMIC GEOLOGY, v. 88, p. 804–816.

Lesher, C.M., Stone, W.E., 1996, Exploration geochemistry of komatiites, in Wyman, D., ed., Igneous Trace Element Geochemistry: Applications for Massive Sulphide Exploration: Geological Association of Canada,

Short Course Notes, v. 12, p. 153-204.

Lesher C.M., Burnham O.M. 2001. Multicomponent elemental and isotopic mixing in Ni-Cu-(PGE) ores at Kambalda, Western Australia. Canadian Mineralogist, **39**:421–446. Doi: https://doi.org/10.2113/gscanmin.39.2.421.

Lesher C.M., Keays R.R. 2002. Komatiite-associated Ni-Cu-PGE Deposits: Geology, Mineralogy, Geochemistry, and Genesis. The Geology, Geochemistry, Mineralogy and Mineral Beneficiation of PGE.

Lesher, C.M., and Barnes, S.J., 2009, Komatiite-associated Ni-Cu-(PGE) deposits, in Li, C., and Ripley, E.M., eds., Magmatic Ni-Cu-PGE deposits: Genetic models and exploration: Beijing, Geological Publishing House of China, p. 27−101.

Lesher, C.M., Arndt, N.T., and Groves, D.I., 1984, Genesis of komatiite-associated nickel sulphide deposits at Kambalda, Western Australia: A distal volcanic model, in Buchanan, D.L., and Jones, M.J., eds., Sulphide Deposits in Mafic and Ultramafic Rocks: Institution of Mining and Metallurgy, London, p. 70-80.

Lesher, C.M., Barnes, S.-J., Gillies, S.L., and Ripley, E.M., 1999. Ni-Cu-(PGE) sulphides in the Raglan Block, in Lesher CM (Editor), Komatiitic Peridotite-Hosted Fe-Ni-Cu-(PGE) Sulphide Deposits in the Raglan Area, Cape Smith Belt, New Québec. Guidebook Series 2, Mineral Exploration Research Centre, Laurentian University, Sudbury: 177–184.

Li C., Ripley E.M. 2009. Sulfur contents at sulfide-liquid or anhydrite saturation in silicate melts Empirical equations and example applications. Economic Geology, **104**:405–412. doi: https://doi.org/10.2113/gsecongeo.104.3.405

Lightfoot P.C., Keays R.R., Evans-Lamswood D., Wheeler R. 2012. S saturation history of Nain Plutonic Suite mafic intrusions: Origin of the Voisey's Bay Ni-Cu-Co sulfide deposit, Labrador, Canada. Mineralium Deposita, **47**:23–50. doi: https://doi.org/10.1007/s00126-011-0347-6

Lima F.G. 2017.Morro do Níquel: Fragmento de manto exumado na faixa Brasília Meridional: UNIVERSIDADE ESTADUAL PAULISTA - Julio de Mesquita Filho: 127 p.

Lima F.G., Faria Júnior I.R., Zanardo A., Szabó G.A.J., Montibeller C.C. 2021. Caracterização textural e mineralógica das rochas do Morro do Níquel (MG) e correlações com o processo de serpentinização. Geociencias, 567–581.

Luolavirta K. 2018. Magmatic evolution of the Kevitsa igneous complex, northern Finland, and its relation to the associated Ni-Cu-(PGE) mineralization. 68 p. Thesis, University of Oulu, Oulu Mining School, P.O. Box 3000, FIN-90014 Oulun yliopisto, Finland. URL: https://www.researchgate.net/publication/333508201_Magmatic_evolution_of_the_Kevitsa_igneous_complex_northern_Finland_and_its_relation_to_the_associated_Ni-Cu-PGE_mineralization

Lyubetskaya T., Korenaga J. 2007. Chemical composition of Earth's primitive mantle and its variance: 1. Method and results. Journal of Geophysical Research: Solid Earth, 112:1–21.

Maia T.F.A., Ferreira Filho C.F., S. B. Oliveira. (submitted). The komatiite-associated Boa Vista Ni-Cu-(PGE) sulfide deposit, Crixás greenstone belt, Central Brazil: insights into komatiite flow facies and exploration. Journal of South American Earth Sciencen.

Marchetto C.M.L. 1990. Platinum-Group Minerals in the O'Toole (Ni-Cu-Co) Deposit, Brazil. Economic Geology, **85**:921–927.

McClenaghan M.B., Layton-Matthews D., Matile G. 2011. Till geochemical signatures of magmatic Ni–Cu deposits, Thompson Nickel Belt, Manitoba, Canada. Geochemistry: Exploration, Environment, Analysis. 11 (2): 145–159. doi: https://doi.org/10.1144/1467-7873/09-IAGS-021

Mota-e-Silva J., Prichard H.M., Filho C.F.F., Fisher P.C., McDonald I. 2015. Platinum-group minerals in the Limoeiro Ni–Cu–(PGE) sulfide deposit, Brazil: the effect of magmatic and upper amphibolite to granulite

metamorphic processes on PGM formation. Mineralium Deposita, 50:1007–1029.

Naldrett, A.J., 1966. The role of sulphurization in the genesis of iron-nickel sulphide deposits of the Porcupine District, Ontario. Can. Inst. Mining Metal. Trans. 69, 147–155.

Naldrett A.J. 2004. Magmatic Sulfide Deposits: Geology, Geochemistry and Exploration, Springer-Verlag Berlin-Heidelberg, 728 pp. Doi: https://doi.org/10.1007/978-3-662-08444-

2011. Fundamentals of Magmatic Sulfide Deposits (C. Li e E. M. Ripley, Orgs.). Magmatic Ni-Cu and PGE Deposits: Geology, Geochemistry, and Genesis, 1–50.

Naldrett A.J., BARNES, S.-J. (1986): The behavior of platinum group elements during fractional crystallization and partial melting with special reference to the composition of magmatic sulfide ores. Fortschr. Mineral. 64, 113-133.

Oliveira E.P., McNaughton N.J., Zincone S.A., Talavera C. 2020. Birthplace of the São Francisco Craton, Brazil: Evidence from 3.60 to 3.64 Ga Gneisses of the Mairi Gneiss Complex. Terra Nova, **32**:281–289.

Perring C.S., Barnes S.J., Hill R.E.T. 1995. The physical volcanology of Archaean komatiite sequences from Forrestania, Southern Cross Province, Western Australia. LITHOS, **34**:189–207. doi: https://doi.org/10.1016/0024-4937(95)90021-7

Pimentel M.M., Ferreira Filho C.F. 2002. Idade Sm-Nd de komatiitos do Greestone Belt do Morro do Ferro, Fortaleza de Minas (MG). Revista Brasileira de Geociências, **32**:147–148.

Pinheiro M.A.P., Guice G.L., Reis Magalhães J. 2021. Archean–Ediacaran evolution of the Campos Gerais Domain — a reworked margin of the São Francisco paleocontinent (SE Brazil): Constraints from metamafic–ultramafic rocks. Geoscience Frontiers, 101201.

Pronost J., Harris C., Pin C. 2008. Relationship between footwall composition,

crustal contamination, and fluid-rock interaction in the Platreef, Bushveld Complex, South Africa. Mineralium Deposita, 43:825–848.

Ripley E.M., Li C. 2013. Sulfide saturation in mafic magmas: Is external sulfur required for magmatic Ni-Cu-(PGE) ore genesis? Economic Geology, **108**:45–58.

Ripley E.M., Li C., 2017. A review of the application of multiple s isotopes to magmatic Ni-Cu-PGE deposits and the significance of spatially variable $\Delta^{33}S$ Values. Economic Geology; 112 (4): 983–991. doi: https://doi.org/10.2113/econgeo.112.4.983

Robertson J., Ripley E.M., Barnes S.J., Li C. 2015. Sulfur liberation from country rocks and incorporation in mafic magmas. Economic Geology, **110**:1111–1123. doi: https://doi.org/10.2113/econgeo.110.4.1111

Samalens N., Barnes S.-J., Sawyer E.W. 2017. The role of black shales as a source of sulfur and semimetals in magmatic nickel-copper deposits: Example from the Partridge River Intrusion, Duluth Complex, Minnesota, USA. Ore Geology Reviews, **81**:173–187.

Staude S., Barnes S.J., Le Vaillant M. 2017. Thermomechanical erosion of ore-hosting embayments beneath komatiite lava channels: Textural evidence from Kambalda, Western Australia. Ore Geology Reviews, **90**:446–464.

Staude, S., Oelze, M. & Markl, G. 2022. Multi-stage sulfide evolution of the Moran Ni sulfide ore, Kambalda, Western Australia: insights into the dynamics of ore forming processes of komatiite-hosted deposits. Miner Deposita 57, 889–909 Doi: https://doi.org/10.1007/s00126-021-01060-5

Teixeira N.A., Gaspar J.C., Brenner T.L., Cheney J.T., Marchetto C.M.L. 1987. Geologia e implicações Teotectônicas do Greestone Belt Morro do Ferro (Fortaleza de Minas, MG). Revista Brasileira de Geociências, **17**:209–220.

Törmänen T., Konnunaho J.P., Hanski E., Moilanen M., Heikura P. 2016. The Paleoproterozoic komatiite-hosted PGE mineralization at Lomalampi, Central Lapland Greenstone Belt, northern Finland. Mineralium Deposita, **51**:411–430. doi: https://doi.org/10.1007/s00126-015-0615-

y

Turbay C.V.G., Valeriano C. de M., Rossi A., Silva V.G.M. da R. e 2013. Geologia Do Complexo Campos Gerais Ao Sul De Alpinópolis, Sudoeste De Minas Gerais. Geonomos, **16**:79–90.

Virnes A. B., Fiorentini M. L., Barnes S. J., Caruso S., Martin L. A. J, Aleshin M., Schoneveld L. E, Roberts M. P., Masurel Q., Thebaud N. 2023. Decoupling of Sulfur Isotope Signatures from Platinum Group Elements in Komatiite-Hosted Ore Systems: Evidence from the Mount Keith MKD5 Ni-(Co-Cu) Deposit, Western Australia. Economic Geology; 118 (8): 1813–1834. doi: https://doi.org/10.5382/econgeo.5030

Appendix B

R-factor calculus of the Fortaleza de Minas deposit

	Komatiite				
	As	Sb	Bi	Se	Te
$C_L = X_i^0$	0.1	0.014	0.008	0.16	0.02
	ppm	ppm	ppm	ppm	ppm
$C_A = Y_i^0$	6.75	0.09	0.50	3.40	1.83
$D_i^{Sul/Sil}$	25	16	875	425	2550

	$C_S = Y_i^f$				
R	As	Sb	Bi	Se	Te
1	6.59	0.10	0.50	3.55	1.85
3	6.29	0.11	0.52	3.85	1.89
5	6.04	0.12	0.53	4.15	1.93
10	5.54	0.14	0.57	4.89	2.02
30	4.43	0.18	0.71	7.66	2.40
50	3.92	0.19	0.85	10.20	2.78
100	3.35	0.21	1.16	15.70	3.69
300	2.83	0.22	2.16	30.13	7.01
500	2.70	0.22	2.86	38.32	9.89
1000	2.60	0.22	3.97	48.73	15.68
3000	2.54	0.22	5.53	59.98	28.41
5000	2.52	0.22	6.03	62.94	34.39
10000	2.51	0.22	6.48	65.37	41.01
30000	2.50	0.22	6.82	67.10	47.15
50000	2.50	0.22	6.89	67.46	48.61
100000	2.50	0.22	6.94	67.73	49.78
300000	2.50	0.22	6.98	67.91	50.59
500000	2.50	0.22	6.99	67.95	50.75
1000000	2.50	0.22	6.99	67.97	50.87

Sulfur isotopic data from Fortaleza de Minas ore and BIF country rock

Sample ID	$\delta^{34}S$ ‰ (V-CDT)	Mineral sulfide	Type of Rock	Type of ore
1A	6.5	Pyrrhotite>Pentlandite>Chalcopyrite	ore	matrix breccia
1D	6.4	Pentlandite>Pyrrhotite>Chalcopyrite	ore	net-texture
1F	6.2	Pyrrhotite>Pentlandite>Chalcopyrite	ore	net-texture
2C	5.9	Pyrrhotite> Chalcopyrite	BIF	-
2D	6.5	Pyrrhotite>Pentlandite>Chalcopyrite	ore	matrix breccia
2H	6.3	Pyrrhotite>Pentlandite>Chalcopyrite	ore	matrix breccia
2M	6.2	Pyrrhotite> Chalcopyrite>Pentlandite	ore	net-texture
2E	6.1	Pyrrhotite> Chalcopyrite>Pentlandite	ore	net-texture
FMD04_55_50	6.7	Pyrrhotite	Graphitic Chert	-
FMD04_181_30	9.5	Chalcopyrite>Pentlandite>Pyrrhotite	BIF	-
FMD04_180_85	9.5	Pyrrhotite>Pentlandite>Chalcopyrite	BIF	-

Standard ID	**$\delta^{34}S$ ‰ vs VCDT**
NBS127	20.2
NBS127	20.4
IAEA-SO-6	-34.0
IAEA-SO-6	-34.0

3. CAPÍTULO 3

Avaliação dos komatiitos brasileiros para mineralização de sulfeto de Ni-Cu-PGE

3.1. Introdução

Os depósitos de sulfeto de Ni-Cu-PGE associados a komatiitos estão exclusivamente associados ou hospedados em greenstone belts Arqueanos e Paleoproterozoicos, e quase sempre estão relacionados a regiões cratônicas (Naldrett, 2004; Arndt et al., 2008). Para formar mineralização econômica de sulfeto de Ni--PGE, é necessária a erosão termomecânica de uma rocha fonte externa de S, a saturação de S em magma, com subsequente segregação e cristalização do líquido de sulfeto imiscível, e uma saturação de líquido de sulfeto no magma de silicato (Li e Ripley, 2005; Li e Ripley, 2009; Keays e Lightfoot 2010; Robertson et al., 2015). O fator R (Campbell e Naldrett, 1979; Lesher e Burnham 2001), mecanismos de transporte de sulfeto fundido (Lesher 2017; Lesher, 2019;), distribuição de minério e variação espacial, geoquímica e textural (Hill 2001; Lesher e Keays, 2002; Barnes, 2006; Arndt et al., 2008), dinâmica do ambiente magmático e geodinâmica do manto e da crosta (Begg et al., 2010; Mole et al., 2014; Magee et al., 2016) também têm sua relevância para a formação desse tipo de minério.

O contato direto dessa rocha com rochas ricas em S é um importante critério geológico; sem ele, a probabilidade de formação de sulfeto magmático é baixa (Hill, 2001; Barnes, 2006). Diferentes rochas encaixantes foram descritas como associadas a komatiitos que hospedam sulfetos magmáticos, como formações ferríferas em bandas (por exemplo, Brenner, 2006; Hiebert et al., 2016) e grafita xistos (Maia et al., (submetido). No entanto, vários depósitos de Ni-Cu-(PGE) associados a komatiitos têm rochas ígneas como encaixantes (por exemplo, basaltos – Kambalda: Lesher e Campbell, 1993; tufos félsicos – Perseverança: Barnes et al., 1995), demonstrando que não se restringe a rochas sedimentares. No contexto mais local, a presença de sequências metavulcano-sedimentares com vulcanismo komatiítico intercaladas com rochas sedimentares ricas em S, com evidências de canalização de fluxo de lava e erosão termomecânica, é o cenário ideal (Naldrett, 1999; Hill, 2001; Naldrett, 2004; Barnes, 2006).

Devido às suas características geológicas de ser um fluxo vulcânico fluido e em ebulição, os fluxos komatiíticos tendem a esfriar rapidamente tanto da borda para o centro do fluxo quanto da base e topo para a porção central; isso

gera um processo de cristalização dos minerais (olivina, cromita e clinopiroxênio) dentro da lava espacial e texturalmente diferente (spinifex) (Lesher e Keays 2002; Gole e Barnes, 2020). Combinado com isso, há o fato de que há derramamentos sucessivos empilhados uns sobre os outros (Hill, 2001). Assim, ter o controle vulcanológico e estratigráfico é essencial para identificar as fácies dos derrames e as áreas mais dinâmicas de canalização da lava. Outro ponto é mapear zonas espessas ricas em olivina com texturas de adcumulus e mesocumulus, nas quais a rocha muitas vezes se apresenta como dunito e/ou peridotito (Gole e Barnes, 2020), bem como, suas contrapartes metamórficas. Essas zonas são favoráveis para uma erosão termomecânica mais eficiente, formação e segregação de um líquido sulfetado imiscível.

A assembleia mineral primária de sulfeto caracteristicamente compreende pirrotita, pentlandita, calcopirita e pirita. Também é necessário destacar o fato de que muitas dessas rochas são fortemente metamorfizadas e tectonizadas, causando mobilização e modificação da textura e mineralogia do minério de sulfeto, podendo até mesmo concentrar PGE nesse processo (e.g., Almeida et al., 2007; Le Vaillant et al., 2016).

O contexto tectônico favorável para esse tipo de mineralização possui regiões cratônicas com grandes estruturas crustais adequadas a um fluxo magma, que podem estar associadas a regiões marginais e paleomargens de crátons, e temporalmente pode ser correlacionadas a plumas do manto (Mole et al., 2014). Ambientes de rifte que foram tectonicamente invertidos também são favoráveis a esse tipo de mineralização (Fiorentini et al., 2012). Portanto, o ambiente tectônico, o tipo de fonte, bem como o tipo de komatiito não afetam seu potencial de formar mineralização Ni-Cu-PGE (Arndt et al., 2008; Barnes e Fiorentine, 2012; Perring, 2015).

O reconhecimento de áreas e ambientes prospectivos, em termos de sulfetos de Ni-Cu-PGE associados a komatiítos pode ser delineado em cinco pontos: I) presença de grandes derrames de magma na sequência komatiítica (ou presença de magmatismo de alto Mg em primeiro lugar); II) presença de rochas encaixantes ricas em enxofre, III) evidências de saturação e segregação de líquido sulfetado; IV) evidências de contaminação crustal; e V) determinação

do controle estrutural e/ou nível de erosão atual da sequência komatiítica (Barnes et al., 2004, Ardnt et al., 2008; Barnes et al., 2016).

Praticamente, cumulatos espessos são mais prospectivos do que fluxos de lava mais finos. No entanto, diferentes técnicas funcionam em diferentes áreas e escalas e, em geral, não há um método absoluto para explorar komatiítos em todo o mundo (Barnes et al., 2004; Barnes, 2006; Konnunaho, et al., 2015; Le Vaillant et al., 2016). Nos métodos geofísicos, por exemplo, levantamentos magnéticos e eletromagnéticos são importantes para localizar áreas potenciais, particularmente em terrenos metamórficos (Le Vaillant et al., 2016), devido à formação de magnetita na serpentinização, os metakomatiitos ficam com anomalias magnéticas positivas. No entanto, a magnetita não é formada durante o metassomatismo rico em CO_2. Além disso, a deformação e a alteração pós-magmática podem limitar o uso de sinais geoquímicos tradicionais na detecção de contaminação e/ou segregação do sulfeto (Jahn et al., 1982; Tourpin et al., 1991; Barnes et al., 2004; Le Vaillant et al., 2016).

3.2. Komatiitos brasileiros

Os komatiitos brasileiros são raros; eles ocorrem em greenstone belts arqueanos em diferentes crátons e faixas móveis, neste último como um bloco arqueano dentro da faixa móvel. O Brasil possui apenas duas ocorrências do depósito de sulfeto de Ni-Cu-(PGE) associado à komatiito até então descobertos, Boa Vista e Fortaleza de Minas. Outras 24 ocorrências de komatiitos foram descritas na literatura. Uma compilação das informações sobre eles encontra-se na **Tabela 5**.

Tabela 5 Compilação dos dados geológicos dos komatiitos brasileiros.

Unidade geológica /Estado	Descrição	Rochas sedimentares associadas	Mineralização ou Ocorências
Craton São Francisco			
Pitangui - Mg	Muito alterados, compostos por uma mineralogia secundária e são considerados talco-xistos. A	intercalados com intervalos BIFs,	Não

	textura e mineralogia originais foram completamente obliteradas, exceto por raros spinifex identificados em afloramentos intemperizados. (Soares et al., 2020)	metaarenitos turbidíticos e metapelitos	
Rio das Velhas (Quebra Osso) - Mg	Os komatiitos maciços são caracterizados por uma textura spinifex, camadas com cumulus olivina / intercumulus ortopiroxênio e uma camada de brecha do tipo lahar. O fluxo komatiítico de 0,5 a 1,5 m de espessura é composto por uma camada de spinifex. (Verma et al., 2017).	localmente intercalados com sedimentos carbonáceos marinhos	não
Rio Manso - Mg (Morro da Onça?)	A textura cumulática é configurada como um nível basal de peridotito de fluxos, e o nível superior é mais piroxenítico, que pode conter texturas spinifex, brechas superiores e textura vítrea ou amorfa. (Andreatta e Silva & Carneiro, 2009).	nenhuma rocha sedimentar associada	não
Umburanas - Ba	As amostras de komatiito consistem principalmente em três grupos de rochas. Um grupo é caracterizado por textura spinifex com morfologia paralela e triangular de agregados de olivina. O outro grupo é maciço e é tipicamente de granulação fina exibindo cor verde, cinza-	intercalações de sedimentos químicos e siliciclásticos,	não

	esverdeada a verde escura e um último é cumulático, com raros cristais de olivina preservados, sendo substituídos por serpentina, talco e clorila (Teixeira et al., 2012; Menezes Leal et al., 2015; Menezes Leal et al., 2016).		
Ibitira-Ubiraçaba - Ba	Preservar texturas reliquiares de spinifex como pequenas agulhas aleatórias de tremolita substituindo cristais primários de piroxênio e olivina. Às vezes com relíquias de cumulus de olivina e em uma estrutura aparentemente fragmentária, típica do topo dos fluxos (Cunha et al. 2012, Santos, 2022).	intercalações subordinadas de BIF, e cherts.	não
Brumado - Ba	Komatiitos extensivamente modificados e obliterados por ação metamórfica e tectônica. Os fluxos são maciços, finos a laminados, não exibindo texturas claras de spinifex, com texturas típicas de fluxo vulcânico, com texturas típicas de spinifex. (Cunha et al. 2012).	intercalados por sedimentos químicos (calcissilicatos, cherts e BIF) e terrígenos (quartzitos).	não
Guajeru- Ba	Rochas verde-claras a escuras, geralmente de granulação fina, por vezes apresentando cristais mais desenvolvidos, foliadas, apresentando, geralmente, traços de textura cumulática e spinifex, mas em geral, a textura cumulada	intercalações de quartzitos, metacarbonatos, formações ferríferas e rochas quartzo-feldspáticas.	não

	é predominante (Cunha et al. 2012).		
Mundo Novo - Ba	Microestrutura de spinifex relíquiar. A microestrutura spinifex de granulação fina é identificada apenas em amostras de mão e no microscópio (Spreafico et al., 2020; Teles et al., 2022).	nenhuma rocha sedimentar associada	não
Gavião - Ba	Encalves de Serpentinitos, com geoquímica de rocha cumulática de olivina (Teixeira, 2012).	?	não
Lagoa do Alegre - Ba	Composto essencialmente por tremolita-actinolita e menos comumente diopsídio e tem uma textura spinifex. Os xistos de talco têm uma cor verde clara. (Cunha et al. 2012).	?	não
Boquira - Ba	Rochas com textura spinifex, com geoquímica de komatiito (Cunha et al., 2012)	?	não
Riacho de Santana - Ba	Rochas com texturas spinifex, maciço e cumulato, com parte semelhante com peridotito e píroxenito, tectonizado e metamofizado. Observa-se pseudomorfo da olivina com serpentina e tremolita (Silveira & Garrido, 2000; Meira, 2023)	associadas a formações ferríferas bandadas (BIFs), quartzitos, metacherts, calciosilicáticas e xistos aluminosos.	não
Tiquara- Ba	Incluem tremólitos e xistos tremolitos e serpentinos, geralmente com textura	nenhuma rocha sedimentar associada	não

	nematoblástica, às vezes com características que sugerem texturas paleospinifex, com tamanhos variados de anfibólios na mesma rocha, anfibólios em uma fina matriz de clorito e cadeias de grânulos de magnetita (Cunha et al., 2012).		
Riacho dos Machados - Ba	Xisto de tremolita-clorito esverdeado e xistos de clorita-tremolita-serpentina. Essas rochas apresentam uma matriz composta por cristais serpentinos fibrosos a lamelares de granulação muito fina (Leal et al. 2021).	nenhuma rocha sedimentar associada	não
Rio Salitre - Ba	Rochas verdes maciças a ligeiramente foliadas. Em alguns lugares, é perceptível a textura micro-spinifex que é formada por serpentina, carbonato e tremolita. Os komatiitos menos deformados apresentam textura decussada compreendendo tremolita, serpentina e carbonato (Garcia et al., 2021).	pequena participação de metassedimentos exalativos clásticos e químicos	não
Cinturão orogênico a NW da borda do Craton São Francisco			

Piumhi - Mg	As características do spinifex aparecem como aciculares no tipo, com a actinolita substituindo os clinopiroxênios	?	não
Fortaleza de Minas-Morro do Ferro - Mg	Quatro ciclos ou unidades de fluxo de serpentinito, clino-piroxenito e gabro. Os fluxos cumulados de olivina são discretos e mostram a textura de forma pontual (Brenner, 2006).	Intercalações de formação ferrífera bandada	sim
Barbacena	serpentinito com texturas maciças e spinifex, e lava localmente em pillow (Rodrigues, 2000).	?	não
Brasília Belt			
Faina and Serra de Santa Rita - Go	As rochas com texturas cumuladas preservadas, além de ser também maciças e caracterizadas por pseudomorfos de olivina cumulus totalmente substituída por serpentina. texturas reliquiares mesocumuladas e ortocumuladas foram descritas, (Borges et al., 2017).	Intercalado com formações ferríferas bandadas	não
Crixás - Go	Foram reconhecidos quatro fluxos diferentes, com texturas de olivina ad-mesocumulada, maciça, platy e radom spinifex. As rochas são serpentinitos e tremolititos, ambos com talco, e em algumas amostras, olivina metamórfica (Maia et al., submetido)	Intercalado com grafita xisto.	sim

Pilar - Go	Serpentinito, talco e clorita- filito, com fluxos piroxeníticos e basáticos subordinados. Características primárias, como texturas spinifex, raramente são vistas (Jost et al., 2014).	Intercalado com formações ferríferas bandadas	não
Guarinos - Go	Semelhantes ao de Pilar.	Intercalado com formações ferríferas bandadas	não
Província Mineral de Carajás			
Selva - Pa	Talco-xisto, serpentinito e komatiito com textura spinifex. uma sequência de fluxos que consiste em uma camada superior texturizada de spinifex e uma camada inferior de acumulado de olivina. a mineralogia primária dos komatiitos foi completamente substituída por minerais metamórficos de fácies xisto verde (Sierpiesky e Ferreira Filho, 2016).	?	não
Sapucaia - Pa	Serpentinitos, onde as texturas spinifex não são facilmente reconhecidas. Ela pode ser vista ao longo do plano de foliação XY, platy e random spinifex também foram reconhecidos. A mineralogia primária foi completamente substituída por	?	não

	minerais metamórficos, como clorito, serpentina, talco, tremolita e actinolita. (Costa et al., 2023)		
Seringa - Pa	As rochas são xistos de tremolita e xistos de talco-tremolita, onde, mostram relíquias de texturas de spinifex. uma sucessão de fluxos máficos para ultramáficos, nos quais distinguiram três zonas: 1) acumula na base; 2) fácies de granulação média a grossa com texturas abundantes de spinifex; e 3) rochas de granulação fina com margens resfriadas e fraturadas e bolsas de brecha, no topo (Souza et al., 1997).	?	não
Província Borborema			
Porção central do Domínio Rio Grande do Norte	serpentinitos, anfibólios-xistos e anfibolitos, os serpentinitos ocorrem como exposições relativamente pequenas de corpos alongados dentro de paragnaisses, e com química de komatiito (Santos et al., 2020)	paragnaisse	não

Uma informação relevante mostrada na **Tabela 5** é a associação ou não dos komatiitos com rochas sedimentares que pode ser rica em enxofre, especificamente aquelas portadoras de enxofre, como são os casos das formações ferríferas bandadas, os folhelhos negros e seus produtos metamórficos (itabiritos, filitos carbonosos e grafita xistos), metasedimentares químicas/exalativas, e outras rochas sedimentares ricas em matéria orgânica. Destaque para os komatiitos não mineralizados dos greenstone belts de Pitangui, Quebra Osso, Umburanas, Ibitiba-Ubiraçaba, Guajeru, Riacho de

Santana, Rio Salitre, Pilar e Guarinos. Também há aqueles que não foram encontrados dados na literatura sobre associação/intercalação com rochas sedimentares, que são todos os komatiitos que estão com uma interrogação (?) nesta coluna.

Avaliando a descrição os komatiitos não mineralizados, para as rochas com textura cumulática, destaque para os komatiitos dos greenstone belts de Quebra Osso, Rio Manso, Riacho de Santana, Faina, Serra de Santa Rita, Selva e Seringa. É importante mencionar que a ausência de descrição de textura cumulática, não implica diretamente que ela não exista no greenstone belt em questão, pode ser que ele não tenha sido descrito/mapeado, não aflore ou ainda que tenha sido erodido.

Foi feita também uma compilação de dados geoquímicos disponível na literatura, a fim de avaliar e identificar zonas de alto fluxo de magma, potenciais para segregação de líquido sulfetado nos komatiitos brasileiros, através de diagramas específicos (**Fig. 31**). Razões Ni/Ti e Ni/Cr podem ser usados para identificar ambiente de maior fluxo de magma/lava em zonas de conduto/canais. Além de indicar um campo de segregação de líquido sulfetado (Le Vaillant et al., 2015). Para os komatiitos brasileiros, (**Fig. 31A**), observa-se a ausência de dados para tais elementos, deixando o diagrama com poucos pontos, destaque para Crixás e Quebra Osso, com razões Ni/Ti e Ni /Cr elevadas >1. Vale enfatizar aqui que nenhuma amostra dos komatiitos de Crixás está mineralizada. Outro aspecto importante é o fato de ter amostras de Quebra Osso no campo denominado sulfide bearing-cumulate, que é o campo indicativo de segregação de líquido sulfetado em rochas cumuláticas.

Algumas rochas sedimentares ricas em enxofre são também ricas em outros elementos que podem ser usados como traçadores de contaminação/assimilação crustal, como é o caso do Zn no depósito de Boa Vista em Crixás. Uma abordagem para Zn vs. Ni foi feita nos komatiitos brasileiros (**Fig. 31B**), nele novamente destaque para a já conhecida associação entre Ni e Zn para os komatiitos de Crixás (Maia et al., 2025), e para Quebra Osso, com algumas anomalias bem altas tanto de Ni quanto Zn aproximadamente 3900 e 280 ppm respectivamente, indicando que essa correlação pode ser usada para

esses komatiitos. O último diagrama (**Fig. 31C**) somente há dados de Pd para os komatiitos do Quebra Osso, nele $(Pd/Al)_{NM}$ vs. $(Pd/Ti)_{NM}$ é usado para avaliar se houve ou não um processo de enriquecimento de metais por um processo de captura desses metais pelo líquido sulfetado (Fiorentine et al., 2010). Mesmo somente tendo dados de Quebra Osso, é possível inferir que houve sim essa captura de metais, em parte dos komatiitos de Quebra Osso. No caso usou-se o Pd, mas pode ser inferido para outros PGE, Ni e Cu, e que foi formado um líquido sulfetado numa fase anterior.

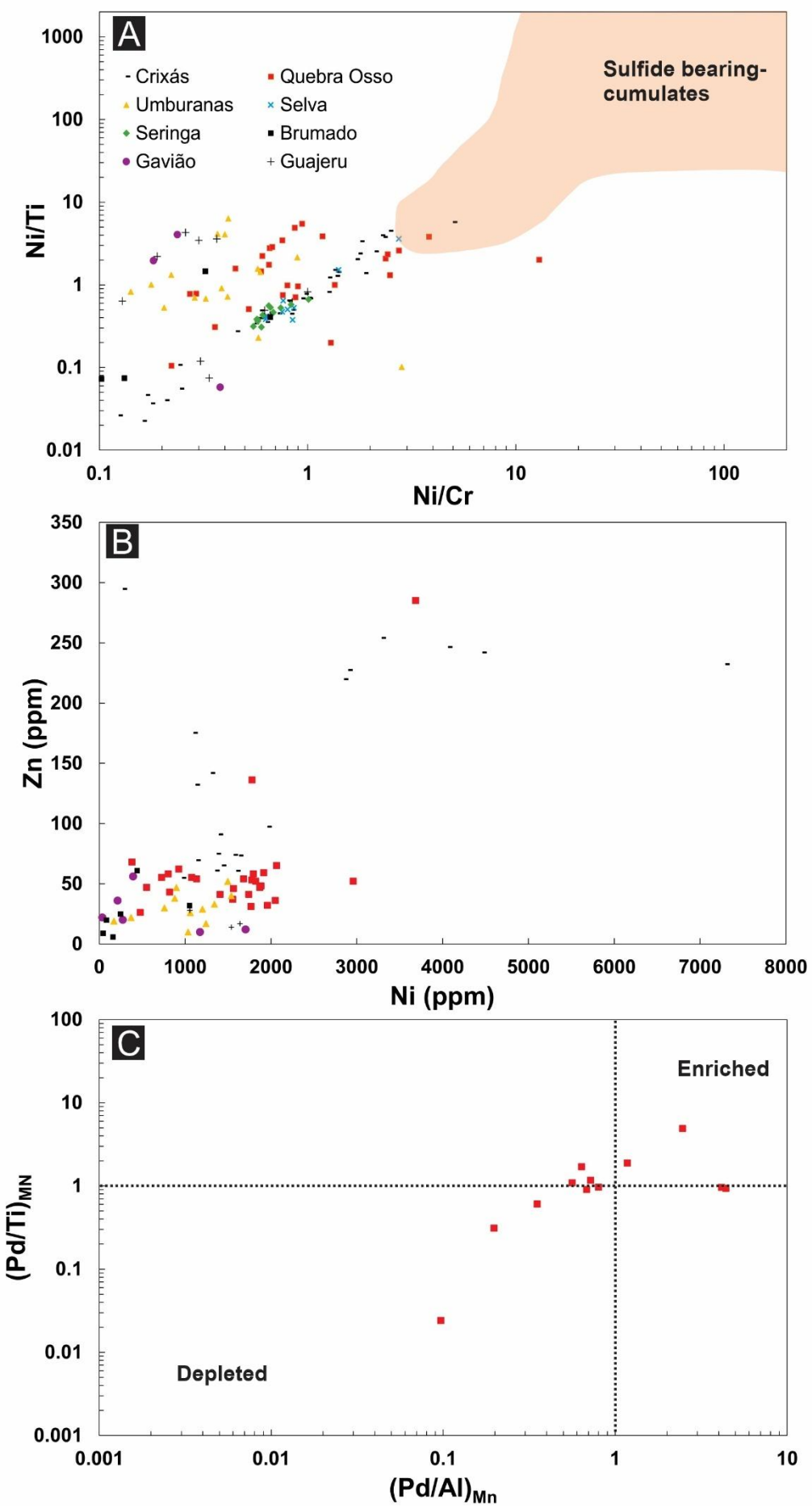
A
Crixás
Quebra Osso
Umburanas
Selva
Seringa
Brumado
Gavião
Guajeru
Sulfide bearing-cumulates
Ni/Ti
Ni/Cr
1000
100
10
1
0.1
0.01
0.1
1
10
100
B
Zn (ppm)
Ni (ppm)
350
300
250
200
150
100
50
0
0
1000
2000
3000
4000
5000
6000
7000
8000
C
Enriched
Depleted
(Pd/Ti)MN
(Pd/Al)Mn
100
10
1
0.1
0.01
0.001
0.001
0.01
0.1
1
10

Figura 31 Diagramas geoquímicos para komatiitos. (A) Ni/Cr vs. Ni/Ti baseado em Le Vaillant et al. (2015), (B) Ni vs. Zn e (C) $(Pd/Al)_{NM}$ vs. $(Pd/Ti)_{MN}$, baseado em Fiorentini et al. (2010) e Heggie et al. (2013). Normalização feita pelo manto primitivo de McDonald e Sun (1995).

Com base nos dados sumarizados e compilados na **Tabela 5**, e dos diagramas geoquímicos feitos (**Fig. 31**), e nos pré-requisitos necessários para formação de sulfetos Ni-Cu-PGE associados a komatiitos, já mencionados foi elaborada uma tabela simples, onde são elencados esses pré-requisitos e marcados com X os komatiitos que os têm (**Tabela 6**). Destaque para Quebra Osso como o único que atendeu todos os quatro pré-requisitos. Um ponto importante é que a ausência de um ou mais pré-requisitos não necessariamente implica em não ter tal pré-requisito(s), pode ser apenas por falta de dados, principalmente geoquímicos, ou não ter sido devidamente mapeado. Isso abre margens para outros komatiitos poderem atender mais pré-requisitos.

Tabela 6 Avaliação dos pré-requisitos necessários para formação de sulfetos Ni-Cu-PGE associados a komatiitos, para os komatiitos brasileiros. X indica que o komatiito tem esse pré-requisito. Em vermelho os dois komatiitos mineralizados, Fortaleza de Minas e Crixás

Unidade Geológica - Estado	Presença de rocha cumulática	Geoquímica de rocha meso-adcumulática (>34% MgO)	Associação espacial com rocha sedimentar que podem ter enxofre	Indicativo geoquímico de contaminação crustal e segregação de Líquido sulfetado com captura de metais	Presença de sulfetos magmáticos
Craton São Franscisco					
Pitangui - MG			X		
Rio das Velhas (Quebra Osso) - MG	X	X	X	X	
Rio Manso - MG (Morro da Onça?)	X	X			
Umburanas - BA	X	X	X		
Ibitira-Ubiraçaba - BA			X		
Brumado - BA	X	X			
Guajeru - BA	X	X	X		
Mundo Novo - BA					
Lagoa do Alegre - BA	X				
Boquira - BA					
Riacho de Santana - BA	X		X		
Gavião	X	X			
Tiquara- BA					
Riacho dos Machados - BA					
Rio Salitre - BA			X		
Cinturão orogêmico na borda SW do Cráton São Francisco					
Piumhi - MG	X	X			
Fortaleza de Minas/Morro do Ferro - MG	X	X	X	X	X
Barbacena - MG	X				
Cinturão/Faixa Brasília					
Faina e Serra de Santa Rita - GO	X		X		
Crixás - GO	X	X	X	X	X
Guarinos - GO			X		
Pilar - GO			X		
Província mineral de Carajás					
Selva - PA	X	X			
Sapucaia - PA					
Seringa - PA	X				
Provícia Borborema					
NE da faixa Seridó - RN		X			

Por fim, é importante destacar que há regiões como por exemplo, a Província Mineral de Carajás e a Província Rio Maria no Cráton Amazônico, com ainda muitas áreas com greenstone belts, que carecem de mapeamento

geológico básico, sem mapeamento de detalhe, sem geoquímica sem geocronologia, como é o caso do greenstone belts de Tucumã. Essas áreas são uma oportunidade exploratória importante, que as empresas de mineração, junto com Serviço Geológico do Brasil (SGB-CPRM), precisam focar e investir em pesquisa.

3.3. Sugestões e critérios para avaliação do potencial para depósitos de Ni-Cu-PGE associados a komatiitos no Brasil

Pensando na escala continental do Brasil e no grau de conhecimento geológico atual sobre os komatiitos brasileiros, foram elaboradas sugestões importantes que estão organizadas de forma sequencial, onde não obtendo resultados positivos, deve-se refazer o ponto em questão novamente na mesma área ou recomeçar tudo, a partir do 1, em outra área, dependendo da escala. Tais sugestões foram baseadas numa integração de vários trabalhos (exemplo: Costa Jr. et al., 1997; Hill, 2001. Lesher e Keays, 2002; Naldrett, 2004; Barnes et al., 2004; Barnes, 2006; Brenner, 2006; Ardnt et al., 2008; Fiorentine et al., 2010; Barnes e Fiorentine, 2012; Barnes et al., 2013; Heggie et al., 2013; Perring, 2015, Le Vaillant et al., 2015; Konnunaho et al., 2015; Lesher, 2017; Barnes et al., 2023; Staude et al., 2022 e 2024; Maia et al., 2025).

i. Focar a pesquisa mineral em terrenos geológicos com ocorrência de greenstone belts, preferencialmente Arqueanos, com foco nas sequências inferiores, onde já foram descritos/mapeados komatiitos e/ou rochas ultramáficas.
ii. Avaliar a zonas de transporte de magma através da crosta. Isso deve ser feito através da geração de mapas gravimétricos, magnetométricos de estruturas complexas, com foco em margens da litosfera continental, por exemplo, falhas penetrantes de grande escala/profundas; rochas contemporâneas ou indicadoras de rifteamento. Outra sugestão ainda nesse ponto, é gerar mapas das bordas dos paleocratons através de isótopos radiogênicos (ex: Sm-Nd). Além de mapas litológicos específicos de rochas contemporâneas ao komatiito.
iii. Combinar dados geoquímicos e geológicos para identificar zonas de alto fluxo de magma. A geoquímica vai ajudar a encontrar rochas

cumuláticas usando mapas geoquímicos de MgO >35%, razões Ni/Ti, Ni/Cr. A geologia deve ser aplicada na descrição e interpretação de rochas para definir a sucessão de fácies komatiiticas, com o objetivo final de identificar fácies de conduto/canal.

iv. Avaliar a adição e saturação de enxofre. A litogeoquímica irá avaliar o nível de contaminação crustal. Para tanto, é necessário que inclua a TABS, Se e EGP nas análises químicas. Fazer mapas e diagramas específicos irão ajudar nisso, contudo, como pode haver uma variedade grande de rochas encaixantes, os diagramas e mapas podem ser bem variados. Outro aspecto importante é garantir que os elementos usados não tenham sido mobilizados em outros processos pós-magmáticos. A sugestão final é focar em elementos que estejam positivamente anómalos nos komatiitos e que só a contaminação crustal explicaria tal anomalia. Usar isótopos de enxofre para identificar fontes externas de enxofre é uma ferramenta útil. Além de gerar mapas de concentração de S nos komatiitos e nas rochas associadas a ele. Todos esses mapas devem ser comparados com um mapa geológico da rocha assimilada.

v. Avaliar o potencial de captura de metais que o líquido sulfetado tem. Esse ponto se faz, uma vez encontrado sulfeto. Isso deve ser feito através da concentração e distribuição de Ni nos sulfetos, por meio de geoquímica do minério, de preferência, separando por tipo de textura. Outra recomendação é avaliar o teor de Ni em olivina e piroxênios, onde por exemplo, baixo teor de Ni em silicatos pode indicar alto teor de Ni em sulfetos. Enfatizo aqui o fato de buscar sempre minerais essencialmente ígneos. Gerar mapas de tenor (concentração de um metal em uma massa de 100% sulfeto) de Ni e de teores de Ni nos silicatos irão permitir tal avaliação, com foco nas áreas com alto tenor no sulfeto e baixo teor no silicato.

vi. Avaliar a concentração física de sulfetos ricos em metais. Essa concentração é causada por uma redução abrupta no fluxo de magma para acumular alta proporção de sulfetos. Isso implica em mudança na morfologia dos canais de komatiítos, para tanto, é sugerido fazer um mapa/modelo geológico das fácies primárias/magmáticas do

komatiito.

vii. Avaliar as modificações pós-magmáticas que o corpo de minério pode ter tido, isso inclui modificações tectônicas e hidrotermais. Gerar mapas de dobras, de intersecção de falhas e zonas de cisalhamento, além de mapear zonas de remobilização de sulfeto maciço, com formação de brechas tectônicas, vão avaliar o aspecto tectônico, já mapas de alteração mineral e de anomalias geoquímicas, junto com o mapeamento de minério associado a veios, vão avaliar o aspecto hidrotermal.

Segue abaixo um fluxograma simplificado das sete etapas:

1. **Definição da Área-Alvo Inicial**
    - Foco em terrenos com *greenstone belts* Arqueanos e eventualmente paleoproterozóicos;
    - Priorizar sequências inferiores com presença de komatiítos/rochas ultramáficas.
2. **Avaliação de Estruturas Crustais Profundas**
    - Gerar mapas gravimétricos e magnetométricos;
    - Identificar falhas profundas e zonas de rifteamento.
    - Mapear bordas de paleocrátons com isótopos (ex: Sm-Nd);
    - Mapas litológicos de rochas contemporâneas aos komatiitos.
3. **Identificação de Zonas de Alto Fluxo de Magma**
    - Aplicar geoquímica: mapas de MgO >35%, Ni/Ti, Ni/Cr;
    - Aplicar geologia: descrever fácies komatiíticas → buscar fácies de canal/conduto.
4. **Avaliação da Adição e Saturação de Enxofre**
    - Análises geoquímicas incluindo S, TABS, Se, EGP;
    - Criar mapas/diagramas de contaminação crustal;
    - Usar isótopos de S para identificar fontes externas;
    - Mapas de concentração de S e correlação com mapa da rocha assimilada.
5. **Avaliação do Potencial de Captura de Metais pelo Líquido Sulfetado**
    - Geoquímica de minério: concentração/distribuição de Ni nos sulfetos;
    - Avaliar teores de Ni em olivinas e eventualmente em piroxênios, ambos magmáticos;
    - Modelagem geoquímica para cálculo de R-factor, incluindo EGP.
6. **Avaliação da Concentração Física dos Sulfetos**
    - Interpretar mudanças na morfologia dos canais
    - Mapear fácies primárias/magmáticas dos komatiítos
7. **Avaliação das Modificações Pós-Magmáticas**
    - Mapas estruturais: dobras, falhas, zonas de cisalhamento

- Identificar zonas de remobilização de sulfetos (brechas tectônicas)
- Mapas de alteração mineral, geoquímica e minério em veios

3.4. Conclusões

Como conclusões desse capítulo, vale destaque para a pouquíssima quantidade de komatiitos brasileiros descritos na literatura, um total de apenas 26, sendo apenas 2 mineralizados, Fortaleza de Minas e Crixás. Destes 26, poucos tem dados geoquímicos robustos que permitam avaliar o potencial para mineralização desses komatiitos. Outros tantos, estão bastante alterados, metamorfizados e tecnonizados, dificultando o reconhecimento de feições e texturas primárias. Muitos trabalhos focam no komatiitos e não avaliam as rochas encaixantes e suas relações espaciais. Poucos trabalhos fazem uma interpretação das fácies, bem como do ambiente do derrame komatiítico.

Sobre a avaliação dos komatiitos brasileiros em relação aos pré-requisitos para formação de depósitos de sulfetados de Ni-Cu-PGE associados a komatiitos. Com o pouco de dados disponível, foi possível indicar que os komatiitos de Quebra Osso do grenstone belt Rio das Velhas no Quadrilátero Ferrifero - Craton São Francisco, tem bons indicativos de ter formado um líquido sulfetado imiscível que capturou metais e formou sulfetos. Isso não quer dizer que este sulfeto tenha volume e teores relevantes, ou que ele ainda esteja lá preservado, somente uma campanha com sondagem diamantada, integrada geoquímica e geofísica podem confirmar esses detalhes. Outro ponto importante é que para a grande maioria dos outros komatiitos, não há dados suficiente para afirmar ou negar essas possibilidades. Há a necessidade de se estudar os komatiitos com uma sistemática que inclua avaliar o potencial metalogenético dessas rochas.

Localizar os principais condutos de magma em terrenos metamórficos, deformados e mal expostos, avaliar fontes adequadas de enxofre, a presença de armadilhas químicas e físicas para a formação do minério, e restringir o efeito da modificação pós-magmática à geoquímica dos komatiitos regionalmente, se torna essencial para a exploração de depósitos de Ni-Cu-PGE associados a komatiitos, principalmente no Brasil.

Portanto, com base nos dados compilados sobre os komatiitos brasileiros e avaliando-os nos aspectos geológicos, petrológicos e geoquímicos, eles não são diferentes dos daqueles encontrados por exemplo, na Austrália, Canada e África do Sul. Contudo, lá eles estão bem mais e melhor expostos, são mais mapeados e analisados, com abordagens integradas que possibilitam avaliar melhor o seu potencial metalogenético, que por fim aumentam as chances de se encontra depósitos sulfetados de Ni-Cu-PGE associados a komatiitos.

Referências

Almeida C.M., Olivo G.R., Carvalho S.G. de 2007. The Ni-Cu-PGE sulfide ores of the komatiite-hosted Fortaleza de Minas deposit, Brazil: Evidence of hydrothermal remobilization. Canadian Mineralogist, 45:751–773.

Andreatta e Silva G.P., Carneiro M.A. 2009. A suíte metatholeiítica da seqüência metavulcanos- sedimentar Rio Manso, Quadrilátero Ferrífero (MG). Rem: Revista Escola de Minas. V. 62, I.4, 423-430p. doi: 10.1590/S0370-44672009000400003

Arndt N.T., Lesher C.M., Barnes S.J. 2008. Komatiite (N. T. Arndt, Ed.). Komatiite, 295–327.

Barnes S.J. 2006. Komatiite-Hosted Nickel Sulfide Deposits: Geology, Geochemistry, and Genesis. Komatiite-Hosted Nickel Sulfide Deposits: Geology, Geochemistry, and Genesis, 51–97.

Barnes S.J., Lesher C.M., Keays R.R. 1995. Geochemistry of mineralised and barren komatiites from the Perseverance nickel deposit, Western Australia. Lithos, 34:209–234.

Barnes, S.J., Hill, R.E.T., Perring, C.S., and Dowling, S.E., 2004, Lithogeochemical exploration for komatiite-associated Ni-sulfide deposits: Strategies and limitations: Mineralogy and Petrology, v. 82, p. 259–293.

Barnes S.J., Fiorentini M.L. 2012. Komatiite magmas and sulfide nickel deposits: A comparison of variably endowed archean terranes. Economic Geology, 107:755–780.

Barnes S.J., Godel B., Gürer D., Brenan J.M., Robertson J., Paterson D. 2013. Sulfide-olivine fe-ni exchange and the origin of anomalously ni rich magmatic sulfides. Economic Geology, 108:1971–1982.

Barnes S.J., Cruden A.R., Arndt N., Saumur B.M. 2016. The mineral system approach applied to magmatic Ni–Cu–PGE sulphide deposits. Ore Geology Reviews, 76:296–316.

Barnes S.J., Yao Z. Sen, Mao Y.J., Jesus A.P., Yang S., Taranovic V., Maier W.D. 2023. Nickel in olivine as an exploration indicator for magmatic Ni-Cu sulfide deposits: A data review and re-evaluation. American Mineralogist, 108:1–17.

Begg G.R.C.B., Ronsky J.O.N.A.M.H., Rndt N.I.T.A., Riffin W.I.L.G. 2010. The Craton Margin Model: A Brief History and Description. 1057–1070.

Borges C.C.A., Toledo C.L.B., Silva A.M., Chemale F., Jost H., Lana C. de C. 2017. Geochemistry and isotopic signatures of metavolcanic and metaplutonic rocks of the Faina and Serra de Santa Rita greenstone belts, Central Brazil: Evidences for a Mesoarchean intraoceanic arc. Precambrian Research, 292:350–377.

Brenner T.L. 2006.The Fortaleza De Minas Nickel, Copper and Platinoids Deposit : Ore Types , Tectonics and Volcanological Aspects a Jazida De Níquel , Cobre E Platinóides De Fortaleza De Minas : Aspectos Tectônicos , Vulcanológicos E Tipos De Minérios .: A Universidade Estadual Paulista Júlio de Mesquita Filho.

Campbell I.H., Naldrett A.J. 1979. The influence of silicate: sulfide ratios on the geochemistry of magmatic sulfides. Economic Geology, 74:1503–1506.

Costa JR. C.N., Ferreira Filho C.F., Araujo G.A.O.S.M., Lopes R.O. 1997. Geology and Geochemistry of the Boa Vista Nickel Sulfide Deposit, Crixás Greenstone Belt, Central Brazil. Revista Brasileira de Geociências, 27:365–376.

Costa F.G., Silva R.C.S., Santos P.A., Silva C.M.G. 2023. Spinifex texture in the Mesoarchean komatiites of the Sapucaia greenstone belt, Carajás

province, Brazil. 17º Simpósio de geologia da Amazônia - Geotecnologias e sustentabilidade: A geologia na Amazônia atual. Expanded abstract.

Cunha, J.C., Barbosa, J.S.F., Mascarenhas, J.F. 2012. Greenstone Belts e Sequências Similares. In: Barbosa, J. S. F. (Coordenação Geral), Geologia da Bahia: Pesquisa e atualização (v. 1, 101-199). Salvador: CPBM; UFBA.

Fiorentini, M.L., Barnes, S.J., Lesher, C.M., Heggie, G.J., Keays, R.R., Burnham, M., 2010. Platinum group element geochemistry of mineralized and nonmineralized komatiites and basalts. Econ. Geol. 105, 795–823.

Fiorentini M., Beresford S., Barley M., Duuring P., Bekker A., Rosengren N., Cas R., Hronsky J. 2012. District to camp controls on the genesis of komatiite-hosted nickel sulfide deposits, agnew-wiluna greenstone belt, western australia: Insights from the multiple sulfur isotopes. Economic Geology, 107:781–796.

Garcia P.M.P., Carrilho E.L.V., Ribeiro B.P., Misi A., Sá J.H.S., Rios D.C., 2021. Geology, petrogenesis, and geochronology of the Rio Salitre Complex: Implications for the Paleoproterozoic evolution of the northern São Francisco Craton, Brazil, Journal of South American Earth Sciences, Volume 107, 103112, ISSN 0895-9811, doi: https://doi.org/10.1016/j.jsames.2020.103112.

Gole M.J., Barnes S.J. 2020. The association between Ni-Cu-PGE sulfide and Ni-Co lateritic ores and volcanic facies within the komatiites of the 2.7 Ga East Yilgarn Craton Large Igneous Province, Western Australia. Ore Geology Reviews, 116:103231.

Heggie, G. J., Barnes, S. J. & Fiorentini, M. L. 2013. Application of lithogeochemistry in the assessment of nickel- sulfide potential in komatiite belt from northern Finland and Norway. Bulletin of the Geological Society of Finland 85 (1–2), 107–126.

Hiebert R.S., Bekker A., Houlé M.G., Wing B.A., Rouxel O.J. 2016. Tracing sources of crustal contamination using multiple S and Fe isotopes in

the Hart komatiite-associated Ni–Cu–PGE sulfide deposit, Abitibi greenstone belt, Ontario, Canada. Mineralium Deposita, 51:919–935.

Hill R.E.T. 2001. Komatiite volcanology, volcanological setting and primary geochemical properties of komatiite-associated nickel deposits. Geochemistry: Exploration, Environment, Analysis, 1:365–381.

Jahn B. ming, Gruau G., Glikson A.Y. 1982. Komatiites of the Onverwacht Group, S. Africa: REE geochemistry, Sm/Nd age and mantle evolution. Contributions to Mineralogy and Petrology, 80:25–40.

Jost, H., Carvalho, M.J., Rodrigues, V.G., Martins, R., 2014. Metalogênese dos greenstone belts de Goiás. In: Silva, M.G., Neto, M.B.R., Jost, H., Kuyumjian, R. M. (Orgs.), Metalogênese das províncias tectônicas brasileiras, Belo Horizonte, CPRM, pp. 141–168.

Keays R.R., Lightfoot P.C. 2010. Crustal sulfur is required to form magmatic Ni-Cu sulfide deposits: Evidence from chalcophile element signatures of Siberian and Deccan Trap basalts. Mineralium Deposita, 45:241–257.

Konnunaho J., Halkoaho T., Hanski E., Törmänen T., 2015. Chapter 3.2 - Komatiite-Hosted Ni-Cu-PGE Deposits in Finland, Editor(s): Wolfgang D. Maier, Raimo Lahtinen, Hugh O'Brien, Mineral Deposits of Finland, Elsevier, Pages 93-131, ISBN 9780124104389, Doi: https://doi.org/10.1016/B978-0-12-410438-9.00004-2.

Le Vaillant M., Fiorentini M.L., Barnes S.J. 2016. Review of lithogeochemical exploration tools for komatiite-hosted Ni-Cu-(PGE) deposits. Journal of Geochemical Exploration, 168:1–19.

Leal V.L.S, Kuchenbecker M., Barbuena D., Queiroga G., Pinheiro M.A.P., Freimann M.A. 2021. Geochemistry and U–Pb zircon ages of the metamafic-ultramafic rocks of the Riacho dos Machados metavolcanosedimentary sequence: Evidence of a late Rhyacian back-arc basin during the assembly of São Francisco-Congo paleocontinent, Journal of South American Earth Sciences, Volume 105, 102972, ISSN 0895-9811, doi: https://doi.org/10.1016/j.jsames.2020.102972.

Lesher C.M. 2017. Roles of xenomelts, xenoliths, xenocrysts, xenovolatiles, residues, and skarns in the genesis, transport, and localization of magmatic Fe-Ni-Cu-PGE sulfides and chromite. Ore Geology Reviews, 90:465–484.

Lesher C.M. 2019. Up, down, or sideways: Emplacement of magmatic Fe–Ni–Cu–PGE sulfide melts in large igneous provinces. Canadian Journal of Earth Sciences, 56:756–773.

Lesher C.M., Burnham O.M. 2001. Multicomponent elemental and isotopic mixing in Ni-Cu-(PGE) ores at Kambalda, Western Australia. Canadian Mineralogist, 39:421–446.

Lesher C.M., Keays R.R. 2002. Komatiite-associated Ni-Cu-PGE Deposits: Geology, Mineralogy, Geochemistry, and Genesis. The Geology, Geochemistry, Mineralogy and Mineral Beneficiation of PGE, .

Li C., Ripley E.M. 2005. Empirical equations to predict the sulfur content of mafic magmas at sulfide saturation and applications to magmatic sulfide deposits. Mineralium Deposita, 40:218–230.

Li C., Ripley E.M. 2009. Sulfur contents at sulfide-liquid or anhydrite saturation in silicate melts:Empirical equations and example applications. Economic Geology, 104:405–412.

Magee C., Muirhead J.D., Karvelas A., Holford S.P., Jackson C.A.L., Bastow I.D., Schofield N., Stevenson C.T.E., McLean C., McCarthy W., Shtukert O. 2016. Lateral magma flow in mafic sill complexes. Geosphere, 12:809–841.

Maia T.F.A., Ferreira Filho C.F., S. B. Oliveira. (2025). The komatiite-associated Boa Vista Ni-Cu-(PGE) sulfide deposit, Crixás greenstone belt, Central Brazil: insights into komatiite flow facies and exploration. Journal of South American Earth Sciencen. Volume 156, 2025, 105436, ISSN 0895-9811, https://doi.org/10.1016/j.jsames.2025.105436.

McDonough W.F., Sun S. s. 1995. The composition of the Earth. Chemical Geology, 120:223–253.

Meira M.M., 2023. Evidências de acreção crustal riaciana em sequências metavulcanossedimentares do setor noroeste do orógeno do oeste da Bahia, Brasil: Contribuições ao estudo do supercontinente Columbia. Dissertação de mestrado, Universidade Federal da Bahia, Salvador, Brasil, 162p.

Menezes Leal A.B., Santos A.L.D., Bastos Leal L.R., Cunha J.C. 2015. Geochemistry of contaminated komatiites from the Umburanas greenstone belt, Bahia State, Brazil. Journal of South American Earth Sciences, 61:1–13.

Menezes Leal A.B., Barbosa N.S., Bastos Leal L.R., Cunha J.C. 2016. Geocronologia U-Pb em zircão do greenstone belt Umburanas, Bloco Gavião, Cráton do São Francisco. 48º Congresso Brasileiro de geologia. Resumo.

Mole D.R., Fiorentini M.L., Thebaud N., Cassidy K.F., Campbell McCuaig T., Kirkland C.L., Romano S.S., Doublier M.P., Belousova E.A., Barnes S.J., Miller J. 2014. Archean komatiite volcanism controlled by the evolution of early continents. Proceedings of the National Academy of Sciences of the United States of America, 111:10083–10088.

Naldrett A.J. 1999. World-class Ni-Cu-PGE deposits: Key factors in their genesis. Mineralium Deposita, 34:227–240.

Naldrett A.J. 2004. Magmatic Sulfide Deposits. Geology, geochemistry and exploration. 730 p.

Nesbitt R.W., Sun S.-S., Purvis A.C. 1979. Komatiites: Geochemistry and genesis. Canadian Mineralogist, 17:165–186.

Perring C.S., 2015; Volcanological and structural controls on mineralization at the Mount Keith and Cliffs komatiite-associated nickel sulfide deposits, Agnew-Wiluna belt, Western Australia-implications for ore genesis and targeting. Econ Geol 110:1669–1695

Robertson J., Ripley E.M., Barnes S.J., Li C. 2015. Sulfur liberation from country rocks and incorporation in mafic magmas. Economic Geology, 110:1111–1123.

Rodrigues, A.C.P. 2000. Rochas metamórficas máficas e ultramáficas do greenstone belt Barbacena na região de Itutinga, Mg. Dissertação de mestrado, Universidade Estadual de Campinas, Instituto de Geociências, Programa de Pós-graduação em Geociências. 137p.

Santos J.N., 2022. Greenstone belt Guajeru, porção sul do Bloco Gavião: caracterização geológica, petrográfica e geoquímica. Dissertação de mestrado. Universidade Federal da Bahia, Salvador. 58p.

Santos F.G., Cavalcanti Neto M.T.O., Ferreira V.P., Bertotti A.L., 2020. Eo to Paleoarchean metamafic-ultramafic rocks from the central portion of the Rio Grande do Norte Domain, Borborema Province, northeast Brazil: The oldest South American platform rocks, Journal of South American Earth Sciences, Volume 97, 102410, ISSN 0895-9811, doi: https://doi.org/10.1016/j.jsames.2019.102410.

Siepierski L., Ferreira Filho C.F. 2016. Spinifex-textured komatiites in the south border of the Carajas ridge, Selva Greenstone belt, Carajás Province, Brazil. Journal of South American Earth Sciences, 66:41–55.

Silveira W.P. & Garrido I.A.A. 2000. Geologia, Pesquisa Mi- neral e Potencialidade Econômica do Greenstone Belt Riacho de Santana. S.A.Abertos, CBPM, 14, 39p.

Soares M.B, Corrêa Neto A.V., Fabricio-Silva W. 2020. The development of a Meso- to Neoarchean rifting-convergence-collision-collapse cycle over an ancient thickened protocontinent in the south São Francisco craton, Brazil. Gondwana Research, 77:40–66.

Souza, Z.S., Dall'Agnol, R., , Claudinei G.O., Huhn S.R.B. 1997. Geochemistry and petrogenesis of metavolcanic rocks from Archaean greenstone belts: Rio Maria region (southeast Pará, Brazil). Revista Brasileira de Geociências. 27. doi: 10.25249/0375-7536.1997169180.

Spreafico, R.R., Barbosa J.S.F., Moraes A.M.V., Souza Júnior F.D., 2020. Geology, petrology and U-Pb geochronology of metavolcanic rocks in the Mundo Novo greenstone belt, eastern São Francisco Craton, NE

Brazil: considerations about its tectonic setting. Brazilian Jornal Geology, 50 (03).

Staude S., Oelze M., Markl G. 2022. Multi-stage sulfide evolution of the Moran Ni sulfide ore, Kambalda, Western Australia: insights into the dynamics of ore forming processes of komatiite-hosted deposits. Mineralium Deposita.

Staude, S., Martin, L.A., Aleshin, M., et al. (2024). The multiple sulfur isotope architecture of the Kambalda nickel camp, Western Australia. Miner Deposita 59, 505–518 Doi: https://doi.org/10.1007/s00126-023-01223-6.

Teixeira L.R., 2012. Projeto Brumado-Condeúba estado da Bahia - Relatório temático de litogeoquímica. Salvador, Serviço Geológico do Brasil Relatório.

Teles G.S., Chemale F., Ávila J.N., Ireland T.R., 2022. The Paleoarchean Northern Mundo Novo Greenstone Belt, São Francisco Craton: Geochemistry, U–Pb–Hf–O in zircon and pyrite δ34S-Δ33S-Δ36S signatures, Geoscience Frontiers, Volume 13, Issue 5, 101252, ISSN 1674-9871, Doi: https://doi.org/10.1016/j.gsf.2021.101252.

Tourpin S., Gruau G., Blais S., Fourcade S. 1991. Resetting of REE, and Nd and Sr isotopes during carbonitization of a komatiite flow from Finland. Chemical Geology, 90:15–29.

Verma S.K., Oliveira E.P., Silva P.M., Moreno J.A., Amaral W.S. 2017. Geochemistry of komatiites and basalts from the Rio das Velhas and Pitangui greenstone belts, São Francisco Craton, Brazil: Implications for the origin, evolution, and tectonic setting, Lithos, Volumes 284–285, Pages 560-577, ISSN 0024-4937, doi: https://doi.org/10.1016/j.lithos.2017.04.024.

CONCLUSÕES DA TESE

Em função das indisponibilidades analíticas ($\Delta^{33}S$ e análise química de PGE), dados analíticos ruins ou não aplicáveis (Sm-Nd e química mineral de olivina metamórfica), as técnicas aplicadas e os artigos planejados foram modificados e adaptados. No entanto, a tese teve seus objetivos propostos alcançados inicialmente, que foi responder a seguinte pergunta: “Existe alguma justificativa geológica/petrológica para a escassez de depósitos sulfetados de Ni-Cu-EGP associados aos komatiitos brasileiros?”

As concussões detalhadas da tese foram divididas em 3 parte e podem ser encontradas no final de cada um dos 3 capítulos que compõem a tese. Toda via, elas podem ser resumidas da seguinte forma:

1) Sobre o depósito de Boa Vista

a) O depósito de Ni-Boa Vista é hospedado por uma unidade indiferenciada de fácies de canalização/conduto de acumulado de olivina intercalada com xistos de grafite contendo sulfeto.
b) As assinaturas isotópicas $\delta^{34}S$ do minério de Ni-Cu foram de +16 até +19 e para o grafita xisto, como rocha encaixante, foi de +30 a +34., razões S/Se muito altas (>10.000) sugerem que o grafita xisto foi a fonte externa de S para a origem do depósito de Boa Vista.
c) O minério mobilizado é caracterizado por zonas ricas em pirita associado a óxido/hidróxido de ferro e brecha de matriz dobrada. O processo de mobilização reduziu os teores de Ni e Cu, as concentrações de ETR, mas não alterou a relação Ni/Cu.
d) O depósito de Ni-Cu de Boa Vista é um depósito do Tipo I (contato basal), deformado de forma variável e mobilizado ao longo das zonas de cisalhamento. O depósito contém duas zonas mineralizadas separadas, ambas consistindo em Pn + Po ± Ccp dentro de brecha de minério de matriz de sulfeto, brecha tectônica é localmente encontrada em zonas de cisalhamento, além do minério ter raras texturas semi-maciça com inclusão de silicato e disseminada.

e) Os teores relativamente baixos dos minérios são atribuíveis a tenors relativamente baixos, o que é consistente com uma relação magma: sulfeto (R factor) <600.
f) A combinação de altos teores de Ni, MgO e Zn, associada à avaliação descritiva e interpretativa para identificar a fácies cumulus canalizados/condutos, em um ambiente komatiítico subvulcânico/vulcânico, pode ser um bom critério de exploração mineral.

2) Sobre o Depósito de Fortaleza de Minas

a) As assinaturas $\delta^{34}S$ dos sulfetos da jazida da Fortaleza de Minas (+5,70 e +6,83‰) são consistentes com a assimilação dos BIF (+9,5‰).
b) O BIF é uma importante fonte externa de S + TABS + Se para os depósitos de sulfeto de Ni-Cu-PGE, e foi a fonte para o depósito de Fortaleza de Minas.
c) O depósito de Fortaleza de Minas tem um baixo fator R entre 100-400, que é comum em depósitos de sulfeto de Ni-Cu-PGE associados à komatiito.
d) A fácies de escoamento em lagoa não é compatível com o fator R do depósito de Fortaleza de Minas, que apresenta erosão termomecânica eficiente e formação de sulfeto de minério de Ni-Ci-PGE. Houve uma combinação e superposição de dois ambientes diferentes, um com um conduíte / fluxo canalizado no início e outra fácies de fluxo em lagoa (lago de lava) por último.
e) O alto teor de Cr no depósito de Fortaleza de Minas pode ser explicado pela assimilação de oxigênio pelo BIF hospedeiro, que ocasionou a cristalização da cromita.

3) Sobre a Avaliação do potencial metalogenético dos komatiitos brasileiros para depósitos sulfetados de Ni-Cu-PGE

a) Há pouquíssimos komatiitos descritos na literatura brasileira, com poucos dados geoquímicos robustos que dificulta uma avaliação

mais abrangente do potencial metalogenético dos komatiitos brasileiros.

b) Não é implementada uma sistemática descritiva e de mapeamento dos komatiitos inclua uma interpretação de facies vulcânica/subvulcânica dos derrames komatiitos, que facilita o reconhecimento de ambientes favoráveis para formação do minério sulfetado de Ni-Cu, bem como o mapeamento das rochas encaixantes que possam ser ricas em enxofre.
c) Com o pouco de dados disponível, foi possível indicar que os komatiitos de Quebra Osso no grenstone belt Rio das Velhas no Quadrilátero Ferrifero - Craton São Francisco, tem bons indicativos de ter formado um líquido sulfetado imiscível que capturou metais e formou sulfetos.
d) A ausência de dados, principalmente geoquímicos, dificulta uma análise mais detalhada dos komatiitos brasileiros.
e) Localizar os principais condutos de magma em terrenos metamórficos, deformados e mal expostos, avaliar fontes adequadas de enxofre, a presença de armadilhas químicas e físicas para a formação do minério, e restringir o efeito da modificação pós-magmática à geoquímica dos komatiitos regionalmente, se torna essencial para a exploração de depósitos de Ni-Cu-PGE associados a komatiitos, principalmente no Brasil.
f) Os komatiitos brasileiros não são diferentes dos daqueles encontrados por exemplo, na Austrália, Canada e África do Sul, e seu potencial metalogenético existe. Eles só precisam serem melhor mapeados, descritos, interpretados e analisados, com foco em avaliar os pré-requisitos necessários para a formação de depósitos sulfetados de Ni-Cu-PGE.